

# **UNIWERSYTET OPOLSKI**

# **Instytut Chemii**

# PRACA DOKTORSKA

# Kacper Rzepiela

The role of hydrogen bonding in determining stability of biologically active compounds: molecular modelling and experimental studies

Rola wiązania wodorowego w oszacowaniu stabilności związków biologicznie czynnych: modelowanie molekularne i badania eksperymentalne

Praca napisana pod kierunkiem prof. dr hab. Teobald Kupka dr Aneta Buczek

**Opole 2025** 

Pragnę złożyć najserdeczniejsze podziękowania Mojej Mamie i Mojemu Tacie za nieocenione wsparcie, cierpliwość, wyrozumiałość i wiarę we mnie przez wszystkie lata mojej naukowej drogi.

Składam również serdeczne podziękowania
Panu Profesorowi Teobaldowi Kupce,
Pani Doktor Anecie Buczek oraz
Pani Profesor Małgorzacie Brodzie
za wieloletnią i owocną współpracę nad publikacjami naukowymi,
cenne wskazówki oraz wsparcie merytoryczne.

Wyrazy wdzięczności kieruję także do Pani Profesor Birgit Strodel i Pani Doktor Hebah Fatafta za możliwość odbycia stażu naukowego oraz za inspirującą współpracę.

# **Table of Contents**

1.	<b>List of Abbreviations</b>	 4
2.	Summary	 5
3.	Streszczenie	 7
4.	Introduction	 9
	4.1 Hydrogen bonding	9
	4.2 Studied systems: selected	13
	biologically active compounds	13
	4.3 Methods	 15
	4.4 Scientific problem	 18
	4.4.1 The object of studies	 18
5.	Overview of Achievements	 20
6.	Discussion of results	 27
	6.1 P1	 27
	6.2 P2	 30
	6.3 P3	 33
	6.4 P4	 36
	6.5 P5	 40
7.	Conclusions	 42
8.	Acknowledgments	 42
9.	References	 43
10	. Appendices to the Articles	
	Constituting the Doctoral	 46
	Dissertation	
	10.1 P1	 46
	10.2 P2	 47
	10.3 P3	 66
	10.4 P4	 134
	10.5 P5	 155
11	Co-author statements	156

#### 1. List of Abbreviations

Abbreviation Full name

2-TU 2-thiouracil

Å Angstrom

**BSSE** Basis Set Superposition Error

**CBD** Cannabidiol

**CBS** Complete Basis Set

CCSD(T) Coupled-Cluster with Single, Double, and

perturbative Triple excitations

**CP** Counterpoise method

**CPCM** Conductor-like Polarizable Continuum Model

**DFT** Density Functional Theory

**DHB** Dihydrogen Bond

**DNA** Deoxyribonucleic Acid

FT-IR Fourier-Transform Infrared spectroscopy

GIAO Gauge-Independent Atomic Orbital

Gaussian-Type Orbitals

HF Hartree–Fock

**LCAO** Linear Combination of Atomic Orbitals

LDBS Locally Dense Basis Set

MD Molecular Dynamics

MP2 Møller–Plesset Perturbation Theory

NMA *N*-methylacetamide

NMR Nuclear Magnetic Resonance
PCM Polarizable Continuum Model

PES Potential Energy Surface

**RNA** Ribonucleic Acid

SSCC Spin-Spin Coupling Constant

STO Slater-Type Orbitals
UW Uracil-Water system

**ZPVC** Zero-Point Vibrational Corrections

#### 2. Summary

This doctoral dissertation consists of five thematically related research articles (P1–P5) and investigates the role of hydrogen bonding in determining the stability of selected biologically active compounds, such as uracil and cannabidiol (CBD), and their complexes with water molecules. The study employed an approach combining various computational methods including quantum-chemical calculations (DFT, MP2, and CCSD(T)) with Molecular Dynamics (MD) simulations, which enabled the determination of key hydrogen bond parameters, identification of the most stable conformations and water complexes, and estimation of hydrogen bond energy. Experimental studies using Fourier-Transform Infrared (FT-IR) and Nuclear Magnetic Resonance (NMR) spectroscopy complemented the computational results.

Studies on uracil—water complexes (P1) revealed that, in addition to the well-known five arrangements with single or double hydrogen bonds, two less stable complexes exist, bonded by a single hydrogen bond, representing shallow energy minima. These complexes are not visible in FT-IR spectra but significantly expand the understanding of nucleobase—water interactions.

In the next study (**P2**), it was shown that hydrogen bond strength in uracil and *N*-methylacetamide (NMA) complexes with water depends on the inclusion of dispersion corrections and solvent polarity, highlighting the importance of precise modeling of hydrogen-bond interactions.

A methodological study (**P3**) demonstrated that accurate NMR parameter calculations for 2-thiouracil and third-period hydrides require appropriate basis sets and vibrational corrections. These methods were subsequently applied to bioactive compounds, improving the reliability of spectroscopic predictions.

FT-IR and NMR studies on weak hydrogen bonds in CBD (**P4**) showed that one hydroxyl group is free while the other participates in intramolecular hydrogen bonding, affecting characteristic vibrational bands and proton chemical shifts. These observations agree with theoretical data showing that the dominant conformer is stabilized by an intramolecular  $O-H\cdots\pi$  hydrogen bond. It underlines the role of intramolecular hydrogen bonding in shaping the spectroscopic properties of bioactive compounds.

Quantum-chemical DFT calculations (P5) revealed that the diequatorial CBD conformer is the most stable, stabilized by an  $O-H\cdots\pi$  intramolecular hydrogen bond. MD simulations confirmed the presence of this stable conformer and further showed that in aqueous environments, only one hydroxyl group is partially solvated while the other is

stabilized by intramolecular hydrogen bonding. This limited availability promotes CBD aggregation and explains its low solubility, despite the presence of polar groups.

The dissertation concludes that hydrogen bonds are decisive not only for molecular stability but also for solubility and aggregation behavior. The balance between intramolecular and intermolecular interactions determines molecular bioavailability, providing important guidance for the design of pharmaceutical drugs and other bioactive compounds, where hydrogen bonds play a key role in shaping biological properties.

#### 3. Streszczenie

Niniejsza rozprawa doktorska składa się z pięciu powiązanych tematycznie artykułów naukowych (P1–P5). Jej celem było zbadanie roli wiązań wodorowych w kształtowaniu trwałości wybranych związków biologicznie czynnych, takich jak uracyl i kannabidiol (CBD), a także ich kompleksów z cząsteczkami wody. W pracy zastosowano podejście łączące różne metody obliczeniowe, w tym obliczenia kwantowo-chemiczne (DFT, MP2 i CCSD(T)) oraz symulacje dynamiki molekularnej (MD), które pozwoliły na określenie kluczowych parametrów wiązań wodorowych, identyfikację najtrwalszych konformacji i kompleksów z wodą oraz oszacowanie wpływu wiązań wodorowych na energię badanych układów. Badania eksperymentalne z wykorzystaniem spektroskopii w podczerwieni z transformacją Fouriera (FT-IR) i magnetycznego rezonansu jądrowego (NMR) uzupełniły i zweryfikowały wyniki obliczeń.

Badania kompleksów uracyl—woda (P1) wykazały, że oprócz dobrze znanych pięciu układów uracylu związanych dwoma lub pojedynczymi wiązaniami wodorowymi z wodą, istnieją również dwa mniej trwałe kompleksy połączone za pomocą pojedynczego wiązania wodorowego, które stanowią rzeczywiste, choć płytkie minima energetyczne. Kompleksy te pozostają niewidoczne w widmach FT-IR, ale istotnie poszerzają wiedzę na temat tworzenia kompleksów zasad nukleinowych z wodą.

W kolejnej pracy (**P2**) pokazano, że siła wiązań wodorowych w kompleksach uracylu i *N*-metyloacetamidu (NMA) z wodą zależy od uwzględnienia poprawki dyspersyjnej i polarności rozpuszczalnika. Wyniki te podkreślają znaczenie precyzyjnego modelowania oddziaływań wodorowych.

Istotnym elementem było opracowanie metodologii (**P3**), która wykazała, że dokładność obliczeń parametrów NMR na przykładzie 2-tiouracylu i wodorków pierwiastków trzeciego okresu, wymagają odpowiedniego doboru baz funkcyjnych i poprawek wibracyjnych. Metody te zostały następnie zastosowane do analizy układów substancji bioaktywnych, zwiększając wiarygodność przewidywań spektroskopowych.

Badania FT-IR i NMR (**P4**) słabych wiązań wodorowych kannabidiolu (CBD) wykazały, że jedna grupa hydroksylowa jest wolna, a druga zaangażowana w wewnątrzcząsteczkowe wiązanie wodorowe, co wpływa na charakterystyczne pasma drgań w podczerwieni oraz przesunięcia chemiczne protonów na widmach <sup>1</sup>H NMR. Wyniki te są zgodne z danymi teoretycznymi, wskazującymi, że dominujący konformer jest stabilizowany przez wewnątrzcząsteczkowe wiązanie wodorowe O–H···π. Uzyskane wyniki wskazują na istotną rolę wewnątrzcząsteczkowych wiązań wodorowych.

Obliczenia kwantowo-chemiczne metodą DFT (**P5**) wykazały, że najtrwalsza jest konformacja diekwatorialna, stabilizowana przez wewnątrzcząsteczkowe wiązanie wodorowe O–H···π. Symulacje MD potwierdziły występowanie tej konformacji. Ponadto, wyniki uzyskane metodą MD w środowisku wodnym, wskazują, iż tylko jedna grupa hydroksylowa w ograniczonym stopniu uczestniczy w solwatacji, natomiast druga jest stabilizowana przez wewnątrzcząsteczkowe wiązanie wodorowe O–H···π. Pomimo obecności w strukturze CBD grup hydroksylowych, ich ograniczona dostępność sprzyja agregacji i tłumaczy jego niską rozpuszczalność w wodzie.

Wnioski uzyskane w niniejszej rozprawie doktorskiej pokazują, że wiązania wodorowe występujące w CBD są czynnikiem decydującym nie tylko o trwałości, lecz także o jego rozpuszczalności i zdolności do agregacji. Równowaga między oddziaływaniami wewnątrz- i zewnątrzcząsteczkowymi determinuje biodostępność CBD. Stanowi to istotną wskazówkę podczas projektowania leków farmaceutycznych oraz innych substancji bioaktywnych, w których wiązania wodorowe mają kluczowe znaczenie dla ich właściwości.

#### 4. Introduction

#### 4.1. Hydrogen bonding

Intermolecular interactions are central to many essential biological processes, including protein folding, ligand-receptor binding, and Deoxyribonucleic Acid (DNA) base pairing. Notably, in proteins N–H···O hydrogen bonds are key factor for stabilization of α-helices and β-sheets. While N-H···N hydrogen bonds, though less common, also contribute to protein stability, particularly in systems involving proline. These interactions underscore their fundamental importance to life. Likewise, water molecules are recognized as a central component of biological systems. They prevent oppositely charged moieties of biological macromolecules from aggregating, thereby helping to maintain the three-dimensional topology essential for proper biological function. In addition, by forming extensive hydrogen-bonding networks, in which oxygen atoms are connected via O-H···O interactions, water functions as a high-dielectric insulator.<sup>2</sup> Therefore, these interactions must be carefully considered when designing new drugs. Computational chemistry provides valuable insights into the formation and role of hydrogen bonds in biological systems. For instance, the stabilizing hydrogen bonds between nitrogen bases and water offer a simple, yet informative model for understanding how intermolecular interactions influence both structural and spectroscopic properties. A proper classification of hydrogen bonds is essential. In addition to valence interactions, such as covalent and ionic bonds that hold atoms together within a molecule, there are also weak interactions between molecules. These non-covalent forces significantly influence the macroscopic properties of substances, such as viscosity, solubility, melting and boiling points. Because their interaction energy decreases more slowly with distance compared to that of covalent (valence) bonds, intermolecular forces are often referred to as long-range interactions. They are categorized based on their physical origin and interaction energy, and include: dipole dipole interactions, dipole–induced dipole interactions, hydrogen bonding and dispersion forces (instantaneous dipole-induced dipole interactions). Both intermolecular and intramolecular interactions are often dominated by their electrostatic nature, arising from the specific arrangement of electron charge within a system and governed by Coulomb's law. Hydrogen bond strength depends on both distance and angle, giving it a directional character. While slight deviations from linearity have minimal impact, bond strength decreases exponentially with increasing distance.

Traditionally, hydrogen bonding is viewed as primarily electrostatic with some covalent character (**Figure 1**).<sup>3</sup>

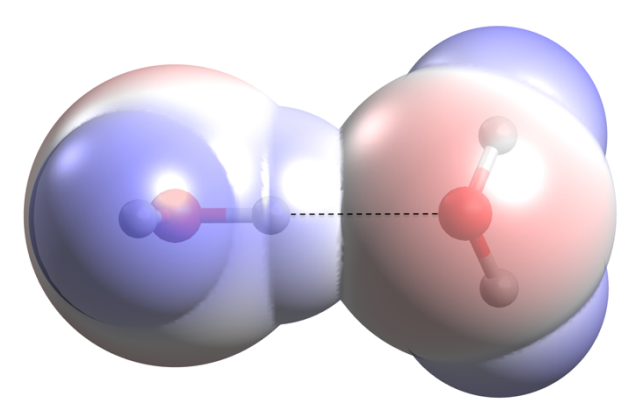


**Fig. 1.** The illustration of the hydrogen bonding  $A-H\cdots B$  in the most stable water dimer.

Hydrogen bonding is a distinct type of dipole-dipole interaction, typically represented as A-H···B. Although weaker than covalent or ionic bonds, hydrogen bonds can have a decisive impact on the properties of substances. In systems where hydrogen bonding is possible, it is often the dominant type of intermolecular interaction. A hydrogen bond is considered to form when atoms A and B are positioned closer to each other than they would be without the presence of the hydrogen atom. This interaction arises due to the electrostatic attraction between opposite partial charges. For a hydrogen bond to form, atom A must be significantly more electronegative than hydrogen, while atom B must possess a region of high electron density, typically a lone electron pair. This arrangement enhances the acidity of the hydrogen, with atom A acting as the hydrogen donor and atom B as the hydrogen acceptor. Hydrogen bonds can be classified according to their energy, the donor and acceptor type, and the number of centres involved in the interaction. In terms of energy, hydrogen bonds are usually grouped as very strong, strong, or weak. Their corresponding bond energy ranges are approximately 15–40 kcal/mol, 4–15 kcal/mol and less than 4 kcal/mol, respectively. The typical distances between the hydrogen bond donor and acceptor atoms (B.A.) fall within 2.2–2.5 Å for very strong, 2.5– 3.2 Å for strong, and 3.0–4.0 Å for very weak hydrogen bonds.<sup>4</sup> Atoms capable of forming strong hydrogen bonds as donors (A) include fluorine, nitrogen, and oxygen. Weaker hydrogen bonds may involve atoms like carbon, phosphorus, sulfur, chlorine, bromine, and iodine. Similarly, atoms acting as strong acceptors (B) are F, N, and O, while weaker acceptors include C, P, S, Cl, Br, and I. The ability to form hydrogen bonds increases in halide ions such as Cl<sup>-</sup>, Br<sup>-</sup>, and I<sup>-</sup>, due to their negative charge. A representative example is provided by the bifluoride anion (FHF), in which the exceptionally short H···F distance of 1.138 Å is associated with a large negative interaction energy ( $E_{int} = -61.1 \text{ kcal/mol}$ ), illustrating the strength of very strong hydrogen bonds.

The approach based on donor and acceptor type highlights the character of the atoms or groups involved in hydrogen bonding. Classical systems involve electronegative donors and acceptors, such as O-H···O, N-H···O, O-H···N, N-H···N, and F-H···F hydrogen bonds. These are often referred to as Pauling-type hydrogen bonds, and they are described as three-centre, four-electron (3c-4e) systems. In this model, the hydrogen atom bridges two electronegative atoms, labelled A and B. The interaction involves four electrons: one electron pair from the covalent  $\sigma$  A–H bond and one lone pair from the Lewis base centre B. Hydrogen bonding, however, extends well beyond classical Pauling-type systems. Donors need not always be strongly electronegative. For instance, C-H bonds can act as weak proton donors, giving rise to C-H···O, C-H···N, or C-H···S interactions. Such bonds are classified as hydrogen bonds with non-electronegative donors. Although they are generally weak, with stabilization energies between -1 and -2 kcal/mol, they occur frequently in protein-ligand complexes and crystal packing. In some cases, C-H···O=C hydrogen bonds in proteins may reach -4 kcal/mol, highlighting their potential biological significance. Likewise, acceptors need not be strongly electronegative either. Interactions such as O-H···C or F-H···C have been identified, although they are weak compared to the other types.<sup>5</sup>

Moreover, the classification of hydrogen bonds can be expanded further by multicentre interactions. In bifurcated hydrogen bonds, a single donor may interact with two acceptors, or conversely, one acceptor may interact with two donors (e.g. **Figure 2**).

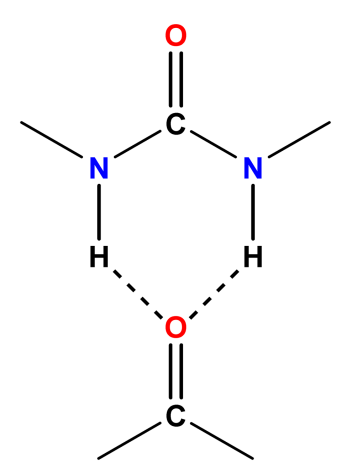


**Fig. 2.** The scheme of the bifurcated bond, the two N-Hs are proton donors, whereas C=O is a proton acceptor.<sup>6</sup>

Cooperative effects often modulate the strength of these bifurcated hydrogen bonds. Intermolecular bifurcated hydrogen bonds typically exhibit negative cooperativity, making them weaker than two-center hydrogen bonds. In contrast, intramolecular bifurcated bonds can display positive or negative cooperativity, or may be additive, showing no net effect on bond strength. More complex multicenter hydrogen bonds also exist, involving  $\pi$ - and  $\sigma$ -electron systems; for example, in A–H··· $\pi$  interactions, an electron-rich  $\pi$ -system such as an aromatic ring or alkyne serves as the proton acceptor. Recent studies demonstrate that when two intramolecular bifurcated hydrogen bonds coexist in the same molecule, they can mutually reinforce each other. The total interaction energy of two hydrogen bonds might exceed the sum of their separate contributions. Model systems analyzed in that work show that the simultaneous presence of bifurcated donors and acceptors strengthens each bond beyond the sum of their independent contributions and that the second bifurcated bond reinforces the first. These results indicate that, although individually weaker than conventional two-center hydrogen bonds, bifurcated hydrogen bonds can achieve significant stabilization through intramolecular cooperativity.<sup>7</sup>

The Dihydrogen Bond (DHB) is a distinct subclass of hydrogen bonds, in which a conventional proton donor, such as N–H or O–H, interacts with a negatively polarized hydrogen atom (hydride) bound to an electropositive element. This interaction, denoted as A–H···H–E, involves a positively polarized hydrogen approaching a negatively polarized hydride, resulting in unusually short H···H contacts in the range of 1.7–1.9 Å, which is significantly shorter than the sum of the van der Waals radii of two hydrogen atoms. The hydride hydrogen is also bonded to elements such as transition metals or boron. The strength of DHB, estimated from the heat of interaction, generally falls in the range of 3–7 kcal/mol, indicating moderate but meaningful stabilization.<sup>8</sup>

Techniques such as infrared (FT-IR) spectroscopy and Nuclear Magnetic Resonance (NMR) are useful for detecting the presence and strength of hydrogen bonds. In FT-IR spectroscopy, hydrogen bonding, such as O–H···O=C, causes the stretching bands of OH and C=O groups to shift to lower frequencies, and become more intense and broader. In dilute alcohol solutions, the OH stretching region typically shows two bands, one from free OH groups and the other from hydrogen-bonded OH groups. In ¹H NMR spectroscopy, hydrogen bonds are indicated by a downfield chemical shift of the hydrogen signal. This occurs because the electronegative atom A decreases the electron density around the proton, reducing its shielding. Additionally, electrostatic attraction from atom B draws the proton closer and pushes bonding electrons toward A, further deshielding the hydrogen nucleus.

Molecular modelling also provides valuable complementary insights into hydrogen bonding, offering parameters such as bond lengths, angles, and interaction energies that are not directly accessible from spectroscopy. Computational methods allow the analysis of effects, such as cooperativity and conformational preferences. These aspects will be discussed in detail in the following chapter.

#### 4.2. Studied systems: selected biologically active compounds

This doctoral dissertation focuses on the theoretical and experimental characterization of biologically active compounds (drugs) and their interactions with water molecules. The research encompasses both the isolated biologically active substances and their hydrated complexes, with particular emphasis on the role of hydrogen bonding in determining structural stability, solubility and biological relevance.

One of the studied substances is uracil (**Figure 3**). It is one of the four pyrimidine bases found in Ribonucleic Acid (RNA). Uracil pairs with adenine through the formation of two hydrogen bonds, playing a crucial role in stabilizing the RNA structure. It is also a key component of nucleic acids that serves as the structural basis for several chemotherapeutic agents, such as 5-fluorouracil. Due to the presence of two oxygen atoms and two amide groups, uracil can exist in several tautomeric forms. Both, in cells and in vitro, it predominantly adopts the diketo form, as also confirmed by DFT calculations.<sup>9</sup>

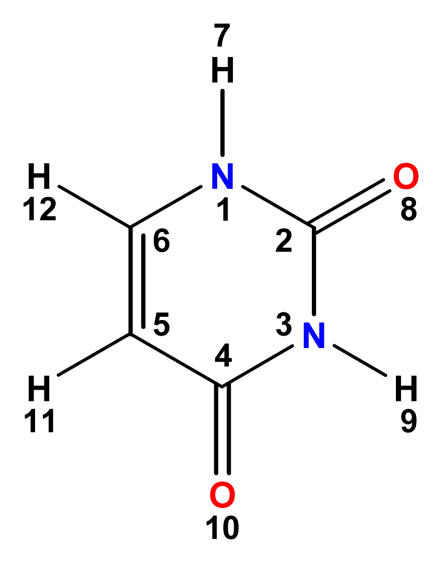


Fig. 3. Molecular structure of uracil with atom numbering.

In this work, the NMR parameters of 2-thiouracil (**Figure 4**) were studied. The results obtained in this work served as a reference for prediction of accurate NMR parameters, subsequently critically compared with experiment. Although the primary focus of this publication was a series of benchmark calculations of NMR parameters, it connects conceptually to the previous article through the inclusion of 2-thiouracil and to the spectroscopic NMR, FT-IR and theoretical studies of hydrogen bonding of cannabidiol.<sup>10</sup>

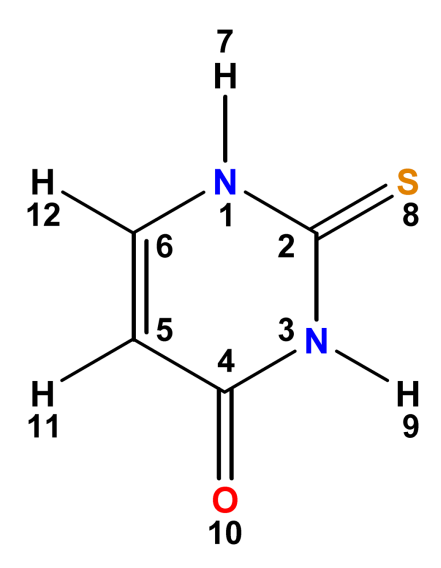


Fig. 4. Molecular structure of 2-TU with atom numbering.

Another biologically important molecule examined in this dissertation is cannabidiol (**Figure 5**), a compound belonging to the phytocannabinoid class.

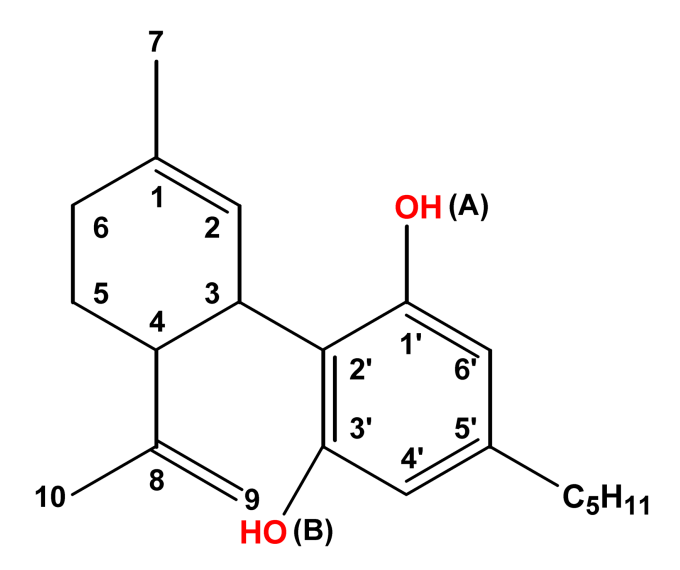


Fig. 5. Molecular structure of CBD with atom numbering.

Phytocannabinoids have attracted significant interest due to their remarkable biological properties, and to date, around 125 such compounds have been identified in *Cannabis sativa*. This plant has been known throughout history, particularly in China and India, for its use in pain management. CBD itself was first isolated by Roger Adams<sup>11</sup> in 1940. Unlike tetrahydrocannabinol, the primary psychoactive component of hashish, CBD does not produce psychoactive effects. Among its biological activities, CBD exhibits anti-inflammatory, antiviral, antioxidant, and anxiolytic properties. It is already used in the treatment of epilepsy and is currently the subject of research for potential applications in cancer and schizophrenia therapy. The CBD molecule consists of a benzene ring with two hydroxyl groups attached, a flexible n-pentyl chain, and a limonene moiety. As shown by calculations<sup>12</sup>, the rotational barrier of the bond connecting the benzene ring to the limonene moiety (bond 2'-3) is relatively high, thereby restricting the molecule's conformational flexibility.

#### 4.3. Methods

By employing both computational chemistry and experimental methods, a deeper understanding of biologically active compounds can be achieved. Currently, the quality of theoretical modeling of individual biologically active compounds and their complexes, have improved in parallel with the rapid advancement of computer technologies and processing power. Moreover, the use of computational resources helps to overcome some of the limitations associated with experimental methods, including high costs and limited access to instrumental tools. In cases where both computational and experimental data are available, theoretical predictions can be verified through experimental results. Conversely, when certain outcomes are accessible through only one of the approaches, the two methods serve as complementary tools, together contributing to a more comprehensive analysis. In this dissertation, the computational methods employed include Density Functional Theory<sup>13, 14</sup> (DFT), Møller–Plesset Perturbation Theory<sup>15</sup> (MP2), Coupled-Cluster with Single, Double, and perturbative Triple excitations<sup>16-18</sup> (CCSD(T)) and Molecular Dynamics<sup>19</sup> (MD) simulations. The experimental methods applied are NMR and FT-IR.

DFT is a widely used computational method, implemented in many software packages, due to its excellent balance between computational cost and accuracy. It is founded on the two theorems of Hohenberg and Kohn<sup>13</sup>:

- 1) The first theorem states that the external potential, and therefore all ground-state properties of a many-electron system, are uniquely determined by its electron density  $\rho(r)$ , where r = (x, y, z) denotes the spatial coordinates.
- 2) The second theorem establishes that the ground-state energy of the system,  $E_0$  can be expressed as a functional F of the electron density:  $E_0 = F[\rho(r)]$

In contrast to *ab initio* methods, which require explicit consideration of the many-electron wavefunction depending on 3N spatial coordinates and the spin of each of the N electrons, DFT reduces computational complexity by relying on the electron density, while still maintaining a high level of accuracy.

A more practical formulation of DFT was developed by Kohn and Sham<sup>14</sup>, who expressed the total electronic energy as a functional of the electron density:

$$E_{\mathrm{DFT}}[\rho] = T[\rho] + E_{\mathrm{ne}}[\rho] + J[\rho] + E_{\mathrm{xc}}[\rho]$$

Here, T is the kinetic energy of the electrons,  $E_{ne}$  the electrostatic nucleus-electron attraction, J the classical Coulomb repulsion between electrons, and  $E_{xc}$  the exchange-correlation energy. Each of these terms is a functional of the electron density. Among them, the exact form of  $E_{xc}$  is unknown, and approximating it, is the central challenge of DFT.

The most commonly used exchange—correlation functionals can be grouped into three major classes:

- Local Density Approximation (LDA):
   The simplest approach, which assumes that the electron density ρ is locally uniform within small volume elements dτ. LDA is most accurate for systems with slowly varying electron densities, such as metals and semiconductors.
- Generalized Gradient Approximation (GGA) improves upon LDA by accounting for the gradient of the electron density, thus incorporating information about its spatial variation. Examples of GGA functionals include exchange functionals PBE<sup>20</sup>, PW91<sup>21</sup>, B3<sup>22</sup>, and correlation functionals such as PBEC<sup>20</sup>, P86C<sup>23</sup>, PW91C<sup>21</sup>, and LYP<sup>24</sup>.
- Hybrid Functionals combine a fraction of Hartree–Fock<sup>25</sup> (HF) exchange with DFT exchange–correlation functionals to improve accuracy. The most widely used is the B3LYP functional, which mixes exchange and correlation energies from different

sources: LDA, Becke's GGA exchange (B88), the LYP correlation functional, and HF exchange. The general form is:

$$E_{xc} = (1-a_0) E_x (LDA) + a_0 E_x (HF) + a_x E_x (B88_x) + a_c E_c (LYP88_c) + (1-a_c) E_c (VWN80_c)$$
  
with parameters  $a_0 = 0.20$ ,  $a_x = 0.72$ , and  $a_c = 0.81$ .

Owing to its versatility and reliability, B3LYP<sup>22, 24</sup> has become one of the most popular functionals, applicable even to organic systems containing several hundred atoms.

Molecular orbitals are solutions of the Schrödinger equation and describe the wave-like nature of electrons. For molecules larger than H<sub>2</sub><sup>+</sup>, exact analytical solutions are impossible, so approximations are required. A common approach is to represent molecular orbitals as a Linear Combination of Atomic Orbitals (LCAO). To describe these atomic orbitals, predefined sets of mathematical functions, called basis sets, are employed. In computational chemistry, Gaussian-Type Orbitals (GTOs) are most widely used, since they simplify the evaluation of integrals, although they represent electron density less accurately than Slater-Type Orbitals (STOs). To overcome this, multiple GTOs are combined to approximate a single STO, leading to minimal basis sets of the form STO-n $G^{26}$  (where n is the number of Gaussians per STO). Expanding beyond minimal bases, Double-Zeta (DZ) and Triple-Zeta (TZ) basis sets use two or three functions per orbital, respectively. A common strategy is to employ split-valence basis sets, which treat core and valence electrons differently: minimal functions describe core orbitals, while DZ or TZ functions describe valence orbitals. Well-known examples are the Pople-type basis sets<sup>27</sup> (e.g., 3-21G, 6-31G). To improve flexibility, diffuse functions (+) are added to describe the outermost regions of wavefunctions, particularly important for anions, lone pairs, and excited states (e.g., 6-31+G)<sup>28</sup>. To further enhance the accuracy of calculations, polarization functions (\*, d, or p) are introduced. These functions allow orbitals to deviate from spherical symmetry and better represent the directional character of chemical bonds. Examples of basis sets incorporating polarization functions include 3-21G\* and 6-31G\*\*.<sup>29</sup>

In addition to quantum chemical methods, MD simulations<sup>19</sup> represent a complementary computational approach. Unlike electronic structure methods, MD describes the classical motion of atoms and molecules by numerically integrating Newton's equations of motion. This method enables the exploration of time-dependent processes and the structural dynamics of larger molecular systems, including those beyond the practical reach of *ab initio* calculations.

### 4.4. The scientific problem

Despite many theoretical and experimental studies on hydration of bioactive compounds, some information is still lacking. Thus, the detailed knowledge of hydrogen bonding pattern and energetics in the first hydration sphere of uracil and cannabidiol is still missing. However, in line with progress in theoretical methodology and computer hardware combined with specially designed spectroscopic experiments, it is possible to get a deeper insight into the mechanism of uracil and CBD hydration. This information could lead to a better understanding of interactions between water and these or similar drugs. The aim of this study was to determine the role of hydrogen bonds in the stabilization of biologically active systems. The obtained results provide a better understanding of the structural, energetic, and spectroscopic properties of hydrated uracil and cannabidiol systems. This goal was achieved using selected theoretical methods supported by experimental methods.

### 4.4.1 The objects of studies

The **uracil** molecule, due to the presence of two carbonyl groups and two amide groups arranged alternately, exhibits notable flexibility in forming complexes with a single water molecule, allowing for the formation of both single and double hydrogen-bonded ring structures. From a structural perspective, investigating the arrangement of these hydrogen bonds is crucial, as it governs uracil's ability to form stable complexes through specific interactions with water and other molecular partners.

Additionally, to support the investigation of these biologically active molecules, a series of calculations evaluated the performance of various basis sets for theoretical NMR predictions. This study focused on selected compounds containing third-row elements, including **2-thiouracil**, a bioactive derivative of uracil. The findings provided valuable benchmarks for the accurate modeling of spectroscopic properties in systems containing third-row elements.

**Cannabidiol** exhibits a wide range of potential therapeutic effects. However, its biological activity is limited by its poor solubility in aqueous environments. CBD readily dissolves in oils but not in water. To better understand the molecular basis of this property, a conformational analysis of CBD was performed. Notably, its two hydroxyl groups could provide sites capable of forming hydrogen bonds with water molecules.

At the same time, CBD is capable of forming the intramolecular hydrogen bonding O-H $^{...}\pi$  that has a stabilizing effect on conformations of the molecule. Moreover, this internal stabilization may influence the hydrogen bonding with solvent molecules. The scientific problem therefore lies in understanding the balance between intra- and intermolecular hydrogen

bonding in CBD and its consequences for conformational preferences and solubility. Addressing this problem requires a detailed conformational analysis, supported by molecular modeling and complemented with experimental data. In this study, the conformational analysis of CBD was performed to explore how hydrogen bonding patterns govern its stability and solvent interactions.

#### 5. Overview of Achievements

My research work comprises five interrelated scientific articles, all of which have been published in peer-reviewed scientific international journals indexed in the Philadelphia list (Journal Citation Reports) and one in domestic journal. These articles are referred to as **P1** through **P5**. The figures presented in this dissertation were modified from those in the published articles.

# Publications included in my doctoral thesis:

P1. Buczek, A.\*; Rzepiela, K.; Kupka, T.; Broda, M. A.; Kar, T.\*

Uracil—water interaction revisited – in search of single H-bonded secondary minima.

Physical Chemistry Chemical Physics 2024, 26 (6), 5169-5182.

DOI: 10.1039/D3CP04057G, IF: 2.9, Ministerial Points<sup>a</sup>: 100, Citations: 0.

aMinisterial Points = Punkty Ministerialne

## P2. Rzepiela, K.; Buczek, A.; Kupka, T.; Kar, T.; Broda, M. A.\*

Modelowanie właściwości wiązań wodorowych na przykładzie kompleksów układ amidowywoda.

Wiadomości Chemiczne 2023, 77 (7-8), 629-645.

DOI: 10.53584/wiadchem.2023.07.1, IF: -, Ministerial Points: 20, Citations: -.

#### P3. Rzepiela, K.; Kaminský, J.\*; Buczek, A.; Broda, M. A.; Kupka, T.\*

Electron correlation or basis set quality: how to obtain converged and accurate NMR shieldings for the third-row elements?

Molecules 2022, 27 (23), 8230.

DOI: 10.3390/molecules27238230, IF: 4.6, Ministerial Points: 140, Citations: 10.

#### P4. Buczek, A.\*; Rzepiela, K.; Kupka, T.; Broda, M. A.

Impact of OH···  $\pi$  Hydrogen Bond on IR and NMR Parameters of Cannabidiol: Theoretical and Experimental Study.

Molecules 2025, 30 (12), 2591.

DOI: 10.3390/molecules30122591, IF: 4.6, Ministerial Points: 140, Citations: 1.

P5. Buczek, A.\*; Rzepiela, K.; Broda, M. A.; Kupka, T.; Strodel, B.; Fatafta\*, H.

Water modulated influence of intramolecular hydrogen-bonding on the conformational properties of Cannabidiol (CBD).

Journal of Molecular Liquids 2025, 423, 127033.

DOI: 10.1016/j.molliq.2025.127033, IF: 5.2, Ministerial Points: 100, Citations: 0.

#### Other publications:

# X1. Rzepiela, K.; Buczek, A.; Kupka, T.\*; Broda, M. A.\*

Factors governing the chemical stability and NMR parameters of uracil tautomers and Its 5-halogen derivatives.

Molecules 2020, 25 (17), 3931.

DOI: 10.3390/molecules25173931, IF: 4.412, Ministerial Points: 140, Citations: 9.30

# X2. Rzepiela, K.; Buczek, A.; Kupka, T.\*; Broda, M. A.\*

On the aromaticity of uracil and its 5-halogeno derivatives as revealed by theoretically derived geometric and magnetic indexes.

Structural Chemistry 2021, 32 (1), 275-283.

DOI: 10.1007/s11224-020-01682-x, IF: 1.795, Ministerial Points: 70, Citations: 2.9

X3. Buczek, A.\*; **Rzepiela, K.**; Stępniak, A.; Buczkowski, A.; Broda, M. A.; Pentak, D.\* Xanthohumol in liposomal form in the presence of cyclodextrins: Drug delivery and stability analysis.

Food Chemistry 2025, 145453.

DOI: 10.1016/j.foodchem.2025.145453, IF: 9.8, Ministerial Points: 200, Citations: 1.31

# X4. Rzepiela, K.; Gajda, T.; Buczek, A.; Broda, M. A.; Kupka, T.\*

Benzen i metan jako wzorce przesunięcia chemicznego <sup>1</sup>H I <sup>13</sup>C NMR w obliczeniach teoretycznych.

Wiadomości Chemiczne **2020**, 74 (9-10), 609-627.

DOI: -, IF: -, Ministerial Points: 20, Citations: -.<sup>32</sup>

X5. Buczek, A.\*; Rzepiela, K.

Teoretyczne badania właściwości konformacyjnych kannabidiolu i tetrahydrokannabinolu.

Wiadomości Chemiczne 2024.

DOI: 10.53584/wiadchem.2024.05.5, IF: -, Ministerial Points: 20, Citations: -.<sup>33</sup>

Publication:	IF:	Ministerial Points:	Citations (excluded self-citations):
P1	2.9	100	0
P2	-	20	-
P3	4.6	140	10
P4	4.6	140	1
P5	5.2	100	0
X1	4.412	140	9
X2	1.795	70	2
X3	9.8	200	1
X4	-	20	-
X5	-	20	-
Total published	The sum of IF:	The sum of	The sum of
articles:	The sum of ir.	Ministerial Points:	citations:
10	33.31	950	23
Total articles from the Philadelphia list:	The average of IF:	The average of Ministerial Points:	The average of citations:
7	4.76	95	3.29

*h*-index: 3

Data downloaded on October 8, 2025.

#### **Conferences and Presentations:**

# 1. K. Rzepiela, M. A. Broda, A. Buczek, T. Kupka,

Inclusion complexes of cannabidiol and tetrahydrocannabinol with  $\beta$ -cyclodextrin: a DFT study with dispersion correction.

International Conference: Modeling and Design of Molecular Materials 2022 (MDMM 2022), Uniwersytet Gdański, Gdańsk, 09/19–09/22/2022 (poster).

# 2. K. Rzepiela, A. Buczek, M. A. Broda, T. Kupka,

Conformational landscape and hydrogen bonding in CBD and THC.

X Łódzkie Sympozjum Doktorantów Chemii,

Uniwersytet Łódzki, Łódź, 05/18–05/19/2023 (oral presentation).

# 3. K. Rzepiela, T. Kupka, A. Buczek,

Charakterystyka teoretyczna i eksperymentalna leków i ich niekowalencyjnych kompleksów z wybranymi nośnikami molekularnymi i nanostrukturalnymi (Theoretical and Experimental Characterization of Drugs and Their Non-covalent Complexes with Selected Molecular and Nanostructured Carriers).

in the research group of Prof. dr hab. Palusiak, Faculty of Chemistry, Uniwersytet Łódzki, 05/19/2023 (invited lecture).

#### 4. K. Rzepiela, H. Fatafta,

Investigating the Interplay between Platinum-based Derivatives and Lipids: Implications for Biomolecular Design and Cancer Therapy.

International Conference: Biomolecular Evolution, Function, and Assembly – Theory Meets Experiment, Forschungszentrum Jülich, Jülich, 04/24–04/26/2024 (poster).

## 5. K. Rzepiela, M. A. Broda, T. Kupka, A. Buczek,

Theoretical and experimental NMR studies of cannabidiol.

International Conference: XXV International Symposium on Advances in Chemistry of Heteroorganic Compounds, Centrum Materiałów Molekularnych i Supramolekularnych PAN, Łódź, 11/21–11/22/2024 (poster).

### 6. K. Rzepiela, A. Buczek, M.A. Broda,

Water modulated influence of intramolecular hydrogen-bonding on the conformational properties of Cannabidiol (CBD).

seminar at the Forschungszentrum Jülich, 04/09/2025 (oral presentation).

### 7. A. Buczek, K. Rzepiela,

Water Modulated Influence of Intramolecular Hydrogen-Bonding on the Conformational Properties of Cannabidiol (CBD).

International Conference: European Congress on Molecular Spectroscopy, Uniwersytet Wrocławski, Wrocław, 08/24–08/29/2025 (poster).

# Scholarships, Grants and Research Stays

- 1. Participation in HPC grant WCSS (Wrocław Supercomputing and Networking Center), project HPC-c2cbroda-1692967353, 09/2021–09/2025.
- 2. Erasmus+ scholarship internship, Forschungszentrum Jülich, research group of Prof. Birgit Strodel.

Work on project: Study of the interactions between cisplatin derivatives and liposomes using computational methods, 09/01/2024–08/31/2025.

#### Collaboration visits and popularization of science:

- 1. Computer workshops entitled Komputerowa Alchemia (Computer Alchemy) for visiting high school students at the Uniwersytet Opolski Summer School, 06/23–06/24/2022.
- 2. Application for PhD research funds at the Institute of Chemistry, Uniwersytet Opolski. (Wniosek o sfinansowanie badań prowadzonych przez doktorantów Instytutu Chemii będących słuchaczami Szkoły Doktorskiej UO), 2022-2024.
- 3. Laboratory workshops: Miareczkowania alkacymetryczne (Acid-base titration) during the Opole Science Festival, Uniwersytet Opolski, 05/29/2023.

- 4. Visit to Uniwersytet Łódzki: scientific collaboration with Dr. Artur Stępniak (Uniwersytet Łódzki). Experimental Research Isothermal titration calorimetry (ITC) studies of interactions between CBD released from liposomes and carriers (β-cyclodextrin and hydroxypropyl-β-cyclodextrin), Uniwersytet Łódzki, 07/04–07/06/2023.
- 5. Laboratory classes entitled Reakcje z miedzią (Reactions with copper) for students of II Liceum Ogólnokształcące im. Adama Mickiewicza, Racibórz, 09/25/2024.
- 6. Visit to Forschungszentrum Jülich 04/06–04/11/2025:
- a) Initiated collaboration on Molecular Dynamics simulations of β-cyclodextrin, HP-β-cyclodextrin, and xanthohumol together with Dr. Hebah Fatafta, Prof. Dr. Dirk Reith and Dr. Karl N. Kirschner.
- b) Conducted scientific consultations with Prof. Dr. Birgit Strodel regarding the already submitted manuscript: "Molecular Insights into the Incorporation of Platinum-Based Drugs into Lipid Aggregates". Ongoing collaborations with Dr. Hebah Fatafta and Prof. Birgit Strodel.

The work is centered on the cisplatin and its carboxylic acid derivatives. In this study, atomistic MD simulations were performed to investigate the interactions between a series of Pt-based compounds, including cisplatin and its fatty acid—conjugated analogs and biologically relevant phospholipids.

The abstract from this work is presented below:

#### Abstract

Platinum-based (Pt-based) compounds remain a cornerstone of chemotherapy, yet their clinical use is limited by poor tumor specificity and systemic toxicity. Fatty acid conjugation has emerged as a promising strategy to enhance the lipophilicity of Pt-based compounds and modify their physicochemical properties. These modifications can improve Pt-based compounds compatibility with lipid-based delivery systems and potentially facilitate their incorporation. In this study, we employed atomistic molecular dynamics (MD) simulations to investigate the interactions between a series of Pt-based compounds, including cisplatin and fatty acid—conjugated analogs (CapryP, ArP, SteariP, ElaidP, and OleP), and biologically relevant phospholipids (DOPC, DSPE, and DPPG). Simulations revealed spontaneous self-assembly of lipid—drug mixtures into micelle-like aggregates, driven by hydrophobic interactions and modulated by the chemical structure of the conjugated moieties. Cluster analysis demonstrated variation

in aggregation dynamics among compounds, with hydrophobic chain length and unsaturation influencing the rate and stability of complex formation. These findings provide molecular-level insights into the incorporation of Pt-based compounds into lipid assemblies and highlight the potential of structural modifications to enhance delivery in lipid-based systems.

#### 6. Discussion of results

P1. Buczek, A.\*; Rzepiela, K.; Kupka, T.; Broda, M. A.; Kar, T.\*

Uracil—water interaction revisited – in search of single H-bonded secondary minima.

Physical Chemistry Chemical Physics 2024, 26 (6), 5169-5182.

DOI: 10.1039/D3CP04057G, IF: 2.9, Ministerial Points: 100, Citations: 0.

Hydration of uracil is important for its functioning in RNA, due to the possibility of forming different hydrogen bond patterns. The computational analyses presented in the article P1<sup>34</sup> provide new insights into the hydration patterns of uracil, particularly the existence of complexes stabilized by two hydrogen bonds for the most stable complex with water. Traditionally, it was assumed that the interaction between uracil and a water molecule is dominated by double H-bonded configurations, which offer higher stability due to cooperative effects. However, our results challenge this view by demonstrating that weaker, single hydrogen-bonded structures represent distinct secondary minima on the Potential Energy Surface (PES) of the Uracil-Water (UW) system. All calculations were performed with the Gaussian 16 program<sup>35</sup>. Initial geometries of seven different UW complexes (UW1–UW7) were prepared in GaussView 5. Geometry optimizations of the complexes and isolated monomers were carried out primarily using the M06-2X<sup>36, 37</sup> functional with the aug-cc-pVTZ basis set, which was applied throughout this work. For comparison, B3LYP and B3LYP-D3 calculations were performed to assess dispersion effects, while additional MP2 optimizations and singlepoint CCSD(T) calculations at MP2 geometries were used to benchmark the DFT results. Optimizations were unconstrained for double H-bonded systems, whereas minor restrictions were initially applied in single H-bonded cases, as discussed in the paper. All structures were confirmed as true minima by harmonic frequency calculations.

The vibrational frequency shifts of selected infrared bands, summarized in **Table 1**, confirm that our M06-2X theoretical predictions closely reproduce the experimental trends observed for the UW1–UW4 monohydrates, which have been previously detected in FT-IR spectroscopic studies conducted in low-temperature argon matrices and helium nanodroplets<sup>38</sup>.

**Table 1.** Comparison of experimental and computed and data: harmonic frequency shifts of OH and NH stretch frequencies (cm<sup>-1</sup>) due to formation of uracil monohydrates.

M06-2X/aug-cc-pVTZ values					
Complex	Complex OH		N1H/N1H(HB)	N2H/N2H(HB)	
UW1	-28.8	-180.9	-187.3	0.7	
UW2	-26.9	-144.8	0.4	-167.5	
UW3	-28.7	-174.2	0.4	-181.1	
UW4	-28.1	-167.8	-1.1	-0.4	
UW5	-18.1	-11.9	-133.3	7.0	
UW6ª	-59.0	-168.5	-28.8	-13.5	
UW7ª	-41.8	-27.8	-26.6	-263.7	
Experimental shifts <sup>b</sup>					
Complex	ОН	OH(HB)	N1H	N2H (HB)	
UW1	-7.2	-170.5	-117.7	-42.3	
UW2	-12.0	-170.5	6.6	-164.0	
UW3	-6.5	-137.3	6.6	-183.0	
UW4	-11.2	-129.6	6.6	7.7	

<sup>&</sup>lt;sup>a</sup> In water (CPCM); <sup>b</sup> Gas and Ar data for water.

Among them, the complex UW1 is the most stable (**Figure 6**). Theoretically predicted UW5–UW7 hydrates are not observed experimentally.

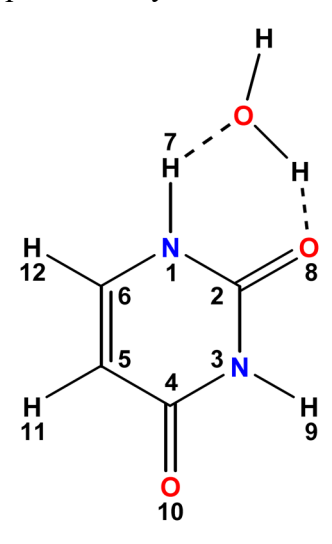


**Fig. 6.** Scheme of hydrogen bonds in the lowest energy uracil complex with a water molecule.

One of the central technical challenges in this work was the identification of secondary minima corresponding to single hydrogen-bonded structures. In standard geometry optimizations, such shallow minima are often bypassed because the PES naturally directs the optimization pathway toward deeper, double hydrogen-bonded minima. To overcome this, we employed a "fixing-and-relaxing" strategy, in which selected intermolecular distances and angles (notably N–H···O and O–H···O geometries) were temporarily constrained during early optimization steps, followed by incremental relaxation to full optimization. This approach allowed us to trap the system in weaker single-bonded configurations, long enough for all vibrational modes to be confirmed as real (absence of imaginary frequencies).

The newly identified single hydrogen-bonded complexes UW5–UW7 differ from their double-bonded counterparts in two key respects: bond lengths and angles. Both N–H···O and O–H···O interactions tend toward shorter and more linear geometries than in double hydrogen-bonded configurations. This is consistent with the absence of cooperative effect from a second hydrogen bond. In cyclic arrangements, hydrogen-bond angles deviate significantly from linearity, resulting in reduced stabilization energy compared to the additive effects of two fully optimized hydrogen bonds. Overall binding energies are lower for single-bonded structures, yet thermodynamic analysis shows that their free energies remain favorable under low-temperature conditions typical for matrix isolation or nanodroplet experiments.

# P2. Rzepiela, K.; Buczek, A.; Kupka, T.; Kar, T.; Broda, M. A.\*

Modelowanie właściwości wiązań wodorowych na przykładzie kompleksów układ amidowywoda.

Wiadomości Chemiczne **2023**, 77 (7-8), 629-645.

DOI: 10.53584/wiadchem.2023.07.1, IF: -, Ministerial Points: 20, Citations: -.

Hydrogen bonding is a cornerstone of molecular stabilization, shaping systems from DNA double helices to protein folding and ligand-receptor interactions. Despite its apparent simplicity, its energetic and structural description requires careful consideration of dispersion effects. In this DFT study<sup>39</sup>, hydrogen bonding was investigated in two biologically relevant model systems: N-methylacetamide (NMA) and uracil, each interacting with a single water molecule. NMA-water complex was examined in both cis and trans configurations, each capable of forming hydrogen bonds via its C=O and N-H groups. All calculations were performed with Gaussian 16 program suite using the B3LYP hybrid functional and the aug-ccpVTZ<sup>40</sup> basis set. The Polarizable Continuum Model (PCM)<sup>41</sup> was applied to account for solvent effects. All optimized structures were verified as true minima by harmonic frequency analysis. To evaluate the contribution of dispersion interactions, calculations were carried out both with and without Grimme's 42 D3 dispersion correction. The interaction energy (E<sub>int</sub>) was determined as the difference between the total energy of the complex and the sum of the energies of the isolated monomers in water. In the gas phase, the Counterpoise method (CP)<sup>43</sup> was employed to correct for the Basis Set Superposition Error (BSSE). Two stable complexes of trans-NMA were identified. The first complex was stabilized by C=O···H-O hydrogen bonding, and the second was stabilized by N-H···O hydrogen bonding. In the literature<sup>44</sup>, a third geometry has been reported, which is similar to the first but differs only in the orientation of the water molecule. This variation has only a minor effect on the interaction energy and geometric parameters. For cis-NMA, two complexes were optimized: the first is stabilized by a C=O···H–O hydrogen bond, while in the second the water molecule simultaneously interacts with both the C=O and N-H groups. Attempts to isolate a pure N-H···O interaction failed, suggesting such an arrangement is inherently unstable. Dispersion corrections (B3LYP-D3) increased binding energies by  $\approx 1.5$  kcal/mol and slightly shortened H···O distances. Solvent effects reduced interaction energies by  $\approx 30\%$  but often shortened hydrogen bonds, indicating increased directionality in a polar environment. Notably, in cis-NMA, solvent enhanced C=O···H-O bonding while elongating N-H···O by  $\approx 0.3$  Å, reflecting competitive

stabilization. Electron density difference maps confirmed localized density depletion near the bridging proton and accumulation near oxygen lone pairs, characteristic of hydrogen bonding. The cooperativity of hydrogen bonds was also explored. For trans-NMA with two water molecules, a cooperative effect increased the total interaction energy by  $\approx 0.7$ –0.9 kcal/mol beyond the sum of isolated interactions. By contrast, two water molecules binding the same C=O group exhibited anti-cooperativity, lowering the total binding energy by  $\approx 0.6$  kcal/mol. For cis-NMA, no cooperative enhancement was detected. These effects highlight how electronic redistribution within the amide group influences its donor/acceptor properties.

In UW complexes, uracil which is a pyrimidine base, offers a closer parallel to nucleic acids hydration. Six uracil—water complexes (UW-1 to UW-6) were optimized in both gas phase and polar medium (water), with and without dispersion corrections. UW-1 (C=O···H-O and N-H···O) was the most stable, with interaction energy -9.9 kcal/mol at B3LYP and -11.7 kcal/mol with dispersion (Figure 6). Its geometry differed from cis-NMA, the C=O···H-O bond was longer by 0.09 Å, while the N-H···O bond was shorter by -0.17 Å. UW-2 to UW-4 corresponded to other dual hydrogen-bonding arrangements previously reported in the literature<sup>45, 46</sup>, while UW-5 and UW-6, stabilized by single hydrogen bonds, were characterized for the first time in our previous work.34 Importantly, the two donor sites of uracil, N1-H and N3–H, displayed different bonding propensities. UW-2 (involving N3–H) was ≈2 kcal/mol less stable than UW-1, confirming weaker donor ability of N3–H. Similarly, UW-5 (N1–H···O) was  $\approx 2$  kcal/mol more stable than UW-6 (N3–H···O). As with NMA, solvent consistently weakened hydrogen bonds by 1.5–5 kcal/mol. A linear correlation was observed, the stronger the hydrogen bond in the gas phase, the larger the reduction upon solvation. Unlike cis-NMA(D), solvent-induced elongation of uracil's N–H···O bond was more modest, emphasizing structural differences between cyclic uracil and acyclic NMA.

From these results, it appears that in our studied systems dispersion contributions are essential, accounting for up to  $\approx 30\%$  of total interaction energy. Solvent effects systematically reduce binding energies but can simultaneously increase hydrogen bond linearity. Cis-NMA is only a partial model for uracil hydration: although both adjacent C=O and N-H groups exist, the cyclic scaffold of uracil alters hydrogen bond geometry and electronic redistribution. Newly characterized complexes (UW-5 and UW-6) clarify the differing donor strengths of N1-H vs. N3-H in uracil. These findings reinforce that hydrogen bonding in biomolecules is site-specific, cooperative, and highly solvent-dependent. For nucleic acids, uracil hydration plays a role not

only in RNA stability but also in recognition processes involving hydrogen-bonded base-water networks.

P3. Rzepiela, K.; Kaminský, J.\*; Buczek, A.; Broda, M. A.; Kupka, T.\*

Electron correlation or basis set quality: how to obtain converged and accurate NMR shieldings for the third-row elements?

Molecules 2022, 27 (23), 8230.

DOI: 10.3390/molecules27238230, IF: 4.6, Ministerial Points: 140, Citations: 10.

In order to accurately predict the NMR parameters in my studies, calculations with varying basis sets were tested. Therefore, the article 10 systematically evaluates nuclear magnetic shielding constants for a series of small molecules and biologically relevant 2-thiouracil (2-TU) (Figure 4) using high-accuracy quantum chemical protocols. The computational strategy combined CCSD(T) and DFT approaches with an extensive basis set analysis, including Dunning's aug-cc-pVXZ<sup>40</sup> (abbreviated as aVXZ), core-valence aug-cc-pCVXZ (where cardinal number X is D,T,Q,5 and 6), and Jensen's aug-pcSseg-n<sup>47</sup> series (where n is 0,1,2,3 and 4), to establish reliable Complete Basis Set (CBS) limits. The Gauge-Independent Atomic Orbital (GIAO)<sup>48</sup> NMR parameters calculations were performed using Gaussian 16, CFOUR-2.149, and S450 (for Zero-Point Vibrational Corrections). A key issue was the determination of accurate <sup>31</sup>P, <sup>33</sup>S, and <sup>1</sup>H shielding constants in molecules such as PN, H<sub>2</sub>S, PH<sub>3</sub>, and 2-TU, where third-row elements exhibit significant basis-set effect (Table 2). The findings confirm that for heavier atoms (S and P), standard valence-only correlation-consistent basis sets (augcc-pVXZ) converge slowly and irregularly, while the inclusion of tight s and p functions (augcc-pCVXZ) or optimized polarization-consistent sets (aug-pcSseg-n) markedly improves smooth convergence. CBS extrapolation via the two-parameter formula<sup>51</sup> Y(X) = Y(CBS) + $A/X^3$  provided robust estimates of the infinite-basis limit for all tested systems.

In case of PN, the comparative analysis of the B3LYP/CBS revealed similar trends in nuclear shielding of the studied <sup>31</sup>P nuclei convergence. However, Traditional Dunning sets and Jensen's aug-pcJ-*n* series showed a clear difference for NMR shieldings. The aug-cc-pVXZ basis set family underscored <sup>31</sup>P shielding by 4.4% relative to the extrapolated CBS value, while aug-pcJ-n lagged behind by nearly 7.0%.

**Table 2.** Computed CBS nuclear shielding values (ppm) for selected studied systems and deviation  $\Delta$  from CCSD(T) used as reference.

Methods	HF-SCF	B3LYP	CCSD(T)	Δ (%)			
				HF-SCF	B3LYP		
PH <sub>3</sub>							
aVXZ(Q-6)	576.501	553.876	596.957	-3.4	-7.2		
aCVXZ(T-5)	581.367	557.847	603.326	-3.6	-7.5		
apcSseg-n(2-4)	580.892	557.661	588.578	-1.3	-5.3		
	PN <sup>a</sup>						
aVXZ(5-6)	-91.460	-58.882	58.080	-257.5	-201.4		
aCVXZ(5-6)	-91.560	-60.030	59.090	-255.0	-201.6		
apcSseg-n(3-4)	-90.720	-58.833	58.780	-254.3	-200.1		
H <sub>2</sub> S							
aVXZ(Q-6)	708.776	694.933	736.852	-3.8	-5.7		
aCVXZ(T-5)	712.644	698.246	741.209	-3.9	-5.8		
apcSseg-n(2-4)	715.929	698.071	742.245	-3.5	-6.0		
Ar							
aVXZ(Q-6)	1237.659	1238.172	1237.509	0.0	0.1		
aCVXZ(T-5)	1237.660	1237.868	1237.924	0.0	0.0		
apcSseg-n(2-4)	1237.534	1237.930	1237.516	0.0	0.0		

<sup>&</sup>lt;sup>a</sup> Results of this work and partially from [<sup>52</sup>]. <sup>b</sup> CBS(5-6) denotes Dunning-type basis set extrapolation using aV5Z and aV6Z. CBS(2-4) obtained with Jensen basis sets aug-pc-Sseg-n (abbreviated as apcSseg-n).

The Locally Dense Basis Set (LDBS)<sup>53</sup> approach proved to be an effective strategy for large systems like 2-TU, where only the "heavy" sulphur atom was described by a large aug-cc-pCV5Z basis, and all other atoms used a smaller 6-31G\* basis. This scheme maintained high accuracy (<sup>33</sup>S isotropic shielding: 287 ppm for the combined scheme *vs.* 258 ppm for the full aug-cc-pCV5Z calculation) while significantly reducing the computational cost, from 20 days of CPU time for the full B3LYP/aug-cc-pCV5Z calculation to just 27.5 minutes. The success of LDBS aligns with earlier observations that the calculated magnetic shieldings are highly localized around selected nuclei, allowing for selective basis set enlargement without global computational overhead.

The CCSD(T) calculations served as the reference standard for assessing electron correlation effects. For PN, the Hartree-Fock method overestimated <sup>31</sup>P shielding by roughly 10 ppm, underscoring the role of correlation for the triple bond. DFT methods, particularly B3LYP, delivered results close to CCSD(T) for simple hydrides (H<sub>2</sub>S, PH<sub>3</sub>), with typical deviations of 3–4 ppm.

Zero-Point Vibrational Corrections (ZPVC) were found to be essential for achieving sub-ppm agreement with experimental NMR shifts.<sup>54</sup> Anharmonic vibrational averaging was performed using the Perturbation Theory<sup>55</sup> with normal-mode expansions of the shielding

tensor (up to quartic terms). For light hydrides (H<sub>2</sub>S, PH<sub>3</sub>), ZPVC contributed between 1.5–2.0 ppm to the final shielding constants, consistent with previously reported vibrational corrections in similar systems.<sup>56</sup> Thermal corrections at 298 K introduced a further adjustment of 0.3–0.5 ppm, however this correction is smaller than the vibrational contributions.

In summary, the results presented in this article demonstrate that the basis set choice, especially core—valence and property-optimized families, is a decisive factor for accurate NMR shielding predictions involving third-row elements. Moreover, electron correlation must be included at least at the hybrid DFT level, with CCSD(T) providing reliable benchmark references. Additionally, vibrational corrections are non-trivial, particularly for heavy atoms like sulfur, and should be incorporated into composite schemes. Furthermore, LDBS strategies offer a practical balance between accuracy and computational efficiency for large heteroaromatic systems. By combining these elements into a coherent computational protocol, it is possible to achieve sub-ppm agreement with experimental data, thereby extending high-level quantum chemical NMR predictions to increasingly complex biological and functional materials.

P4. Buczek, A.\*; Rzepiela, K.; Kupka, T.; Broda, M. A.

Impact of OH $\cdots$   $\pi$  Hydrogen Bond on IR and NMR Parameters of Cannabidiol: Theoretical and Experimental Study.

Molecules 2025, 30 (12), 2591.

DOI: 10.3390/molecules30122591, IF: 4.6, Ministerial Points: 140, Citations: 1.

CBD (**Figure 5**) is a pharmacologically active cannabinoid with a wide range of therapeutic effects.  $^{57, 58}$  Its structural complexity, including two hydroxyl groups, an aromatic ring and a limonene group, provides multiple opportunities for intramolecular interactions that shape its conformational preferences. Among these, the O–H··· $\pi$  hydrogen bond plays a central role. Although weak, this interaction can stabilize specific conformers, thereby influencing CBD's vibrational and magnetic resonance spectra. Despite the availability of FT-IR and NMR studies of CBD, the direct relationship between hydrogen bonding and spectroscopic parameters has remained partly unresolved. Understanding this link is not only crucial for accurate molecular characterization but also for insights into receptor binding, solubility, and conformational dynamics in biologically relevant environments.

In our study<sup>66</sup>, quantum chemical calculations were carried out using Gaussian 16. Geometry optimizations were performed at the B3LYP-D3BJ<sup>67</sup>/6-311++G level, and single-point energy refinements were obtained with MP2/6-311++G\*\* in chloroform. For the calculation of NMR parameters, the aug-cc-pVTZ basis set was employed, following the methodology established in previous studies.<sup>10</sup>

These calculations revealed the diequatorial conformer 1a as the lowest-energy structure in chloroform, stabilized by an  $OH(A)\cdots\pi$  hydrogen bond and a C-H···O interaction involving the second hydroxyl group. The small energy gap between 1a and 1b indicates an equilibrium dominated by these two conformers (**Figure 7**).

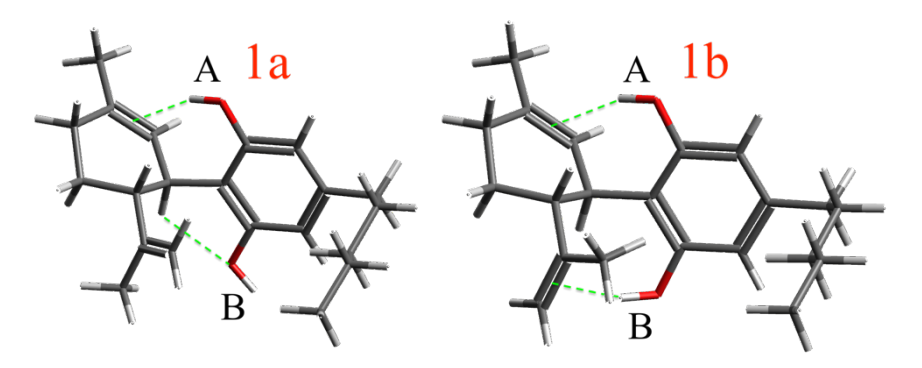


**Fig. 7.** Structures of diequatorial CBD conformers 1a and 1b with the lowest energies, highlighting different OH(A) and OH(B) group settings. Hydrogen bonds are marked by dotted lines.

The central stabilizing factor is consistently the  $OH(A)\cdots\pi$  bond, which dictates the relative energetics of the conformers. This theoretical result provides a clear structural hypothesis: CBD in chloroform solution should exhibit spectroscopic band of intramolecular  $OH\cdots\pi$  bonding, particularly associated with the OH(A) group.

The FT-IR spectra of CBD in chloroform revealed two distinct vs(O–H) stretching bands: 3603 cm<sup>-1</sup> corresponding to a free hydroxyl group, and 3425 cm<sup>-1</sup> corresponding to a hydrogen-bonded OH group. The absence of concentration-dependent changes confirmed that these bands arise from monomeric intramolecular interactions rather than intermolecular associations. Comparison with computed spectra showed excellent agreement for conformer 1a (**Figure 8**).

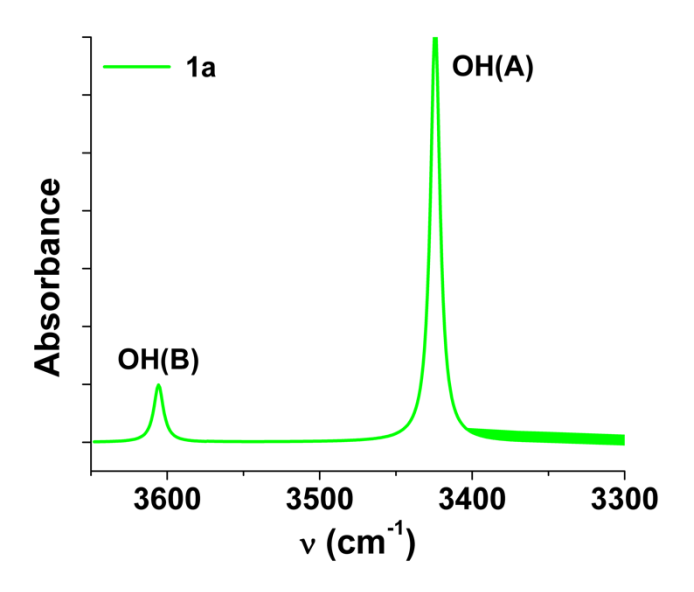


**Fig. 8.** The computed FT-IR spectra (OH stretching region) of the CBD conformer 1a, calculated at the level of theory: B3LYP-GD3BJ/6-311++G\*\* in chloroform, including a scaling factor of 0.938.<sup>68</sup>

Importantly, the magnitude of frequency shifts differentiated the two hydroxyl groups:  $OH(A)\cdots\pi$  caused a larger redshift ( $\approx$ 175 cm<sup>-1</sup>),  $OH(B)\cdots\pi$  caused a smaller shift ( $\approx$ 130 cm<sup>-1</sup>). This indicates that the OH(A) bond is stronger and more structurally relevant, consistent with the calculated conformer stability. Hydrogen bonding also impacted the fingerprint region (1700–1300 cm<sup>-1</sup>), notably shifting the C=C stretching and aromatic skeletal vibrations, further demonstrating the pervasive influence of weak internal interactions on CBD's FT-IR response.

Multinuclear  $^{1}$ H and  $^{13}$ C NMR experiments in CDCl<sub>3</sub> confirmed the computational predictions. The proton chemical shift of OH(A) displayed a strong dependence on the presence of the OH··· $\pi$  bond ( $\approx$  6.6 ppm when bonded vs.  $\approx$  4.4 ppm when free). For OH(B), the effect was weaker but still noticeable ( $\approx$  5.8 vs. 4.5 ppm). The overall best agreement between experimental and calculated shifts was obtained for conformer 1a, reinforcing its predominance in solution.  $^{13}$ C shifts showed similar trends, with the C1 carbon moving downfield (147 ppm)

in the presence of OH(A)··· $\pi$  bonding, compared to  $\approx$  136 ppm when absent. Indirect Spin-Spin Coupling Constants (SSCCs) further supported the conclusions. While variations were modest ( $\approx$ 1 Hz), they were consistent with changes expected from hydrogen bonding, particularly at the methyl and olefinic sites. The combined FT-IR and NMR evidence converges on a coherent picture: CBD exists primarily as the 1a conformer in chloroform, The OH(A)··· $\pi$  bond is the key stabilizing feature, dominating both energetic and spectroscopic behavior, The OH(B) group participates in weaker or alternative interactions, but its contribution is secondary. This work provides one of the clearest demonstrations that weak hydrogen bonds, often considered negligible, can significantly shape vibrational and magnetic resonance signatures, thereby serving as indirect probes of conformational stability.

The study highlights the importance of intramolecular hydrogen bonding as a subtle but decisive factor in determining the molecular behavior of bioactive compounds. For CBD, the predominance of conformer 1a stabilized by  $OH\cdots\pi$  bonding suggests a level of conformational restriction that may influence receptor binding and solubility. More generally, this research shows how spectroscopic techniques combined with quantum chemical modeling can uncover weak internal interactions that are otherwise difficult to detect. Such insights extend beyond cannabinoids to other natural products and biomolecules where intramolecular hydrogen bonding governs conformational flexibility, recognition, and activity.

This work establishes the  $OH\cdots\pi$  hydrogen bond as a central factor in CBD's conformational stability and spectroscopic behavior. By integrating FT-IR and NMR spectroscopy with DFT modeling, we provide a comprehensive understanding of how weak hydrogen bonds affect electronic environments, vibrational frequencies, and coupling constants. These findings enhance the structural basis for CBD research and lay the groundwork for future investigations of weak interactions in pharmacologically relevant molecules.

P5. Buczek, A.\*; Rzepiela, K.; Broda, M. A.; Kupka, T.; Strodel, B.; Fatafta\*, H.

Water modulated influence of intramolecular hydrogen-bonding on the conformational properties of Cannabidiol (CBD).

Journal of Molecular Liquids 2025, 423, 127033.

DOI: 10.1016/j.molliq.2025.127033, IF: 5.2, Ministerial Points: 100, Citations: 0.

CBD, discussed above (**Figure 5**), is an increasingly important phytocannabinoid whose therapeutic potential is limited by poor aqueous solubility.<sup>69</sup> Although formulation strategies such as lipid carriers and cyclodextrin complexes improve its bioavailability<sup>70</sup>, the fundamental molecular determinants of solubility remain insufficiently understood. A key open question concerns the role of intramolecular hydrogen bonding, particularly  $O-H\cdots\pi$  interactions, in shaping CBD's conformational preferences and thereby modulating its interactions with solvent molecules. Addressing this question is essential not only for CBD but also for a broader class of bioactive molecules where internal stabilization competes with solvation.

Our DFT analysis<sup>71</sup>, conducted in Gaussian 16, identified diequatorial conformers as the most stable arrangement of CBD, stabilized by a combination of O–H··· $\pi$  and C–H···O hydrogen bonding. The O–H group directed toward the limonene double bond consistently forms a short, stabilizing hydrogen bond with  $\pi$  electrons, while the second hydroxyl group prevents a formation of an additional intramolecular contact. These results support our previous FT-IR and NMR studies<sup>66</sup>, but crucially, they highlight the internal stabilization of CBD by hydrogen bonds that reduce its capacity to fully engage in hydrogen bonding with water. Interestingly, the inclusion of a polar environment via PCM models did not significantly alter the relative energetics or geometries of these conformers. This suggests that intramolecular interactions dominate over solvent stabilization in dictating the conformational preferences of isolated CBD molecules.

Additionally, MD simulations of the CBD molecule, placed in a water box, were performed in the GROMACS<sup>72</sup> package. Force field parameters were derived from CGenFF (version 2.5), which is based on CHARMM General Force Field version 4.6.<sup>73</sup> It was shown that in aqueous solution, the lowest-energy diequatorial conformer dominates, which is consistent with DFT calculations. However, the hydroxyl groups exhibit differential solvation behavior: OH(A) remains preferentially engaged in intramolecular  $O-H\cdots\pi$  bonding, limiting water access. By contrast, OH(B) is more solvent-exposed, forming transient hydrogen bonds with surrounding water molecules. Thus, only one hydroxyl group effectively participates in solvation, while the

other is "locked" internally. This asymmetry contributes to the limited water compatibility of CBD.

When ten CBD molecules were simulated in a water box, the picture shifted further: clustering occurred spontaneously, driven largely by hydrophobic interactions of the limonene and aliphatic n-pentyl chain regions, with only loose and labile intermolecular contacts. This aggregation minimizes solvent exposure, but also effectively moves hydroxyl groups from sustained water interaction. The result is a self-assembly mechanism consistent with experimentally observed poor aqueous solubility.

The combined findings of DFT and MD underscore a competition between intra- and intermolecular hydrogen bonding: Intramolecular  $O-H\cdots\pi$  interactions stabilize low-energy conformers, effectively "shielding" donor groups from hydration and water molecules preferentially engage with only one hydroxyl group, limiting overall solvation. Aggregation further restricts hydrogen bonding with water, reinforcing the hydrophobic character of CBD in aqueous environments. This delicate balance of interactions explains why CBD remains sparingly soluble despite possessing polar hydroxyl functionalities.

The insights obtained here extend beyond CBD: many bioactive natural compounds formed by a hydrophobic scaffold decorated with a small number of polar groups display similar duality. Intramolecular hydrogen bonding may provide a general mechanism that stabilizes conformations at the cost of solubility. For CBD, this trade-off has direct pharmacological consequences, as bioavailability depends on overcoming aggregation and enabling water compatibility. These results suggest two potential strategies: formulation approaches that disrupt internal hydrogen bonds (e.g., cyclodextrin inclusion, solvent polarity tuning). Chemical modification strategies targeting hydroxyl orientation or introducing solubilizing groups to bias external hydrogen bonding.

This work provides a coherent molecular explanation of CBD's limited aqueous solubility by integrating quantum chemical and MD approaches. The water-modulated balance of intramolecular hydrogen bonds and external solvation emerges as a central determinant of conformational stability and aggregation. These findings not only clarify a persistent scientific problem but also lay the groundwork for rational design of improved CBD formulations with higher bioavailability.

#### 7. Conclusions

The results of this thesis demonstrate that hydrogen bonding, whether internal or external, plays a decisive role in stabilizing biologically relevant molecules such as uracil and CBD. In uracil, hydration reveals not only the dominant double hydrogen-bonded complexes but also weaker single-bonded secondary minima, which had been overlooked in earlier models. In amide and uracil systems, dispersion corrections, solvent effects, and basis set selection (particularly augmented correlation-consistent and polarization-consistent families) were shown to be crucial for achieving accurate geometric structures and interaction energies. For CBD, the studies revealed that intramolecular O–H $\cdots\pi$  interactions strongly stabilize preferred conformers, reducing the accessibility of hydroxyl groups for external hydrogen bonding with water. This internal stabilization explains CBD's limited solubility in aqueous environments and its tendency to aggregate, despite the presence of polar functionalities. Solvent models and MD confirmed that one hydroxyl group remains largely solvent-shielded, while the other engages only transiently in hydration. These findings highlight that intramolecular hydrogen bonding stabilizes specific conformations of the molecule, while simultaneously reducing its ability to form external hydrogen bonds with the solvent, which contributes to its low aqueous solubility. For future research, the choice of computational methods, especially basis sets and inclusion of electron correlation and dispersion, will remain essential for capturing the subtle balance between intra- and intermolecular interactions. More importantly, hydrogen bonding should be regarded as a central determinant not only of molecular stability but also of drug solubility, aggregation, and bioavailability. Understanding and controlling this balance may guide the rational design of new drugs and formulations, where disrupting or enhancing hydrogen bonding could tune pharmacokinetic properties and therapeutic performance.

# 8. Acknowledgments

I would like to express my sincere gratitude to the University of Opole for providing me with the opportunity to conduct this research and pursue my doctoral studies. I gratefully acknowledge the Erasmus+ program for supporting my one year internship through a scholarship. The computational resources generously provided by Wrocławskie Centrum Superkomputerowo-Sieciowe (WCSS) and Forschungszentrum Jülich were essential for carrying out the calculations presented in this thesis. Their support is deeply appreciated.

#### 9. References

- (1) Deepak, R. N. V. K.; Sankararamakrishnan, R. Unconventional NH... N hydrogen bonds involving proline backbone nitrogen in protein structures. *Biophysical journal* **2016**, *110* (9), 1967-1979.
- (2) Jeffrey, G. A.; Saenger, W. Hydrogen bonding in biological structures; Springer Science & Business Media, 2012.
- (3) Grabowski, S. J. Hydrogen bonding: new insights; Springer, 2006.
- (4) Desiraju, G. R.; Steiner, T. *The weak hydrogen bond: in structural chemistry and biology*; International Union of Crystal, **2001**.
- (5) Grabowski, S. J. Understanding hydrogen bonds: theoretical and experimental views; Royal Society of Chemistry, 2020.
- (6) Bella, J.; Humphries, M. \*Cα-H···O=C hydrogen bonds contribute to the specificity of RGD cell-adhesion interactions. *BMC structural biology* **2005**, *5*, 4.
- (7) Parra, R. D.; Ohlssen, J. Cooperativity in intramolecular bifurcated hydrogen bonds: an ab initio study. *The Journal of Physical Chemistry A* **2008**, *112* (15), 3492-3498.
- (8) Grabowski, S. J. Dihydrogen bond and X–H... σ interaction as sub-classes of hydrogen bond. *Journal of Physical Organic Chemistry* **2013**, *26* (6), 452-459.
- (9) Rzepiela, K.; Buczek, A.; Kupka, T.; Broda, M. A. On the aromaticity of uracil and its 5-halogeno derivatives as revealed by theoretically derived geometric and magnetic indexes. *Structural Chemistry* **2021**, *32* (1), 275-283.
- (10) Rzepiela, K.; Kaminský, J.; Buczek, A.; Broda, M. A.; Kupka, T. Electron correlation or basis set quality: how to obtain converged and accurate NMR shieldings for the third-row elements? *Molecules* **2022**, *27* (23), 8230.
- (11) Adams, R.; Hunt, M.; Clark, J. H. Structure of Cannabidiol, a Product Isolated from the Marihuana Extract of Minnesota Wild Hemp. I. *Journal of the American Chemical Society* **1940**, *62* (1), 196-200.
- (12) Baranović, G. Understanding the conformational, electronic and vibrational properties of Tetrahydrocannabinol (THC) and Cannabidiol (CBD). Pharmacophoric similarities and differences. *Journal of Molecular Structure* **2021**, *1244*, 130945.
- (13) Hohenberg, P.; Kohn, W. Inhomogeneous electron gas. Physical review 1964, 136 (3B), B864.
- (14) Kohn, W.; Sham, L. J. Self-consistent equations including exchange and correlation effects. *Physical review* **1965**, *140* (4A), A1133.
- (15) Frisch, M. J.; Head-Gordon, M.; Pople, J. A. A direct MP2 gradient method. *Chemical Physics Letters* **1990**, *166* (3), 275-280.
- (16) Čížek, J. On the Use of the Cluster Expansion and the Technique of Diagrams in Calculations of Correlation Effects in Atoms and Molecules. In *Advances in Chemical Physics*, Advances in Chemical Physics, 1969; pp 35-89.
- (17) Raghavachari, K.; Trucks, G. W.; Pople, J. A.; Head-Gordon, M. A fifth-order perturbation comparison of electron correlation theories. *Chemical Physics Letters* **1989**, *157* (6), 479-483.
- (18) Purvis, G. D., III; Bartlett, R. J. A full coupled-cluster singles and doubles model: The inclusion of disconnected triples. *The Journal of Chemical Physics* **1982**, *76* (4), 1910-1918.
- (19) Alder, B. J.; Wainwright, T. E. Studies in molecular dynamics. I. General method. *The Journal of Chemical Physics* **1959**, *31* (2), 459-466.
- (20) Perdew, J. P.; Burke, K.; Ernzerhof, M. Generalized gradient approximation made simple. *Physical review letters* **1996**, 77 (18), 3865.
- (21) Perdew, J. P.; Chevary, J. A.; Vosko, S. H.; Jackson, K. A.; Pederson, M. R.; Singh, D. J.; Fiolhais, C. Atoms, molecules, solids, and surfaces: Applications of the generalized gradient approximation for exchange and correlation. *Physical review B* **1992**, *46* (11), 6671.
- (22) Becke, A. D. Density-functional exchange-energy approximation with correct asymptotic behavior. *Physical review A* **1988**, *38* (6), 3098.
- (23) Perdew, J. P. Density-functional approximation for the correlation energy of the inhomogeneous electron gas. *Physical review B* **1986**, *33* (12), 8822.
- (24) Lee, C.; Yang, W.; Parr, R. G. Development of the Colle-Salvetti correlation-energy formula into a functional of the electron density. *Physical review B* **1988**, *37* (2), 785.
- (25) Roothaan, C. C. J. New developments in molecular orbital theory. *Reviews of modern physics* **1951**, *23* (2), 69.
- (26) Hehre, W. J.; Stewart, R. F.; Pople, J. A. Self-consistent molecular-orbital methods. I. Use of Gaussian expansions of Slater-type atomic orbitals. *The Journal of Chemical Physics* **1969**, *51* (6), 2657-2664.
- (27) Binkley, J. S.; Pople, J. A.; Hehre, W. J. Self-consistent molecular orbital methods. 21. Small split-valence basis sets for first-row elements. *Journal of the American Chemical Society* **1980**, *102* (3), 939-947.

- (28) Clark, T.; Chandrasekhar, J.; Spitznagel, G. W.; Schleyer, P. V. R. Efficient diffuse function-augmented basis sets for anion calculations. III. The 3-21+ G basis set for first-row elements, Li–F. *Journal of Computational Chemistry* **1983**, *4* (3), 294-301.
- (29) Frisch, M. J.; Pople, J. A.; Binkley, J. S. Self-consistent molecular orbital methods 25. Supplementary functions for Gaussian basis sets. *The Journal of chemical physics* **1984**, *80* (7), 3265-3269.
- (30) Rzepiela, K.; Buczek, A.; Kupka, T.; Broda, M. A. Factors governing the chemical stability and NMR parameters of uracil tautomers and Its 5-halogen derivatives. *Molecules* **2020**, *25* (17), 3931.
- (31) Buczek, A.; Rzepiela, K.; Stępniak, A.; Buczkowski, A.; Broda, M. A.; Pentak, D. Xanthohumol in liposomal form in the presence of cyclodextrins: Drug delivery and stability analysis. *Food Chemistry* **2025**, 145453.
- (32) Rzepiela, K.; Gajda, T.; Buczek, A.; Broda, M. A.; Kupka, T. Benzen i metan jako wzorce przesunięcia chemicznego 1 HI 13 C NMR w obliczeniach teoretycznych. *Wiadomości Chemiczne* **2020**, *74* (9-10), 609-627.
- (33) Buczek, A.; Rzepiela, K. Teoretyczne badania właściwości konformacyjnych kannabidiolu i tetrahydrokannabinolu. *Wiadomości Chemiczne* **2024**, *78* (5-6), 527-543.
- (34) Buczek, A.; Rzepiela, K.; Kupka, T.; Broda, M. A.; Kar, T. Uracil-water interaction revisited-in search of single H-bonded secondary minima. *Physical Chemistry Chemical Physics* **2024**, *26* (6), 5169-5182.
- (35) Frisch, M. J.; Trucks, G. W.; Schlegel, H. B.; Scuseria, G. E.; Robb, M. A.; Cheeseman, J. R.; Scalmani, G.; Barone, V.; Petersson, G. A.; Nakatsuji, H.; et al. Gaussian 16 Rev. C.01. Wallingford, CT, **2016**.
- (36) Wang, Y.; Verma, P.; Jin, X.; Truhlar, D. G.; He, X. Revised M06 density functional for main-group and transition-metal chemistry. *Proceedings of the National Academy of Sciences* **2018**, *115* (41), 10257-10262.
- (37) Zhao, Y.; Truhlar, D. G. The M06 suite of density functionals for main group thermochemistry, thermochemical kinetics, noncovalent interactions, excited states, and transition elements: two new functionals and systematic testing of four M06-class functionals and 12 other functionals. *Theoretical chemistry accounts* **2008**, *120* (1), 215-241.
- (38) Choi, M. Y.; Miller, R. E. Multiple isomers of uracil—water complexes: infrared spectroscopy in helium nanodroplets. *Physical Chemistry Chemical Physics* **2005**, *7* (20), 3565-3573.
- (39) Rzepiela, K.; Buczek, A.; Kupka, T.; Kar, T.; Broda, M. A. Modelowanie właściwosci wiązań wodorowych na przykładzie kompleksów układ amidowy-woda. *Wiadomości Chemiczne* **2023**, *77* (7-8), 629-645.
- (40) Dunning Jr, T. H. Gaussian basis sets for use in correlated molecular calculations. I. The atoms boron through neon and hydrogen. *The Journal of chemical physics* **1989**, *90* (2), 1007-1023.
- (41) Tomasi, J.; Mennucci, B.; Cammi, R. Quantum Mechanical Continuum Solvation Models. *Chemical Reviews* **2005**, *105* (8), 2999-3094.
- (42) Grimme, S.; Antony, J.; Ehrlich, S.; Krieg, H. A consistent and accurate ab initio parametrization of density functional dispersion correction (DFT-D) for the 94 elements H-Pu. *The Journal of Chemical Physics* **2010**, *132* (15), 154104.
- (43) Kestner, N. R.; Combariza, J. E. Basis set superposition errors: Theory and practice. *ReViews in computational chemistry* **1999**, 99-132.
- (44) Zhang, R.; Li, H.; Lei, Y.; Han, S. Structures and interactions in N-methylacetamide-water mixtures studied by IR spectra and density functional theory. *Journal of molecular structure* **2004**, *693* (1-3), 17-25.
- (45) Fornaro, T.; Burini, D.; Biczysko, M.; Barone, V. Hydrogen-bonding effects on infrared spectra from anharmonic computations: uracil-water complexes and uracil dimers. *The Journal of physical chemistry A* **2015**, *119* (18), 4224-4236.
- (46) Fornaro, T.; Biczysko, M.; Bloino, J.; Barone, V. Reliable vibrational wavenumbers for C=O and N-H stretchings of isolated and hydrogen-bonded nucleic acid bases. *Physical Chemistry Chemical Physics* **2016**, *18* (12), 8479-8490.
- (47) Jensen, F. Polarization consistent basis sets: Principles. *The Journal of Chemical Physics* **2001**, *115* (20), 9113-9125.
- (48) Wolinski, K.; Hinton, J. F.; Pulay, P. Efficient implementation of the gauge-independent atomic orbital method for NMR chemical shift calculations. *Journal of the American Chemical Society* **1990**, *112* (23), 8251-8260.
- (49) Matthews, D. A.; Cheng, L.; Harding, M. E.; Lipparini, F.; Stopkowicz, S.; Jagau, T.-C.; Szalay, P. G.; Gauss, J.; Stanton, J. F. Coupled-cluster techniques for computational chemistry: The CFOUR program package. *The Journal of Chemical Physics* **2020**, *152* (21).
- (50) Bouř, P. Program S4. Czech Academy of Sciences: Prague, Czech Republic: 2009.
- (51) Helgaker, T.; Klopper, W.; Koch, H.; Noga, J. Basis-set convergence of correlated calculations on water. *The Journal of chemical physics* **1997**, *106* (23), 9639-9646.
- (52) Kupka, T.; Leszczyńska, M.; Ejsmont, K.; Mnich, A.; Broda, M.; Thangavel, K.; Kaminský, J. Phosphorus mononitride: A difficult case for theory. *International Journal of Quantum Chemistry* **2019**, *119* (24), e26032.
- (53) Chesnut, D. B.; Moore, K. D. Locally dense basis sets for chemical shift calculations. *Journal of Computational Chemistry* **1989**, *10* (5), 648-659.

- (54) Ruud, K.; Åstrand, P.-O.; Taylor, P. R. An efficient approach for calculating vibrational wave functions and zero-point vibrational corrections to molecular properties of polyatomic molecules. *The Journal of Chemical Physics* **2000**, *112* (6), 2668-2683.
- (55) Daněček, P.; Bouř, P. Comparison of the numerical stability of methods for anharmonic calculations of vibrational molecular energies. *Journal of Computational Chemistry* **2007**, *28* (10), 1617-1624.
- (56) Antu ek, A.; Jaszuński, M. Coupled cluster study of NMR shielding constants and spin-rotation constants in SiH4, PH3 and H2S molecules. *Molecular Physics* **2006**, *104* (09), 1463-1474.
- (57) Burstein, S. Cannabidiol (CBD) and its analogs: a review of their effects on inflammation. *Bioorganic & medicinal chemistry* **2015**, *23* (7), 1377-1385.
- (58) Pisanti, S.; Malfitano, A. M.; Ciaglia, E.; Lamberti, A.; Ranieri, R.; Cuomo, G.; Abate, M.; Faggiana, G.; Proto, M. C.; Fiore, D. Cannabidiol: State of the art and new challenges for therapeutic applications. *Pharmacology & therapeutics* **2017**, *175*, 133-150.
- (59) Espel Grekopoulos, J. Construction and validation of quantification methods for determining the cannabidiol content in liquid pharma-grade formulations by means of near-infrared spectroscopy and partial least squares regression. *Medical Cannabis and Cannabinoids* **2019**, *2* (1), 43-55.
- (60) Tay, L.-L.; Hulse, J.; Paroli, R. M. FTIR and Raman spectroscopic characterization of cannabinoids. *Canadian Journal of Chemistry* **2022**, *100* (10), 751-758.
- (61) Geskovski, N.; Stefkov, G.; Gigopulu, O.; Stefov, S.; Huck, C. W.; Makreski, P. Mid-infrared spectroscopy as process analytical technology tool for estimation of THC and CBD content in Cannabis flowers and extracts. *Spectrochimica Acta Part A: Molecular and Biomolecular Spectroscopy* **2021**, *251*, 119422.
- (62) Colella, M. F.; Salvino, R. A.; Gaglianò, M.; Litrenta, F.; Oliviero Rossi, C.; Le Pera, A.; De Luca, G. NMR spectroscopy applied to the metabolic analysis of natural extracts of cannabis sativa. *Molecules* **2022**, *27* (11), 3509
- (63) Choi, Y. H.; Hazekamp, A.; Peltenburg-Looman, A. M. G.; Frédérich, M.; Erkelens, C.; Lefeber, A. W. M.; Verpoorte, R. NMR assignments of the major cannabinoids and cannabiflavonoids isolated from flowers of Cannabis sativa. *Phytochemical Analysis: An International Journal of Plant Chemical and Biochemical Techniques* **2004**, *15* (6), 345-354.
- (64) Siciliano, C.; Bartella, L.; Mazzotti, F.; Aiello, D.; Napoli, A.; De Luca, P.; Temperini, A. 1H NMR quantification of cannabidiol (CBD) in industrial products derived from Cannabis sativa L.(hemp) seeds. 2019, IOP Publishing: Vol. 572, p 012010.
- (65) Reggio, P. H. Endocannabinoid binding to the cannabinoid receptors: what is known and what remains unknown. *Current medicinal chemistry* **2010**, *17* (14), 1468-1486.
- (66) Buczek, A.; Rzepiela, K.; Kupka, T.; Broda, M. A. Impact of OH···  $\pi$  Hydrogen Bond on IR and NMR Parameters of Cannabidiol: Theoretical and Experimental Study. *Molecules* **2025**, *30* (12), 2591.
- (67) Grimme, S.; Ehrlich, S.; Goerigk, L. Effect of the damping function in dispersion corrected density functional theory. *Journal of computational chemistry* **2011**, *32* (7), 1456-1465.
- (68) Scott, A. P.; Radom, L. Harmonic vibrational frequencies: an evaluation of Hartree–Fock, Møller–Plesset, quadratic configuration interaction, density functional theory, and semiempirical scale factors. *The Journal of Physical Chemistry* **1996**, *100* (41), 16502-16513.
- (69) Tavčar, E.; Vidak, M. Experimental investigation and thermodynamic modelling of cannabidiol and curcumin in different solvents. *Journal of molecular liquids* **2024**, *410*, 125511.
- (70) Li, H.; Chang, S.-L.; Chang, T.-R.; You, Y.; Wang, X.-D.; Wang, L.-W.; Yuan, X.-F.; Tan, M.-H.; Wang, P.-D.; Xu, P.-W. Inclusion complexes of cannabidiol with  $\beta$ -cyclodextrin and its derivative: Physicochemical properties, water solubility, and antioxidant activity. *Journal of Molecular Liquids* **2021**, *334*, 116070.
- (71) Buczek, A.; Rzepiela, K.; Broda, M. A.; Kupka, T.; Strodel, B.; Fatafta, H. Water modulated influence of intramolecular hydrogen-bonding on the conformational properties of Cannabidiol (CBD). *Journal of Molecular Liquids* **2025**, *423*, 127033.
- (72) Berendsen, H. J. C.; van der Spoel, D.; van Drunen, R. GROMACS: A message-passing parallel molecular dynamics implementation. *Computer physics communications* **1995**, *91* (1-3), 43-56.
- (73) Vanommeslaeghe, K.; Hatcher, E.; Acharya, C.; Kundu, S.; Zhong, S.; Shim, J.; Darian, E.; Guvench, O.; Lopes, P.; Vorobyov, I. CHARMM general force field: A force field for drug-like molecules compatible with the CHARMM all-atom additive biological force fields. *Journal of computational chemistry* **2010**, *31* (4), 671-690.

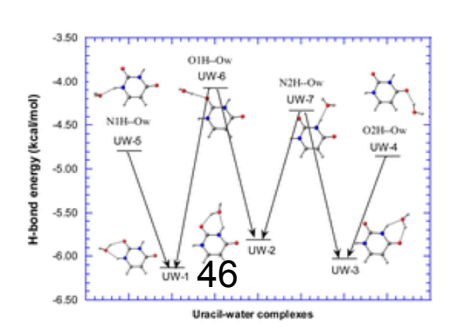
# 10. Appendices to the Articles Constituting the Doctoral Dissertation

# 10.1 P1: Uracil-water interaction revisited - in search of single H-bonded secondary



#### **Abstract**

Monohydrated uracil (UW) complexes are stabilized by both O···HO and NH···O hydrogen bonds (H-bonds), simultaneously participating in forming three stable cyclic structures. The role and contribution of these individual H-bonds (O···HO and NH···O) to the stability of the three UW complexes are still not understood, because of the technical problems in obtaining their optimized structures by standard geometry optimization. The present study explores a non-standard approach to identify three single H-bonded local minima structures without imaginary frequency using DFT (M06-2X, B3LYP and B3LYP-D3), MP2 and CCSD(T) theories and Dunning's correlation-consistent aug-cc-pVTZ basis set, in both vacuum and aqueous media (CPCM method). The results reveal that these new structures are very shallow secondary minima between two deep wells or next to a deep well of primary minima (double H-bonded structures) in the potential energy surface. The H-bond energy of these single Hbonded complexes is found to be less sensitive to a wide range (about 15-20 degrees) of O··· HO and NH···O angles, and the linearity is preferred in the stable three single H-bonded structures. The technical method used to locate such a shallow minimum is described in detail and may be useful for identifying local minima in other cases where consecutive multiple H-bonded structures are global minima. Energy decomposition (using symmetry adapted perturbation theory (SAPT)) of interaction energy, electron redistribution, and relevant vibrational modes are discussed.



10.2 P2: Modelowanie właściwosci wiązań wodorowych na przykładzie kompleksów układ amidowy-woda (MODELING THE PROPERTIES OF HYDROGEN BONDS.

AN EXAMPLE OF AMIDE-WATER COMPLEX)

DOI: 10.53584/wiadchem.2023.07.1

# MODELOWANIE WŁAŚCIWOŚCI WIĄZAŃ WODOROWYCH NA PRZYKŁADZIE KOMPLEKSÓW UKŁAD AMIDOWY - WODA

MODELING THE PROPERTIES OF HYDROGEN BONDS. AN EXAMPLE OF AMIDE-WATER COMPLEX

# Kacper Rzepiela<sup>1</sup>, Aneta Buczek<sup>1</sup>, Teobald Kupka<sup>1</sup>, Tapas Kar<sup>2</sup>, Małgorzata A. Broda<sup>1</sup> \*

<sup>1</sup>Uniwersytet Opolski, Wydział Chemii, ul. Oleska 48, 45-052 Opole, <sup>2</sup> Utah State University, Logan, United States \*email: broda@uni.opole.pl

# Praca dedykowana

### Panu Profesorowi Jerzemu Piotrowi Hawrankowi

Abstract

Wykaz stosowanych symboli i oznaczeń

Wprowadzenie

- 1. Kompleksy N-metyloacetamidu z cząsteczką wody
- 2. Kompleksy uracyl woda

Uwagi końcowe

Podziękowania

Piśmiennictwo cytowane



Mgr Kacper Rzepiela jest absolwentem studiów magisterskich na Wydziale Chemii Uniwersytetu Opolskiego. W 2021 obronił pracę magisterską pt. "Modelowanie oddziaływań uracylu i fluorouracylu z cząsteczkami wody". Obecnie jest doktorantem Szkoły Doktorskiej UO. Zajmuje się badaniem właściwości leków i ich niekowalencyjnych oddziaływań z wybranymi nośnikami molekularnym i nanostrukturalnymi.



Dr Aneta Buczek studiowała chemię w latach 2003 – 2008 na Uniwersytecie Opolskim, (Wydział Chemii, kierunek Chemia Podstawowa i Stosowana). W 2008 uzyskała tytuł magistra chemii (promotor: dr hab. Małgorzata Broda, prof. UO). W latach 2008 – 2014 doktorantka Środowiskowego Studium Doktoranckiego Uniwersytetu Opolskiego i Politechniki Wrocławskiej. W 2014 uzyskała tytuł doktora nauk chemicznych. Obecnie zatrudniona na stanowisku adiunkta w Instytucie Chemii UO w Katedrze Chemii Fizycznej i Modelowania Molekularnego. Działalność badania właściwości naukowa: konformacyjnych pochodnych α,β-dehydrofenyloalaniny, badanie siły wiązań tworzonych przez modelowe dehydropeptydy, wyznaczanie

częstości anharmonicznych małych molekuł.



Prof. dr hab. Teobald Kupka Tytuł magistra chemii uzyskał w roku 1978 w Instytucie Chemii Wydziału Matematyki-Fizyki i Chemii Uniwersytetu Śląskiego w Katowicach. Od 1980 roku pracował w zespole profesora Jana O. Dzięgielewskiego w Zakładzie Chemii Nieorganicznej i Radiacyjnej zajmując się głównie zastosowaniem spektroskopii NMR w badaniach związków organicznych i kompleksów metali przejściowych. Na podstawie wyników tych badań uzyskał w roku 1992 tytuł doktora nauk chemicznych. Pracował w zespołach dr Mika Pintara i Harta Peemoeller'a w Ontario, Kanada, w Argonne

National Laboratory, Chicago (zespoły dr Bob Botto, Branko Ruscic i Larry Curtiss) oraz w Academia Sinica (Tajpei, Tajwan). W roku 2011 uzyskał stopień doktora habilitowanego na Wydziale Chemii, Uniwersytetu Wrocławskiego a w roku 2020 tytuł profesora nauk ścisłych i przyrodniczych (Instytut Chemii, UO Opole). Zainteresowania naukowe koncentrują się obecnie na badaniach eksperymentalnych z zastosowaniem technik NMR, IR i Ramana oraz modelowaniu molekularnym układów biologicznie ważnych i nanomateriałów.





https://orcid.org/0000-0002-6252-3822



**Dr Tapas Kar** uzyskał tytuł mgr inż w roku1983 i stopień doktora w 1988 w Burdwan University, Indian Institute of Technology (Indie) pod kierunkiem prof. AB Sannigrahi. Od 1990 r. pracował w renomowanych ośrodkach naukowych w Europie Zachodniej, Brazylii i USA. Ponadto, w latach 1991-1993 przebywał na prestiżowym stypendium naukowym w Niemczech (Alexander von Humboldt Fellowship). Ostatnio pracował w zespole prof. Steve Scheiner w Utah State University w Logan (USA). Współpracuje z wieloma ośrodkami naukowymi, w tym z Wydziałem Chemii Uniwersytetu Opolskiego.





http://orcid.org/0000-0001-8493-4254



#### Prof. dr hab. Małgorzata A. Broda

Studia magisterskie w latach 1977-1982 w Instytucie Chemii Uniwersytetu Wrocławskiego. Od 1982 asystent w Zakładzie Chemii Fizycznej Uniwersytetu Wrocławskiego w zespole prof. J. P. Hawranka. Praca doktorska pt: "Relaksacja oscylacyjna w halogenofenolach" przygotowana pod kierunkiem prof. J. P. Hawranka. Habilitacja w 2009 r. na

Wydziale Chemii Uniwersytetu Wrocławskiego. Tytuł rozprawy habilitacyjnej: "Stereoelektronowe właściwości pochodnych α,β-dehydroaminokwasów". Od 1993 roku adiunkt w Katedrze Chemii Organicznej Uniwersytetu Opolskiego. Od 2011 – kierownik Zakładu Chemii Fizycznej i Modelowania Molekularnego. W roku 2020 – tytuł profesora nauk chemicznych. Zainteresowania naukowe: Spektroskopia oscylacyjna układów z wiązaniem wodorowym; badanie relaksacji oscylacyjnej na podstawie analizy kształtu pasm; właściwości modelowych peptydów i α,β-dehydropeptydów; modelowanie molekularne właściwości strukturalnych i spektroskopowych związków o znaczeniu biologicznym.





http://orcid.org/0000-0002-4092-3593

#### **ABSTRACT**

The energy and structure of intermolecular hydrogen bonds between water molecule and *N*-methylamide (NMA) or uracil (U) are discussed on the basis of DFT calculations. Theoretical methods are applied to calculate properties of *cis*- and *trans*-NMA complexes with one water molecule. Subsequently, H-bonds in six uracil – water complexes are analyzed. The influence of dispersion interactions and the polar environment on the hydrogen bond energy was analyzed. Results obtained by B3LYP functional with and without Grimme D3 dispersion correction indicate that dispersion interaction plays a significant role in an association process. In addition, the polar solvent reduces the hydrogen bond energy and this reduction is directly proportional to the hydrogen bond energy.

<u>Keywords:</u> hydrogen bond, binding energy, Grimme D3 dispersion correction, uracil, amide bond

<u>Słowa kluczowe</u>: wiązanie wodorowe, energia oddziaływania, poprawka dyspersyjna Grimme'a, uracyl, wiązanie amidowe

# WYKAZ STOSOWANYCH SKRÓTÓW

B3LYP - hybrydowy funkcjonał gęstości (ang. Becke three parameter, Lee, Young i Parr)

DFT - teoria funkcjonału gęstości (ang. density functional theory)

NMA - *N*-metyloacetamid (ang. *N*-methylacetamide)

D3 - empiryczna poprawka Grimme'a na energię dyspersyjną

PCM - model rozpuszczalnika ciągłego (ang. polarized continuum model)

WCSS - Wrocławskie Centrum Sieciowo-Superkomputerowe

a.u. - jednostki atomowe (ang. atomic unit)

# **WPROWADZENIE**

Wiązanie wodorowe odgrywa bardzo istotną rolę pośród oddziaływań stabilizujących układy molekularne i jest obiektem badań prowadzonych w wielu obszarach chemii, na przykład z zakresu nanotechnologii [1,2], projektowania leków [3,4] czy poszukiwania nowych materiałów [5-7]. Wiązanie wodorowe jest wyjątkowym, niekowalencyjnym oddziaływaniem występującym w wielu cząsteczkach organicznych. Najbardziej znanym i przytaczanym przykładem jest cząsteczka DNA będąca głównym nośnikiem informacji genetycznej. Rdzeń helisy DNA utrzymywany jest poprzez komplementarne pary zasad azotowych połączonych ze sobą za pomocą dwóch lub trzech wiązań wodorowych. Tworzenie podobnych oddziaływań w peptydach i białkach prowadzi do powstania fragmentów o regularnej strukturze, które określa się jako elementy struktury drugorzędowej. Są one o tyle ważne, że stają się rusztowaniem, wokół którego powstaje ostateczna struktura trójwymiarowa białka – struktura trzeciorzędowa, decydująca o jego funkcji. Ponadto wiązania wodorowe są niezbędne do tworzenia oddziaływań pomiędzy receptorami a ligandami, co ma ogromne znaczenie w działaniu leków.

Badanie właściwości wiązania wodorowego ma ponad 100 – letnią historię. Pierwsze wzmianki o tego typu oddziaływaniach pojawiły się w 1902 r. [8]. Natomiast Pauling w 1939 roku zauważył, że "w pewnych warunkach atom wodoru przyciągany jest przez dwa atomy zamiast jednego, co może świadczyć o rodzaju pewnej więzi pomiędzy nimi" [9]. Złożona natura tego oddziaływania spowodowała, że na przestrzeni wielu lat definicja wiązania wodorowego ewoluowała i nawet obecnie jest tematem wielu dyskusji [10-13]. Niemniej jednak najnowsza z nich wypracowana została przez IUPAC [14]. Wg niej wiązanie takie tworzy się zawsze pomiędzy atomem wodoru związanym kowalencyjnie z atomem lub jonem o większej od niego elektroujemności (X) a wolną parą elektronową drugiego atomu (Y) występującego w tej samej lub innej cząsteczce. Wiązanie to zaznacza się linią przerywaną X-H···Y-Z. Pomiędzy atomami H i Y występuje głównie oddziaływanie elektrostatyczne. Ponadto dochodzi do przeniesienia ładunku z akceptora na atom wodoru i związane z nim atomy oraz do polaryzacji chmury elektronowej zarówno akceptora jak i donora wiązania wodorowego [15]. Energia wiązań wodorowych mieści się w granicach od ok. 1 do 40 kcal/mol [16]. Pod tym kątem można je sklasyfikować jako wiązania silne, umiarkowane i słabe.

Prace eksperymentalne dotyczące właściwości i różnorakich skutków występowania wiązania wodorowego są wspomagane metodami modelowania molekularnego. Aby stwierdzić obecność wiązania wodorowego w układzie należy określić kryteria, na podstawie których można to stwierdzić w strukturach krystalicznych czy otrzymanych za pomocą modelowania molekularnego [17-22]. W większości prac dotyczących tego zagadnienia przyjmuje się że odległość pomiędzy atomami H···A powinna być krótsza niż suma promieni van der Waalsa akceptora i wodoru. Geometrię wiązań wodorowych określa się podając odległość pomiędzy atomami H···Y i X···Y oraz wartość kąta walencyjnego utworzonego przez atomy X-H···Y. Wiązanie wodorowe tworzy się, gdy

odległość pomiędzy atomami H···Y jest mniejsza od 3,0 Å (w przypadku słabych oddziaływań granicę można przesunąć do 3,2 Å a kąt zawarty pomiędzy atomami X-H···Y powinien być większy od 90° [16, 18].

Celem prezentowanej pracy jest przybliżenie czytelnikowi problemów związanych z wiarygodnym przewidywaniem energii wiązania wodorowego i właściwości strukturalnych kompleksów z jedną cząsteczką wody wybranych związków o znaczeniu biologicznym - *N*-metyloacetamidu i uracylu. Obliczenia przeprowadzono przy zastosowaniu teorii funkcjonału gęstości (DFT) [23, 24]. Wpływ rozpuszczalnika modelowano przy pomocy teorii rozpuszczalnika ciągłego (PCM) [25, 26].

# 1. KOMPLEKSY N-METYLOACETAMIDU Z CZĄSTECZKĄ WODY

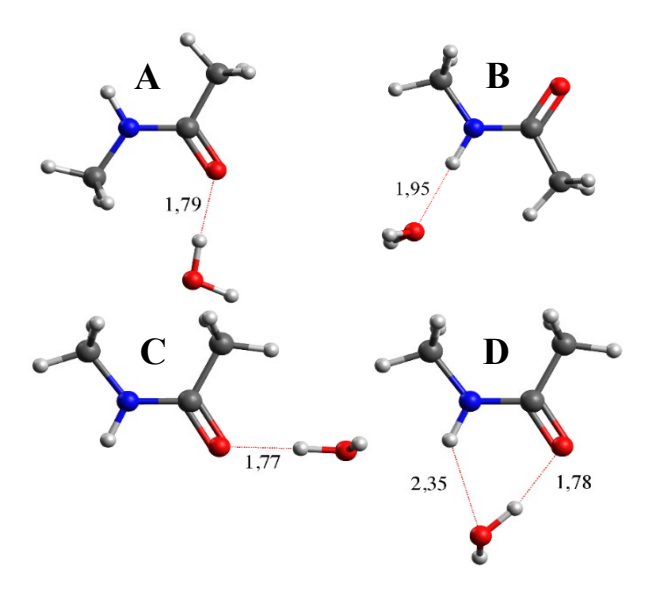
Wszystkie obliczenia, których wyniki będą prezentowane w tej pracy wykonano przy pomocy programu Gaussian 16 [27]. Użyty został funkcjonał hybrydowy B3LYP [28] i baza funkcyjna Dunninga aug-cc-pVTZ [29]. Funkcjonał B3LYP jest jednym z najczęściej stosowanych do modelowania właściwości związków organicznych ale ma poważny mankament - nie uwzględnia oddziaływań dyspersyjnych. Z tego powodu, aby sprawdzić jaki jest wpływ tych oddziaływań na energię i strukturę geometryczną wiązań wodorowych tworzonych przez układy amidowe, zastosowaliśmy empiryczną poprawkę Grimme'a uwzględniającą dyspersję [30]. Wpływ rozpuszczalnika wzięty został pod uwagę przez zastosowanie modelu ciągłego dielektryka (PCM) [25]. Każda zoptymalizowana struktura została zweryfikowana jako minimum energetyczne poprzez obliczenie częstości drgań harmonicznych i sprawdzenie, że wszystkie one są rzeczywiste. Energia międzycząsteczkowego oddziaływania (Eint) w badanych kompleksach została obliczona jako różnica pomiędzy energią kompleksu i sumą energii monomerów. W fazie gazowej została ona dodatkowo skorygowana metodą CP (ang. counterpoise correction) ze względu na błąd superpozycji bazy (BSSE) [31].

Pierwszym analizowanym układem był kompleks NMA – woda. *N*-Metyloacetamid może występować w dwóch konfiguracjach – *cis* i *trans*. Obliczono kompleksy dla obu tych izomerów, bo chociaż *cis*-NMA jest, zgodnie z wynikami obliczeń DFT [32], o około 3 kcal/mol mniej trwały niż *trans*-NMA to w polarnym otoczeniu różnica energii między nimi zmniejsza się do ∼1,5 kcal/mol. Ponadto, w kolejnym etapie analizowane będą wiązania wodorowe tworzone przez uracyl, którego fragmenty strukturalne są podobne do *cis*-NMA.

Układ amidowy ma dwa ugrupowania zdolne do tworzenia wiązań wodorowych o średniej energii – grupę karbonylową C=O i grupę N-H. Zoptymalizowano dwa kompleksy *trans*-NMA stabilizowane wiązaniami wodorowymi C=O···H-O<sub>w</sub> i N-H···O<sub>w</sub>, odpowiednio *trans*-NMA-H<sub>2</sub>O (A) i *trans*-NMA-H<sub>2</sub>O (B). Istnieje jeszcze jeden kompleks stabilizowany wiązaniem C=O···H-O<sub>w</sub>, który różni się od struktury

(A) ułożeniem cząsteczki wody [33] co jedynie w nieznacznym stopniu wpływa na energię i parametry geometryczne oddziaływania. Dla izomeru *cis*-NMA również otrzymano dwa kompleksy, z których jeden jest stabilizowany przez wiązanie wodorowe C=O···H-O<sub>w</sub> (*cis*-NMA-H<sub>2</sub>O (C) ), a w drugim cząsteczka wody tworzy oddziaływanie zarówno z grupą C=O jak i N-H (*cis*-NMA-H<sub>2</sub>O (D) ). Pomimo wielokrotnych prób optymalizacji struktury kompleksu *cis*-NMA z wodą, w której występowałoby wyłącznie wiązanie N-H···O<sub>w</sub> nie udało się uzyskać takiego minimum. Takiej struktury nie otrzymano również metodą Hartree-Focka [34].

Struktury wszystkich obliczonych kompleksów NMA – woda z zastosowaniem poprawki Grimme'a i w otoczeniu wody jako ciągłego dielektryka przedstawione są na **rysunku 1**. Wybrane parametry energetyczne i strukturalne dla tych kompleksów oraz uzyskane również bez poprawki na oddziaływania dyspersyjne lub/i w fazie gazowej są zebrane w **Tabeli 1**. Już na wstępie warto zaznaczyć, że dla stosowanej w naszych obliczeniach bazy funkcyjnej aug-cc-pVTZ błąd wynikający z superpozycji bazy jest mały i wynosi od 1% do 2% energii oddziaływania i nie ma praktycznego znaczenia dla interpretacji otrzymanych wyników.



Rysunek 1. Struktury kompleksów trans- i cis-NMA z cząsteczką wody otrzymane metodą B3LYP/aug-ccpVTZ z zastosowaniem poprawki Grimme'a D3 i metody PCM. Wiązania wodorowe zaznaczone są czerwonymi liniami przerywanymi

Figure 1. Structures of *trans*- and *cis*-NMA complexes with water molecule obtained by B3LYP/aug-cc-pVTZ method using Grimme D3 correction and PCM method. Hydrogen bonds are indicated by red dashed lines

Analizując wyniki obliczeń zebrane w **Tabeli 1**, można stwierdzić, że uwzględnienie w obliczeniach poprawki na oddziaływania dyspersyjne dla struktur

w fazie gazowej zwiększa energie oddziaływania o około 1,6 kcal/mol w przypadku wiązań C=O···HO<sub>w</sub>, i o około 1,3 kcal/mol dla oddziaływania N-H··· O<sub>w</sub>, co oznacza wzrost energii wiązania wodorowego o około 20%. Towarzyszy temu niewielkie (od 0,007 do 0,049 Å) skrócenie odległości H···O. Jeżeli próbujemy modelować wpływ polarnego rozpuszczalnika metodą PCM, to energia oddziaływania w badanych kompleksach jest mniejsza niż w fazie gazowej o około 30%, a dodanie poprawki na oddziaływania dyspersyjne ma podobny wpływ na energię oddziaływania jak w przypadku kompleksów w próżni. Różnica pomiędzy energią wiązania wodorowego obliczona bez poprawki Grimme'a i z ta poprawka wynosi, dla układów modelowanych w otoczeniu polarnego ośrodka, około 1,5 kcal/mol. W przypadku kompleksów stabilizowanych przez pojedyncze wiązanie wodorowe, czyli (A), (B) i (C), uwzględnienie w obliczeniach wpływu polarnego rozpuszczalnika powoduje (pomimo znacznie mniejszej energii wiązania wodorowego) skrócenie odległości O···H o około 0,08 Å, zarówno w przypadku wiązań C=O···HO<sub>w</sub> jak i N-H··· O<sub>w</sub>. Natomiast w przypadku kompleksu (D) polarne otoczenie powoduje zmniejszenie odległości C=O···HO<sub>w</sub> i jednoczesne znaczne wydłużenie wiązania N-H··· O<sub>w</sub> (o około 0,3 Å).

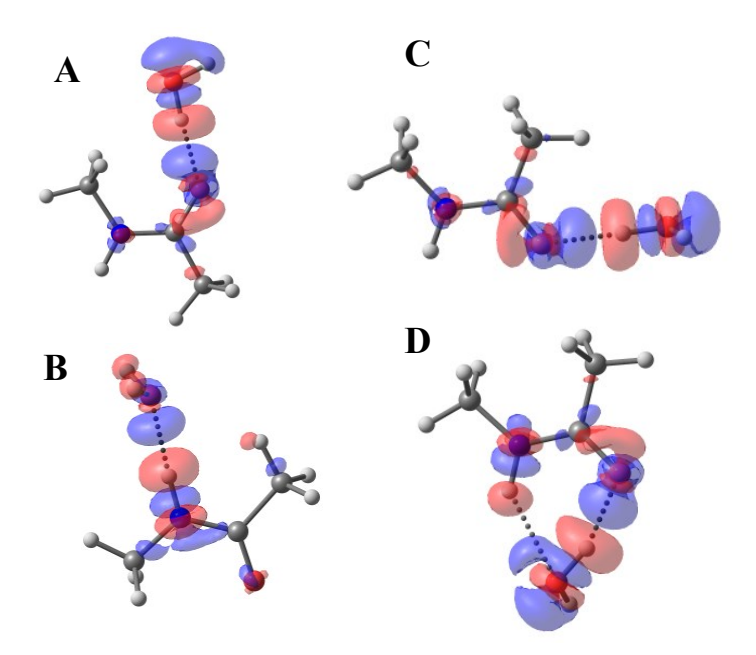
Tabela 1. Energie oddziaływania E<sub>int</sub> [kcal/mol] i długości wiązań wodorowych [Å] w kompleksach transi cis-NMA z cząsteczką wody otrzymane metodą B3LYP/aug-cc-pVTZ. E<sub>int</sub>(kor) oznacza energie oddziaływania skorygowane ze względu na błąd superpozycji bazy

Table 1. E<sub>int</sub> interaction energies [kcal/mol] and hydrogen bond lengths [Å] in trans- and cis-NMA complexes with a water molecule obtained by the B3LYP/aug-cc-pVTZ method. E<sub>int</sub>(kor) denotes interaction energies corrected for base superposition error

Kompleks	Faza gazowa		Woda	
	B3LYP	B3LYP-D3	B3LYP	B3LYP-D3
trans-NMA-H <sub>2</sub> O	(A)			
$\mathrm{E}_{\mathrm{int}}$	-6,92	-8,83	-4,52	-6,18
$E_{int}(kor)$	-6,82	-8,73	-	-
$C=O\cdots HO_w$	1,871	1,850	1,807	1,791
trans-NMA-H <sub>2</sub> O	(B)			
$\mathrm{E}_{\mathrm{int}}$	-4,10	-5,38	-2,61	-4,07
E <sub>int</sub> (kor)	-4,01	-5,28	-	-
$N-H\cdots O_w$	2,089	2,040	1,992	1,954
cis-NMA-H <sub>2</sub> O (C	)			
$\mathrm{E}_{\mathrm{int}}$	-7,18	-8,78	-4,97	-6,36
$E_{int}(kor)$	-7,09	-8,69	-	-
$C=O\cdots HO_w$	1,848	1,840	1,799	1,768
cis-NMA-H <sub>2</sub> O (D	)			
$\mathrm{E}_{\mathrm{int}}$	-9,48	-11,19	-4,94	-6,66
E <sub>int</sub> (kor)	-9,37	-11,08	-	-
$C=O\cdots HO_w$	1,837	1,839	1,776	1,779
$N\text{-}H\cdots O_w$	2,088	2,080	2,439	2,351

W przypadku kompleksu (C) uwzględnienie w obliczeniach wpływu rozpuszczalnika nie tylko skraca wiązanie C=O···HO<sub>w</sub>, ale również powoduje zmianę wzajemnego ułożenia cząsteczek w kompleksie. W kompleksie zoptymalizowanym w fazie gazowej, cząsteczka wody leży w płaszczyźnie wiązania amidowego, natomiast w polarnym otoczeniu płaszczyzna cząsteczki wody jest w przybliżeniu prostopadła do płaszczyzny układu amidowego.

W literaturze jest wiele prac, gdzie analizowane są energie wiązań wodorowych pomiędzy NMA a dwoma cząsteczkami wody [32, 35-38]. W przypadku kiedy trans-NMA tworzy wiązania wodorowe z cząsteczkami wody poprzez grupę karbonylową i grupę N-H, obserwowany jest efekt kooperatywny, czyli energia wiązań wodorowych w takim przypadku jest większa niż suma energii dwóch pojedynczych oddziaływań, a różnica wynosi około 0,7 – 0,9 kcal/mol w zależności od metody obliczeń, w szczególności 0,7 dla B3LYP/PCM. Natomiast jeśli obie cząsteczki wody oddziałują z grupą karbonylową amidu występuje efekt antykooperatywny, czyli energia oddziaływania w takim układzie jest o około 0,6 kcal/mol mniejsza niż suma dwóch wiązań wodorowych C=O···HO<sub>w</sub> [35]. W przypadku *cis*-NMA autorzy [35] stwierdzają, że ich obliczenia nie wskazują na występowanie kooperatywnego efektu. Jednak ze względu na efekt sprzężenia π-elektronowego w układzie amidowym można się spodziewać, że utworzenie wiązania wodorowego z cząsteczką wody zmieni rozkład gęstości elektronowej, a tym samym protono-donorowe lub akceptorowe właściwości amidu. Aby to lepiej zobrazować, na rysunku 2 przedstawiona została zmiana gęstości elektronowej po utworzeniu wiązania wodorowego w kompleksach trans- i cis- NMA z cząsteczką wody. Niebieskie i czerwone obszary wskazują odpowiednio zwiększenie lub zmniejszenie gęstości elektronowej w kompleksie w porównaniu do gęstości w izolowanych cząsteczkach. Uzyskane rezultaty wskazują, że zgodnie z oczekiwaniami, największe zmiany gęstości elektronowej występują w obszarze utworzonego wiązania wodorowego H···O, przy czym w okolicy protonu mostkowego następuje zmniejszenie gęstości elektronowej, a w pobliżu atomu tlenu (jego wolnych par elektronowych) gestość elektronowa rośnie po utworzeniu kompleksu. Jest to typowy obraz dla wiązania wodorowego [39, 40]. Oprócz tego, w układzie amidowym, obserwowane są niewielkie zmiany gęstości elektronowej na sąsiedniej grupie zdolnej do tworzenia wiązania wodorowego. To pozwala zrozumieć, dlaczego energia oddziaływania w kompleksie D (-6,66 kcal/mol obliczona metodą PCM//B3LYP-D3/aug-cc-pVTZ) nie jest równa sumie takich energii w kompleksach C i B (odpowiednio -6,36 i -4,07 kcal/mol) oraz dlaczego wiązanie wodorowe N-H···O<sub>w</sub> w kompleksie D pod wpływem polarnego otoczenia znacznie się wydłuża, podczas gdy w pozostałych kompleksach rozpuszczalnik powoduje zmniejszenie odległości H···O.



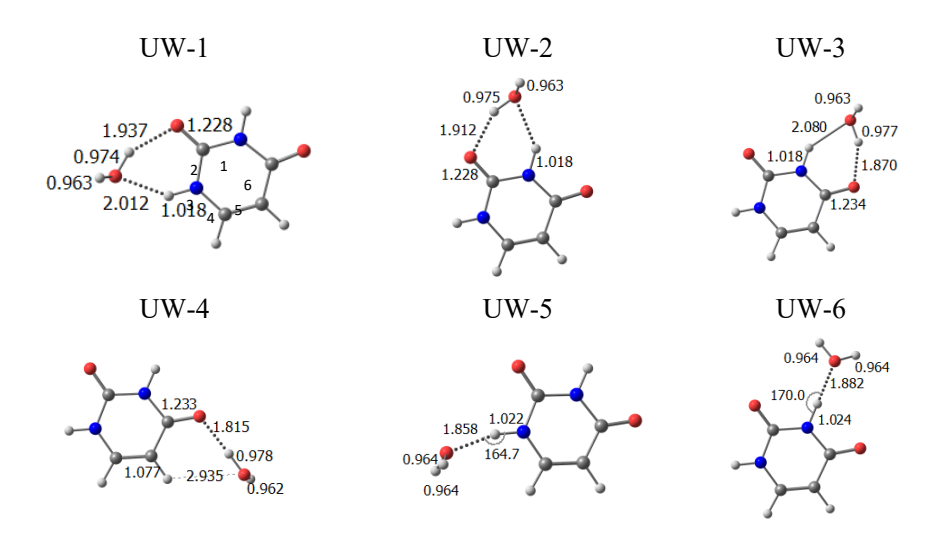
Rysunek 2. Zmiana gęstości elektronowej (kontur dla wartości 0.001 e/a.u.³) dla kompleksów trans i cis NMA z jedną cząsteczką wody otrzymane metodą PCM//B3LYP-D3/aug-cc-pVTZ

Figure 2. Change in electron density (contour for 0.001 e/a.u.<sup>3</sup> value) for *trans* and *cis* NMA complexes with one water molecule obtained by PCM//B3LYP-D3/aug-cc-pVTZ method

#### 2. KOMPLEKSY URACYL-WODA

Kolejnym modelowym układem, którego oddziaływanie z cząsteczką wody jest analizowane w tej pracy to uracyl, tj. jedna z pirymidynowych zasad azotowych. Istnieje sześć tautomerów uracylu, z których forma zawierająca dwie grupy karbonylowe i dwa fragmenty N-H jest najbardziej stabilna, co wykazały zarówno badania eksperymentalne jak i teoretyczne [41-44]. Tylko taki tautomer uwzględniono w obliczeniach.

Struktury geometryczne sześciu kompleksów uracylu z cząsteczką wody (**Rysunek 3**) zostały obliczone w fazie gazowej i w wodzie, bez uwzględnienia poprawki Grimme'a oraz z tą poprawką. Ich energie względne i energie wiązań wodorowych zostały zebrane w **tabeli 2**. Cztery pierwsze z tych kompleksów, mające dwa wiązania wodorowe pomiędzy składnikami kompleksu, zostały już wcześniej opisane w literaturze [45, 46]. Natomiast dwa pozostałe, stabilizowane przez jedno wiązanie wodorowe pomiędzy uracylem i cząsteczką wody, są prezentowane po raz pierwszy.



Rysunek 3. Struktury kompleksów uracylu z cząsteczką wody otrzymane metodą PCM/B3LYP-D3/aug-cc-pVTZ. Wiązania wodorowe zaznaczono liniami przerywanymi. W kompleksie UW-1 podano numerację atomów w cząsteczce uracylu

Figure 3. Structures of uracil complexes with water molecule obtained by PCM/B3LYP-D3/aug-cc-pVTZ method. Hydrogen bonds are marked with dashed lines. In the UW-1 complex, the numbering of atoms in the uracil molecule is given

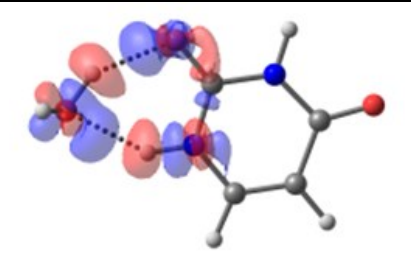
W fazie gazowej najniżej energetycznym jest kompleks UW-1 stabilizowany przez dwa wiązania wodorowe: C=O···HO<sub>w</sub> i N-H··· O<sub>w</sub>, których długości, bez poprawki Grimme'a, wynoszą odpowiednio 1,925 Å i 1,950 Å, a energia oddziaływania w tym układzie jest równa -9,9 kcal/mol. Uwzględnienie oddziaływań dyspersyjnych, zwiększa energię oddziaływania do -11,7 kcal/mol i nieco skraca oba wiązania. Chociaż energia oddziaływania w tym kompleksie jest bardzo podobna jak w układzie cis-NMA (D) to wiązania wodorowe mają inną geometrię. Mianowicie wiązanie C=O···HO<sub>w</sub> jest w kompleksie UW-1 o 0,09 Å dłuższe a wiązanie N-H···O<sub>w</sub> o 0,17 Å krótsze niż w kompleksie (D). Otoczenie polarnego rozpuszczalnika modelowane metodą PCM powoduje, podobnie jak dla kompleksów NMA, znaczne zmniejszenie energii oddziaływania oraz modyfikuje geometrie wodorowych, ale ta modyfikacja jest inna niż w przypadku kompleksu (D) dla NMA. Oba wiązania stają się dłuższe, ale wydłużenie wiązania N-H···O<sub>w</sub> nie jest tak duże jak w przypadku kompleksu NMA(D). Oznacza to, że *cis*-NMA wcale nie jest tak dobrym modelem wiązań wodorowych uracylu z cząsteczką wody. Różnice najprawdopodobniej wynikają z cyklicznej budowy uracylu, chociaż obliczone zmiany rozkładu gęstości elektronowej pod wpływem utworzenia wiązania z jedną

cząsteczką wody (na przykładzie kompleksu UW-1) wcale nie wskazują na to, że zmiany są zdelokalizowane poza fragment wiązań wodorowych stabilizujących kompleks (Rysunek 4).

Tabela 2. Energie względne ( $E_{rel}$ ) i energie oddziaływania  $E_{int}$  [kcal/mol] w kompleksach uracyl - woda otrzymane metodą B3LYP/aug-cc-pVTZ.  $E_{int}$ (kor) oznacza energie oddziaływania skorygowane ze względu na błąd superpozycji bazy. Wpływ wody jako rozpuszczalnika modelowano metodą PCM

Table 2. Relative energies  $(E_{rel})$  and interaction energies  $E_{int}$  [kcal/mol] in uracil-water complexes obtained by the B3LYP/aug-cc-pVTZ method.  $E_{int}$  (kor) denotes interaction energies corrected for base superposition error. The effect of water as a solvent was modeled by the PCM method

Kompleks	Faza gazowa		Woda	
	B3LYP	B3LYP-D3	B3LYP	B3LYP-D3
UW-1				
$\mathrm{E}_{\mathrm{rel}}$	0,00	0,00	0,04	0,04
E <sub>rel</sub> E <sub>int</sub>	-9,94	-11,72	-4,43	-6,25
$E_{int}$ $E_{int}(kor)$	-9,82	-11,72	-4,43	-0,23
$C=O\cdots HO_w$	*	1,932	1,928	1,937
	1,925	*	· · · · · · · · · · · · · · · · · · ·	
N-H···O <sub>w</sub>	1,950	1,941	2,029	2,012
UW-2	2.05	2.04	0.25	0.26
$E_{rel}$	2,07	2,04	0,37	0,36
E <sub>int</sub>	-7,41	-9,23	-4,11	-5,92
$E_{int}(kor)$	-7,29	-10,21	-	-
$C=O\cdots HO_w$	1,949	1,956	1,905	1,912
N-H···O <sub>w</sub>	2,023	2,009	2,108	2,087
UW-3				
$E_{rel}$	1,38	1,36	0,00	0,00
$\mathrm{E}_{\mathrm{int}}$	-8,09	-9,90	-4,48	-6,29
$E_{int}(kor)$	-7,98	-9,81	-	-
$C=O\cdots HO_w$	1,909	1,914	1,864	1,970
$N-H\cdots O_w$	1,994	1,983	2,098	2,080
UW-4				
$E_{rel}$	3,10	3,16	0,40	0,84
$\mathrm{E}_{\mathrm{int}}$	-6,37	-8,10	-4,08	-5,45
E <sub>int</sub> (kor)	-6,29	-8,01	=	=
C=O···HO <sub>w</sub>	1,904	1,894	1,828	1,815
C-H···O <sub>w</sub>	2,475	2,410	3,347	2,935
UW-5	<u> </u>	<u> </u>		·
$E_{rel}$	3,12	3,66	0,60	1,07
E <sub>int</sub>	-6,36	-7,60	-3,88	-5,21
E <sub>int</sub> (kor)	-6,25	-7,51	-	-
N-H···O <sub>w</sub>	1,948	1,921	1,879	1,858
UW-6	-7	- 7	-,~	-,
$E_{rel}$	5,17	5,62	1,28	1,72
E <sub>int</sub>	-4,30	-5,64	-3,20	-4,56
E <sub>int</sub> (kor)	-4,20	-5,53	-	-
N-H···O <sub>w</sub>	1,949	1,929	1,910	1,882

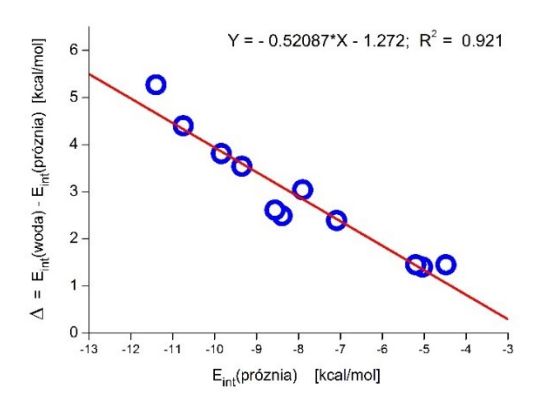


Rysunek 4. Zmiana gęstości elektronowej (kontur dla wartości 0.001 e/a.u.³) w kompleksie UW-1 w porównaniu w otrzymana metodą PCM//B3LYP-D3/aug-cc-pVTZ

Figure 4. The change in electron density (contour for the value of 0.001 e/a.u.<sup>3</sup>) in the UW-1 complex in comparison with that obtained by the PCM//B3LYP-D3/aug-cc-pVTZ method

Warto zauważyć, że dwie grupy protonodonorowe uracylu, N1-H i N3-H mają różne otoczenie chemiczne, co wpływa na energie i struktury geometryczne tworzonych przez nie wiązań wodorowych. Z tego powodu kompleks UW-2 w fazie gazowej jest o około 2 kcal/mol mniej stabilny niż kompleks UW-1 co wynika ze słabszych protonodonorowych właściwości grupy N3-H. Zgodnie z tym, energia oddziaływania kompleksu UW-5 (stabilizowanego wiązaniem N1H···Ow) jest w fazie gazowej o około 2 kcal/mol większa niż w przypadku UW-6 (stabilizowanego wiązaniem N3H···Ow).

Dla wszystkich sześciu kompleksów uracyl–woda polarny rozpuszczalnik powoduje znaczne zmniejszenie energii wiązania wodorowego, podobnie jak to zaobserwowaliśmy dla kompleksów NMA z jedną cząsteczką wody. Co ciekawe zmniejszenie energii oddziaływania jest tym większe im większa jest energia wiązania wodorowego. Ta liniowa zależność przedstawiona jest na rysunku 5.



Rysunek 5. Zależność (otrzymana metodą B3LYP-D3/aug-cc-pVTZ) różnicy energii oddziaływań w wodzie i fazie gazowej (Δ= E<sub>int</sub> (woda) –E<sub>int</sub> (faza gazowa)) od energii oddziaływań w fazie gazowej z cząsteczką wody NMA lub uracylu

Figure 5. Dependence (obtained by the method B3LYP-D3/aug-cc-pVTZ ) of the difference in energy of interactions in water and gas phase (Δ= Eint (water)-Eint (gas phase)) on the energy of interactions in the gas phase with the water molecule NMA or uracil

# **UWAGI KOŃCOWE**

Zrozumienie i poprawne modelowanie metodami teoretycznymi oddziaływania uracylu z wodą jest bardzo ważne w kontekście badania struktury i funkcji DNA/RNA. W niniejszej pracy przedstawiono wyniki obliczeń funkcjonałem B3LYP czterech kompleksów *N*-metyloacetamidu i sześciu kompleksów uracylu z jedną cząsteczką wody. Modelowanie prowadzone było z zastosowaniem poprawki Grimme'a aby uwzględnić oddziaływania dyspersyjne. Zastosowano średniej wielkości bazę funkcyjną aug-cc-pVTZ a wpływ wody jako polarnego otoczenia uwzględniono stosując metodę ciągłego dielektryka (PCM). Analizując otrzymane wyniki można wyciągnąć następujące wnioski:

- Zoptymalizowanie struktur geometrycznych dwóch, nie opisanych wcześniej w literaturze, kompleksów uracyl – woda (UW-5 i UW-6) stabilizowanych przez tylko jedno wiązanie wodorowe pozwoliło lepiej scharakteryzować i porównać protono-donorowe właściwości grup N1-H i N3-H uracylu.
- Energia hydratacji uracylu w polarnym środowisku (metoda PCM) jest o 1,5 do 5 kcal/mol mniejsza niż w fazie gazowej. Najsilniejszy efekt obserwowany jest dla najsilniejszych wiązań wodorowych.
- Przeprowadzając modelowanie funkcjonałem B3LYP wiązań wodorowych amidów w cząsteczką wody koniecznie należy wziąć pod uwagę oddziaływania dyspersyjne. Udział tych oddziaływań w całkowitej energii wiązania może sięgać nawet 30%.

#### **PODZIĘKOWANIA**

Wszystkie obliczenia wykonano przy pomocy sprzętu i oprogramowania WCSS. Autorzy dziękują również za wsparcie finansowe w ramach Uniwersytetu Opolskiego.

#### PIŚMIENNICTWO CYTOWANE

- [1] Y. Liu, C. Hu, A. Comotti, M.D. Ward, Science, 2011, 333, 436.
- [2] M.L. Bushey, T.-Q. Nguyen, W. Zhang, D. Horoszewski, C. Nuckolls, Angew. Chem. Int. Ed., 2004, 43, 5446.
- [3] R.E. Babine, S.L. Bender, Chem. Rev., 1997, 97, 1359.
- [4] P. Schmidtke, F. Javier Luque, J.B. Murray, X. Barril, JACS, 2011, 133, 18903.
- [5] W.H. Binder, R. Zirbs, S Adv. Polym. Sci., 2007, 207, 1.
- [6] S. Debrus, H. Ratajczak, J. Venturini, N. Pinçon, J. Baran, J. Barycki, T. Głowiak, A. Pietraszko, Synth. Met., 2002, 127, 99.
- [7] C. Shao, H. Chang, M. Wang, F. Xu, J. Yang, ACS Appl. Mater., 2017, 9, 28305.
- [8] A. Werner, Liebigs Ann. Chem., 1902, 322, 261.

- [9] L. Pauling, The Nature of the Chemical Bond, Cornell University Press, Ithaca, 1960.
- [10] P. Schuster, G. Zundel, C. Sanfordy, The Hydrogen Bond: Recent Developments in Theory and Experiments, Vols. I-III. North Holland, Amsterdam, 1976.
- [11] S.J. Grabowski, Ed. Hydrogen Bonding-New Insights. Springer, Dordrecht, 2006.
- [12] P. Gilli, G. Gilli, The Nature of the Hydrogen Bond. Oxford University Press, Oxford, 2009.
- [13] B. Kojić-Prodić, K. Molćanov, Acta Chim. Slov., 2008, 55, 692.
- [14] E. Arunan, G.R. Desiraju, R.A. Klein, J. Sadlej, S. Scheiner, I. Alkorta, D.C. Clary, R.H. Crabtree, J.J Dannenberg, P. Hobza, H.G. Kjaergaard, A.C. Legon, B. Mennucci, D.J. Nesbitt, Pure Appl. Chem., 2011, 83, 1637.
- [15] G.R. Desiraju, Acc. Chem. Res., 2002, 35, 565.
- [16] G.A. Jeffrey, An Introduction to Hydrogen Bonding. Oxford University Press, Oxford, 1997.
- [17] S. Scheiner, Hydrogen Bonding: A Theoretical Perspective. Oxford University Press, Oxford, 1997.
- [18] T. Steiner, Angew. Chem. Int. Ed., 2002, 41, 48.
- [19] I. Rozas, Phys. Chem. Chem. Phys., 2007, 9, 2782.
- [20] I.Y, Torshin, I.T. Weber, R.W. Harrison, Protein Eng., 2002, 15, 359.
- [21] I.K. McDonald, J.M. Thornton, J. Mol. Biol., 1994, 238, 777.
- [22] G.R. Desiraju, T. Steiner, The Weak Hydrogen Bond. Oxford University Press, Oxford, 1999.
- [23] R.G. Parr, W. Yang, Density-functional theory of atoms and molecules. Oxford University Press, Oxford, 1989.
- [24] J. A. Pople, P. M. W. Gill, B. G. Johnson, Chem. Phys. Lett., 1992, 199, 557.
- [25] S. Miertuš, E. Scrocco, J. Tomasi, Chem. Phys., 1981, 55, 117.
- [26] M. Cossi, V. Barone, R. Cammi, J. Tomasi, Chem. Phys. Lett., 1996, 255, 327.
- [27] M.J. Frisch, G.W. Trucks, H.B. Schlegel, G.E. Scuseria, M.A. Robb, J.R. Cheeseman, G. Scalmani, V. Barone, G.A. Petersson, H. Nakatsuji, X. Li, M. Caricato, A.V. Marenich, J. Bloino, B.G. Janesko, R. Gomperts, B. Mennucci, H.P. Hratchian, J.V. Ortiz, A.F. Izmaylov, J.L. Sonnenberg, Williams, F. Ding, F. Lipparini, F. Egidi, J. Goings, B. Peng, A. Petrone, T. Henderson, D. Ranasinghe, V.G. Zakrzewski, J. Gao, N. Rega, G. Zheng, W. Liang, M. Hada, M. Ehara, K. Toyota, R. Fukuda, J. Hasegawa, M. Ishida, T. Nakajima, Y. Honda, O. Kitao, H. Nakai, T. Vreven, K. Throssell, J.A. Montgomery Jr., J.E. Peralta, F. Ogliaro, M.J. Bearpark, J.J. Heyd, E.N. Brothers, K.N. Kudin, V.N. Staroverov, T.A. Keith, R. Kobayashi, J. Normand, K. Raghavachari, A.P. Rendell, J.C. Burant, S.S. Iyengar, J. Tomasi, M. Cossi, J.M. Millam, M. Klene, C. Adamo, R. Cammi, J.W. Ochterski, R.L. Martin, K. Morokuma, O. Farkas, J.B. Foresman, D.J. Fox, Gaussian 16 Rev. C.01. Wallingford, CT, 2016.
- [28] A. D. Becke, J. Chem. Phys., 1993, 98, 5648.
- [29] R. A. Kendall, T. H. Dunning Jr., R. J. Harrison, J. Chem. Phys., 1992, 96, 6796.
- [30] S. Grimme, J. Antony, S. Ehrlich and H. Krieg, J. Chem. Phys., 2010, 132, 154104.
- [31] S. F. Boys and F. Bernardi, Mol. Phys., 1970, 19, 553.
- [32] A. Panuszko, E. Gojło, J. Zielkiewicz, M. Śmiechowski, J. Krakowiak, J. Stangret, J. Phys. Chem. B, 2008, 112, 2483.
- [33] R. Zhang, H. Li, Y. Lei, S. Han, J. Mol. Struct., 2004, 693, 17.
- [34] D.A. Dixon, K.D. Dobbs, J.J. Valentini, J. Phys. Chem., 1994, 98, 13435.
- [35] W.-G. Han, S. Suhai, J. Phys. Chem., 1996, 100, 3942.
- [36] M.H. Farag, M.F. Ruiz-López, A. Bastida, G. Monard, F. Ingrosso, J. Phys. Chem. B, 2015, 119, 9056.
- [37] N.S. Kang, Y.K. Kang, Chem. Phys. Lett., 2017, **687**, 23.
- [38] X. Xiao, Y. Tan, L. Zhu, Y. Guo, Z. Wen, M. Li, X. Pu, A. Tian, J. Mol. Model., 2012, 18, 1389.
- [39] T. Kar, S. Scheiner, J. Phys. Chem. A, 2004, 108, 9161.
- [40] T. Kar, S. Scheiner, J. Chem. Phys., 2003, 119, 1473.
- [41] K. Rzepiela, A. Buczek, T. Kupka, M.A. Broda, Molecules, 2020, 25, 3931.
- [42] K. Rzepiela, A. Buczek, T. Kupka, M.A. Broda, Struct. Chem., 2021, 32, 275.
- [43] D.D. Colasurdo, M.N. Pila, D.A. Iglesias, S.L. Laurella, D.L. Ruiz, Eur. J. Mass Spectrom., 2018, 24, 214.
- [44] Y. Tsuchiya, T. Tamura, M. Fujii, M. Ito, J. Phys. Chem., 1988, 92, 1760.
- [45] T. Fornaro, M. Biczysko, J. Bloino, V. Barone, Phys. Chem. Chem. Phys., 2016, 18, 8479.

[46] T. Fornaro, D. Burini, M. Biczysko, V. Barone, J. Phys. Chem. A, 2015, 119, 4224.

Praca wpłynęła do Redakcji 13 kwietnia 2023 r.

10.3 P3: Electron correlation or basis set quality: how to obtain converged and accurate NMR shieldings for the third-row elements?





Article

# Electron Correlation or Basis Set Quality: How to Obtain Converged and Accurate NMR Shieldings for the Third-Row Elements?

Kacper Rzepiela <sup>1</sup>, Jakub Kaminský <sup>2</sup>,\*©, Aneta Buczek <sup>1</sup>, Małgorzata A. Broda <sup>1</sup>© and Teobald Kupka <sup>1</sup>,\*©

- Faculty of Chemistry, University of Opole, 48 Oleska Street, 46-052 Opole, Poland
- Institute of Organic Chemistry and Biochemistry of the CAS, Flemingovo nám. 2, 166 10 Prague, Czech Republic
- \* Correspondence: kaminsky@uochb.cas.cz (J.K.); teobaldk@gmail.com (T.K.)

Abstract: The quality of theoretical NMR shieldings calculated at the quantum-chemical level depends on various theoretical aspects, of which the basis set type and size are among the most important factors. Nevertheless, not much information is available on the basis set effect on theoretical shieldings of the NMR-active nuclei of the third row. Here, we report on the importance of proper basis set selection to obtain accurate and reliable NMR shielding parameters for nuclei from the third row of the periodic table. All calculations were performed on a set of eleven compounds containing the elements Na, Mg, Al, Si, P, S, or Cl. NMR shielding tensors were calculated using the SCF-HF, DFT-B3LYP, and CCSD(T) methods, combined with the Dunning valence aug-cc-pVXZ, core-valence aug-cc-pCVXZ, Jensen polarized-convergent aug-pcSseg-n and Karlsruhe x2c-Def2 basis set families. We also estimated the complete basis set limit (CBS) values of the NMR parameters. Widely scattered nuclear shieldings were observed for the Dunning polarized-valence basis set, which provides irregular convergence. We show that the use of Dunning core-valence or Jensen basis sets effectively reduces the scatter of theoretical NMR results and leads to their exponential-like convergence to CBS. We also assessed the effect of vibrational, temperature, and relativistic corrections on the predicted shieldings. For systems with single bonds, all corrections are relatively small, amounting to less than 4% of the CCSD(T)/CBS value. Vibrational and temperature corrections were less reliable for H<sub>3</sub>PO and HSiCH due to the high anharmonicity of the molecules. An abnormally high relativistic correction was observed for phosphorus in PN, reaching ~20% of the CCSD(T)/CBS value, while the correction was less than 7% for other tested molecules.

Keywords: NMR shieldings; basis set dependence; third-row elements



Citation: Rzepiela, K.; Kaminský, J.; Buczek, A.; Broda, M.A.; Kupka, T. Electron Correlation or Basis Set Quality: How to Obtain Converged and Accurate NMR Shieldings for the Third-Row Elements? *Molecules* 2022, 27, 8230. https://doi.org/10.3390/ molecules27238230

Academic Editor: Chao Dong

Received: 2 November 2022 Accepted: 22 November 2022 Published: 25 November 2022

**Publisher's Note:** MDPI stays neutral with regard to jurisdictional claims in published maps and institutional affiliations.



Copyright: © 2022 by the authors. Licensee MDPI, Basel, Switzerland. This article is an open access article distributed under the terms and conditions of the Creative Commons Attribution (CC BY) license (https://creativecommons.org/licenses/by/4.0/).

#### 1. Introduction

Computed NMR parameters are often used to support experimental observations or to predict properties of new compounds. Thus, accurate theoretical predictions of components of nuclear magnetic shieldings, isotropic shielding constants (and chemical shifts, respectively) and shielding anisotropies have always been in great demand [1–4]. The experimental nuclear shielding tensor characterizes the response of a local nuclei to an external magnetic field. Nowadays, theoretical methods allow the prediction of this absolute parameter. In contrast, the experimental observable, chemical shift is a relative parameter, which requires a reference signal. The quality of predicted NMR shieldings depends on various theoretical aspects [1,3,5]. The basis set type and size used in NMR shielding predictions are among the most important factors strongly affecting the quality of predicted values. In the case of a theoretical chemical shift, the results often benefit from accidental error cancellation [1,6–8]. In general, the calculated NMR shieldings are sensitive to a proper description of electrons and they improve with the completeness and the flexibility of the basis sets. The atomic nuclei are shielded by both valence and core

Molecules **2022**, 27, 8230 2 of 22

electrons, which interact with the external magnetic field, inducing a magnetic field in the opposite direction. Thus, any reliable GIAO NMR calculation [9,10] should properly describe both types of electrons. The typical approach in the calculations of shieldings is that a series of basis sets with well-defined quality levels is employed for calculations that, in favorable cases, allow the extrapolation of results to the CBS limit [11,12]. However, the CBS limit of the <sup>1</sup>H, <sup>13</sup>C, <sup>15</sup>N and <sup>17</sup>O NMR shieldings is achievable only for small- or medium-sized isolated molecules [13–15], but yet it is out of reach for larger molecules. Note that generally good results are obtained with dedicated basis sets, optimized for specific methods and properties [16–18].

To aid thermochemical calculations of energy and energy-related parameters performed with relevant basis sets, various basis set families have specifically been designed for accurate predictions of GIAO NMR parameters. For example, the Dunning correlationconsistent (aug)-cc-pVXZ basis set [19–23], where X = D, T, Q, S, and S, was designed to treat reliably and efficiently electron correlation between the valence electrons. The further extension (augmentation) was then used to specifically treat the polarization due to an external electric field. Properties of correlation-consistent basis sets are also reported in detail [19–23]. Later, they were modified to also include core-valence electrons, giving rise to the (aug)-cc-pCVXZ, and aug-cc-pwCVXZ basis sets [21,24,25]. Similarly, Jensen polarization-consistent basis set families (aug)-pc-n [26–29], where n = 0, 1, 2, 3, and 4, were designed and used for accurate calculations of energy and energy related properties (originally for SCF-HF and DFT). The characteristic feature of these basis set families is an exponential-like decrease in energy of an atom or molecule as a result of calculation according to increased cardinal number *X* (or *n*). Later, Jensen designed the aug-pcS-*n*, aug-pcSseg-n and aug-pcJ-n [17,30] basis set families for efficient predictions of nuclear shieldings and indirect spin–spin coupling constants. It is generally accepted that GIAO NMR parameters calculated with the smaller Dunning basis set (significantly truncated for lower X) are inferior to those obtained with the larger basis set [4,31,32]. Thus, it is expected that the NMR parameters improve significantly from X to X + 1 in a regular way as was documented in [4,31–33]. In a seminal review on the calculation of nuclear shieldings and coupling constants, Helgaker, Jaszunski, and Ruud [1] noticed some deficiencies of the cc-pVXZ basis set series and proposed their improved version, with the inclusion of core-valence treatment (cc-pCVXZ) in future studies.

Another hierarchy of basis sets, primarily developed by Ahlrichs and coworkers [34], are the so-called Karlsruhe x2c-Def2 basis sets. Despite their compact size, these basis sets have recently been recommended for accurate calculations of nuclear shieldings [35–37]. The Karlsruhe x2c-Def2 basis sets are also suitable for the treatment of scalar relativistic effects but are smaller than Douglas–Kroll modifications of the Dunning type [38].

Most correlated calculations of NMR shieldings are performed with a focus only on valence electrons but core electrons become important even for moderately heavier NMRactive nuclei, such as <sup>27</sup>Al, <sup>31</sup>P, and <sup>33</sup>S. Indeed, neglecting core electrons could perturb a regular convergence of NMR parameters toward the complete basis set limit, which is observed for <sup>1</sup>H, <sup>13</sup>C and <sup>15</sup>N. A completely different picture was observed recently for the <sup>31</sup>P shielding constants in the phosphorus mononitride (PN) molecule [15]. In this case, the phosphorous isotropic shielding  $\sigma$ iso (and similarly shielding anisotropy,  $\Delta \sigma$ ) calculated with the SCF-HF, DFT-KT3, MP2, CCSD and CCSD(T) methods, and combined with the (aug)-cc-pVXZ basis sets, were scattered, evincing nonstandard convergence with increasing basis set size. In addition, the scatter patterns were very similar for all the studied methods. Going from double- to triple-ζ, the <sup>31</sup>P isotropic shielding in PN calculated with the CCSD(T) method dropped by approximately 190 ppm and then went back up by 20 ppm for the quadruple- $\zeta$  basis set and again decreased by 70 ppm with the quintuple-ζ basis set. Finally, a saturation of phosphorous isotropic shielding was observed for X = 5 and 6. At the same time, regular exponential decreases in total energy as well as the <sup>15</sup>N isotropic shielding were observed.

Molecules **2022**, 27, 8230 3 of 22

The importance of including the core-valence basis sets in accurate calculation of nuclear shieldings has been demonstrated in several wave-function and density-functional studies [39-41]. For example, Field-Theodore et al. [40] studied nuclear shieldings of NF<sub>3</sub>, PF<sub>3</sub>, and AsF<sub>3</sub> using all-electron CCSD(T) calculations with the valence and corevalence basis sets. However, there is no clear general picture of regular nuclear shielding convergence for the third-row nuclei upon improving the cc-pVXZ or cc-pCVXZ basis set series in the literature. We can find some studies on selected third-row nuclei, though. Recently, a HF/aug-cc-pVXZ study on <sup>27</sup>Al NMR chemical shift of Al(OH)<sub>4</sub><sup>-</sup> appeared [42], showing a similar scatter of <sup>27</sup>Al nuclear isotropic shielding upon increasing the cardinal number of Dunning basis set, as was observed for PN [15]. The calculated values in the series differed by -48 ppm when changing X from D to T, by +20 ppm when going from T to Q, and finally by -20 ppm for the changes from Q to 5. The authors modified the standard aug-cc-pVQZ Dunning basis set by the addition of a tight p-function and the scatter of the calculated nuclear shieldings disappeared. Interestingly, the use of the core-valence aug-cc-pCVXZ basis set family produced regularly converging <sup>31</sup>P NMR parameters in PN [15]. Unfortunately, no analysis of <sup>31</sup>P shielding components in PN was performed in the work [15]. These parameters should be more sensitive to the basis set quality than the total isotropic value which is calculated as one-third of the trace average of the nuclear magnetic shielding tensor. Further, no direct comparison of the convergence patterns of the <sup>31</sup>P NMR shieldings in small molecules has been published so far. From the aforementioned literature compilation, it is apparent that a systematic test of nuclear shieldings convergence for third-row elements using the SCF-HF, B3LYP, and CCSD(T) methods combined with the aug-cc-pVXZ, aug-cc-pCVXZ, aug-pcSseg-n, and Karlsruhe-type basis sets has not been reported.

Given all the above, there is still an open question that is the behavior of calculated NMR shieldings obtained with the aug-cc-pVXZ basis set for all chemical elements in the third row of periodic table, namely Na, Mg, Al, Si, P, S, Cl and Ar. NMR spectroscopy for <sup>25</sup>Mg, <sup>35</sup>Cl and <sup>39</sup>Ar (a radioactive isotope) is not common. Most of the NMR-active nuclei from the third row are quadrupolar, with a spin of 3/2 (<sup>23</sup>Na, <sup>33</sup>S, <sup>35</sup>Cl, or <sup>37</sup>Cl) or 5/2 (<sup>25</sup>Mg, <sup>27</sup>Al), and therefore their signal broadens with asymmetry of the environment. Only  $^{29}$ Si and  $^{31}$ P have  $\frac{1}{2}$  spin. The sensitivity of the aforementioned nuclei is from low (25Mg and 33S) to medium (23Na, 29Si and 31P) or even high (27Al). 35Cl is more sensitive than <sup>37</sup>Cl; on the contrary, <sup>37</sup>Cl provides a slightly higher resolution than <sup>35</sup>Cl. Therefore, <sup>35</sup>Cl is usually preferred over <sup>37</sup>Cl. In general, quadrupolar nuclei have broader signals than silicon and phosphorus (1/2 spin) that yield sharp lines. The main use of sodium, magnesium or aluminum NMR is to determine their presence, or to monitor their binding, e.g., to biomolecules (Mg). Silicon NMR is mainly applied in material science, battery materials, civil engineering, or geology as the solid-state <sup>29</sup>Si NMR [43]. Since  $^{31}$ P is a naturally abundant active nucleus that is more sensitive than  $^{13}$ C or  $^{15}$ N, it was utilized in a wide range of fields, such as cellular biochemistry, metabolomics, medicine, or synthetic chemistry [44]. Ultimately, accurate theoretical calculations for these isotopes could complete the picture about the sensitivity of predicted NMR features (e.g., shieldings) to individual computational approaches (e.g., to increased basis set cardinal number X). As result, this knowledge could help to design reliable, accurate, but simplified tools for simulation of a nuclear shielding tensor for these elements.

We need to mention that the quality of gauge-including atomic orbital (GIAO) NMR calculations of shieldings is generally also sensitive to the description of the electron correlation. Thus, the precision of methods commonly used for shielding predictions decreases in the following order:  $CCSD(T) > MP2 \approx DFT > SCF - HF$ . Since the DFT approximation may often lead to a comparable quality of results as computationally more demanding MP2, the choice of a particular density functional from their great variety is also of prime importance [1,4]. Additionally, predicted NMR shieldings are often improved by inclusion of the zero-point vibrational correction (ZPVC) [45,46], the temperature correction (TC) [32,45,46], and also relativistic corrections (RCs) when the system contains heavy

Molecules **2022**, 27, 8230 4 of 22

atoms [47–50]. For practical reasons, the solvent effect needs to be considered often to allow a direct comparison of calculated NMR parameters with experiment, mainly conducted in solution.

Finally, we want to clarify some issues related to the use of estimated theoretical nuclear shieldings at the CBS limit and experimentally determined gas-phase chemical shifts (and nuclear shieldings). Obviously, the CBS shielding values are only values obtained by simply fitting the data obtained for a set of consecutive incomplete basis sets. Thus, the quality of any computational method, for example HF, DFT or CCSD(T), in predicting gas-phase or solution-phase NMR properties could be assessed from an error of the CBS value from experiment, when all aforementioned effects are considered (the ZPVC, the TC, RCs, and the solvent effect). According to earlier studies, the quality of theoretical predictions of experimental chemical shifts also depends on the following factors: (1) selection of a proper (similar) reference compound [6,51,52]; (2) statistical treatment of possible conformers, especially those stabilized by intramolecular H bonds [7,8]; and (3) proper inclusion of an explicit solvent effect, especially for polar protic solvents [51,52]. In the latter case, the compromise of including only the first solvation/hydration sphere is useful. This can significantly change the order of various signals in the theoretically predicted NMR spectrum and accurately reproduce the experimental image [53].

The aim of this study is to find a simple remedy to improve the irregular convergence patterns towards CBS of nuclear shielding tensors of simple molecules (or atoms) preferentially containing the third-row elements, calculated with the aug-cc-pVXZ basis set families, leading to the exponential-like behavior of the calculated NMR parameters. All benchmark NMR calculations were performed for free molecules in the gas phase and the results were compared with available experimental data (the solvent effect was not considered). However, ZPV, TC and RC corrections were included for direct comparison of theoretical results with experiment.

#### 2. Results

For the convenience of the reader, we will use several abbreviations, including basis sets, instead of their full names in the following sections. All abbreviations are summarized in Table 1.

Table 1.	List of appl	ied basis set	s and their	abbreviations.
IUDIC I.	List of appr	ica basis sci	s and then	abbititions

Basis Set/Full Name	Abbreviation	
(aug)-cc-pVXZ	(a)XZ	
(aug)-cc-pCVXZ	(a)CXZ	
(aug)-cc-pwVXZ	(a)wXZ	
(aug)-cc-pwCVXZ	(a)wCXZ	
aug-pc-n	арсп	
aug-pcSseg-n	apcSseg <i>n</i>	
aug-pcJ-n	apcJn	
Karlsruhe-type basis set	x2c-Def	
x2c-SVPall-s	x2cSV	
x2c-TZVPPall-s	x2cTZ	
x2c-QZVPPall-s	x2cQZ	
Complete basis set limit	CBS	
Zero-point vibration correction	ZPVC	
Temperature correction	TC	
Relativistic correction	RC	
Gauge-including atomic orbital	GIAO	
Polarized continuum model of solvent	PCM	

# 2.1. Sensitivity of Total Shieldings of the Third-Row Nuclei to the Basis Set Quality

We have recently reported the irregular basis set convergence of theoretical <sup>31</sup>P isotropic shieldings of PN, calculated using the Hartree–Fock, but also DFT and coupled-

Molecules **2022**, 27, 8230 5 of 22

cluster methods [15]. We obtained such irregularity for Dunning aug-cc-pVXZ or aug-cc-pV(X+d)Z basis sets, while a smooth convergence was observed for the core-valence aug-cc-pCVXZ basis set. On the other hand, we achieve a smooth basis set convergence of <sup>15</sup>N NMR shieldings in PN with all the basis set families [15]. We decided to inspect whether the irregularity observed for <sup>31</sup>P in PN is a general behavior of all elements of the third row. Therefore, we extended our test set by small systems (mainly hydrides) containing magnetic active nuclei of the third row, namely <sup>23</sup>Na, <sup>25</sup>Mg, <sup>27</sup>Al, <sup>29</sup>Si, <sup>31</sup>P, <sup>33</sup>S, <sup>35</sup>Cl, and <sup>39</sup>Ar as a free atom, and calculated their isotropic shieldings using various methods and basis set families. We will discuss most of the findings of an important NMR nucleus, <sup>31</sup>P, as an example, using the three model molecules. The results for other third-row nuclei will be briefly summarized afterwards.

# 2.1.1. Sensitivity of <sup>31</sup>P NMR Parameters to the Basis Set Quality

As model compounds for a thorough analysis of  $^{31}P$  nuclear shieldings, we have selected systems where phosphorus is joined to other atoms by a single or multiple bond. A popular hydride,  $PH_3$  contains only three single bonds. As a system with a double bond, we picked up phosphine oxide,  $H_3PO$ . We also extended our recent study on another molecule, PN, present in the interstellar space [15]. Note that the bond in PN, a molecule also briefly discussed here, is not strictly speaking a triple bond, but rather something between a double and a triple bond [15].

For brevity, most individual data discussed in this section are gathered in tables and figures in the Supplementary Material, as indicated in the text.

First, individual <sup>31</sup>P nuclear shielding values for PH<sub>3</sub>, calculated with the SCF-HF, B3LYP and CCSD(T) methods and with four selected basis set series (the aug-cc-pVXZ, augcc-pCVXZ, aug-pcSseg-n and x2c-XZVPall-s basis set families) are gathered in Table S1A. Total energies of phosphine calculated at the B3LYP and CCSD(T) levels with two selected correlation-consistent basis sets are included in Table S1B. In Figure S1, we can see a regular convergence of the B3LYP/aug-cc-pVXZ and B3LYP/aug-cc-pCVXZ energies for PH3 towards the complete basis set limit. On the contrary, Figure 1 displays quite irregular convergence patterns of NMR shielding constants for <sup>31</sup>P in PH<sub>3</sub>, calculated with the HF-SCF, B3LYP, and CCSD(T) methods and the aug-cc-pVXZ basis set, unsuitable for any extrapolation with more than than two-points to the CBS limit. Calculated isotropic shieldings (obtained, e.g., at CCSD(T)/aug-cc-pVXZ; cf. Table S1A) change upon increasing the basis set size by:  $\Delta = -44$ , 5, -29, and 0.3 ppm, respectively, where  $\Delta$  is calculated for  $T \rightarrow D$ ,  $Q \rightarrow T$ ,  $S \rightarrow Q$ , and  $S \rightarrow S$ . On the other hand, shieldings obtained with the Dunning core-valence basis set family smoothly converge towards the CBS limit, following the exponential decay curve (e.g., see converging HF-SCF data for X = T, Q and S in Figure 1A). The estimated CBS <sup>31</sup>P isotropic nuclear shielding, calculated at the CCSD(T)/aug-ccpCVXZ level of theory in  $PH_3$  is 603.326 ppm (see Table S1A). When vibrational, thermal, and relativistic corrections were included (see Table 4), we obtained the final CCSD(T) value of 611.38 ppm. Apart from aug-cc-pCVXZ, the Jensen aug-pcSseg-n basis set hierarchy also yields a regular and smooth convergence (see Figure 1) of phosphorus shielding towards the CBS limit (580.892 ppm for HF-SCF, 557.661 ppm for B3LYP, and 588.578 ppm for CCSD(T)). It is important that these results are nearly converged already for aug-pcSseg-2, with only 128 basis functions. The last tested basis sets are from the Karlsruhe family. These basis sets are relatively small (45, 96 and 172 basis functions for x2c-SVPall-s, x2c-TZVPPall-s, and x2c-QZVPPall-s, resp.). All of these basis sets provide shieldings that are fairly close to the CBS limit estimated with the aug-cc-pCVXZ and aug-pcSseg-n series (see Figure 1 and Table S1A). The approximate CBS limit, estimated using the Karlsruhe basis sets, is 601.348 ppm (the CCSD(T) level). Nevertheless, we cannot call the convergence smooth in this series due to the small number of values.

Molecules **2022**, 27, 8230 6 of 22

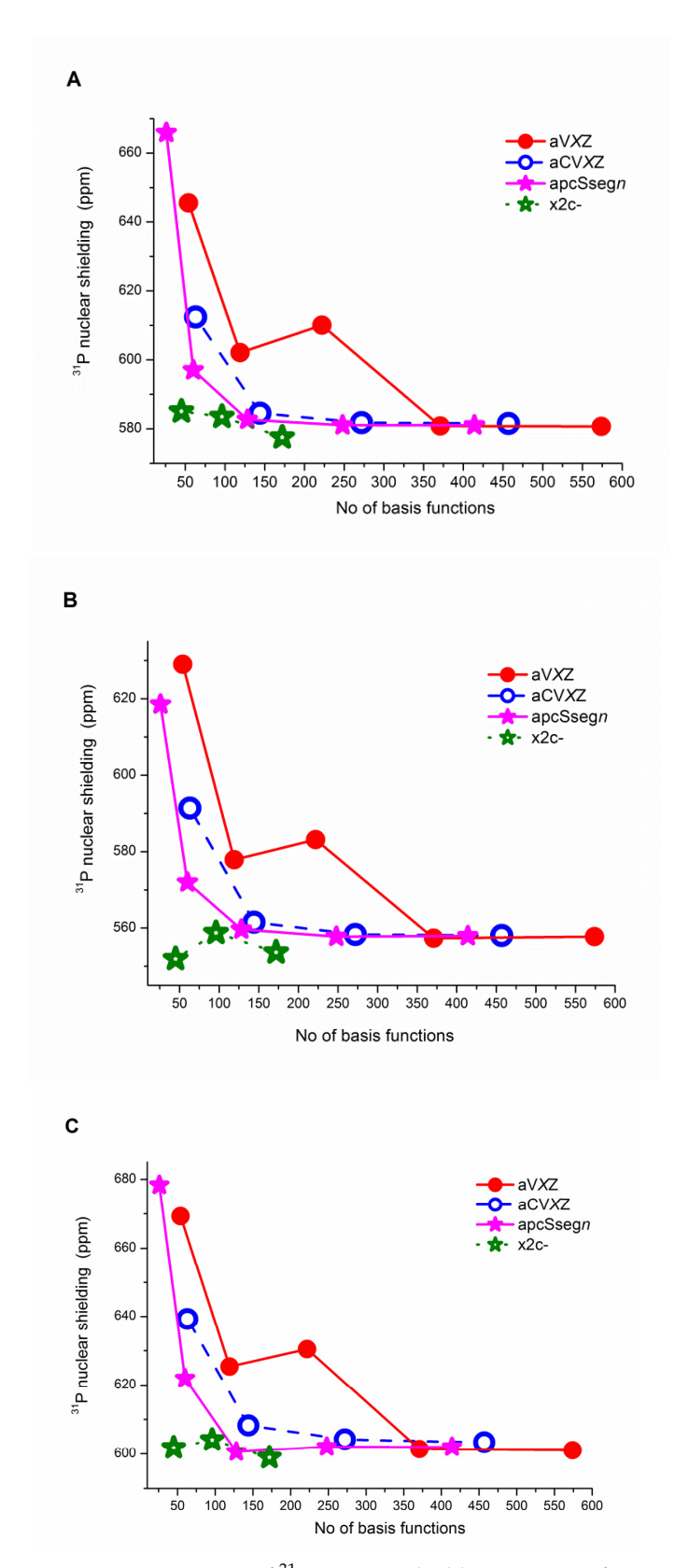


**Figure 1.** Convergence of  $^{31}$ P isotropic shielding constants for PH<sub>3</sub> vs. the number of basis functions, calculated with the (**A**) HF-SCF, (**B**) B3LYP and (**C**) CCSD(T) methods combined with the aug-cc-pVXZ, aug-cc-pCVXZ, aug-pcSseg-n and x2c-XZVPall-s basis set families.

To extend our recent study on <sup>31</sup>P NMR shieldings of PN [15], we performed here additional DFT-B3LYP calculations to also determine the sensitivity of individual shielding

Molecules **2022**, 27, 8230 7 of 22

components, isotropic and anisotropic shieldings of P and N nuclei to the selected basis sets and their size (Tables S2–S4) if calculated at the DFT level. In Figures S2 and S3, the B3LYP/aug-cc-pVXZ-calculated  $^{31}$ P shielding constants and their components are shown according to the cardinal number X (Figure S3A) and the number of basis functions (Figure S3B). Note that the shielding convergence patterns plotted against X or the number of basis sets are essentially the same. We observed significantly scattered results obtained with aug-cc-pVXZ basis for X = D, T and Q, and only the results for X = 5 and 6 seem to converge to the complete basis set limit.

The analysis of components suggests that the main source of the irregularity originates in the paramagnetic contribution of the nuclear shielding. We inspected the diamagnetic (DSO) and paramagnetic (PSO) contributions to total phosphorus shielding in PN calculated at the B3LYP level with the aug-cc-pVXZ, aug-cc-pCVXZ, aug-pcSseg-n, aug-pc-n, and aug-pcJ-n basis sets (Table S2B). We can see that while DSO calculated with the aug-ccpVXZ basis set converges relatively smoothly, PSO exhibits the scattering of data. As expected, the results obtained with the aug-cc-pwCVXZ basis set family, better describing the core-valence electrons, provide less scattered shielding components upon increasing the basis set size. The shielding components calculated with the latter basis set family are also more regularly converging toward the CBS limit. For brevity, similar correlation patterns of <sup>31</sup>P nuclear shielding components in PN, obtained with aug-cc-pCVXZ, aug-ccpwCVXZ, aug-pc-n, aug-pcJ-n and aug-Sseg-n basis sets vs. X are shown in Figure S3A in the Supplementary Material (see also Table S2A). No matter whether we plot the shielding components against X or the number of basis functions, the same convergence pattern was observed (Figures S2 and S3), only for the latter case, the size of individual basis sets is more imaginable. Note the break on the y-axis and different scaling for individual components in Figures S2 and S3; thus, the  $\sigma_{xx}$  component varies by approximately 160 ppm, while  $\sigma_{zz}$  changes only by approximately 1 ppm.

It is also apparent from Figures S2 and S3 that the NMR results obtained with the aug-cc-pVXZ basis sets are highly scattered and unreliable for X = D, T and Q and evince saturation for X = 5 and 6. On the other hand, the results obtained with the core-valence basis sets (aug-cc-wCVXZ) regularly converge within the whole set, reaching values close to CBS already for aug-cc-wCVTZ. Thus, highly reliable  $^{31}P$  shielding components for larger system can be achieved with properly chosen core-valence triple- $\zeta$  basis set. Considering the performance of Jensen basis sets, all available series converge exponentially, perform fairly well and the CBS values are within  $\pm 5$  ppm from each other (see Table 2 and Figure S4). Obviously, results obtained with Jensen basis sets using too small values of n (0 and 1) are unreliable. Finally, one can observe that the Douglas–Kroll modification of polarized-valence Dunning-type basis sets also produces scattered  $^{31}P$  shieldings for PN (Figure S5).

Detailed comparison of the B3LYP/CBS values of <sup>31</sup>P NMR parameters obtained for PN with selected basis set families are in Table 2. In general, the CBS values, estimated according to *X* (see Table S4) or the numbers of basis functions (Table 3), are very similar and differ by less than 1%. Only in the case of isotropic shielding calculated with the aug-cc-pV*XZ* and aug-pcJ-*n* basis set families are the differences slightly larger (4.4 and 7.0%). Corresponding <sup>15</sup>N CBS values of PN are significantly closer to each other and differ by less than 0.5%. Gathered NMR parameters are also compared with earlier reported values. As expected, the <sup>31</sup>P nuclear isotropic shielding calculated at the B3LYP level is nearly 120 ppm smaller than the CCSD(T) results, but the shielding anisotropy is approximately 180 ppm larger. Obviously, the DFT methods usually do not provide reliable predictions of <sup>31</sup>P NMR parameters [4]. However, in the current study, we aimed at converged results close to the CBS limit for a selected method and at the behavior of calculated values with increasing basis set, rather than at precise predictions of a particular NMR property.

Molecules **2022**, 27, 8230 8 of 22

**Table 2.** Calculated B3LYP/CBS  $^{a\ 31}$ P and  $^{15}$ N nuclear shielding components, isotropic shieldings and shielding anisotropy of PN  $^{b}$  with respect to the number of basis functions (b.f.).

		31	l P			15	5N	
CBS Type	$\sigma_{xx}$	$\sigma_{zz}$	$\sigma_{iso}$	$\sigma_{aniso}$	$\sigma_{xx}$	$\sigma_{zz}$	$\sigma_{iso}$	$\sigma_{aniso}$
			aVX	Z				
(5-6)	-575.605	966.522	-61.563	1542.127	-829.620	341.858	-439.128	1171.478
			aCV	ΧZ				
(Q-5)	-572.407	966.332	-59.494	1538.739	-827.668	341.860	-437.825	1169.527
			awCV	XXZ				
(Q-5)	-572.721	966.333	-59.703	1539.052	-828.236	341.860	-438.204	1170.095
			Apc	n				
(3-4)	-572.069	966.686	-59.150	1538.755	-829.711	341.862	-439.186	1171.573
			apcSs	egn				
(3-4)	-572.596	966.399	-59.598	1538.995	-828.249	341.870	-438.210	1170.119
			apcJ	n				
(3-4)	-573.360	966.087	-60.210	1539.447	-828.154	341.853	-438.151	1170.007
Method				Liter	ature			
CCSD(T)/aVXZ c			58.080	1362.090				
CCSD(T)/aCVXZ <sup>c</sup>			59.090	1361.250				
B3LYP/6-311++G** <sup>d</sup>			-57.48				-406.54	
CCSD(T)/15s12p4d3f2g e			49.0					

<sup>&</sup>lt;sup>a</sup> Basis sets selected for fitting are in parenthesis (e.g., CBS(5-6) is calculated using the Dunning basis sets aV5Z and aV6Z; for Jensen basis sets, CBS(3-4) denotes extrapolation with apc3 and apc4). <sup>b</sup> All NMR calculations were performed using the CCSD(T)/aug-pc-4 geometry (1.49466464  $^{\circ}$ ). <sup>c</sup> From [15]. <sup>d</sup> From [54], where the authors also cited the experimental value of 53.0 ppm. <sup>e</sup> From [55].

**Table 3.** Calculated CBS nuclear shielding values (in ppm) for studied species <sup>a,b</sup>.

Methods	HF-SCF	B3LYP	CCSD(T)	$\Delta$ (%) from	n CCSD(T)
				SCF	B3LYP
		N	аН		
aVXZ(T-5)	562.384	565.305	549.057	2.4	3.0
aCVXZ(T-5)	565.269	572.698	569.555	-0.8	0.6
apcSseg- $n(2-4)$	565.478	572.789	572.180	-1.2	0.1
1 0 . ,		M	$gH_2$		
aVXZ(T-5)	475.048	397.813	441.802	7.5	-10.0
aCVXZ(T-5)	462.948	426.089	447.156	3.5	-4.7
apcSseg- $n(2-4)$	460.706	426.588	443.87	3.8	-3.9
1 0 \ /		A	$lH_3$		
aVXZ(Q-6)	340.417	260.370	301.061	13.1	-13.5
aCVXZ(T-5)	346.671	267.211	307.762	12.6	-13.2
apcSseg- $n(2-4)$	344.362	265.630	305.775	12.7	-13.1
1 0 ( )		Si	$iH_4$		
aVXZ(T-5)	489.275	445.37	483.294	1.2	-7.8
aCVXŽ(T-5)	477.703	435.416	470.854	1.5	-7.5
apcSseg- $n(2-4)$	473.790	434.990	468,972	1.0	-7.2
1 9 ()			≡ CH		
aVXZ(T-5)	917.646	498.605	619.338	48.2	-19.5
aCVXZ(T-5)	907.666	501.293	630.101	44.1	-20.4
apcSseg- $n(2-4)$	915.536	501.697	628,762	45.6	-20.2
	, 20.000		H <sub>3</sub>		
aVXZ(Q-6)	576.501	553.876	596,957	-3.4	-7.2
aCVXZ(T-5)	581.367	557.847	603.326	-3.6	-7.5
apcSseg-n(2-4)	580.892	557.661	588.578	-1.3	-5.3
			3PO	-10	
aVXZ(5-6)	398.514	349.201	-	-	-
aCVXZ(T-5)	397.276	346.109	-	-	_
apcSseg- $n(2-4)$	396.549	347.681	-	-	-

Molecules **2022**, 27, 8230 9 of 22

Table 3. Cont.

Methods	HF-SCF	B3LYP	CCSD(T)	$\Delta$ (%) fron	CCSD(T)
				SCF	B3LYP
		Pi	y a		
aVXZ(5-6)	-91.460	-58.882	58.080	-257.5	-201.4
aCVXZ(5-6)	-91.560	-60.030	59.090	-255.0	-201.6
apcSseg- $n(3-4)$	-90.720	-58.833	58.780	-254.3	-200.1
1 0		Н	$_2$ S		
aVXZ(Q-6)	708.776	694.933	736.852	-3.8	-5.7
aCVXZ(T-5)	712.644	698.246	741.209	-3.9	-5.8
apcSseg- $n(2-4)$	715.929	698.071	742.245	-3.5	-6.0
1 0		Н	Cl		
aVXZ(Q-6)	944.476	930.256	955.745	-1.2	-2.7
aCVXZ(T-5)	931.858	946.403	957.943	-2.7	-1.2
apcSseg- $n(2-4)$	946.06	931.705	957.3498	-1.2	-2.7
1 0		A	\r		
aVXZ(Q-6)	1237.659	1238.172	1237.509	0.0	0.1
aCVXZ(T-5)	1237.660	1237.868	1237.924	0.0	0.0
apcSseg- $n(2-4)$	1237.534	1237.930	1237.516	0.0	0.0

<sup>&</sup>lt;sup>a</sup> Results of this work and partially from [15]. <sup>b</sup> CBS(5-6) denotes Dunning-type basis set extrapolation using V5Z and aV6Z. CBS(2-4) obtained with Jensen basis sets is constructed with apc2, apc3 and apc4.

Similar to PN, we wanted to inspect whether an analogously irregular convergence pattern of <sup>31</sup>P shielding is also obtained for other P-containing molecules with multiple bonds when the aug-cc-pVXZ family is used. Phosphine oxide includes a double P=O bond and their shielding differs markedly from PH<sub>3</sub>. For brevity, the individual <sup>31</sup>P nuclear shieldings for H<sub>3</sub>PO calculated at the B3LYP, HF, and partially also at the CCSD(T) level with the aug-cc-pVXZ, aug-cc-pCVXZ, and aug-pc-Sseg-*n* basis sets are gathered in Table S5A and shown in Figure S6. Once again, the nuclear shieldings obtained using Dunning valence basis sets are scattered and do not follow a smooth convergence pattern. On the contrary, NMR parameters predicted with polarized-consistent basis sets show regular convergence. Due to convergence problems, we did not obtain the full series of the CCSD(T) values for all basis sets (see Table S5A). However, it is already evident that <sup>31</sup>P shieldings at HF match the CCSD(T) values.

#### 2.1.2. Other Third-Row Elements

On concluding the analysis of <sup>31</sup>P nuclear shieldings convergence in selected systems, we will perform a brief analysis of nuclear shieldings for other third-row elements. We start with the <sup>23</sup>Na NMR parameters of NaH calculated using the Hartree–Fock, B3LYP, and CCSD(T) methods and various basis sets. In addition, we calculated <sup>23</sup>Na nuclear shieldings for NaF using the B3LYP hybrid function combined with the aug-cc-pVXZ, aug-cc-pCVXZ, and aug-pcsSeg-*n* basis set families. Then, we will move to hydrides of the remaining elements calculated at various levels of theory as indicated in the text. The tests will end with hypothetical NMR parameters predicted for an isolated argon atom. Indeed, the NMR-active <sup>39</sup>Ar isotope does not exist in nature but analysis of its hypothetical NMR parameters will complete the GIAO NMR studies of the third-row elements. Obtained results will be commented only briefly, but the fully detailed text is in Supplementary Materials (Sections S1.1–S1.7).

Before we analyze all calculated shieldings, we tested the eligibility of the B3LYP geometries in further calculations of NMR shieldings of the third-row elements. NaH served us as a model system. First, we calculated interatomic distances of NaH at the B3LYP level with the cc-pVTZ and cc-pCVTZ basis sets and compared them with the CCSD(T) geometries obtained with the same basis sets. Reported [56] distances for the CCSD(T)/cc-pVTZ and CCSD(T)/cc-pCVTZ levels were 1.916  $A^{\circ}$  and 1.893  $A^{\circ}$ , respectively. We observed slightly shorter distances for the B3LYP but also for the CCSD(T)—1.8832  $A^{\circ}$  (B3LYP/aug-cc-pVTZ), 1.8801  $A^{\circ}$  (CCSD(T)/aug-cc-pVTZ), and

Molecules **2022**, 27, 8230 10 of 22

1.8947 A° (CCSD(T)/aug-cc-pCVTZ). Later, we obtained Na–H distances of 1.8808 A° and 1.8811 A° at the B3LYP/aug-cc-pV5Z and B3LYP/aug-cc-pCV5Z levels that are very close to the CCSD(T) values. These values are also close to the experimental distance of 1.8874 A° [56]. Subsequent estimations of  $^{23}$ Na nuclear shieldings at the B3LYP/aug-cc-pV5Z level of theory for the B3LYP/aug-cc-pV5Z and B3LYP/aug-cc-pCV5Z geometries provide similar values of 559.698 and 559.729 ppm. Note also that the calculated CCSD(T) nuclear shieldings achieved for the DFT and CCSD(T) geometry (quintuple- $\zeta$  basis set) were very close (541.910 and 540.964 ppm, respectively). Thus, the B3LYP/aug-cc-pV5Z geometries appear to be good estimates achievable relatively easily and will be used to gain 3D structures of several other model compounds (NaH, NaF, MgH<sub>2</sub>, AlH<sub>3</sub>, and HCl) in this study. However, for the sake of comparison with earlier studies, the PN, PH<sub>3</sub>, SiH<sub>4</sub> and H<sub>2</sub>S geometries from recent reports [15,56,57] were used.

The <sup>23</sup>Na nuclear shielding values calculated at the B3LYP/aug-cc-pVXZ and B3LYP/aug-cc-pCVXZ levels for NaH are gathered in Table S6A. For a better perspective, the convergence patterns of <sup>23</sup>Na isotropic shieldings of NaH calculated at the HF-SCF, B3LYP-DFT and CCSD(T) levels of theory and with the aug-cc-pVXZ, aug-cc-pCVXZ, aug-pcSseg-*n* and x2c-Def2 basis set families are shown in Figure S7. Similarly to <sup>31</sup>P, the aug-cc-pVXZ series produces scattered <sup>23</sup>Na isotropic shieldings, while a smooth convergence is seen for the aug-pcSseg-*n* family. Interestingly, despite their small size, the x2c-Def2 basis family performs fairly accurate in comparison to Jensen or core-valence basis. We observed the analogous behavior of <sup>23</sup>Na shieldings for another sodium-containing molecule, NaF (Table S6A, Figure S8). Note that energies for all calculated sodium models exhibit presumed exponential patterns (see Table S6B, Figure S9).

We observed analogous basis set convergences of isotropic shieldings also for <sup>25</sup>Mg (MgH<sub>2</sub>), <sup>27</sup>Al (AlH<sub>3</sub>), <sup>29</sup>Si (SiH<sub>4</sub>), <sup>33</sup>S (H<sub>2</sub>S), and <sup>35</sup>Cl (HCl). In all cases, the Dunning basis set family provided irregular convergence patterns, whereas other tested basis sets behave as expected, giving smooth (exponential-like) patterns. All isotropic shieldings calculated at various levels are summarized in Table S7A (MgH<sub>2</sub>), Table S8A (AlH<sub>3</sub>), Table S9A (SiH<sub>4</sub>), HSi  $\equiv$  CH [58] (Table S9C), Table S10A (H<sub>2</sub>S), and Table S11A (HCl). For a better idea of different convergences, we plotted the CCSD(T) shieldings obtained with different basis sets in Figure S10A (MgH<sub>2</sub>), Figure S11A (AlH<sub>3</sub>), Figure S12A (HF-SCF results for SiH<sub>4</sub>), Figure S13A (H<sub>2</sub>S) and Figure S14A (HCl). In Figure S12C, the results of B3LYP calculations with augcc-pVXZ and aug-pcSseg-n basis sets for <sup>29</sup>Si nuclear shieldings in the Hsi  $\equiv$  CH molecule are graphically presented. Corresponding energy estimates of all systems are gathered in Tables S7B, S8B, S9B, S10B, and S11B or Figures S10B, S11B, S12B, S13B and S14B. Similarly to phosphorus, all tested basis sets provided smooth convergence patterns of estimated energies (all systems) with increasing basis set size. Interestingly, the difference between shieldings calculated using the highest Dunning basis set (aug-cc-pV5Z) and the lowest basis set (aug-cc-pVDZ) usually depends on the level of theory. For example, we observe for <sup>25</sup>Mg  $(MgH_2)$  the difference of -35, -98 and -73 ppm for HF-SCF, B3LYP, CCSD(T), respectively. Since the <sup>25</sup>Mg CBS value is approximately 400 ppm (see Table 3), this means that these differences account for 8 to 25% of the CBS value. As indicated above, the differences between values calculated with consecutive Dunning basis sets change unpredictably producing a scattered convergence pattern. For example, <sup>27</sup>Al isotropic shieldings in AlH<sub>3</sub> calculated at the CCSD(T)/aug-cc-pVXZ level vary by -74, -4, -15 ppm for  $X = T \rightarrow D$ ,  $Q \rightarrow T$  and  $5 \rightarrow Q$ , respectively. The absolute changes (but also relative to the CBS value) according to increasing basis set size depend on the individual methods (see Tables S7A, S8A, S9A, S10A and S11A, and Sections S1.1–S1.7 for more comments on individual data).

Table S12A analogously summarizes NMR shieldings for isolated Ar, as calculated using different methods and basis sets. Figure S15A then depicts the shielding convergence patterns corresponding to the different basis sets. Contrary to the aforementioned hydrides, we can see a fairly regular convergence pattern of <sup>39</sup>Ar shielding even for the aug-cc-pVXZ family. Changes in the shielding with increasing basis set size are rather cosmetic (less than 0.1% of the CBS value). On the other hand, smaller Karlsruhe basis sets provided

Molecules 2022, 27, 8230 11 of 22

<sup>39</sup>Ar shieldings more distinct from the CBS value resulting thus in an unusually scattered convergence pattern. Nevertheless, even the highest change between consecutive shieldings does not exceed 1% of the CBS value. Estimated energies for Ar are gathered in Table S12B and Figure S15B revealing their standard convergence for all methods and basis sets.

#### 2.1.3. Estimated CBS Nuclear Shielding Values of the Studied Systems

As documented in most figures (see, e.g., Figures 1, S5, S6 or S7), theoretical isotropic shielding constants for individual third-row nuclei estimated with double- $\zeta$  quality basis sets are problematic. The aug-cc-pVDZ values are far from the fitted CBS values and also from the convergence trendline estimated using the triple- $\zeta$ , quandruple- $\zeta$ , and quintuple- $\zeta$  basis set. Although the aug-cc-pCVDZ results more or less follow trends estimated using larger basis sets, they are still far from the convergence. Therefore, any reasonable CBS isotropic shielding of the third-row elements should be estimated excluding the double- $\zeta$  data. The CBS nuclear shieldings estimated using the 2-parameter fit of values obtained with the aug-cc-pVXZ and aug-cc-pCVXZ basis sets at the HF-SCF, B3LYP, and CCSD(T) levels are summarized in Table 3. The table also reveals the CBS values estimated using the Jensen basis sets. Corresponding CBS shieldings for the Karlsruhe x2c-XZVPPall-s basis sets can be found in Tables S5A–S12A.

We can observe a difference of nuclear shieldings calculated with the core-valence and valence basis sets. Nevertheless, the difference does not exceed for any molecule and any method 7% of the CBS(aug-cc-pCVXZ) value. This difference is due to the overestimation of shieldings obtained with smaller aug-cc-pVXZ (X = D, T, and even Q) basis sets that as a result deteriorates the finals CBS(aug-cc-pVXZ) value, as documented in Tables S5A–S12A. Therefore, we can consider the results obtained with the aug-cc-pVXZ basis set family less reliable. On the other hand, both basis set families produced very similar results for isolated argon atom.

The impact of the electron correlation on calculated nuclear shieldings of the third-row elements can be clearly demonstrated by comparing the HF-SCF and CCSD(T) values of the molecules studied (see the  $\Delta$  values in Table 3). The most significant discrepancy between the HF and coupled cluster results is observed for PN ( $\sim$ 250%) and Hsi  $\equiv$  CH (>40%). In both compounds, the element of interest is bonded by a triple bond (the PN bond is, strictly speaking, something between a double and triple bond). This  $\Delta$  is comparable for all tested basis set families. A significant deviation is also observed for AlH<sub>3</sub> (approximately ~13%). We can assume that the importance of electron correlation for accurate prediction of nuclear shieldings of the third-row elements increases, especially when these atoms are bonded to other atoms by a multiple bond. On the other hand, we were not able to achieve the full set of the CCSD(T) shieldings for H<sub>3</sub>PO (due to convergence problems) that would confirm this assumption. However, partial data show that HF provides shieldings very close to CCSD(T), in contrast to B3LYP with an average error of ~10%. As observed before, the differences of the CBS values for the Hartree–Fock, B3LYP, and coupled cluster methods are negligible for argon [32]. Interestingly, the  $\Delta$  compared for HF-SCF and B3LYP indicates the slightly better performance of the Hartree-Fock method than B3LYP for saturated molecules. This could be due to overestimation of paramagnetic term of shielding by B3LYP (see [4,59,60]).

#### 2.2. <sup>33</sup>S shielding Components and Total Shielding of 2-Thiouracil (2-TU)

So far, we have mostly discussed systems where the heavy element was bonded with hydrogen (with the exception of HSiCH, PN, and  $H_3PO$ ). In this section, we will deal with a more realistic molecule containing a third-row element and other heavy atoms. Uracil is an important component related to information transfer and replication in living systems. Its 5-halogen modifications are used in anticancer and antifungal treatment [59,61–63]. Modifications of uracil, including replacing the oxygen atom with sulfur [64], also changes its biological activity. The presence of a sulfur atom can be exploited to easily identify the molecule by  $^{33}$ S NMR. Therefore, accurate theoretical predictions of sulfur shielding tensor in 2-thiouracil (2-TU)

Molecules **2022**, 27, 8230 12 of 22

are valuable to help clarify the structure-spectrum relationship. The size of this molecule makes NMR calculations at the CCSD(T) level unavailable; therefore, all calculations had to be performed at the DFT (B3LYP) level as a reasonable compromise. The previously reported use of a relatively small basis set [65] (6-31G\* containing 132 basis functions) for all atoms allowed fast but inaccurate calculations of nuclear shieldings of 2-thiouracil. To improve calculation reliability, we will show the effect of the locally dense basis set (LDBS) approach [66–69], where only the atom of interest is described with a higher basis set, while the rest of the molecule is described with some low-level basis set. Here, within the LDBS approach, all atoms were calculated with the 6-31G\* basis set, while the aug-cc-phisVXZ basis set families are employed for sulfur (see Table S10C in Supplementary Materials). Note that the complete description of 2-thiouracil with, e.g., a very reliable aug-cc-pCV5Z basis set containing 1804 basis functions, lies beyond any practical use. On the other hand, the proposed LDBS approach with, e.g., aug-cc-pCV5Z/6-31G\* basis sets, requires only 323 basis functions.

The corresponding  $^{33}$ S isotropic shielding estimated by the B3LYP/6-31G\* calculation was 335 ppm compared to 258 ppm obtained at the B3LYP/aug-cc-pCV5Z level. The total CPU time for the former level was 3.5 min and was almost 20 days for the latter. Using the LDBS approach (aug-cc-pCV5Z/6-31G\*), we obtained the  $^{33}$ S isotropic shielding of approximately 287 ppm (see Figure 2), which is much closer to the full aug-cc-pCV5Z value of 258 ppm. At the same time, a very impressive reduction in CPU time was observed, which dropped to 27.5 min. Figure 2 also compares convergence patterns of the  $^{33}$ S isotropic shieldings for 2-TU calculated at the B3LYP level with the aug-cc-pVXZ and aug-cc-pCVXZ basis sets. For the first family of basis sets, we observe a scatter of calculated values comparable to H<sub>2</sub>S, while a smooth convergence is evident for the latter. Same behavior can be noticed if we employ the LDBS approach (Figure 2B). The change in estimated CBS values due to the LDBS approach is ~10% of the CBS value when all atoms were described using aug-cc-pVXZ or aug-cc-pCVXZ.

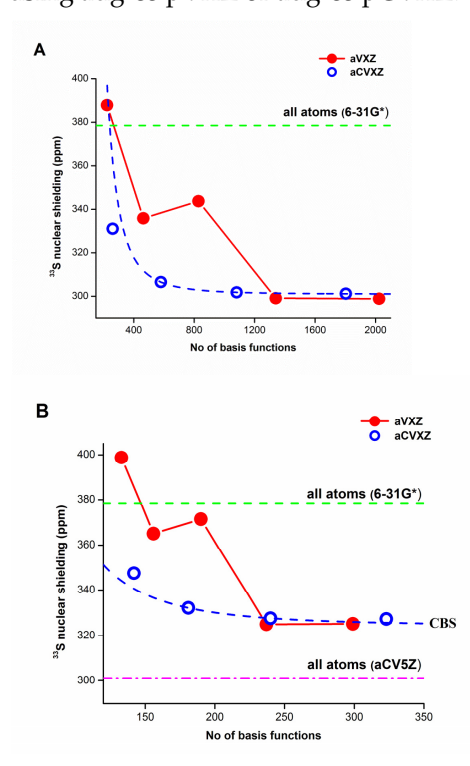


**Figure 2.** <sup>33</sup>S nuclear isotropic shielding constants of 2-thiouracil calculated at the **(A)** B3LYP/aug-cc-pVXZ and B3LYP/aug-cc-pCVXZ levels of theory, and **(B)** using the LDBS approach, where only the sulfur atom was described using either the aug-cc-pVXZ or aug-cc-pCVXZ and 6-31G\* basis set on H, C, N and O atoms. The green dashed line indicates the value obtained at the B3LYP/6-31G\* level. The pink dash-and-dot line on the right shows the value obtained at the B3LYP/aug-cc-pCV5Z level (all atoms).

Molecules **2022**, 27, 8230 13 of 22

#### 2.3. Corrections to Isotropic Nuclear Magnetic Shieldings of Third Row Elements

We compared our best isotropic shieldings for all our molecules that were estimated using the CCSD(T)/aug-cc-pCVXZ data with available literature data in Table 4. It has been documented before that the equilibrium value (calculated for the optimized geometry) is often not precise enough, as vibrational effects, thermal effects, or relativistic corrections may become significant, especially for heavier elements [47,48,50,70,71].

Therefore, our CCSD(T)/CBS values were later corrected by the zero-point vibrational, thermal and relativistic corrections (the TC and the RC). Thus, the final values were obtained as: final value = equilibrium CCSD(T)/CBS  $\sigma$  + ZPVC + TC + RC. Our correction terms were also compared with available reported corrections (see Table 4). Note, there are no available equilibrium shieldings reported in the literature for NaH, MgH<sub>2</sub>, AlH<sub>3</sub>, H<sub>3</sub>PO, or HSi  $\equiv$  CH. Jaszunski et al. performed accurate coupled cluster estimates of nuclear shielding also considering the ZPVC and the TC for SiH<sub>4</sub> [57], PH<sub>3</sub> [55,57], H<sub>2</sub>S [57], and HCl [72]. The relativistic effects on the total shielding value were considered only for HCl [72]. Argon nuclear shieldings were studied by Hada [73]. Sauer et al. also estimated the relativistic contribution to the argon isotropic value [32].

We first discuss the TC and the ZPVC separately for hydrides, as the selected systems with multiple bonds ( $H_3PO$ ,  $HSi \equiv CH$ , and PN) appeared to be exceptional or even problematic. Note that the TC is negligible for all third-row element shieldings in the hydrides studied. The ZPVC estimated at the B3LYP/aug-cc-pVQZ level ranges from ~0.05% for the  $^{23}$ NaH to >4% for  $^{29}$ Si in SiH<sub>4</sub>. Other noticeable (>2%) ZPVCs were observed for MgH<sub>2</sub>, and H<sub>2</sub>S. All other ZPVCs were lower than 2% of the isotropic value. Interestingly, positive ZPVCs to isotropic shieldings were observed for NaH, MgH<sub>2</sub> and SiH<sub>4</sub>, while negative values were obtained for AlH<sub>3</sub>, PH<sub>3</sub>, H<sub>2</sub>S, and HCl. Note that the ZPVC may depend on the level of theory used for calculating the anharmonic potential and shielding derivatives. Therefore, we alternatively calculated the anharmonic force fields at the CCSD(T)/aug-pc-2 level and combined them with shielding derivatives at the BHandHLYP/aug-pcSseg-4 level. A similar combination of different levels for the anharmonic potential and for the property derivatives has previously been shown as an economical approach for reliable estimations of ZPVCs of medium-sized molecules [32,41,74]. We noticed significant differences between the fully B3LYP and the mixed ZPVCs, especially for SiH<sub>4</sub> (20.28 versus 1.85 ppm). Nevertheless, the higher B3LYP values still represent only ~2% of the total shielding value. In general, we consider the mixed approach closer to the fully coupled-cluster ZPVC value and thus likely more reliable for unsaturated molecules.

Predictions of the ZPVC for the selected molecules with multiple bonds, HSi  $\equiv$  CH, H<sub>3</sub>PO, and PN, appeared to be more interesting. Due to their nature, a standard perturbational approach used for calculating the ZPVC failed when some of the lowest vibrational modes were included in the PT2 formula. As a result, the unrealistic ZPVC or TC, as well as vibrational frequencies, were obtained. Therefore, we had to exclude the contribution of the two lowest vibrational modes for HSi  $\equiv$  CH, and even three lowest modes for H<sub>3</sub>PO. Even so, ZPVCs calculated using both methods (B3LYP and CCSD(T)/BHandHLYP) vary significantly. We obtained for example -0.69 ppm (B3LYP) and 30.77 ppm (CCSD(T)/BHandHLYP) for HSi ≡ CH. The ZPVC contribution thus makes -0.1% or 4.9% of the CCSD(T)/CBS equilibrium value. This discrepancy may be due to various reasons. For example, a different basis set convergence of the two methods, inadequate numerical steps in the ZPVC calculation, significant contribution of quartic constants, or more general failure of the methodology used. An even larger deviation is observed for  $H_3PO$ , where we calculated the ZPVC of -4.72 ppm (B3LYP) and 69.39 ppm (CCSD(T)/BHandHLYP), which makes -1.4% and 20.0% of the equilibrium value. Note that we were not able to obtain the CCSD(T)/CBS equilibrium value, only the B3LYP/CBS, and therefore the final percentage contribution may change. On the other hand, ZPVCs for PN are comparable for both methods. We conclude that ZPVC calculations for compounds with double or triple bonds deserve further investigation and we can only speculate that the B3LYP values reported here represent more reliable estimates.

Molecules **2022**, 27, 8230 14 of 22

**Table 4.** Zero-point vibrational, thermal, and relativistic corrections to NMR shieldings of the thirdrow elements (in ppm).

	NaH	MgH <sub>2</sub>	AlH <sub>3</sub>	SiH <sub>4</sub>	HSi≡CH	PH <sub>3</sub>	H <sub>3</sub> PO	PN	H <sub>2</sub> S	HCl	Ar
					Th	nis work					
Isotropic σ	569.56	447.16	307.76	470.85	628.76	603.33	389.34 *	59.09	741.21	957.94	1237.92
ZPVC <sup>mixed</sup>	1.03	6.61	-0.13	1.85	30.77	-5.60	69.39	-4.40	-21.12	-17.35	-
$ZPVC^{B3LYP}$	0.29	10.66	-1.06	20.28	-0.69	-10.81	-4.72	-6.21	-22.36	-18.29	-
TC (273K)	-0.01	1.36	0.01	-0.75	-1.30	-0.42	-0.15	-0.04	-0.51	-0.42	-
RCKT2	8.08	9.96	11.52	14.87	20.99	20.80	18.31	11.45	27.26	33.21	33.72
$RC^{B3LYP}$	7.74	9.97	11.97	14.92	25.84	18.86	22.35	12.37#	24.80	32.16	-
Final value	577.59	467.79	278.12	506.05	653.91	611.38	406.97	65.25	743.65	971.81	1271.64
					Li	terature					
Isotropic σ				470.64 <sup>a</sup>		605.83 a			737.92 <sup>a</sup>	961.92 <sup>f</sup>	1237.50 <sup>e</sup> ; 1237.76 <sup>g</sup>
ZPVC				$-1.41^{a}$		−9.50 <sup>c</sup>			-20.86 a	-17.09 f	
TC (273K)				0.01 a		$-0.32^{a}$			$-0.89^{a}$	$-0.59^{\text{ f}}$	
RC										31.82 <sup>f</sup>	37.52 <sup>e</sup> 1275.02;
Final value				469.24		596.01			716.17	976.06	1275.28; 1273.89 h
Exp. Total						594.45 <sup>d</sup>			717.24 <sup>a</sup>	-	
Ехр. σ				475.3 $\pm$ 10 $^{\rm b}$		−266.10 <sup>e</sup>					

Isotropic values—CCSD(T)/CBS results from the 2-parameter fit of the aug-cc-pCVXZ values. See Table 3 (\* for H3PO—the CCSD(T)/aug-cc-pCVQZ value); PVC<sup>mixed</sup>—CCSD(T)/aug-pc-2 //BHandHLYP/aug-pcSseg-4; ZPVCB3LYP/aug-cc-pVQZ; TC (at 273K)—B3LYP /aug-cc-pVQZ; RCKT2—KT2/pcS-3; RCB3LYP/aug-cc-pVTZ (for PN—the B3LYP /aug-cc-pVQZ value). Final value (this work) = isotropic  $\sigma$  + ZPVCB3LYP + TC + RCB3LYP. a [57] b [75]; c [55]; d [76]; e [77]; f [72]; g [78]; h [73].

As expected, the absolute relativistic correction (see Table 4) increases with atomic mass ranging from ~8 ppm for Na to ~33 ppm for Cl and Ar. Nevertheless, the RC accounts for 1.4–6.5% of the CCSD(T)/CBS equilibrium shielding value for most systems. Two different levels of theory for the RC were tested, yet both DFT approaches provide in most cases comparable results (see Table 4). Interestingly, AlH<sub>3</sub> and H<sub>3</sub>PO had a higher percentage relativistic contribution than H<sub>2</sub>S or HCl. The relativistic correction of PN was completely out of line with the others, accounting for 19% or 33% depending on the method. We estimated the basis set effect on the B3LYP RC for PN, where we obtained a larger contribution. The relativistic correction calculated at the B3LYP level and the aug-cc-pVXZ basis set, where X = D, T, and Q are summarized in Table S13. The double- $\zeta$  basis set provides obviously overestimated results, while the aug-cc-pVQZ value is close to the KT2/pcS-3 value. Nevertheless, the triple- $\zeta$  values may represent a good compromise between accuracy and price.

#### 3. Discussion

Convergence patterns of the third-row elements nuclear shieldings were tested using the SCF-HF, DFT-B3LYP and CCSD(T) methods combined with the aug-cc-pVXZ, aug-cc-pCVXZ, and several polarization-consistent Jensen-type basis set series. The shieldings calculated with the aug-cc-pVXZ basis set family show an irregular convergence towards CBS. An erratic convergence of nuclear shieldings calculated with aug-cc-pVXZ (X = D-5 or 6) was observed for a test set of the simple molecules (NaH, MgH<sub>2</sub>, AlH<sub>3</sub>, SiH<sub>4</sub>, HSi $\equiv$ CH, PH<sub>3</sub>, PN, H<sub>3</sub>PO, H<sub>2</sub>S, and HCl) and Ar atom studied. By improving the valence basis sets to core-valence, a regular (exponential) convergence of shieldings towards CBS could be observed. A similar improvement was also observed for shieldings calculated using the with Jensen-type basis set families.

On the contrary, a relatively smooth convergence was seen for the Ar atom and all basis sets. Such behavior has not been observed for nuclear shielding of lighter atoms, as evidenced, for example, by the example of the PN molecule [15]. In this work, we have demonstrated that the scattering convergence of the aug-cc-pVXZ shieldings holds for the entire third row. Based on our results, we therefore propose to use the core-valence basis

Molecules **2022**, 27, 8230 15 of 22

set families or the Jensen segmented contracted basis sets for calculations of shieldings of these nuclei, which could warrant the CBS estimations of NMR parameters shieldings being more reliable than results obtained using standard Dunning basis sets. The effect of electron correlation was relatively low (below 15%) for all the studied hydrides but increased significantly for systems with multiple bonds (PN, HSiCH). The incomplete results for  $H_3PO$ , on the other hand, show quite good results of the HF method compared to CCSD(T). We can only speculate whether this is just a fortuitous error cancellation or an exception to the rule, and additional calculations on other molecules with multiple bonds are needed.

We also evaluated the effect of vibrational, temperature, and relativistic corrections to nuclear shieldings of the third-row elements considering them as additive factors to the equilibrium CBS values. For systems with single bonds, all corrections are rather small, being less than 4% of the CCSD(T)/CBS value estimated using the core-valence basis sets. The ZPVC and TC estimates were difficult for H<sub>3</sub>PO and HSiCH due to their high anharmonicity and/or method failure and different levels provided significantly different values. On the other hand, this was not observed for PN, where comparable ZPVCs were achieved regardless of what level of theory was used. Interestingly, we obtained the highest relativistic correction to nuclear shielding for phosphorus in PN. The correction was ~20% of the CCSD(T)/CBS value, while it was substantially lower (<7%) for other elements. Note that we estimated the four-component RC at the DFT level for cost/benefit reasons, which turned out to be insufficient for estimating the isotropic PN shielding. Therefore, RC estimates (calculated as the difference between relativistic and non-relativistic values) may also be affected by the inadequacy of the DFT theory. The complete CCSD(T) description may be a solution with correct RC calculations, but this is not available to us and, moreover, this method is too uneconomical for most common molecules.

As an extension of this study, the  $^{33}$ S NMR shieldings of 2-thiouracil were estimated as an example of a real medium-sized molecule. We employed two different approaches. One was based on the standard description of the system using the same basis set for all atoms, while the other employed the locally dense basis set approach [66–69]. For both approaches, we observed a scattering of  $^{33}$ S shieldings for the aug-cc-pVXZ basis set family comparable to  $H_2$ S, while a smooth convergence is seen for aug-cc-pCVXZ. The change in estimated CBS values due to the LDBS approach is ~10% of the CBS value when all atoms were described using aug-cc-pVXZ or aug-cc-pCVXZ.

#### 4. Materials and Methods

Most calculations were performed using the Gaussian 16 [79] and CFOUR-2.1 [80] programs. Zero-point vibrational corrections were calculated with the S4 program [81].

#### 4.1. Geometry

Geometries of all compounds in this work were either taken from previous reports or optimized as described below. The previously reported optimized structure (CCSD(T)/augpc-4) of phosphorus mononitride [15] (PN) was used in this study, with an interatomic separation of 1.49466464 A°. Hydrogen sulfide (H<sub>2</sub>S) geometry parameters of SH = 1.3376 A° and HSH = 92.11 A° obtained by the infrared and microwave spectral analysis were taken from [57]. Phosphine (PH<sub>3</sub>) geometry (PH = 1.42002 A° and HPH = 93.3454 A°) was taken from [57] The X-ray structure of 2-thiouracil (2-TU) was taken from [64] and reoptimized at the B3LYP/aug-cc-pV5Z level to gain accurate C–H and N–H bond lengths. Geometries of all other model compounds (NaH, NaF, MgH<sub>2</sub>, AlH<sub>3</sub>, HsiCH, H<sub>3</sub>PO, and HCl) in this study were achieved by their optimization at the B3LYP/aug-cc-pV5Z level. In order to describe the geometry influence on the resulting NMR property, the B3LYP geometry of NaH was assessed against the CCSD(T) geometry and the experimental geometry ([56]; Na-H = 1.8874 A°).

Molecules **2022**, 27, 8230 16 of 22

#### 4.2. NMR Shieldings

The following basis set families, acquired from EMSL [82–85] were used in the calculations of NMR shieldings: (aug)-cc-pVXZ, where X = D, T, Q, 5 and 6; (aug)-cc-pCVXZ, where X = D, T, Q and 5; aug-cc-pwCVXZ, where X = D, T, Q and 5; and Jensen aug-pcJ-n, and aug-pcSseg-n, where n = 1, 2, 3 and 4. In addition, the Karlsruhe-type all-electron relativistic split-valence (x2c-SVPall-s), triple- $\zeta$  (x2c-TZVPPall-s) and double-polarized quadruple- $\zeta$  (x2c-QZVPPall-s) basis sets for two-component calculations of NMR shieldings, as well as the Douglas–Kroll-type aug-cc-pVXZ-DK, were applied as indicated below and taken from EMSL [82–85].

The GIAO NMR parameters were calculated at the SCF-HF and CCSD(T) levels using the CFOUR program, and at the DFT-B3LYP level with Gaussian 16 [79]. The all-electron CCSD(T) nuclear shieldings were calculated with the CFOUR-2.1 program [80]. The locally dense basis sets (LDBS) approach [66–69] was applied for the B3LYP calculation of the  $^{33}$ S NMR shielding constants in 2-TU to reduce the computational time. Thus, C, H, N, O atoms were described by the 6-31G\* basis set and the sulfur atom was calculated with the aug-cc-pVXZ or aug-cc-pCVXZ basis set families. In the case of hydrogen atom, aug-cc-pCVXZ = aug-cc-pVXZ. Thus, the aug-cc-pVXZ basis sets were used for hydrogen. Shielding constants, shielding anisotropies and individual shielding components were plotted against the basis set cardinal number X, or the number of basis functions (b.f.). The latter approach allowed a better discrimination between the size of different basis set series but essentially produced the same CBS value. Finally, the CBS values of calculated NMR parameters, Y(CBS), were estimated using the 2-parameter formula [86,87] (Equation (1)).

The GIAO NMR parameters were calculated at the SCF-HF and CCSD(T) levels using the CFOUR program, and at the DFT-B3LYP level with Gaussian 16 [79]. The all-electron CCSD(T) nuclear shieldings were calculated with the CFOUR-2.1 program [80]. The locally dense basis sets (LDBS) approach [66–69] was applied for the B3LYP calculation of the  $^{33}$ S NMR shielding constants in 2-TU to reduce the computational time. Thus, C, H, N, O atoms were described by the 6-31G\* basis set and the sulfur atom was calculated with the aug-cc-pVXZ or aug-cc-pCVXZ basis set families. In the case of hydrogen atom, aug-cc-pCVXZ = aug-cc-pVXZ. Thus, the aug-cc-pVXZ basis sets were used for hydrogen. Shielding constants, shielding anisotropies and individual shielding components were plotted against the basis set cardinal number X, or the number of basis functions (b.f.). The latter approach allowed a better discrimination between the size of different basis set series but essentially produced the same CBS value. Finally, the CBS values of calculated NMR parameters, Y(CBS), were estimated using the 2-parameter formula [86,87] (Equation (1)).

$$Y(X) = Y(CBS) + A/X^3$$
 (1)

In this formula, Y(CBS) and A are the fitted parameters and X (or b.f.) is the cardinal number (or the number of basis functions) of the basis set. We used X = n + 1 in the case of Jensen basis sets (i.e., pc-1 basis set corresponds to the double- $\zeta$  quality).

In the case of three systematically growing x2c- basis sets, we expected no regular convergence of energy and related parameters. However, to obtain some indication of trends in calculated nuclear shieldings, we also performed the 2-parameter fit. In this case, the fitting was performed for all three data points. Obviously, this was an empirical treatment of the data (produced by these basis sets). Despite such crude approximations, the obtained CBS-like values were often close to numbers obtained with the Dunning or Jensen-type basis sets.

#### 4.3. Zero-Point Vibrational and Thermal Corrections

The nuclear potential of studied compounds was expanded to a Taylor series up to fourth powers of all normal-mode coordinates according to Equation (2) to estimate the ZPVC effect on calculated NMR shieldings [88].

Molecules **2022**, 27, 8230 17 of 22

$$V = \frac{1}{2} \sum_{i=1} \omega_i^2 Q_i^2 + \frac{1}{6} \sum_{i=1} \sum_{j=1} \sum_{k=1} c_{ijk} Q_i Q_j Q_k + \frac{1}{24} \sum_{i=1} \sum_{j=1} \sum_{k=1} \sum_{l=1} d_{ijkl} Q_i Q_j Q_k Q_l$$
 (2)

We considered only cubic  $(c_{ijk})$  and semi-diagonal quartic constants  $(d_{ijkl})$ ; with two or more identical indices), as a single numerical differentiation of harmonic force fields provides them. Isotropic nuclear magnetic shieldings were calculated for vibrational ground state  $\psi_n$  as  $\sigma_n = \psi_n |\sigma| \psi_n$ , where  $\sigma = \sigma_0 + \sum_i \sigma_{1,i} Q_i + \frac{1}{2} \sum_{i,j} \sigma_{2,ij} Q_i Q_j$ . The  $\sigma_1$  and  $\sigma_2$  are the first and the second normal-mode isotropic shielding derivatives that were obtained numerically as described elsewhere [89]. The wave function is expanded in the harmonic oscillator basis within the second-order degeneracy-corrected perturbational (PT2) approach [90] providing thus the zero-point vibrational corrections (ZPVCs). All geometries were optimized at the B3LYP/aug-cc-pVQZ level. The anharmonic force field and the shielding derivatives were obtained at the same level of theory. Alternatively, we calculated the anharmonic force field (as we did the optimization) at the CCSD(T)/aug-pc-2 level and the shielding derivatives at the BHandHLYP/aug-pcSseg-4 level. The Hessian and NMR computations for displaced geometries (performed in normal modes) were carried out using the Gaussian 16, while the anharmonic vibrational averaging was executed using program S4. The temperature-corrected shieldings (TCS) were obtained as  $\sigma = \sigma_0 + 0.25\sigma_{ii} \exp(-\omega_i/kT)[1 - \exp(-\omega_i/kT)]^{-1}$ . Then, the pure temperature correction was obtained as the TCS-ZPVC. Note that our simplified estimation of the TC does not include centrifugal distortion, which may represent a large contribution to the TC.

#### 4.4. Relativistic Corrections

We employed the Respect 5.2.0 [91] code to obtain the relativistic corrections to theoretical GIAO NMR shielding constants. We compared the full four-component Dirac–Kohn–Sham shieldings [92,93], calculated with the B3LYP functional and the aug-cc-pVTZ basis set, with values achieved with one-component Kohn–Sham Hamiltonian at the same level. For PN, we examined the basis set dependence of relativistic corrections using the aug-cc-pVXZ series, where X = D, T, Q. Alternatively, the relativistic correction was achieved also at the KT2 level with the uncontracted pcS-3 basis set. The correction for Ar was obtained using the uncontracted Dyall aug-cvtz basis set. Moreover, since Ar is not defined as an NMR-active nucleus in by default, we obtained RC for Ar by interpolation of theoretical values of He, Ne, Kr, and Xe using the trendline, where Z is the atomic number of a nucleus.

#### 5. Conclusions

A detailed test of HF-SCF, B3LYP and CCSD(T) of the apparent irregularity of the convergence of nuclear magnetic shielding tensors with respect to increasing the size of the aug-cc-pVXZ basis set has been performed for selected isolated molecules containing nuclides of the third row of the periodic table of elements. The scattered patterns of nuclear shieldings calculated by the three selected methods and using Dunning basis sets with a regularly increasing cardinal number X were observed for the studied compounds. In contrast to NMR shieldings, regular and exponential decays were observed for energies calculated using the same approach. The use of the aug-cc-pCVXZ core-valence basis set family or the segmented-contracted aug-cc-pcSseg-n basis sets (slightly smaller than the former one) improved the behavior of the calculated NMR shieldings with smooth convergence towards the CBS limits. In addition, the x2c-Def2 basis sets, being significantly smaller than the aug-cc-pCVXZ or aug-cc-pcSseg-n basis sets, provided results close to the CBS limit for the latter two families. Obtained results point to the necessity of using the aug-pcSseg-n or aug-cc-pCVXZ basis sets if one attempts to obtain converged (or close to saturation) nuclear shieldings of the third-row elements. As a cheaper alternative, the x2c-Def2 basis sets could also be employed for reliable prediction of nuclear shieldings for compounds containing elements from the third row of the periodic table.

Molecules **2022**, 27, 8230 18 of 22

Additionally, we estimated the effect of vibrational, temperature, and relativistic corrections on the predicted shieldings of the third-row elements. The vibrational corrections were estimated using the second-order degeneracy-corrected perturbational approach. The relativistic corrections were obtained at the full four-component Dirac–Kohn–Sham basis. We can conclude that all corrections are relatively small, amounting to less than 4% of the CCSD(T)/CBS value, for systems containing only single bonds. Estimates of the vibrational and temperature corrections were less reliable for  $H_3PO$  and HSiCH due to the high anharmonicity of these molecules. Abnormally high relativistic corrections, reaching ~20% of the CCSD(T)/CBS value, were observed for phosphorus in PN, while the corrections were substantially lower (~7% of the CCSD(T)/CBS value) for other tested molecules.

**Supplementary Materials:** The following supporting information can be downloaded at: https://www.mdpi.com/article/10.3390/molecules27238230/s1: Additional figures and tables showing convergence patterns of nuclear shieldings of third-row elements in test compounds, calculated with the SCF-HF, B3LYP-DFT, and CCSD(T) methods, combined with the aug-cc-pVXZ, aug-cc-pCVXZ, aug-pcSseg-*n* and x2c-Def2 basis set series. The calculated energies are also included.

**Author Contributions:** K.R.—investigation, methodology, and visualization; J.K.—investigation, supervision, methodology, and writing—review and editing; A.B.—investigation; M.A.B.—funding acquisition; T.K.—supervision, conceptualization, methodology, writing—draft preparation, and project administration. We confirm that neither the manuscript nor any parts of its content are currently under consideration or published in another journal. All authors have read, approved the manuscript and agree with its submission to *Molecules*. All authors have read and agreed to the published version of the manuscript.

**Funding:** This work was partly supported by the Czech Ministry of Education, Youth and Sports (grant No. LTAUSA18085) and the Czech Science Foundation (22-17586S). Additional support was provided by the Faculty of Chemistry, University of Opole. Computational resources were supplied by the project "e-Infrastruktura CZ" (e-INFRA CZ LM2018140) supported by the Ministry of Education, Youth and Sports of the Czech Republic and by Wroclaw Centre for Networking and Supercomputing (WCSS).

Institutional Review Board Statement: Not applicable.

**Informed Consent Statement:** Not applicable.

Data Availability Statement: All data are available in the text and the Supplementary Material.

Acknowledgments: We would like to thank the University of Opole, Institute of Chemistry for a partial internal support. We are particularly grateful to WCSS Wrocław for enabling us an access to its hardware and software facilities. Additional computational resources were supplied by the project "e-Infrastruktura CZ" (e-INFRA LM2018140) provided within the program Projects of Large Research, Development and Innovations Infrastructures. The Czech Ministry of Education, Youth and Sports (grant No. LTAUSA18085) and the Czech Science Foundation (22-17586S) are gratefully acknowledged. Finally, we would like to thank Michał Jaszuński for his help and expertise in CFOUR program and two anonymous reviewers for many detailed comments and helpful suggestions.

Conflicts of Interest: The authors declare no conflict of interest.

Molecules **2022**, 27, 8230 19 of 22

#### References

 Helgaker, T.; Jaszunski, M.; Ruud, K. Ab Initio Methods for the Calculation of NMR shielding and Indirect Spin-Spin Coupling Constants. Chem. Rev. 1999, 99, 293–352. [CrossRef] [PubMed]

- 2. Gauss, J.; Stanton, J.F. Gauge-invariant calculation of nuclear magnetic shielding constants at the coupled-cluster singles and doubles level. *J. Chem. Phys.* **1995**, *102*, 251–253. [CrossRef]
- 3. Gauss, J.; Stanton, J.F. Perturbative treatment of triple excitations in coupled-cluster calculations of nuclear magnetic shielding constants. *J. Chem. Phys.* **1996**, *104*, 2574–2583. [CrossRef]
- 4. Kupka, T.; Stachów, M.; Nieradka, M.; Kaminský, J.; Pluta, T. Convergence of nuclear magnetic shieldings in the Kohn-Sham limit for several small molecules. *J. Chem. Theor. Comput.* **2010**, *6*, 1580–1589. [CrossRef]
- 5. Gauss, J. Calculation of NMR chemical shifts at second-order many-body perturbation theory using gauge-including atomic orbitals. *Chem. Phys. Lett.* **1992**, *191*, 614–620. [CrossRef]
- Crittenden, D.L. A new double-reference correction scheme for accurate and efficient computation of NMR chemical shieldings. Phys. Chem. Chem. Phys. 2022, 24, 27055–27063. [CrossRef]
- 7. Nazarski, R.B.; Wałejko, P.; Witkowski, S. Multi-conformer molecules in solutions: An NMR-based DFT/MP2 conformational study of two glucopyranosides of a vitamin E model compound. *Org. Biomol. Chem.* **2016**, *11*, 3142–3158. [CrossRef] [PubMed]
- 8. Nazarski, R.B. Summary of DFT calculations coupled with current statistical and/or artificial neural network (ANN) methods to assist experimental NMR data in identifying diastereomeric structures. *Tetrahedron Lett.* **2021**, *71*, 152548. [CrossRef]
- 9. Wolinski, K.; Hinton, J.F.; Pulay, P. Efficient implementation of the gauge-independent atomic orbital method for NMR chemical shift calculations. *J. Am. Chem. Soc.* **1990**, *112*, 8251–8260. [CrossRef]
- 10. Ditchfield, R. Self-consistent perturbation theory of diamagnetism I. A gauge-invariant LCAO method for N.M.R. chemical shifts. *Mol. Phys.* **1974**, 27, 789–807. [CrossRef]
- 11. Feller, D. Application of systematic sequences of wave functions to the water dimer. J. Chem. Phys. 1992, 96, 6104–6114. [CrossRef]
- 12. Feller, D. The use of systematic sequences of wave functions for estimating the complete basis set, full configuration interaction limit in water. *J. Chem. Phys.* **1993**, *98*, 7059–7071. [CrossRef]
- 13. Kupka, T.; Ruscic, B.; Botto, R.E. Hartree-Fock and Density Functional Complete Basis-Set (CBS) Predicted Nuclear Shielding Anisotropy and Shielding Tensor Components. *Solid State Nucl. Magn. Reson.* **2003**, *2*, 143–167. [CrossRef]
- 14. Kupka, T.; Ruscic, B.; Botto, R.E. Toward Hartree-Fock- and Density Functional Complete Basis-Set Predicted NMR Parameters. *J. Phys. Chem. A.* **2002**, *106*, 10396–10407. [CrossRef]
- 15. Kupka, T.; Leszczyńska, M.; Ejsmont, K.; Mnich, A.; Broda, M.; Thangavel, K.; Kaminský, J. Phosphorus mononitride: A difficult case for theory. *Int. J. Quantum Chem.* **2019**, *119*, e26032. [CrossRef]
- 16. Jensen, F. The basis set convergence of spin-spin coupling constants calculated by density functional methods. *J. Chem. Theor. Comput.* **2006**, *2*, 1360–1369. [CrossRef] [PubMed]
- 17. Jensen, F. Basis set convergence of nuclear magnetic shielding constants calculated by density functional methods. *J. Chem. Theor. Comput* **2008**, *4*, 719–727. [CrossRef] [PubMed]
- 18. Jensen, F. Unifying General and Segmented Contracted Basis Sets. Segmented Polarization Consistent Basis Sets. *J. Chem. Theory Comput.* **2014**, *10*, 1074–1085. [CrossRef] [PubMed]
- 19. Dunning, T.H., Jr. Gaussian basis sets for use in correlated molecular calculations. I. The atoms boron through neon and hydrogen. *J. Chem. Phys.* **1989**, *90*, 1007–1023. [CrossRef]
- 20. Kendall, R.A.; Dunning, T.H., Jr.; Harrison, R.J. Electron affinities of the first-row atoms revisited. Systematic basis sets and wave functions. *J. Chem. Phys.* **1992**, *96*, 6796–6806. [CrossRef]
- 21. Woon, D.E.; Dunning, T.H., Jr. Gaussian basis sets for use in correlated molecular calculations. III. The atoms aluminum through argon. *J. Chem. Phys.* **1993**, *98*, 1358–1371. [CrossRef]
- 22. Van Mourik, T.; Dunning, T.H., Jr. Gaussian Basis Sets for Use in Correlated Molecular Calculations. VIII. Standard and Augmented Sextuple Zeta Correlation Consistent Basis Sets for Aluminum Through Argon. *Int. J. Quantum Chem.* **2000**, 76, 205–221. [CrossRef]
- 23. Peterson, K.A.; Woon, D.E.; Dunning, T.H., Jr. Benchmark calculations with correlated molecular wave functions. IV. The classical barrier height of the H + H2→H2 + H reaction. *J. Chem. Phys.* **1994**, *100*, 7410–7415. [CrossRef]
- 24. Peterson, K.A.; Dunning, T.H. Accurate correlation consistent basis sets for molecular core–valence correlation effects: The second row atoms Al–Ar, and the first row atoms B–Ne revisited. *J. Chem. Phys.* **2002**, *117*, 10548–10560. [CrossRef]
- 25. Prascher, B.P.; Woon, D.E.; Peterson, K.A.; Dunning, T.H.; Wilson, A.K. Gaussian basis sets for use in correlated molecular calculations. VII. Valence, core-valence, and scalar relativistic basis sets for Li, Be, Na, and Mg. *Theor. Chem. Acc.* **2011**, 128, 69–82. [CrossRef]
- 26. Jensen, F. Polarization consistent basis sets: Principles. J. Chem. Phys. 2001, 115, 9113–9125. [CrossRef]
- 27. Jensen, F. Polarization consistent basis sets. II. Estimating the Kohn-Sham basis set limit. *J. Chem. Phys.* **2002**, *116*, 7372–7379. [CrossRef]
- 28. Jensen, F. Polarization consistent basis sets. III. The importance of diffuse functions. *J. Chem. Phys.* **2002**, 117, 9234–9240. [CrossRef]
- 29. Jensen, F. Polarization consistent basis sets. IV. The basis set convergence of equilibrium geometries, harmonic vibrational frequencies, and intensities. *J. Chem. Phys.* **2003**, *118*, 2459–2463. [CrossRef]

Molecules **2022**, 27, 8230 20 of 22

30. Jensen, F. The optimum contraction of basis sets for calculating spin-spin coupling constants. *Theor. Chem. Acc.* **2010**, *126*, 371–382. [CrossRef]

- 31. Kupka, T.; Stachow, M.; Nieradka, M.; Kaminsky, J.; Pluta, T.; Sauer, S.P.A. From CCSD(T)/aug-cc-pVTZ-J to CCSD(T) complete basis set limit isotropic nuclear magnetic shieldings via affordable DFT/CBS calculations. *Magn. Reson. Chem.* **2011**, *49*, 231–236. [CrossRef]
- 32. Jankowska, M.; Kupka, T.; Stobinski, L.; Faber, R.; Lacerda, E.G.; Sauer, S.P.A. Spin-Orbit ZORA and Four-Component Dirac-Coulomb Estimation of Relativistic Corrections to Isotropic Nuclear Shieldings and Chemical Shifts of Noble Gas Dimers. *J. Comput. Chem.* **2016**, *37*, 395–403. [CrossRef] [PubMed]
- 33. Kupka, T.; Stachów, M.; Chełmecka, E.; Pasterny, K.; Stobińska, M.; Stobiński, L.; Kaminský, J. Efficient modeling of NMR parameters in carbon nanosystems. *J. Chem. Theor. Comput.* **2013**, *9*, 4275–4286. [CrossRef] [PubMed]
- 34. Schäfer, A.; Huber, C.; Ahlrichs, R. Fully optimized contracted Gaussian basis sets of triple zeta valence quality for atoms Li to Kr. *J. Chem. Phys.* **1994**, *100*, 5829–5835. [CrossRef]
- 35. Franzke, Y.J.; Spiske, L.; Pollak, P.; Weigend, F. Segmented Contracted Error-Consistent Basis Sets of Quadruple-ζ Valence Quality for One- and Two-Component Relativistic All-Electron Calculations. *J. Chem. Theory Comput.* **2020**, *16*, 5658–5674. [CrossRef]
- 36. Franzke, Y.J.; Weigend, F. NMR Shielding Tensors and Chemical Shifts in Scalar-Relativistic Local Exact Two-Component Theory. *J. Chem. Theory Comput.* **2019**, *15*, 1028–1043. [CrossRef]
- 37. Franzke, Y.J.; Treß, R.; Pazdera, T.M.; Weigend, F. Error-consistent segmented contracted all-electron relativistic basis sets of double- and triple-zeta quality for NMR shielding constants. *Phys. Chem. Chem. Phys.* **2019**, 21, 16658–16664. [CrossRef]
- 38. de Jong, W.A.; Harrison, R.J.; Dixon, D.A. Parallel Douglas–Kroll energy and gradients in NWChem: Estimating scalar relativistic effects using Douglas–Kroll contracted basis sets. *J. Chem. Phys.* **2001**, *114*, 48–53. [CrossRef]
- 39. Teale, A.M.; Lutnas, O.B.; Helgaker, T.; Tozer, D.J.; Gauss, J. Benchmarking density-functional theory calculations of NMR shielding constants and spin-rotation constants using accurate coupled-cluster calculations. *J. Chem. Phys.* **2013**, *138*, 024111. [CrossRef]
- 40. Field-Theodore, T.E.; Olejniczak, M.; Jaszuński, M.; Wilson, D.J.D. NMR shielding constants in group 15 trifluorides. *Phys. Chem. Phys.* **2018**, 20, 23025–23033. [CrossRef] [PubMed]
- Stoychev, G.L.; Auer, A.A.; Izsák, R.; Neese, F. Self-Consistent Field Calculation of Nuclear Magnetic Resonance Chemical Shielding Constants Using Gauge-Including Atomic Orbitals and Approximate Two-Electron Integrals. J. Chem. Theory Comput. 2018, 14, 619–637. [CrossRef]
- 42. Martinez-Baez, E.; Feng, R.; Pearce, C.I.; Schenter, G.K.; Clark, A.E. Al27 NMR chemical shift of Al(OH)4— calculated from first principles: Assessment of error cancellation in chemically distinct reference and target systems. *J. Chem. Phys.* **2020**, *152*, 134303. [CrossRef] [PubMed]
- 43. Lee, V.Y.; Uhlig, F. Organosilicon Compounds; Academic Press: Cambridge, MA, USA, 2017; p. 59.
- 44. Bhinderwala, F.; Evans, P.; Jones, K.; Laws, B.R.; Smith, T.G.; Morton, M.; Powers, R. Phosphorus NMR and Its Application to Metabolomics. *Anal. Chem.* **2020**, 92, 9536–9545. [CrossRef]
- 45. Ruud, K.; Astrand, P.-O.; Taylor, P.R. An efficient approach for calculating vibrational wave functions and zero-point vibrational corrections to molecular properties of polyatomic molecules. *J. Chem. Phys.* **2000**, *112*, 2668–2683. [CrossRef]
- 46. Ruud, K.; Astrand, P.-O.; Taylor, P.R. Zero-point vibrational effects on proton shieldings: Functional-group contributions from ab initio calculations. *J. Am. Chem. Soc.* **2001**, *123*, 4826–4833. [CrossRef] [PubMed]
- 47. Vıícha, J.; Novotný, J.; Komorovsky, S.; Straka, M.; Kaupp, M.; Marek, R. Relativistic Heavy-Neighbor-Atom Effects on NMR Shifts: Concepts and Trends Across the Periodic Table. *Chem. Rev.* **2020**, *120*, 7065–7103. [CrossRef] [PubMed]
- 48. Lantto, P.; Standara, S.; Riedel, S.; Vaara, J.; Straka, M. Exploring new 129Xe chemical shift ranges in HXeY compounds: Hydrogen more relativistic than xenon. *Phys. Chem. Chem. Phys.* **2012**, *14*, 10944–10952. [CrossRef]
- 49. Krivdin, L.B. Recent advances in computational liquid-phase 77Se NMR. Russ. Chem. Rev. 2021, 90, 265–279. [CrossRef]
- Rusakov, Y.Y.; Krivdin, L.B.; Sauer, S.P.A.; Levanova, E.P.; Levkovskaya, G.G. Structural trends of 77Se-1H spin-spin coupling constants and conformational behavior of 2-substituted selenophenes. Magn. Reson. Chem. 2010, 48, 44–52. [CrossRef] [PubMed]
- 51. Sarotti, A.M.; Pellegrinet, S.C. A Multi-standard Approach for GIAO 13C NMR Calculations. *J. Org. Chem.* **2009**, *74*, 7254–7260. [CrossRef]
- 52. Lodewyk, M.W.; Siebert, M.R.; Tantillo, D.J. Computational Prediction of 1H and 13C Chemical Shifts: A Useful Tool for Natural Product, Mechanistic, and Synthetic Organic Chemistry. *Chem. Rev.* **2012**, *112*, 1839–1862. [CrossRef] [PubMed]
- 53. Gamov, G.A.; Kuranova, N.N.; Pogonin, A.E.; Aleksandriiskii, V.V.; Sharnin, V.A. Hydrogen bonds determine the signal arrangement in 13C NMR spectra of nicotinate. *J. Mol. Struct.* **2018**, *1154*, 565–569. [CrossRef]
- 54. Alkorta, I.; Elguero, J. Ab initio (GIAO) calculations of absolute nuclear shieldings for representative compounds containing 1(2)H, 6(7)Li, 11B, 13C, 14(15)N, 17O, 19F, 29Si, 31P, 33S and 35Cl nuclei. *Struct. Chem.* **1998**, *9*, 187–202.
- 55. Prochnow, E.; Auer, A.A. Quantitative prediction of gas-phase <sup>15</sup>N and <sup>31</sup>P nuclear magnetic shielding constants. *J. Chem. Phys.* **2010**, 132, 064109. [CrossRef]
- 56. NIST. Available online: https://cccbdb.nist.gov/geom2x.asp (accessed on 1 January 2020).
- 57. Antušek, A.; Jaszuński, M. Coupled cluster study of NMR shielding constants and spin-rotation constants in SiH4, PH3 and H2S molecules. *Mol. Phys.* **2006**, *104*, 1463–1474.

Molecules **2022**, 27, 8230 21 of 22

58. Lu, T.; Hao, Q.; Wilke, J.J.; Yamaguchi, Y.; Fang, D.-C.; Schaefer, H.F. Silylidene (SiCH2) and its isomers: Anharmonic rovibrational analyses for silylidene, silaacetylene, and silavinylidene. *J. Mol. Struct.* **2012**, *1009*, 103–110. [CrossRef]

- 59. Blicharska, B.; Kupka, T. Theoretical DFT and experimental NMR studies on uracil and 5-fluorouracil. *J. Mol. Struct.* **2002**, *613*, 153–166. [CrossRef]
- 60. Kupka, T.; Pasterna, G.; Lodowski, P.; Szeja, W. GIAO-DFT Prediction of Accurate NMR Parameters in Selected Glucose Derivatives. *Magn. Reson. Chem.* **1999**, *37*, 421–429. [CrossRef]
- 61. Vincent, J.; Mignot, G.; Chalmin, F.; Ladoire, S.; Bruchard, M.; Chevriaux, A.; Martin, F.; Apetoh, L.; Rébé, C.; Ghiringhelli, F. 5-Fluorouracil Selectively Kills Tumor-Associated Myeloid-Derived Suppressor Cells Resulting in Enhanced T Cell–Dependent Antitumor Immunity. *Cancer Res.* 2010, 70, 3052–3061. [CrossRef]
- 62. Rzepiela, K.; Buczek, A.; Kupka, T.; Broda, M.A. Factors Governing the Chemical Stability and NMR Parameters of Uracil Tautomers and Its 5-Halogen Derivatives. *Molecules* **2020**, *25*, 3931. [CrossRef]
- 63. Rzepiela, K.; Buczek, A.; Kupka, T.; Broda, M.A. On the aromaticity of uracil and its 5-halogeno derivatives as revealed by theoretically derived geometric and magnetic indexes. *Struct. Chem.* **2021**, *32*, 275–283. [CrossRef]
- 64. Jarzembska, K.N.; Kubsik, M.; Kamiński, R.; Woźniak, K.; Dominiak, P.M. From a Single Molecule to Molecular Crystal Architectures: Structural and Energetic Studies of Selected Uracil Derivatives. *Cryst. Growth Des.* **2012**, *12*, 2508–2524.
- 65. Francl, M.M.; Pietro, W.J.; Hehre, W.J.; Binkley, J.S.; Gordon, M.S.; DeFrees, D.J.; Pople, J.A. Self-consistent molecular orbital methods. XXIII. A polarization-type basis set for second-row elements. *J. Chem. Phys.* **1982**, 77, 3654–3665. [CrossRef]
- 66. Chesnut, D.B.; Moore, K.D. Locally dense basis sets for chemical shift calculations. J. Comput. Chem. 1989, 10, 648–659. [CrossRef]
- 67. Reid, D.M.; Kobayashi, R.; Collins, M.A. Systematic study of locally dense basis sets for NMR shielding constants. *J. Chem. Theor. Comp.* **2014**, *10*, 146–152. [CrossRef]
- 68. Provasi, P.F.; Aucar, G.A.; Sauer, S.P.A. The use of locally dense basis sets in the calculation of indirect nuclear spin–spin coupling constants: The vicinal coupling constants in H3C–CH2X (X = H, F, Cl, Br, I). *J. Chem. Phys.* **2000**, *112*, 6201–6208. [CrossRef]
- 69. Semenov, V.A.; Krivdin, L.B. DFT computational schemes for 1H and 13C NMR chemical shifts of natural products, exemplified by strychnine. *Magn. Reson. Chem.* **2020**, *58*, 56–64. [CrossRef]
- Krivdin, L.B. Computational NMR of heavy nuclei involving 109Ag, 113Cd, 119Sn, 125Te, 195Pt, 199Hg, 205Tl, and 207Pb. Russ. Chem. Rev. 2021, 90, 1166–1212.
- 71. Faber, R.; Kaminský, J.; Sauer, S.P.A. Rovibrational and Temperature Effects in Theoretical Studies of NMR Parameters. In *New Developments in NMR. Gas Phase NMR.*; Jackowski, K., Jaszuński, M., Eds.; The Royal Society of Chemistry: Piccadilly, UK, 2016; Volume 6, pp. 218–266.
- 72. Jaszuński, M.; Repisky, M.; Demissie, T.B.; Komorovsky, S.; Malkin, E.; Ruud, K.; Garbacz, P.; Jackowski, K.; Makulski, W. Spin-rotation and NMR shielding constants in HCl. *J. Chem. Phys.* **2013**, 139, 234302. [CrossRef]
- 73. Yoshizawa, T.; Hada, M. Calculations of nuclear magnetic shielding constants based on the exact two-component relativistic method. *J. Chem. Phys.* **2017**, 147, 154104. [CrossRef]
- 74. Stoychev, G.L.; Auer, A.A.; Neese, F. Efficient and Accurate Prediction of Nuclear Magnetic Resonance Shielding Tensors with Double-Hybrid Density Functional Theory. *J. Chem. Theory Comput.* **2018**, 14, 4756–4771. [CrossRef] [PubMed]
- 75. Jameson, C.J.; Jameson, A.K. Absolute shielding scale for 29Si. Chem. Phys. Lett. 1988, 149, 300–305. [CrossRef]
- 76. Jameson, C.J.; de Dios, A.C.; Jameson, A.K. The 31P shielding in phosphine. J. Chem. Phys. 1991, 95, 9042–9053. [CrossRef]
- 77. Lantto, P.; Jackowski, K.; Makulski, W.; Olejniczak, M.; Jaszuński, M. NMR Shielding Constants in PH3, Absolute Shielding Scale, and the Nuclear Magnetic Moment of 31P. *J. Phys. Chem. A* **2011**, *115*, 10617–10623. [CrossRef]
- 78. Kudo, K.; Fukui, H. Calculation of nuclear magnetic shieldings using an analytically differentiated relativistic shielding formula. *J. Chem. Phys.* **2005**, 123, 114102. [CrossRef]
- 79. Frisch, M.J.; Trucks, G.W.; Schlegel, H.B.; Scuseria, G.E.; Robb, M.A.; Cheeseman, J.R.; Scalmani, G.; Barone, V.; Petersson, G.A.; Nakatsuji, H.; et al. Gaussian 16 Rev. C.01. Gaussian, Inc.: Wallingford, CT, USA, 2016.
- 80. Stanton, J.F.; Gauss, J.; Cheng, L.; Harding, M.E.; Matthews, D.A.; Szalay, P.G. CFOUR. Available online: http://www.cfour.de (accessed on 1 January 2020).
- 81. Bouř, P. Program S4; Czech Academy of Sciences: Prague, Czech Republic, 2009.
- 82. Feller, D. The Role of Databases in Support of Computational Chemistry Calculations. *J. Comput. Chem.* **1996**, *17*, 1571–1586. [CrossRef]
- 83. Schuchardt, K.L.; Didier, B.T.; Elsethagen, T.; Sun, L.; Gurumoorthi, V.; Chase, J.; Li, J.; Windus, T.L. Basis Set Exchange: A Community Database for Computational Sciences. *J. Chem. Inf. Model.* **2007**, 47, 1045–1052. [CrossRef]
- 84. Pritchard, B.P.; Altarawy, D.; Didier, B.; Gibson, T.D.; Windus, T.L. New Basis Set Exchange: An Open, Up-to-Date Resource for the Molecular Sciences Community. *J. Chem. Inf. Model.* **2019**, *59*, 4814–4820. [CrossRef]
- 85. EMSL, Basis Set Exchange. Available online: https://bse.pnl.gov/bse/portal (accessed on 1 January 2020).
- 86. Helgaker, T.; Klopper, W.; Koch, H.; Noga, J. Basis-set convergence of correlated calculations on water. *J. Chem. Phys.* **1997**, 106, 9639–9646. [CrossRef]
- 87. Kupka, T.; Lim, C. Polarization-consistent versus correlation-consistent basis sets in predicting molecular and spectroscopic properties. *J. Phys. Chem. A* **2007**, *111*, 1927–1932. [CrossRef]
- 88. Papoušek, D.; Aliev, M.R. Molecular Vibrational-Rotational Spectra: Theory and Applications of High Resolution Infrared, Microwave, and Raman Spectroscopy of Polyatomic Molecules; Elsevier Scientific Pub. Co.: Amsterdam, The Netherlands, 1982.

Molecules **2022**, 27, 8230 22 of 22

89. Kaminský, J.; Buděšínský, M.; Taubert, S.; Bouř, P.; Straka, M. Fullerene C70 characterization by 13C NMR and the importance of the solvent and dynamics in spectral simulations. *Phys. Chem. Chem. Phys.* **2013**, *15*, 9223–9230. [CrossRef]

- 90. Danecek, P.; Bour, P. Comparison of the Numerical Stability of Methods for Anharmonic Calculations of Vibrational Molecular Energies. *J. Comput. Chem.* **2007**, *28*, 1617–1624. [CrossRef] [PubMed]
- 91. Repisky, M.; Komorovsky, S.; Kadek, M.; Konecny, L.; Ekström, U.; Malkin, E.; Kaupp, M.; Ruud, K.; Malkina, O.L.; Malkin, V.G. ReSpect: Relativistic spectroscopy DFT program package. *J. Chem. Phys.* **2020**, *152*, 184101. [CrossRef] [PubMed]
- 92. Komorovský, S.; Repiský, M.; Malkina, O.L.; Malkin, V.G.; Malkin Ondík, I.; Kaupp, M. A fully relativistic method for calculation of nuclear magnetic shielding tensors with a restricted magnetically balanced basis in the framework of the matrix Dirac-Kohn-Sham equation. *J. Chem. Phys.* **2008**, *128*, 104101. [CrossRef] [PubMed]
- 93. Komorovsky, S.; Repisky, M.; Malkina, O.L.; Malkin, V.G. Fully relativistic calculations of NMR shielding tensors using restricted magnetically balanced basis and gauge including atomic orbitals. *J. Chem. Phys.* **2010**, *132*, 154101. [CrossRef]





# Electron Correlation or Basis Set Quality: How to Obtain Converged and Accurate NMR Shieldings for the Third-Row Elements?

Kacper Rzepiela 1, Jakub Kaminský 2,\*, Aneta Buczek 1, Małgorzata A. Broda 1 and Teobald Kupka 1,\*

- <sup>1</sup> Faculty of Chemistry, University of Opole, 48 Oleska Street, 46-052 Opole, Poland <sup>2</sup> Institute of Organic Chemistry and Biochemistry of the CAS, Flemingovo nám. 2, 166 10 Prague, Czech Republic
- \* Correspondence: kaminsky@uochb.cas.cz (J.K.); teobaldk@gmail.com (T.K.)

#### S1.1 Sensitivity of <sup>23</sup>Na parameters to the basis set quality

The <sup>23</sup>Na nuclear shielding values calculated at the B3LYP/aug-cc-pVXZ and B3LYP/aug-cc-pCVXZ levels for NaH, but also for NaF are gathered in Table S6A. Table also presents NMR shieldings for NaF and NaH calculated at the HF-SCF and CCSD(T) levels with same basis sets as for B3LYP. Similarly, Table S6B then summarizes energies for two selected sodium species calculated at the B3LYP, HF-SCF and CCSD(T) levels with the aug-cc-pVXZ and aug-cc-pCVXZ basis sets.

The convergence patterns of <sup>23</sup>Na isotropic shieldings according to the number of basis functions for NaH calculated at the HF-SCF, B3LYP-DFT and CCSD(T) levels of theory, combined with the aug-cc-pVXZ, aug-cc-pCVXZ, aug-pcSseg-n and x2c-Def2 basis set families are shown in Figure S7. It is apparent that <sup>23</sup>Na isotropic shieldings predicted with the aug-cc-pVXZ series produce scattered results and a smooth convergence is for shieldings produced with the aug-pcSseg-n family. Interestingly, despite their small size, the x2c-Def2 basis set family performs fairly accurate in comparison to Jensen's or core-valence basis sets. Thus, apart from aug-cc-pCVXZ basis sets, the x2c-Def2 basis sets could be recommended for shielding calculations of <sup>23</sup>Na nuclei. In addition, Figure S8 depicts very similar <sup>23</sup>Na shielding patterns for NaF as for NaH with respect to the cardinal number X and the number of basis functions calculated with the B3LYP functional and aug-cc-pVXZ and aug-cc-pCVXZ basis set families. Note that the B3LYP/aug-cc-pVXZ and B3LYP/aug-cc-pCVXZ calculated energies of NaH and NaF show typical (exponential) patterns as seen in Figure S9.

According to Table S6A, the CCSD(T)/CBS (estimated with the core-valence basis sets) <sup>23</sup>Na isotropic nuclear shielding in NaH is 569.555 ppm. When we consider also ZPVC of 0.29 ppm,

RC of 7.74 ppm, and TC of -0.01 ppm (Table 4), the total shielding changes to its final value of 577.585 ppm.

#### S1.2 Sensitivity of <sup>25</sup>Mg parameters to the basis set quality

The <sup>25</sup>Mg nuclear shielding values calculated at the B3LYP level with the aug-cc-pVXZ, augcc-pCVXZ, aug-pcSseg-n, and x2c-Def2 basis sets for MgH<sub>2</sub> are gathered in Table S7A, as well as the estimated CBS values. Analogously, Table S6B summarizes electronic energies of MgH<sub>2</sub> calculated at the same levels for the first two basis set families. Figure S10 then, for clearer picture of the magnesium shielding behavior with increasing basis set, depicts convergence patterns of <sup>25</sup>Mg NMR shieldings for MgH<sub>2</sub> calculated with the CCSD(T) method. Again, four basis set families, aug-cc-pVXZ, aug-cc-pCVXZ, aug-pcSseg-n, and x2c-Def2 were used. Similarly to NaH, the results obtained with the aug-cc-pVXZ basis sets exhibit a slightly scattered and not converging behavior with increasing the basis set size. Interestingly, the difference between isotropic shieldings calculated with the lowest and the highest basis set (augcc-pVDZ and aug-cc-pV5Z) are -36, -98, and -73 ppm for HF-SCF, B3LYP and CCSD(T), respectively (see Table 7A). Besides, the difference between the aug-cc-pCV5Z and aug-ccpV5Z <sup>25</sup>Mg shielding calculated with these three methods was 7, -35 and -22 ppm, respectively. As expected, the results obtained with the core-valence basis set family, as well as with Jensen's and Karlsruhe type series smoothly converge towards the CBS limit (Figure S10).

According to Table S7A, the CCSD(T)/CBS (estimated with the core-valence basis sets) <sup>25</sup>Mg isotropic nuclear shielding in MgH<sub>2</sub> is 447.156 ppm. When we consider also ZPVC of 10.66 ppm, RC of 9.97 ppm, and TC of 1.36 ppm (Table 4), the total shielding changes to its final value of 467.786 ppm.

In contrast, we can see a smooth energy convergence for MgH<sub>2</sub> calculated with the B3LYP functional and the two basis sets in Figure S10B.

#### S1.3 Sensitivity of <sup>27</sup>Al parameters to the basis set quality

As in previous sections, convergence patterns of <sup>27</sup>Al NMR shielding constants for AlH<sub>3</sub>, calculated with the HF-SCF, B3LYP and CCSD(T) methods, combined with the aug-cc-pVXZ, aug-cc-pCVXZ, aug-pcSseg-n, and x2c-Def2 basis sets are gathered in Table S8A and the coupled cluster results are shown graphically in Figure S11A. Again, the CCSD(T) results obtained with the aug-cc-pVXZ basis sets show an irregular zig-zag pattern, which doesn't allow any reliable extrapolation of shieldings to the CBS limit. This is solved by utilizing the corevalence or Jensen's basis set family that converge smoothly towards the CBS following an exponential decay curve. The results, calculated with Karlsruhe basis set series are also near the CBS limit. Observed scatter of <sup>27</sup>Al isotropic shieldings calculated at CCSD(T)/aug-cc-pVXZ level of theory is significant (ca. -74, -7, -15 ppm for  $X = T \rightarrow D$ ,  $Q \rightarrow T$  and  $S \rightarrow Q$ ). To extend the choice of core-valence basis sets we also tested the performance of HF-SCF and CCSD(T) calculations with the aug-cc-pwVXZ family. The CCSD(T)/CBS (estimated with the aug-ccpwVXZ basis sets) <sup>27</sup>Al isotropic nuclear shielding in AlH<sub>3</sub> was estimated as 307.762 ppm changing to 318.672 ppm after consideration of ZPVC, RC, and TC (-1.06 ppm, 11.92 ppm, and 0.01 ppm; see Table 4).

Table S8B also adds information of the B3LYP and CCSD(T) calculated energies for AlH<sub>3</sub> using aug-cc-pVXZ and aug-cc-pCVXZ series of basis sets and Figure S11B shows the corresponding regular convergence of the B3LYP/aug-cc-pVXZ and B3LYP/aug-cc-pCVXZ calculated energy of AlH<sub>3</sub>.

#### S1.4 Sensitivity of <sup>29</sup>Si parameters to the basis set quality

Another NMR nucleus in the third row is  $^{29}$ Si. Convergence patterns of  $^{29}$ Si NMR shielding constants for SiH<sub>4</sub> calculated again with the HF-SCF, B3LYP and CCSD(T) methods, combined with the aug-cc-pVXZ, aug-cc-pCVXZ, aug-pcSseg-n, and x2c-Def2 basis sets are gathered in Table S9A and are depicted in Figure S12A. As seen before, the aug-cc-pVXZ basis sets provide again an irregular pattern that is impossible to reliably extrapolate to the CBS limit. However, the core-valence basis set family gives shieldings smoothly converging towards CBS. In case of SiH<sub>4</sub>, the change of isotropic shieldings upon increasing the basis set size observed for aug-cc-pVXZ (-67, 14, -34 ppm for  $X = T \rightarrow D$ ,  $Q \rightarrow T$  and  $5 \rightarrow Q$ ) is comparable to changes of the  $^{27}$ Al NMR parameters. The estimated CCSD(T)/CBS(aug-cc-pCVXZ) of  $^{29}$ Si isotropic nuclear shielding in SiH<sub>4</sub> is 470.854 ppm. When ZPVC, RC, and TC (20.28 ppm, 14.92 ppm, and -0.75 ppm; Table 4) are included the final value increases to 506.054 ppm. As before, the Jensen's and Karlsruhe type basis sets produce regularly converging patterns of  $^{29}$ Si isotropic nuclear shielding.

Table S9B compares the B3LYP and CCSD(T) energies of SiH<sub>4</sub> calculated with the aug-cc-pVXZ and aug-cc-pCVXZ basis sets. In Figure S12B we can see regular energy convergences for SiH<sub>4</sub> calculated using the B3LYP functional and the two Dunning's basis sets.

As an example of a silicon-containing molecule with the triple bond we picked  $HSi \equiv CH$ . Its NMR shieldings were calculated again with the HF-SCF, B3LYP, and CCSD(T) methods, combined with the aug-cc-pVXZ, aug-cc-pCVXZ, aug-pcSseg-n, and x2c-Def2 basis sets. All corresponding silicon nuclear shieldings are gathered in Table S9C. Since  $HSi \equiv CH$  contains a triple bond between silicon and carbon, it represents an interesting model because it is supposed

to be highly anharmonic and ZPVC may play a significant role. This appeared partially true, as seen in Table 4. However, the calculated ZPVC varies with the level of theory (30.77 ppm for the mixed CCSD(T)/BHandHLYP level and -0.69 ppm for B3LYP). Moreover, due to its nature, the standard perturbational approach fails when the lowest vibrational modes were included in the PT2 formula. Thus, the contribution of the three lowest modes had to be excluded from the ZPVC estimates. Nevertheless, ZPVC for HSi = CH may be unreliable and deserves further study in the future. Also, electron correlation is substantial (about 151 ppm on  $^{29}Si$ ) as documented in Table S9C.

#### S1.5 Sensitivity of <sup>33</sup>S parameters to the basis set quality

Another NMR active nucleus of the third row lying in the sixth group is  ${}^{33}$ S. All  ${}^{33}$ S nuclear shielding values are gathered in Table S10A for H<sub>2</sub>S and are calculated using the HF-SCF, B3LYP and CCSD(T) methods combined with the aug-cc-pVXZ, aug-cc-pCVXZ, aug-pcSseg-n, and x2c-Def2 basis sets. In Table S10B there are the corresponding B3LYP and CCSD(T) energies calculated with the aug-cc-pVXZ and aug-cc-pCVXZ basis sets. Obviously, the nuclear shielding results obtained with the aug-cc-pVXZ basis set series are also scattered as we have seen for nuclei in other groups (Figure S13A). Thus, it is difficult to extrapolate these results to the CBS limit. However, the results obtained with the core-valence basis set family again converge towards CBS (see also ref.  $^{12}$ ) for X = T to 5. In case of H<sub>2</sub>S, the magnitude of the scatter of isotropic shieldings calculated with CCSD(T)/aug-cc-pVXZ method is comparable to the  $^{31}$ P NMR parameters (see changes of -29, -3, -22 and -1 ppm for  $X = T \rightarrow D$ ,  $Q \rightarrow T$ ,  $5 \rightarrow Q$  and  $6 \rightarrow 5$ ). The isotropic CCSD(T)/CBS(aug-cc-pCVXZ)  $^{33}$ S nuclear shielding of 741.209 ppm from

Table S10A was corrected using ZPVC, RC, and TC (-22.36 ppm, 24.80 ppm, and -0.51 ppm; Table 4) and the final value of 743.649 ppm was obtained.

As for other elements, Figure S13B in Supporting Information reveals smooth convergences of H<sub>2</sub>S energies calculated at the B3LYP level with the two basis sets.

#### S1.6 Sensitivity of <sup>35</sup>Cl parameters to the basis set quality

Nuclear shielding values calculated using HF-SCF, B3LYP and CCSD(T) methods combined with the aug-cc-pVXZ, aug-cc-pCVXZ, aug-pcSseg-n, and x2c-Def2 basis sets for the 3<sup>rd</sup> row halogen, chlorine, are gathered in Table S11A. The B3LYP and CCSD(T) calculated energies using the aug-cc-pVXZ, aug-cc-pCVXZ basis sets for HCl can be found in Table S11B. Figure S14A shows convergence patterns of <sup>35</sup>Cl NMR shielding constants for HCl calculated with the four selected basis sets and using the CCSD(T) method. As before, the aug-cc-pVXZ basis set family produces unreliable and scattered results upon increasing the basis set size. Similarly as for previous nuclei, it is difficult to extrapolate these results to the CBS limit according to the X =T, Q, 5 and 6 data. On the other hand, corresponding points obtained with the aug-cc-pCVXZ show a nice decaying convergence pattern for X = T to 5. In case of HCl, the scatter of isotropic shieldings calculated with aug-cc-pVXZ is significantly smaller than for <sup>33</sup>S NMR parameters (see changes of about -16, -2, -11 and -1 ppm for  $X = T \rightarrow D$ ,  $Q \rightarrow T$ ,  $S \rightarrow Q$  and  $S \rightarrow S$ ). The CBS (CCSD(T)/aug-cc-pCVXZ) <sup>35</sup>Cl isotropic nuclear shielding in HCl was estimated as 957.943 ppm, which was later corrected by ZPVC (-18.29 ppm), RC (32.16 ppm), and TC (-0.42 ppm) to its final value of 971.813 ppm (see Table 4). There is also a nice convergence of chlorine shieldings calculated with the aug-pcSseg-n basis set family. The x2c-Def2 basis sets produce results close to the CBS value, estimated for the aug-cc-pCVXZ basis set hierarchy.

Theoretical smooth energy convergences for HCl calculated with the B3LYP functional and the two Dunning's type basis sets are shown in Figure S14B in Supplemental Material.

#### S1.7 Sensitivity of <sup>39</sup>Ar parameters to the basis set quality

Convergence patterns of hypothetical <sup>39</sup>Ar NMR shielding constants calculated at the CCSD(T) level using the aug-cc-pVXZ, aug-cc-pCVXZ, aug-pcSseg-n, and x2c-Def2 basis sets are shown in Figure S15A and the individual HF-SCF, B3LYP, and CCSD(T) shieldings, as well as the estimated CBS values, are gathered in Table S12A. In this case, the results obtained with the aug-cc-pVXZ basis sets show a fairly regular convergence pattern. In contrast to previous hydrides, the <sup>39</sup>Ar shieldings are nearly saturated and converge is starting from smaller basis sets (compare results obtained with aug-cc-pCVTZ, aug-cc-pCVQZ and aug-cc-pCV5Z). Thus, scattering of <sup>39</sup>Ar isotropic shieldings calculated at the B3LYP/aug-cc-pVXZ level is significantly smaller (0.18, 0.01, 0.14, and 0.13 ppm for  $X = T \rightarrow D$ ,  $Q \rightarrow T$ ,  $5 \rightarrow Q$ , and  $6 \rightarrow 5$ , resp.) than that, which is observed for the <sup>35</sup>Cl NMR parameters. Note that the estimated CBS (CCSD(T)/aug-ccpCVXZ) value of the <sup>39</sup>Ar isotropic nuclear shielding is 1237.924 ppm, so the observed changes with increasing basis set size are negligible. Besides, the aug-pcSseg-n and aug-cc-pVXZ basis sets perform similarly and their CBS results are about 0.5 ppm lower than the converged values for aug-cc-pCVXZ. On the other hand, shieldings calculated using Karlsruhe basis sets scattered more than expected. When the relativistic correction of 33.72 ppm is considered, we obtain the best value of 1271.644 ppm.

Figure S15B clearly reveals a smooth energy convergence for the argon atom calculated with the B3LYP functional and the two Dunning's basis sets.

**Table S1A.** Theoretical  $^{31}P$  nuclear shielding values (in ppm) of  $PH_3$  calculated at the B3LYP, HF-SCF, and CCSD(T) level using various basis sets.

		$PH_3$		
Basis set	b. f.	B3LYP	HF- SCF	CCSD(T)
aVXZ				
D	54	629.029	645.500	669.295
T	119	577.881	602.124	625.354
Q	222	583.120	610.049	630.431
5	371	557.361	580.829	601.383
6	574	557.782	580.718	601.079
CBS(Q-6)		553.876	576.501	596.957
aCVXZ				
D	63	591.385	612.462	639.239
T	144	561.534	584.555	608.292
Q	272	558.319	581.774	604.194
5	457	558.027	581.523	603.368
CBS(T-5)		557.847	581.367	603.326
apcSseg <i>n</i>				
0	26	618.515	665.870	678.359
1	60	571.99	597.015	621.910
2	128	559.65	582.699	600.605
3	248	557.74	581.030	602.087
4	414	557.89	581.042	602.033
CBS(2-4)		557.661	580.892	602.184
x2c-XZVPPall-				
S				
x2c-SVPall-s	45	551.927	585.077	601.819
x2c-TZVPPall-s	96	558.755	583.521	604.065
x2c-QZVPPall-s	172	553.668	577.512	598.945
CBS(1-3)		556.340	580.073	601.348

Table S1B. The B3LYP and CCSD(T) energies (in a.u.) of  $PH_3$ 

	$PH_3$	
Basis set	B3LYP	CCSD(T)
aVXZ		
D	- 343.16263598	-342.65674477
Т	- 343.18054477	-342.74522177
Q	- 343.18524453	-342.76498669
5	- 343.18943646	-342.89034025
6	- 343.18998064	-342.96350363
CBS(Q-6)	- 343.19246832	-343.04039416
aCVXZ		
D	- 343.16593385	-342.860511137
Т	- 343.18569238	-343.026773502
Q	- 343.19001447	-343.093932239
5	- 343.19061671	-343.121495928
CBS(T-5)	- 343.19234535	-343.146144750

 $\textbf{Table S2A.} \ \ \text{The B3LYP}^{\ 31} P \ \ \text{and}^{\ 15} N \ \ \text{nuclear shielding components, isotropic shieldings and shielding anisotropy of PN}^{a}$ 

Basis set	b. f. <sup>b</sup>		3	¹P			15	N	
		$\sigma_{xx}$	σ <sub>zz</sub>	$\sigma_{\mathrm{iso}}$	σ <sub>aniso</sub>	$\sigma_{xx}$	$\sigma_{zz}$	$\sigma_{\mathrm{iso}}$	<b>G</b> aniso
aVXZ									
aVDZ	50	-414.054	966.072	45.988	1380.126	- 709.558	341.805	-359.104	1051.363
aVTZ	96	-525.830	965.611	-28.683	1491.441	- 789.443	341.523	-412.455	1130.966
aVQZ	164	-472.400	965.436	6.879	1437.835	- 813.679	341.814	-428.514	1155.493
aV5Z	258	-581.863	966.515	-65.737	1548.378	- 824.679	341.831	-435.843	1166.510
aV6Z	382	-577.533	966.520	-62.849	1544.053	- 828.098	341.849	-438.116	1169.948
<b>CBS(5-6)</b>		-575.605	966.522	-61.563	1542.127				
CBS(Q-6)						- 829.013	341.84628	-438.727	1170.860
aCVXZ									
aCVDZ	63	-537.347	966.292	-36.134	1503.638	- 742.096	341.882	-380.770	1083.977
aCVTZ	134	-569.885	966.146	-57.875	1536.031	- 807.266	341.856	-424.226	1149.122
aCVQZ	243	-571.027	966.329	-58.575	1537.356	- 820.945	341.851	-433.346	1162.796
aCV5Z	398	-572.093	966.331	-59.285	1538.424	- 826.138	341.858	-436.806	1167.995
CBS(T-5)		-571.792	966.350	-59.078	1538.142	- 825.545	341.855	-436.411	1167.3988
awCVXZ									
awCVDZ	63	-539.032	966.100	-37.322	1505.132	- 745.086	341.738	-382.811	1086.824

awCVTZ	134	-568.374	966.094	-56.885	1534.468	- 801.810	341.817	-420.601	1143.627
awCVQZ	243	-569.984	966.325	-57.881	1536.309	- 818.980	341.850	-432.037	1160.830
awCV5Z	398	-572.098	966.331	-59.288	1538.428	- 826.129	341.857	-436.800	1167.987
CBS(T-5)		-571.430	966.354	-58.835	1537.783	- 825.133	341.858	-436.136	1166.991
apcn									
apc-1	50	-516.962	966.843	-22.360	1483.806	- 744.540	342.014	-382.355	1086.553
apc-2	96	-561.408	966.691	-52.042	1528.099	- 814.133	341.964	-428.767	1156.097
арс-3	178	-568.151	966.688	-56.538	1534.839	- 826.000	341.860	-436.714	1167.860
apc-4	286	-571.124	966.687	-58.520	1537.811	- 828.816	341.862	-438.590	1170.678
CBS(2-4)		-570.606	966.687	-58.175	1537.293	- 828.886	341.851	-438.641	1170.736
apcSsegn									
apcSseg-1	59	-578.815	966.522	-63.702	1545.337	- 808.622	342.061	-425.061	1150.683
apcSseg-2	111	-579.105	966.435	-63.925	1545.540	- 827.185	342.022	-437.449	1169.206
apcSseg-3	198	-574.961	966.428	-61.165	1541.389	- 828.395	341.851	-438.313	1170.246
apcSseg-4	305	-573.244	966.407	-60.027	1539.650	- 828.289	341.865	-438.238	1170.154
CBS(2-4)		-573.422	966.414	-60.143	1539.835	- 828.475	341.839	-438.371	1170.314
арсЈп									
apcJ-1	76	-619.637	928.452	-103.607	1548.088	-	341.963	-427.553	1154.275

						812.312			
apcJ-2	137	-592.272	954.892	-76.551	1547.164	-	341.864	-438.202	1170.098
						828.234			
apcJ-3	220	-583.702	958.924	-69.493	1542.625	-	341.840	-438.162	1170.002
						828.163			
apcJ-4	332	-576.369	964.003	-62.911	1540.372	-	341.849	-438.154	1170.006
_						828.156			
CDC(2.4)		-577.405	962.963	-63.948	1540.368	-	341.842	-438.150	1169.988
CBS(2-4)						828.146			

<sup>&</sup>lt;sup>a</sup>All NMR calculations were performed at CCSD(T)/aug-pc-4 geometry (1.49466464 Å); <sup>b</sup>Number of basis functions

**Table S2B.** Diamagnetic (DSO) and paramagnetic (PSO) contributions (in ppm) to the phosphorus nuclear shielding of PN calculated at the B3LYP level using various basis sets.

		PN		
	aVDZ	aVTZ	aVQZ	aV5Z
DSO	971.43	971.94	949.46	962.39
PSO	-925.45	-1000.60	-942.54	-1028.41
Tota	45.98	-28.66	6.92	-66.02
1				
	aCVDZ	aCVTZ	aCVQZ	aCV5Z
DSO	974.16	964.91	966.54	967.84
PSO	-1010.31	-1022.79	-1025.12	-1027.13
Tota	-36.15	-57.88	-58.58	-59.29
1				
	apcSseg-1	apcSseg-	apcSseg-	apcSseg-4
		2	3	•
DSO	967.90	966.65	967.93	969.23
PSO	-1031.61	-1030.59	-1029.10	-1029.26
Tota	-63.71	-63.94	-61.17	-60.03
1				
	apc-1	apc-2	apc-3	apc-4
DSO	967.67	966.74	969.19	972.15
PSO	-990.04	-1018.77	-1025.72	-1030.59
Tota	-22.37	-52.03	-56.52	-58.43
1				
	apcJ-1	apcJ-2	apcJ-3	apcJ-4
DSO	933.19	956.84	959.13	959.04
PSO	-1036.80	-1033.42	-1028.64	-1021.98
Tota	-103.62	-76.57	-69.51	-62.95
1				

**Table S3.** The B3LYP  $^{31}$ P and  $^{15}$ N NMR parameters shown as differences between 2 cardinal numbers in PN (ppm)

Basis set		31	P			15	N	
	$\sigma_{xx}$	σ <sub>zz</sub>	σ <sub>iso</sub>	<b>G</b> aniso	$\sigma_{xx}$	σ <sub>zz</sub>	σ <sub>iso</sub>	$\sigma_{\rm aniso}$
aVXZ								
(T → D)	-111.776	-0.461	-74.671	111.315	- 79.885	-0.282	-53.350	79.603
$(Q \rightarrow T)$	53.430	-0.175	35.562	-53.606	- 24.236	0.291	-16.060	24.527
(5 → Q)	-109.464	1.079	-72.616	110.543	- 11.001	0.016	-7.328	11.017
$(6 \rightarrow 5)$	4.330	0.006	2.889	-4.325	-3.419	0.019	-2.273	3.438
aCVXZ								
(T → D)	-32.539	-0.146	-21.741	32.392	- 65.171	-0.026	-43.456	65.145
(Q → T)	-1.142	0.183	-0.700	1.325	- 13.678	-0.005	-9.120	13.673
$(5 \rightarrow Q)$	-1.066	0.002	-0.710	1.068	-5.193	0.007	-3.460	5.200
ONWE								
awCVXZ					_			
(T → D)	-29.342	-0.006	-19.563	29.336	56.725	0.079	-37.790	56.803
$(Q \rightarrow T)$	-1.610	0.231	-0.996	1.841	- 17.170	0.033	-11.436	17.203
$(5 \rightarrow Q)$	-2.113	0.006	-1.407	2.119	-7.149	0.007	-4.764	7.157
apc <i>n</i>								
(2-1)	-44.446	-0.153	-29.681	44.293	69.593	-0.050	-46.412	69.543
(3-2)	-6.743	-0.003	-4.496	6.740	- 11.867	-0.104	-7.946	11.763
(4-3)	-2.973	-0.001	-1.983	2.972	-2.816	0.002	-1.877	2.818
apcSsegn								
(2 → 1)	-0.290	-0.087	-0.223	0.203	18.563	-0.039	-12.388	18.524
$(3 \rightarrow 2)$	4.143	-0.007	2.760	-4.150	-1.210	-0.170	-0.864	1.040
$(4 \rightarrow 3)$	1.718	-0.021	1.138	-1.739	0.106	0.013	0.075	-0.092
apcJn								
(2 → 1)	27.365	26.441	27.057	-0.924	- 15.923	-0.100	-10.649	15.823

$(3\rightarrow 2)$	8.570	4.031	7.057	-4.539	0.072	-0.024	0.040	-0.095
$(4\rightarrow 3)$	7.333	5.080	6.582	-2.253	0.006	0.010	0.008	0.003

**TABLE S4.** Calculated B3LYP/CBS<sup>a 31</sup>P nuclear shielding components, isotropic shieldings and shielding anisotropy of PN<sup>b</sup> with respect to cardinal number (X) The difference (in %) between the CBS values estimated with respect to the cardinal number X and the number of basis functions b.f. is shown as  $\Delta$  (%)

PN							
Basis set	$\sigma_{xx}$	$\sigma_{zz}$	$\sigma_{ m iso}$	σ <sub>aniso</sub>			
aVXZ							
X (5-6)	-571.585	966.527	-58.882	1538.112			
Δ (%)	0.698	0.000	4.355	0.260			
aCVXZ	•	•	•				
X (Q-5)	-573.211	966.333	-60.030	1539.545			
$\Delta\left(\% ight)$	-0.141	0.000	-0.900	-0.052			
awCVXZ							
<i>X</i> (Q-5)	-574.316	966.337	-60.764	1540.651			
$\Delta\left(\% ight)$	-0.279	0.000	-1.778	-0.104			
apc <i>n</i>							
X(3-4)	-574.244	966.685	-60.600	1540.929			
Δ (%)	-0.380	0.000	-2.452	-0.141			
apcSsegn							
<i>X</i> (3-4)	-571.441	966.385	-58.833	1537.826			
$\Delta\left(\% ight)$	0.202	0.001	1.284	0.076			
apcJ <i>n</i>	•	•	•	•			
X (3-4)	-568.675	969.332	-56.005	1538.008			
Δ (%)	0.817	-0.336	6.983	0.093			
CCSD(T)/aVXZ <sup>c</sup>			58.080	1362.090			
CCSD(T)/aCVXZ <sup>c</sup>			59.090	1361.250			
Literature							
PBE1PBE/6-311G(2d,2p) <sup>d</sup>			35.7				
B3LYP/6-311++G**e			53.0				
CCSD(T)/15s12p4d3f2g <sup>f</sup>			53.4				

<sup>&</sup>lt;sup>a</sup>Basis sets selected for fitting are in parenthesis; <sup>b</sup>All NMR calculations were performed using the CCSD(T)/aug-pc-4 geometry (1.49466464 Å); <sup>c</sup>From ref.12; <sup>d</sup>From ref.62; <sup>e</sup>From ref.63; <sup>f</sup>From ref.64

**Table S5A.** <sup>31</sup>P isotropic shieldings in H₃PO calculated at the B3LYP, HF-SCF, and CCSD(T) level in combination with the aug-cc-pV*X*Z, aug-cc-pCV*X*Z, and aug-pcSseg-*n* basis sets. <sup>a</sup>

H <sub>3</sub> PO								
		B3LYP	HF-	CCSD(T)				
Basis set	b. f.		SCF	, ,				
aVXZ								
D	77	458.078	494.411	496.373				
T	165	381.595	431.022	427.424				
Q	302	390.328	441.573	433.032				
5	498	350.188	399.961	_				
6	763	349.475	398.916	-				
CBS(5-6)		349.201	398.514	~396 <sup>b</sup>				
aCVXZ								
D	90	402.100	447.671	451.545				
Т	203	354.785	403.727	397.616				
Q	381	348.954	399.412	389.335				
5	638	348.483	399.028	_				
CBS(T-5)		346.109	397.276	~388 <sup>b</sup>				
apcSseg-n								
0	39	453.796	517.119	510.616				
1	86	377.240	424.750	423.473				
2	180	354.333	403.097	393.977				
3	345	348.303	398.614	405.597				
4	563	348.178	398.391	_				
CBS(2-4)		347.681	396.549	~400 <sup>b</sup>				

 $^aB3LYP/aug\text{-cc-pV5}\overline{Z}$  geometry of  $H_3P\text{-O}$  was used (PO=1.476205; PH=1.412422 and HPO=116.746141);  $^bA$  rough estimate from comparison of convergence patterns obtained with HF-SCF

**Table S5B.** The B3LYP, HF-SCF, and CCSD(T) energies (in a.u.) of  $H_3PO$ .

$H_3PO$							
	b.	B3LYP	HF-SCF	CCSD(T)			
Basis set	f.			, ,			
aVXZ							
D	77	-418.387596198	-417.338510362	-417.71138712			
T	165	-418.442930694	-417.392246562	-417.84168225			
Q	302	-418.457842226	-417.406265295	-417.88070359			
5	498	-418.467265810	-417.412337212	-417.89555662			
6	763	-418.468751518	-417.413440044	-417.90016792			
CBS(Q-6)		-418.46966928	-417.41397975	-417.9008092			
aCVXZ							
D	90	-418.394718919	-417.342068132	-417.71850259			
T	203	-418.456313671	-417.401126555	-417.85452001			
Q	381	-418.467766367	-417.411848696	-417.88841014			
5	638	-418.469661666	-417.413678259	-417.89784511			
CBS(T-5)		-418.46997783	-417.41395163	-417.89721138			
apcSseg <i>n</i>							
1	86	-418.376478710	-417.311315008	-417.68361574			
2	180	-418.457227447	-417.398157629	-417.84214735			
3	345	-418.469109581	-417.411219687	-417.88403616			
4	563	-418.469750122	-417.412294093	-417.89429699			
CBS(2-4)		-418.47056645	-417.41303735	-417.893.84342			

**Table S6A.** Theoretical <sup>23</sup>Na nuclear shielding values (in ppm) of NaF and NaH calculated using various methods.

	NaF				NaH	
Basis set	b. f.	B3LYP	b. f.	B3LYP	HF-SCF	CCSD(T)
aVXZ						
D	50	592.819	36	593.102	580.656	585.782
T	96	581.969	73	573.960	575.525	579.222
Q	164	579.192	130	574.010	563.720	565.539
5	258	572.578	211	559.698	563.753	541.040
CBS(T-5)		574.674		565.305	562.384	549.057
aCVXZ						
D	63	586.976	45	583.678	570.165	579.072
T	134	580.693	98	572.513	564.175	569.292
Q	243	580.332	180	572.662	565.081	569.674
5	398	580.362	297	572.697	565.24	569.408
CBS(T-5)		580.311		572.698	565.269	569.555
apcSseg-n						
0	27	588.892	17	577.289	571.090	579.412
1	46	578.504	29	572.142	563.866	572.481
2	89	580.728	60	572.635	564.406	572.457
3	160	580.113	112	572.729	565.084	572.016
4	249	580.066	186	572.753	565.211	572.371
CBS(2-4)		579.815		572.789	565.478	572.180

**Table S6B.** Calculated energies (in a.u.) of NaF and NaH.

	NaF	NaH		
Basis set	B3LYP	B3LYP	CCSD(T)	
aVXZ				
D	-262.204869156	-162.86387918	-162.422001078	
T	-262.237660615	-162.87141560	-162.44338745	
Q	-262.247642152	-162.87414279	-162.45537297	
5	-262.251590656	-162.87510466	-162.45892442	
CBS(T-5)	-262.25527211	-162.87612472	-162.46348953	
aCVXZ				
D	-262.20827680	-162.86540524	-162.61455950	
Т	-262.24443261	-162.87621861	-162.71919341	
Q	-262.25322055	-162.87802768	-162.77681296	
5	-262.25542162	-162.87831464	-162.80221667	
CBS(T-5)	-262.25881776	-162.87903395	-162.82315118	

**Table S7A.** <sup>25</sup>Mg nuclear shielding values (in ppm) of MgH<sub>2</sub> calculated at the HF-SCF, B3LYP, and CCSD(T) level, combined with the aug-cc-pVXZ, aug-cc-pCVXZ, aug-pcSseg-n, and x2c-Def2 basis sets.

$MgH_2$					
Basis set	b. f.	B3LYP	HF-SCF	CCSD(T)	
aVXZ					
D	45	486.035	503.602	496.843	
T	96	459.192	488.420	473.084	
Q	176	421.519	485.928	469.522	
5	291	388.385	468.158	423.764	
CBS(T-5)		397.813	475.048	441.802	
aCVXZ					
D	54	473.001	489.815	484.616	
T	121	439.339	470.668	457.479	
Q	226	432.012	465.987	451.201	
5	377	423.201	461.617	445.393	
CBS(T-5)		426.089	462.948	447.156	
apcSseg-n					
0	20	459.402	486.743	467.466	
1	38	426.175	462.991	450.642	
2	83	426.234	459.800	447.809	
3	161	426.427	460.467	444.129	
4	272	426.676	460.780	444.226	
CBS(2-4)		426.588	460.706	443.870	
x2c-XZVPPall-					
S					
x2c-SVPall-s	37	425.167	462.634	450.466	
x2c-TZVPPall-s	69	426.580	460.266	449.526	
x2c-QZVPPall-s	135	423.667	457.168	443.334	
CBS(1-3)		424.985	458.225	445.784	

**Table S7B.** The B3LYP and CCSD(T) energies (in a.u.) of  $MgH_2$  calculated with the aug-cc-pVXZ and aug-cc-pCVXZ basis set series.

	$MgH_2$				
Basis set	B3LYP	CCSD(T)			
aVXZ					
D	-201.25953842	-200.80399245			
T	-201.26997915	-200.84155803			
Q	-201.27228212	-200.85863579			
5	-201.27465395	-200.92482476			
CBS(T-	-201.27532589	-200.92390375			
5)	-201.27552569	-200.92390373			
aCVXZ					
D	-201.2615830	-200.975948470			
T	-201.2731550	-201.120087868			
Q	-201.2757430	-201.17385263			
5	-201.2766084	-201.19787045			
CBS(T- 5)	-201.2775821	-201.21736633			

**Table S8A.** <sup>27</sup>Al nuclear shielding values (in ppm) of AlH $_3$  calculated at the HF-SCF, B3LYP, and CCSD(T) level, combined with the aug-cc-pVXZ, aug-cc-pCVXZ, aug-pcSseg-n, and x2c-Def2 basis sets.

		$AlH_3$		
Basis set	b. f.	B3LYP	HF-SCF	CCSD(T)
aVXZ				
D	54	356.842	418.019	398.363
T	119	267.533	352.723	324.075
Q	222	279.900	365.604	319.626
5	371	264.302	344.518	305.039
6	574	261.701	342.906	Not conv.
CBS(Q-6)		260.370	340.417	301.061
aCVXZ			awCVXZ	awCVXZ
D	63	292.346	350.971	318.748
Т	144	270.502	348.433	311.521
Q	272	268.116	347.181	308.498
5	457	266.955	346.512	307.726
CBS(T-5)		267.211	346.671	307.762
apcSseg-n				
0	26	224.919	321.006	264.706
1	60	272.72	347.879	312.927
2	128	266.47	344.749	307.232
3	172	264.03	341.332	305.189
4	414	266.649	346.004	306.424
CBS(2-4)		265.630	344.362	305.775
x2c-XZVPPall-				
S				
x2c-SVPall-s	45	255.610	338.958	306.507
x2c-TZVPPall-s	96	268.910	346.915	311.762
x2c-QZVPPall-s	172	261.219	341.332	305.189
CBS(1-3)		265.443	344.293	308.421

**Table S8B.** The B3LYP and CCSD(T) energies (in a.u.) of  $AlH_3$  calculated with the aug-cc-pVXZ and aug-cc-pCVXZ basis set series.

	$AlH_3$	
Basis set	B3LYP	CCSD(T)
aVXZ		
D	- 244.21922425	-243.747570184
Т	- 244.23360255	-243.837834800
Q	- 244.23939987	-243.83729289
5	- 244.24097337	-243.92943312
6	- 244.24104531	-
CBS(Q-6)	- 244.24197328	-
CBS(T-5)	-	-243.91801437
aCVXZ		
D	- 244.22201311	-243.87445191
Т	- 244.23785921	-244.04698171
Q	- 244.24170076	-244.12311882
5	- 244.24227256	-244.15894233
CBS(T-5)	- 244.24380456	-244.18633069

**Table S9A.** <sup>29</sup>Si nuclear shielding values (in ppm) of SiH<sub>4</sub> calculated at the HF-SCF, B3LYP, and CCSD(T) level, combined with the aug-cc-pVXZ, aug-cc-pCVXZ, aug-pcSseg-n, and x2c-Def2 basis sets.

		SiH <sub>4</sub>		
Basis set	b. f.	B3LYP	HF-SCF	CCSD(T)
aVXZ				
D	63	524.779	548.033	554.575
T	142	450.243	485.124	488.826
Q	268	457.562	506.361	501.517
5	451	435.668	473.932	468.513
CBS(T-5)		445.370	489.275	483.294
aCVXZ				
D	72	473.6513	507.218	516.049
T	167	439.0493	476.680	476.451
Q	318	436.0286	474.938	471.664
5	537	435.4506	479.932	_
CBS(T-5)		435.416	477.703	470.854
apcSseg-n				
0	29	486.947	533.581	540.468
1	69	444.030	483.088	483.900
2	151	436.940	475.284	469.321
3	297	434.980	473.826	469.018
4	500	435.270	473.974	-
CBS(2-4)		434.990	473.79	468.972
x2c-XZVPPall-				
S				
x2c-SVPall-s	53	441.080	480.403	482.139
x2c-TZVPPall-s	113	437.239	475.830	472.508
x2c-QZVPPall-s	205	431.572	470.8032	467.086
CBS(1-3)		433.841	472.744	468.890

Table S9B. The B3LYP and CCSD(T) energies (in a.u.) of SiH<sub>4</sub>

SiH <sub>4</sub>				
Basis set	B3LYP	CCSD(T)		
aVXZ				
D	- 291.89879366	-291.4087569985		
Т	- 291.91847211	-291.5056560050		
Q	- 291.92448059	-291.504971737		
5	- 291.92810244	-291.627661525		
6	- 291.92866588	-		
CBS(Q-6)	- 291.93081935	-		
CBS(T-5)		-291.61247239		
aCVXZ				
D	- 291.90205678	-291.607682461		
Т	- 291.92365987	-291.765560806		
Q	- 291.92870585	-291.827830430		
5	- 291.92937201	-		
CBS(T-5)	- 291.93139466	-		
CBS(D-Q)	-	-291.87327043		

**Table S9C.** <sup>29</sup>Si nuclear shielding values (in ppm) of HSiCH calculated at the HF-SCF, B3LYP, and CCSD(T) level, combined with the aug-cc-pVXZ, aug-cc-pCVXZ, and aug-pcSseg-*n* basis sets.

	HSiCH				
Basis set	b. f.	B3LYP	HF-SCF	CCSD(T)	
aVXZ					
D		556.68	905.47		
D	68	46	5	666.826	
т	14	505.96	903.96		
T	2	67	2	634.782	
0	25	511.87	905.15		
Q	6	6	8	641.418	
5	41	499.51	914.77		
5	8	18	7	624.410	

6	63 6	501.14 38	-	-
CBS(T- 5,6)		498.605	917.646	619.338
aCVXZ				
D	81	514.935	900.384	645.931
T	180	502.124	904.667	630.532
Q	335	501.597	907.255	630.168
5	558	501.171	907.519	-
CBS(T-5)		501.293	907.666	630.101
apcSseg <i>n</i>				
		503.78	922.88	
1	77	13	5	644.709
	15	500.70	914.77	
2	7	14	2	625.185
	29	501.40	916.40	
3	6	64	5	628.228
	47	501.78	914.66	
4	7	46	1	_
CBS(2-4)		501.697	915.536	628.762

**Table S10A.**  $^{33}$ S nuclear shielding values (in ppm) of H<sub>2</sub>S calculated at the HF-SCF, B3LYP, and CCSD(T) level, combined with the aug-cc-pVXZ, aug-cc-pCVXZ , aug-pcSseg-n, and x2c-Def2 basis sets.

		H <sub>2</sub> S		
Basis set	b. f.	B3LYP	HF- SCF	CCSD(T)
aVXZ				
D	45	757.263	768.299	794.741
T	96	721.620	738.199	765.513
Q	176	722.836	736.350	762.929
5	291	699.124	712.597	740.623
6	447	698.200	712.258	740.020
CBS(Q-6)		694.933	708.776	736.852
aCVXZ				
D	54	726.299	740.258	770.194
T	121	702.600	716.827	745.570
Q	226	698.785	713.141	741.832
5	377	698.501	712.906	741.393
CBS(T-5)		698.246	712.644	741.209
apcSseg-n				
0	23	746.908	793.434	804.953
1	51	709.21	726.433	755.754
2	105	700.97	715.123	739.502
3	199	698.26	719.781	743.898
4	328	698.37	712.476	740.381
CBS(2-4)		698.071	715.929	742.245
x2c-XZVPPall-				
S				
x2c-SVPall-s	37	728.757	755.384	770.757
x2c-TZVPPall-s	79	701.935	719.781	743.898
x2c-QZVPPall-s	139	694.072	709.531	736.967
CBS(1-3)		695.877	711.844	738.358

**Table S10B.** The B3LYP and CCSD(T) energies (in a.u.) of H<sub>2</sub>S.

	$H_2S$	
Basis set	B3LYP	CCSD(T)
aVXZ		
D	- 399.41468530	-398.88839956
Т	- 399.43217564	-398.97922094
Q	- 399.43649626	-399.01740712
5	- 399.44059810	-399.13954634
6	- 399.44111883	-399.21382420
CBS(Q-6)	- 399.44355253	-399.28887450
aCVXZ		
D	- 399.41755048	-399.09628617
Т	- 399.43695573	-399.27659357
Q	- 399.44115027	-399.34894772
5	- 399.44175495	-399.37832694
CBS(T-5)	- 399.44343012	-399.40492109

**Table S10C.** The B3LYP calculated  $^{33}$ S nuclear shieldings for 2-thiouracil with aug-cc-pVXZ and aug-cc-pCVXZ basis sets on all atoms and within LDBS approach (all atoms with 6-31G\* basis set and only sulfur with aVXZ and aCVXZ)

	2-TU														
Basis set			All		Ll	DBS									
(X)		H, C, O, N, S: aVXZ		H: aVXZ; C, O, N, S: aCVXZ	(C, O, N and H: 6-31G*)										
	bf	B3LYP/aVXZ	bf		bf	S: aVXZ	bf	S: aCVXZ							
D	224	387.869	261	331.045	133	398.795	142	347.543							
T	464	335.860	580	306.502	156 365.034 181 332.193										

Q	828	343.732	1081	301.800	190	371.328	240	327.708
5	1340	299.099	1804	301.169	237	325.067	323	327.367
6	2024	298.830	-	-	299	325.205	-	-
CBS		298.720		300.970		325.342		325.774
6-31G*	132	378.514						

**Table S11A.**  $^{35}$ Cl nuclear shielding values (in ppm) of HCl calculated at the HF-SCF, B3LYP, and CCSD(T) level, combined with the aug-cc-pVXZ, aug-cc-pCVXZ, aug-pcSseg-n, and x2c-Def2 basis sets.

		HCl		
Basis set	b. f.	B3LYP	HF-SCF	CCSD(T)
aVXZ				
D	36	961.8332	977.258	986.763
T	73	945.2023	961.547	970.798
Q	130	944.7120	958.593	968.566
5	211	932.9930	946.919	957.914
6	320	931.7249	946.089	957.249
CBS(Q-6)		930.256	944.476	955.745
aCVXZ				
D	45	945.4964	961.169	972.344
T	98	933.9553	948.667	958.910
Q	180	932.1409	946.678	958.007
5	297	931.9804	946.561	958.055
CBS(Q-6)		931.858	946.403	957.943
apcSseg-n				
0	20	941.602	980.478	977.953
1	42	935.83	953.008	964.124
2	82	934.08	948.579	956.537
3	150	931.96	946.336	957.071
4	242	931.91	946.272	957.442
CBS(2-4)		931.705	946.060	957.3498
x2c-XZVPPall-				
S				
x2c-SVPall-s	29	982.965	982.965	983.097
x2c-TZVPPall-s	62	957.132	957.131	963.485
x2c-QZVPPall-s	106	944.420	944.419	954.303

CBS(1-3)	948.413	948.412	957.127

**Table S11B.** The B3LYP and CCSD(T) energies (in a.u.) of HCl

	HCl	
Basis set	B3LYP	CCSD(T)
aVXZ		
D	-460.82758530	-460.27881668
T	-460.84426235	-460.37795747
Q	-460.84818174	-460.42666503
5	-460.85164037	-460.54386650
6	-460.85220096	-460.62888464
CBS(Q-6)	-460.85425837	-460.70150484
aCVXZ		
D	-460.830248867	-460.490880368
T	-460.848259238	-460.68548124
Q	-460.852219393	-460.76287445
5	-460.852812828	-460.79423489
CBS(T-5)	-460.85439165	-460.82268904

**Table S12A.** <sup>39</sup>Ar nuclear magnetic shielding values (in ppm) calculated for an isolated atom at the HF-SCF, B3LYP, and CCSD(T) level, combined with the aug-cc-pVXZ, aug-cc-pCVXZ, aug-pcSseg-n, and x2c-Def2 basis sets.

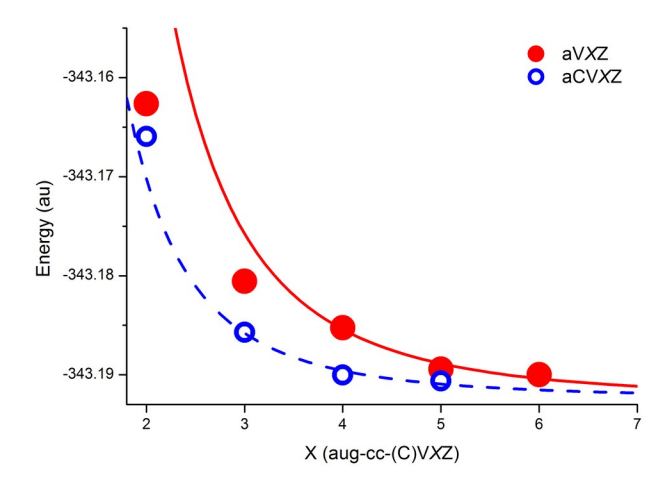
		Ar		
Basis set	b. f.	B3LYP	HF-SCF	CCSD(T)
aVXZ				
D	27	1237.382	1237.602	1237.071
T	50	1237.057	1237.615	1237.246
Q	84	1237.121	1237.651	1237.258
5	131	1237.944	1237.657	1237.394
6	193	1238.049	1237.658	1237.524
CBS(Q-6)		1238.172	1237.659	1237.509
aCVXZ				
D	36	1237.399	1237.570	1237.119
T	75	1237.610	1237.621	1237.644
Q	134	1237.836	1237.655	1237.846
5	217	1237.846	1237.657	1237.937
CBS(T-5)		1237.868	1237.660	1237.924
apcSseg-n				
0	17	1236.404	1236.578	1236.178
1	33	1237.716	1237.155	1236.677
2	59	1237.881	1237.269	1237.004
3	101	1237.936	1237.507	1237.404
4	156	1237.915	1237.498	1237.497
CBS(2-4)		1237.930	1237.534	1237.516
x2c-XZVPPall-				
S				
x2c-SVPall-s	21	1249.189	1248.648	1248.437
x2c-TZVPPall-s	45	1249.336	1248.803	1248.634
x2c-QZVPPall-s	73	1236.887	1236.677	1236.579
CBS(1-3)		1242.409	1242.056	1241.920

**Table S12B.** The B3LYP and CCSD(T) energies (in a.u.) of isolated Ar atom.

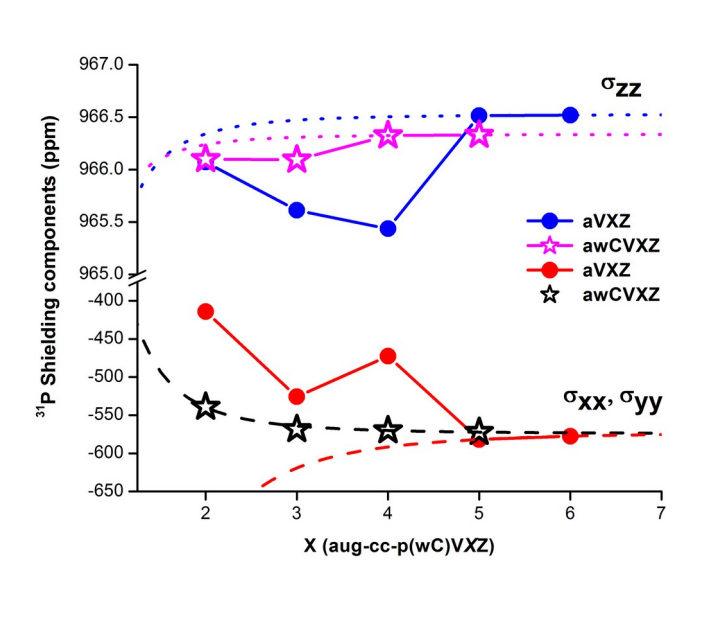
	Ar	
Basis set	B3LYP	CCSD(T)
aVXZ		
D	- 527.54538899	-526.97518862
Т	- 527.56000196	-527.08028270
Q	- 527.56367703	-527.13763465
5	- 527.56633502	-527.25062305
6	- 527.56703390	-527.34980274
CBS(Q-6)	- 527.56805707	-527.38485741
aCVXZ		
D	- 527.54773771	-527.19113752
Т	- 527.56317741	-527.39744948
Q	- 527.56703529	-527.48090156
5	- 527.56763687	-527.51450674
CBS(T-5)	- 527.56917203	-527.54521404

**Table S13.** Relativistic corrections of PN (in ppm) calculated at the B3LYP/aug-cc-pVXZ level (X = D, T, Q)

B3LYP/aVXZ	PN
D	29.82
T	19.50
Q	12.37

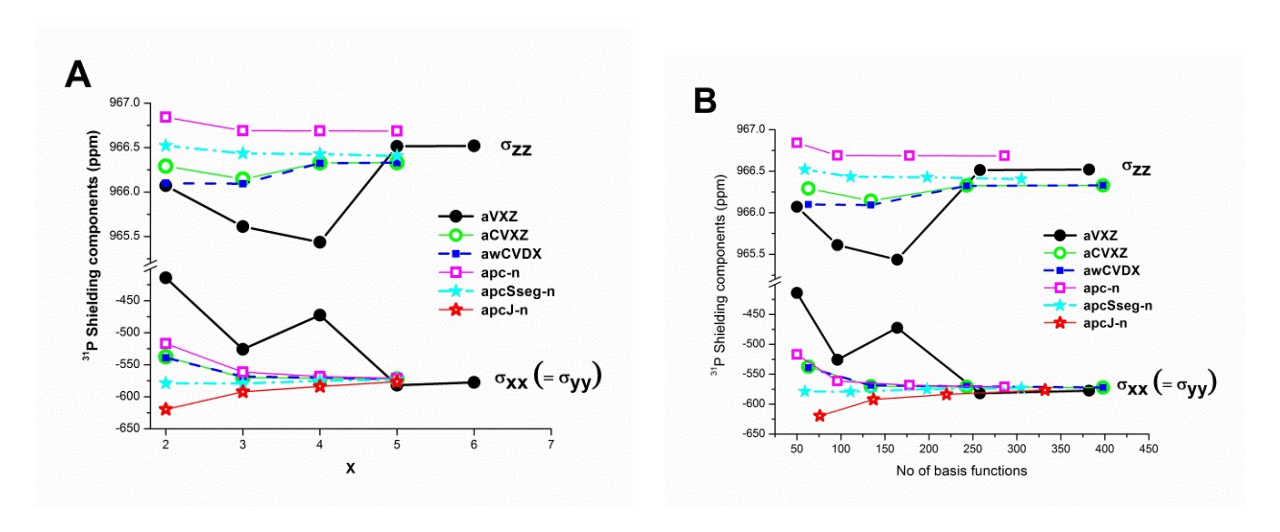


**Figure S1.** Convergences of the B3LYP/aug-cc-pVXZ and B3LYP/aug-cc-pCVXZ energies of  $PH_3$  with fitting lines shown.

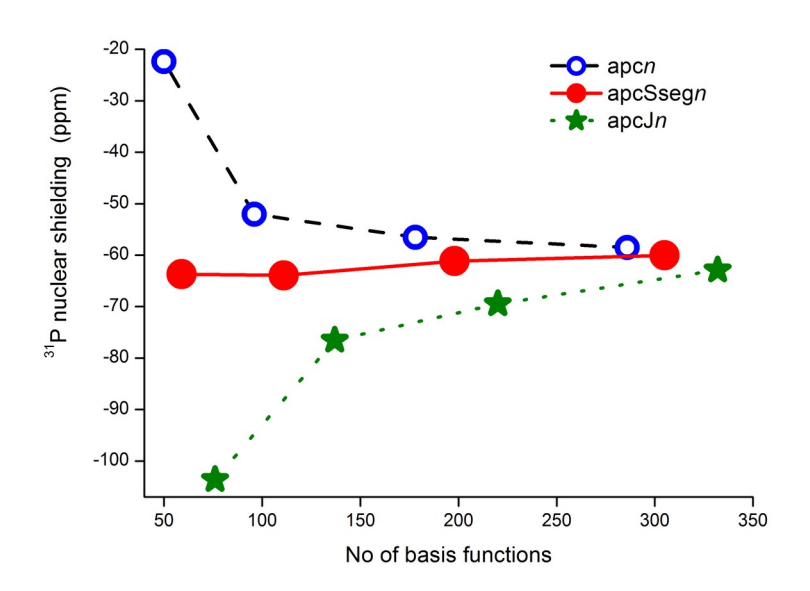


**Figure S2.** Theoretical  $\sigma_{xx}$  (=  $\sigma_{yy}$ ) and  $\sigma_{zz}$  components of  $^{31}P$  nuclear shielding constants in PN calculated at the B3LYP/aug-cc-pVXZ and the B3LYP/aug-cc-pwCVXZ levels, where X=2-5 or 6. The fitting curves estimated with the 2-parameter formula are shown as well.

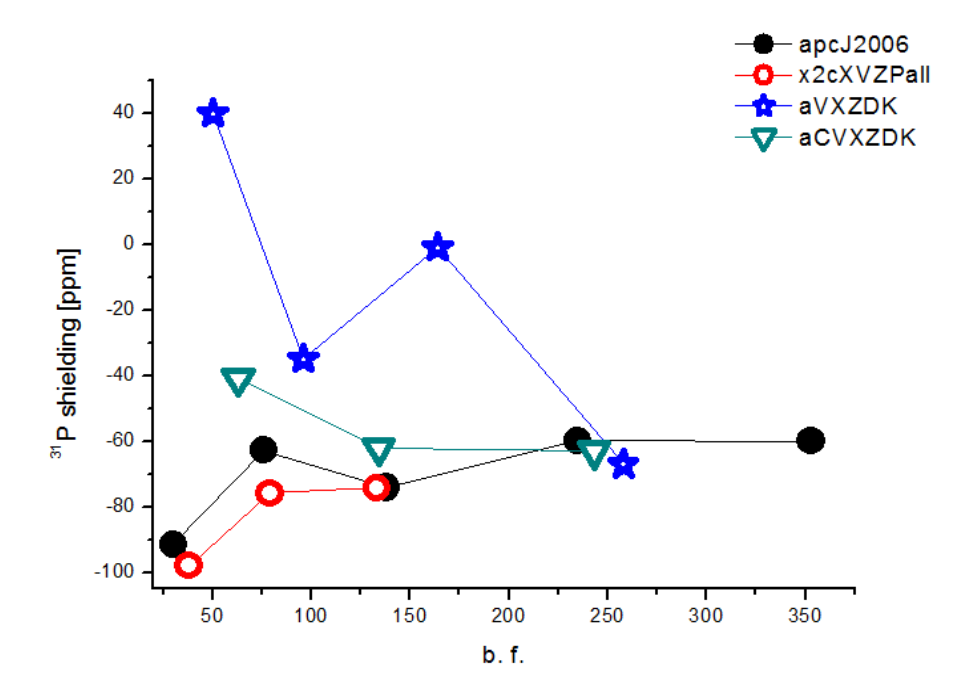
 $\sigma_{xx} = \sigma_{yy}$ 



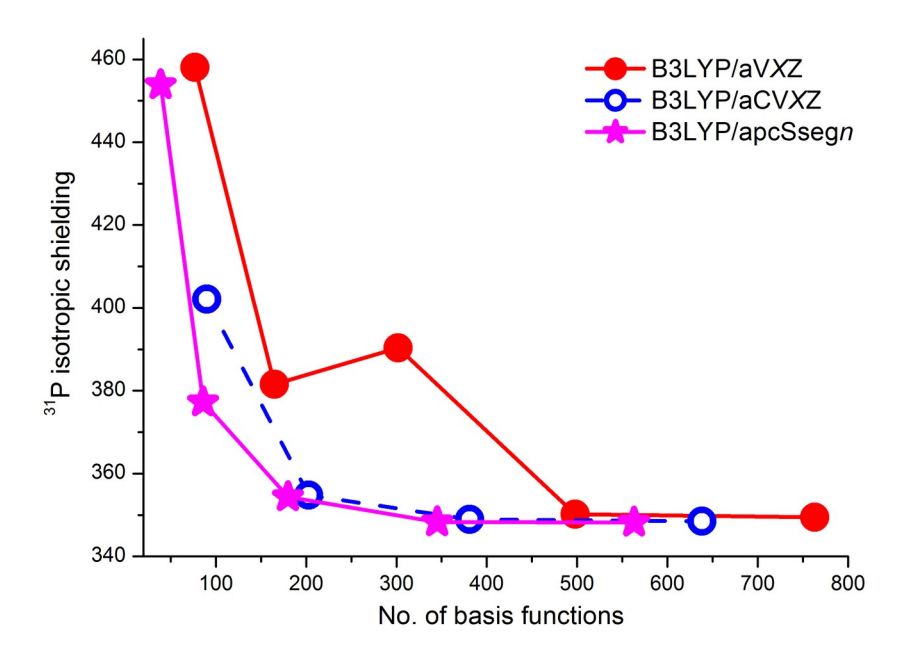
**Figure S3.** B3LYP calculated  $\sigma_{xx}$  (=  $\sigma_{yy}$ ) and  $\sigma_{zz}$  components of the <sup>31</sup>P shielding constants of PN calculated with selected Dunning's and Jensen's basis set families plotted against (A) the cardinal number *X* and (B) the number of basis functions.



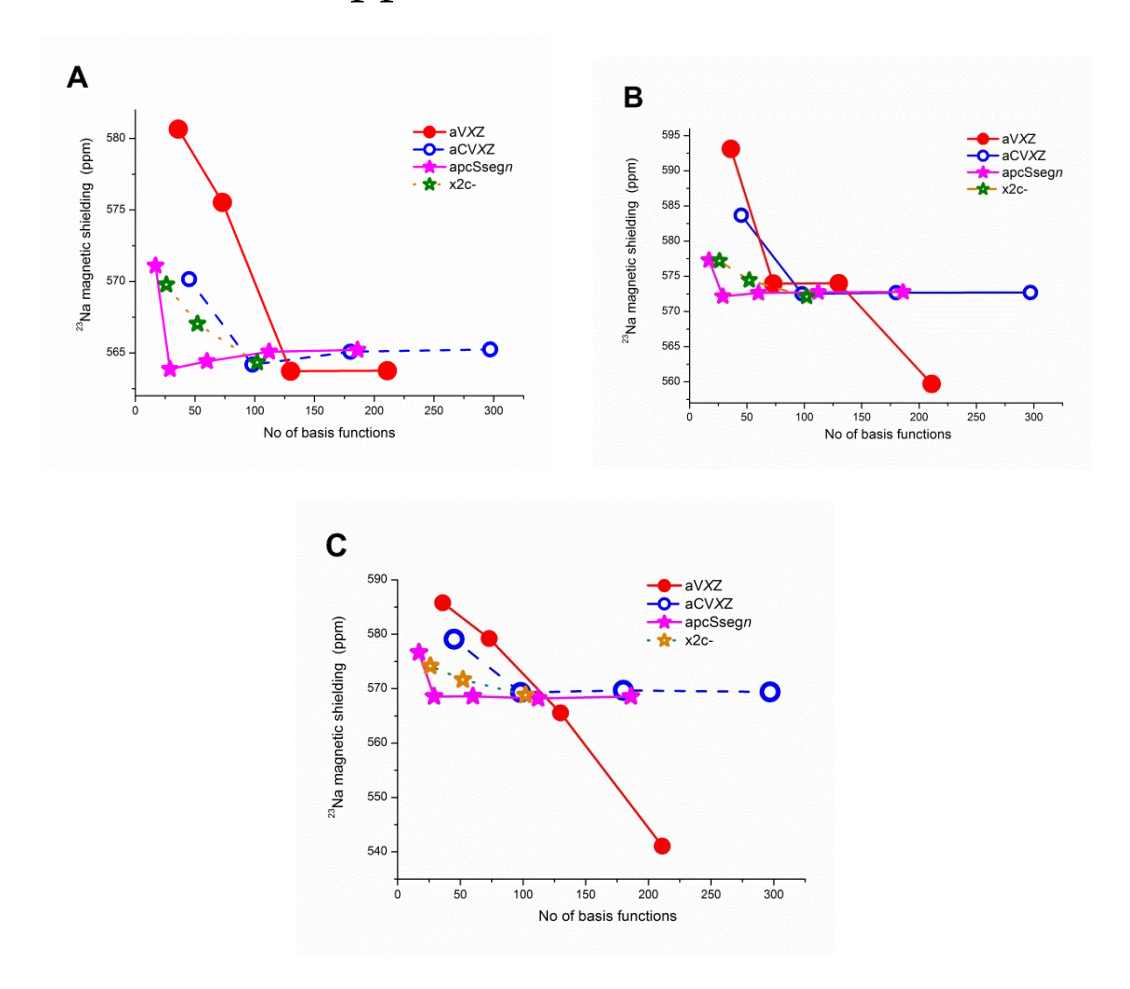
**Figure S4.** Performance of Jensen's basis sets using the B3LYP functional in prediction of <sup>31</sup>P shielding in PN.



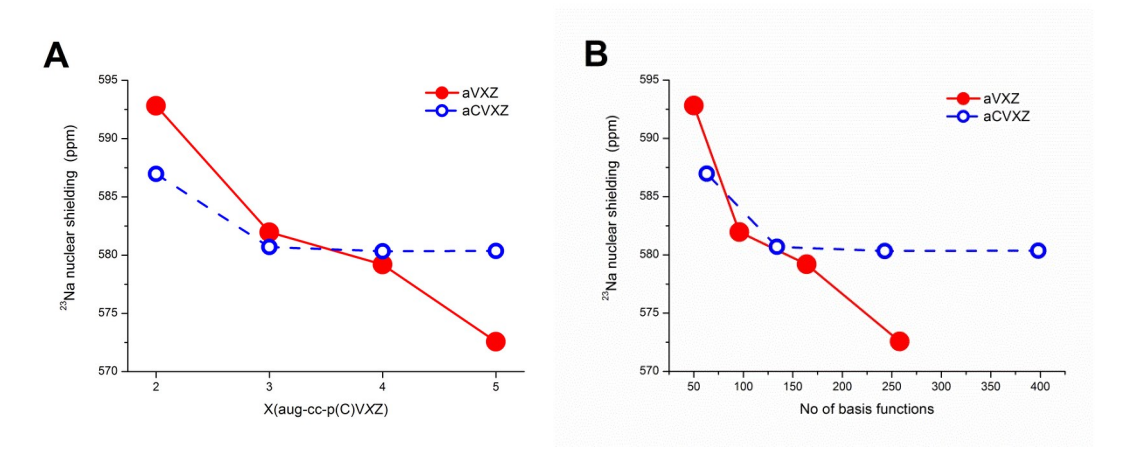
**Figure S5.** Convergence of <sup>31</sup>P shieldings in PN calculated with the B3LYP functional and the aug-pcJ2006, x2c-Def2, aug-cc-pV*X*Z-DK, and aug-cc-pCV*X*Z-DK basis set series.



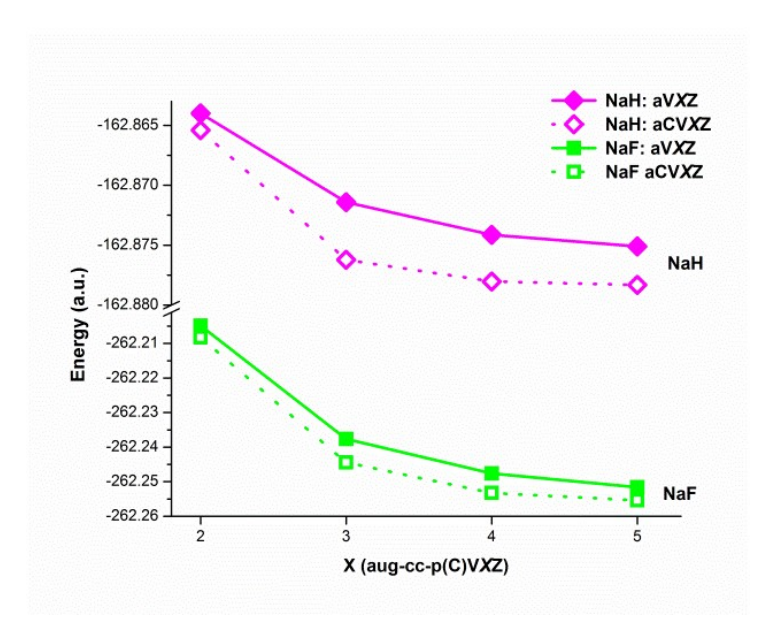
**Figure S6.** Convergence patterns of  $^{31}$ P isotropic shieldings in H<sub>3</sub>PO calculated with B3LYP and HF-SCF in combination with aug-cc-pV*X*Z basis set series and B3LYP/aug-pcSseg-*n* level of theory.



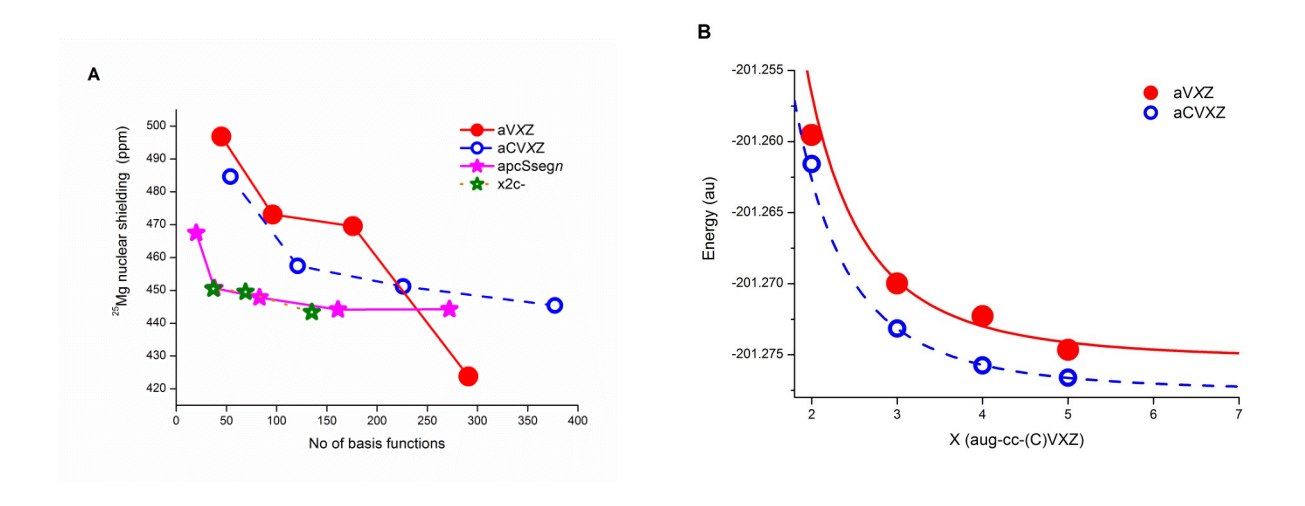
**Figure S7.** <sup>23</sup>Na isotropic shielding constants for NaH calculated with the (A) HF-SCF, (B) B3LYP and (C) CCSD(T) methods, using the aug-cc-pVXZ, aug-cc-pCVXZ, aug-pcSseg-*n* and x2c-Def2 basis set families.



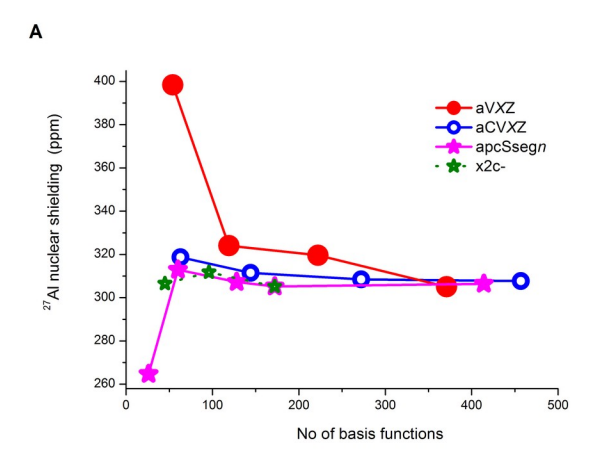
**Figure S8.** The B3LYP  $^{23}$ Na shielding constants with respect to (A) the cardinal number X and (B) the number of basis functions for NaF calculated with the aug-cc-pVXZ and aug-cc-pCVXZ basis set families.



**Figure S9.** Convergence of the B3LYP/aug-cc-pV*X*Z and B3LYP/aug-cc-pCV*X*Z energies of NaH and NaF.



**Figure S10.** Convergence of <sup>25</sup>Mg isotropic shielding constants for MgH<sub>2</sub> calculated with the CCSD(T) method using the aug-cc-pVXZ, aug-cc-pCVXZ, aug-pcSseg-*n* and x2c-XZVPall-s basis set families (A). Convergences of the B3LYP energies of MgH<sub>2</sub> calculated with the aug-cc-pVXZ and aug-cc-pCVXZ basis sets are on the right (B)



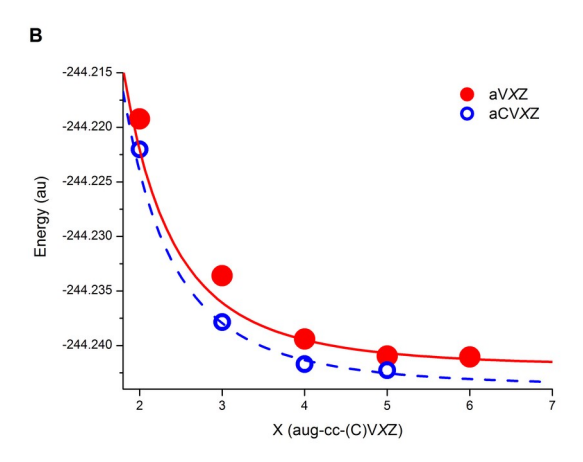


**Figure S11.** <sup>27</sup>Al isotropic shielding constants for AlH<sub>3</sub> predicted with the CCSD(T) method and the aug-cc-pVXZ, aug-cc-pCVXZ, aug-pcSseg-n, and x2c-XZVPall-s basis set families (A). The B3LYP/aug-cc-pVXZ and B3LYP/aug-cc-pCVXZ calculated energies of AlH<sub>3</sub> are on the right (B).

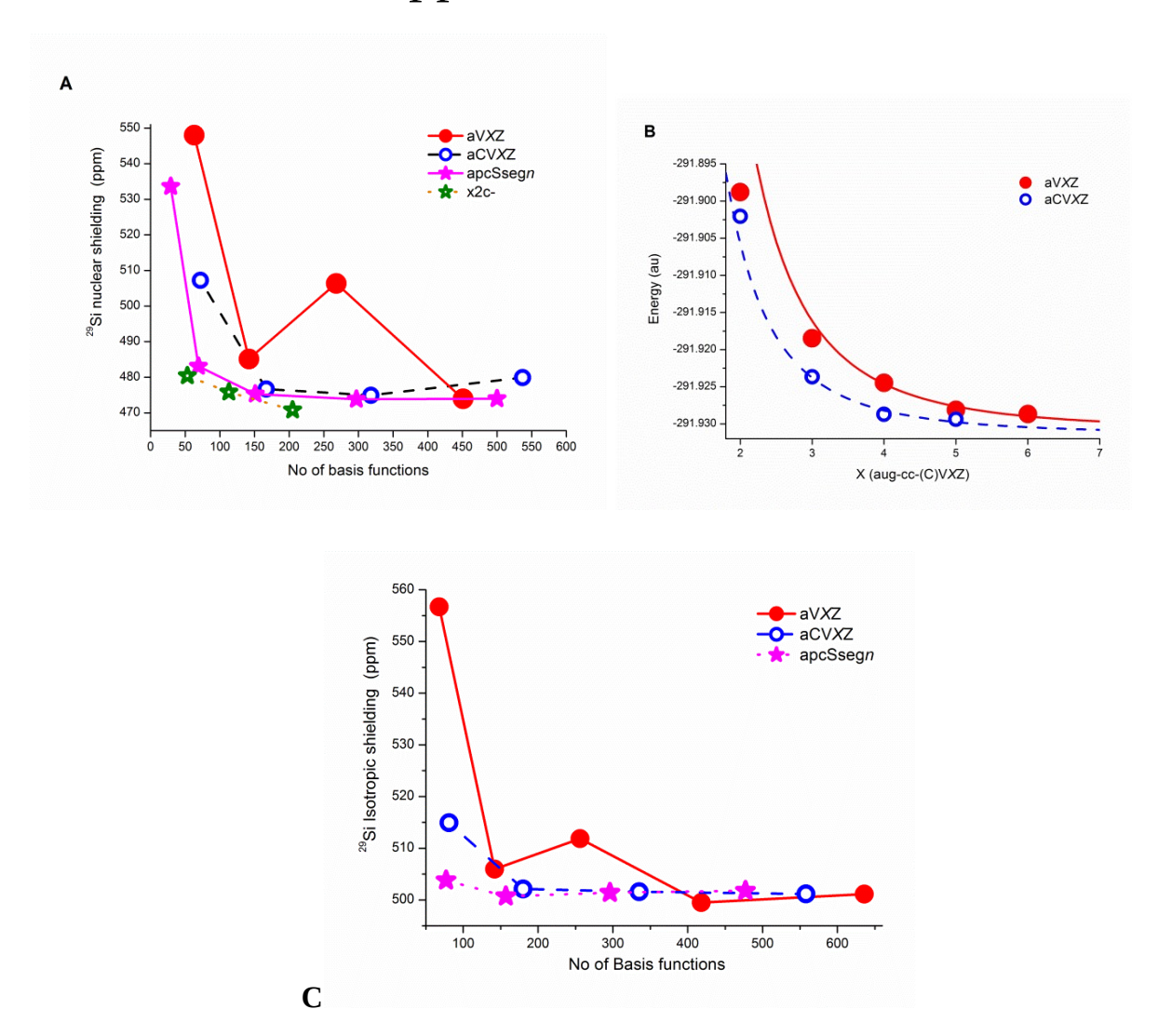


**Figure S12.** <sup>29</sup>Si isotropic shielding constants for SiH<sub>4</sub> calculated with the HF-SCF method and the aug-cc-pVXZ, aug-cc-pCVXZ, aug-pcSseg-*n*, and x2c-XZVPall-s basis set families (A). Convergences of the B3LYP/aug-cc-pVXZ and B3LYP/aug-cc-pCVXZ energies of SiH<sub>4</sub> are on the right (B) and <sup>29</sup>Si isotropic shielding constants for HSiCH, calculated with the B3LYP density functional combined with the aug-cc-pVXZ and aug-pcSseg-*n*, basis set families (C).

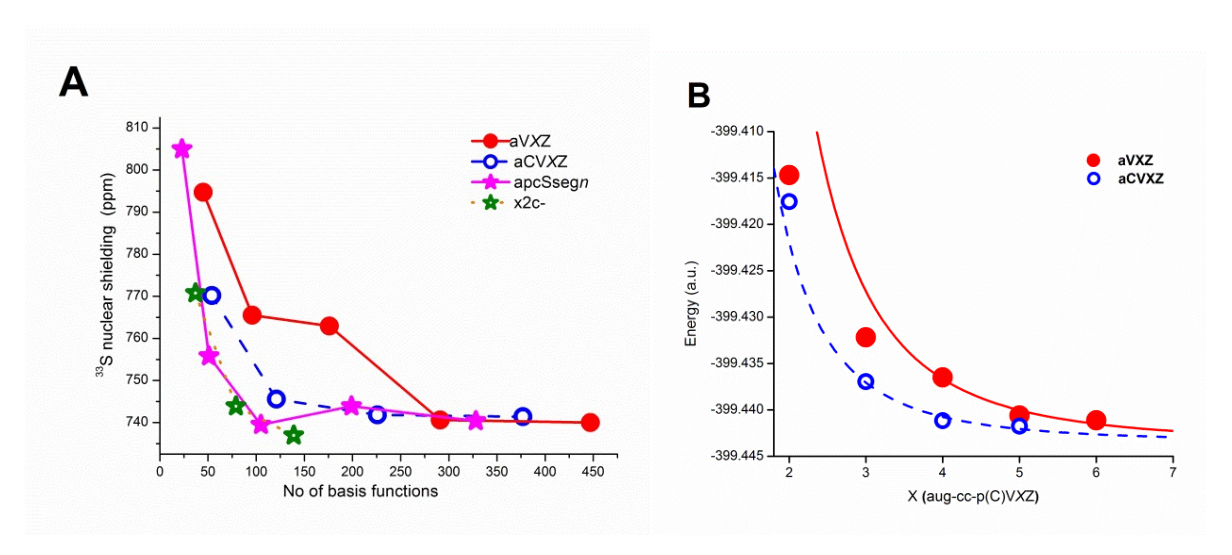


**Figure S13.** <sup>33</sup>S isotropic shielding constants for  $H_2S$  calculated with the CCSD(T) method and the aug-cc-pVXZ, aug-cc-pCVXZ, aug-pcSseg-n, and x2c-XZVPall-s basis set families (A). Convergences of the B3LYP/aug-cc-pVXZ and B3LYP/aug-cc-pCVXZ energies of  $H_2S$  are on the right (B).

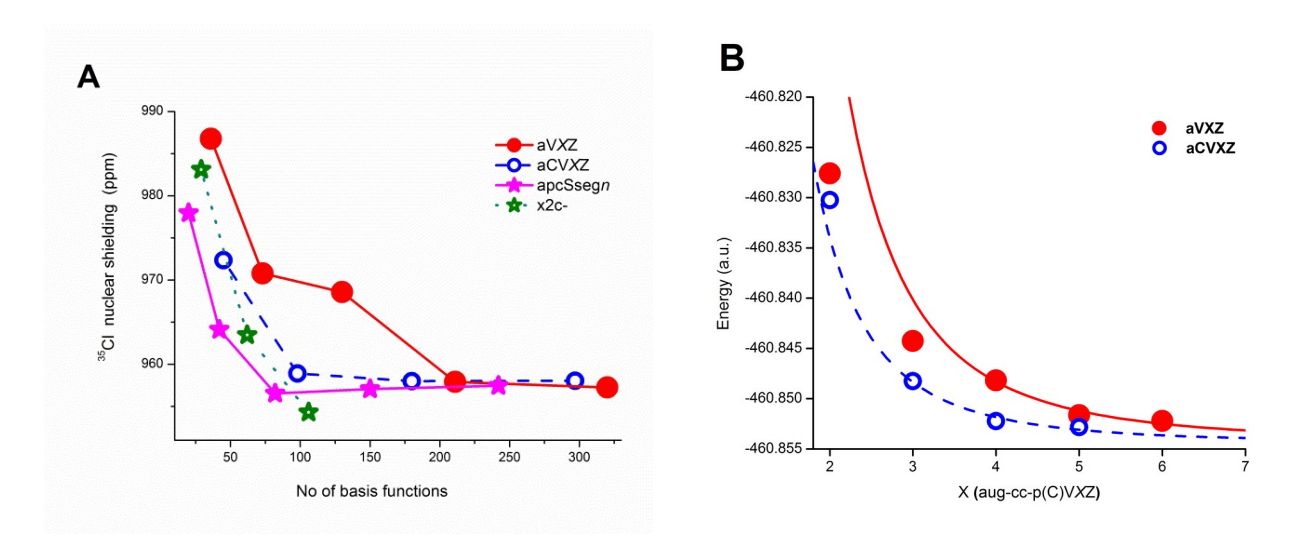


**Figure S14.** <sup>35</sup>Cl isotropic shielding constants for HCl calculated with the CCSD(T) method and the aug-cc-pV*X*Z, aug-cc-pCV*X*Z, aug-pcSseg-*n*, and x2c-*X*ZVPall-s basis set families (A). Convergences of the B3LYP/aug-cc-pV*X*Z and B3LYP/aug-cc-pCV*X*Z energies of HCl are on the right (B).

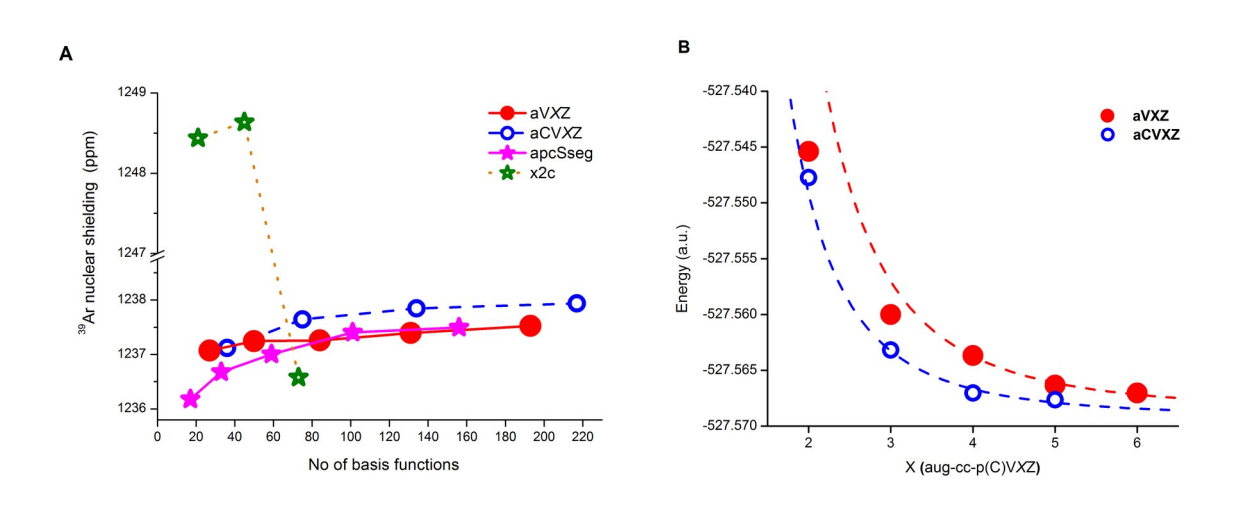


**Figure S15.** <sup>39</sup>Ar isotropic shielding constants for isolated argon atom calculated with the CCSD(T) method using the aug-cc-pVXZ, aug-cc-pCVXZ, aug-pcSseg-*n*, and x2c-Def2 basis set families (A). Convergences of the B3LYP/aug-cc-pVXZ and B3LYP/aug-cc-pCVXZ energies of Ar are on the right (B).

# 10.4 P4: Impact of OH $\cdots$ $\pi$ Hydrogen Bond on IR and NMR Parameters of Cannabidiol: Theoretical and Experimental Study





Article

# Impact of O-H··· $\pi$ Hydrogen Bond on IR and NMR Parameters of Cannabidiol: Theoretical and Experimental Study

Aneta Buczek \*, Kacper Rzepiela D, Teobald Kupka D and Małgorzata A. Broda D

Faculty of Chemistry and Pharmacy, University of Opole, 48, Oleska Street, 45-052 Opole, Poland; 119680@student.uni.opole.pl (K.R.); teobald@uni.opole.pl (T.K.); broda@uni.opole.pl (M.A.B.)

\* Correspondence: abuczek@uni.opole.pl; Tel.: +48-774527130

**Abstract:** This study investigates the influence of weak hydrogen bonds on the conformational properties and spectral characteristics of cannabidiol (CBD). Using a combination of FTIR and NMR spectroscopy, we analyze the effects of intramolecular hydrogen bonding, particularly the O-H $\cdots$  $\pi$  interactions, on the molecular behavior of CBD in chloroform solution. FTIR spectra reveal distinct  $v_s(O-H)$  stretching bands at 3603 cm<sup>-1</sup> and 3425 cm<sup>-1</sup>, corresponding to free and hydrogen-bonded -OH groups, respectively, with experimental results aligning closely with computational data for CBD conformers. Notably, conformer 1a predominates in solution, with weaker hydrogen bonding observed for the -OH(B) group compared to -OH(A). Additionally, the formation of -OH $\cdots\pi$  hydrogen bonds affects key vibrational bands in the 1700–1300 cm<sup>-1</sup> region. NMR analysis shows significant shifts in proton and carbon signals, emphasizing the influence of hydrogen bonding on CBD's electronic environment. The observed changes in coupling constants, although subtle, further highlight the impact of these interactions on spin-spin coupling. Overall, these findings provide deeper insights into the structural and electronic factors governing CBD's behavior in solution, offering a basis for future studies on hydrogen bonding in biomolecules and their pharmacological implications.

Keywords: cannabidiol; IR; NMR; DFT; conformational properties; intramolecular H-bond



Academic Editor: Riccardo Chelli

Received: 21 May 2025 Revised: 10 June 2025 Accepted: 11 June 2025 Published: 14 June 2025

Citation: Buczek, A.; Rzepiela, K.; Kupka, T.; Broda, M.A. Impact of O-H··· $\pi$  Hydrogen Bond on IR and NMR Parameters of Cannabidiol: Theoretical and Experimental Study. *Molecules* **2025**, *30*, 2591. https://doi.org/10.3390/molecules30122591

Copyright: © 2025 by the authors. Licensee MDPI, Basel, Switzerland. This article is an open access article distributed under the terms and conditions of the Creative Commons Attribution (CC BY) license (https://creativecommons.org/licenses/by/4.0/).

#### 1. Introduction

Cannabidiol (CBD, Figure 1) was first discovered by American chemist Roger Adams, who successfully isolated the compound from wild hemp flowers in Minnesota in 1940 [1,2]. This non-psychoactive cannabinoid [3] exhibits significant biological properties, including anti-inflammatory [4–6], antibacterial, antiviral, antioxidative [7–9], and anxiolytic effects. It is widely recognized for its therapeutic applications in the treatment of epilepsy [10–12] and schizophrenia [13]. Additionally, cannabidiol is used in managing various types of cancer and in palliative care to prevent nausea, vomiting, insomnia, and severe chronic pain [14].

The structural complexity of CBD, which includes two hydroxyl groups (-OH) and a polycyclic structure, makes this molecule an ideal candidate for spectroscopic studies aimed at understanding its conformation and molecular interactions. While the IR spectra of CBD in solution and in solid state have been characterized in several studies [15–19], the role of intramolecular interactions, particularly hydrogen bonding, in shaping the spectroscopic properties of CBD remains underexplored. Hydrogen bonding plays a crucial role in molecular recognition processes, particularly in the binding of ligands to proteins. The presence and orientation of intramolecular hydrogen bonds, such as the O–H… $\pi$ 

Molecules **2025**, 30, 2591 2 of 15

interaction observed in CBD conformer 1a, can influence the molecular rigidity and spatial arrangement of functional groups critical for receptor binding. For example, studies have shown that conformationally restricted cannabinoids can exhibit altered binding affinities toward CB1 and CB2 receptors, as well as nuclear receptors such as PPAR $\gamma$  [20,21]. In our previous work [22], we demonstrated that CBD adopts a specific conformation in a solution that is stabilized by intramolecular hydrogen bonds between the hydroxyl groups (-OH) and the  $\pi$ -electron system of the C=C double bonds (denoted as OH··· $\pi$  interactions) [22]. These interactions are known to influence the spatial arrangement of the molecule [23–25], potentially altering the electronic and vibrational properties that are captured in the IR spectra. It is important to note that the crystallographic form of CBD consists of a dimer, in which an intermolecular hydrogen bond (O-H···O) is formed between the hydrogen atom of the -OH(B) group of the first molecule and the oxygen atom of the -OH(A) group of the second molecule, as demonstrated in the study [26]. The presence of intermolecular hydrogen bonding may influence the observed shifts in vibrational frequencies.

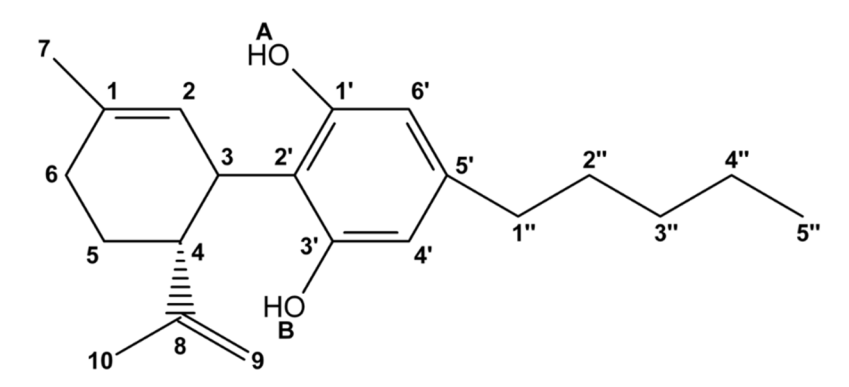


Figure 1. Chemical formula with atom numbering of cannabidiol (CBD).

Molecular modeling of NMR parameters is currently an indispensable tool and an efficient support for deriving the structure of many natural compounds [27,28]. Given its sensitivity, speed, and information delivery capabilities, most hemp extracts are analyzed using <sup>1</sup>H NMR spectroscopy. For instance, Barthlott et al. [29] reported on the screening of cannabinoids in CBD oils using quantitative <sup>1</sup>H NMR spectroscopy. They emphasized that this technique is fast and capable of detecting and determining hemp metabolites from an initial, complex organic matrix without requiring separation or sample preparation. At temperatures of 12 °C, 27 °C, and 42 °C, they observed a gradual collapse of two aromatic signals (H4' and H6') and broadening of another peak, attributed to the -OH(A) proton. These changes were associated with intramolecular dynamic effects in CBD fragments, enhanced by temperature. This dynamic process is probably due to the restricted rotation of the aromatic ring around a C3-C2'single bond.

<sup>13</sup>C NMR spectroscopy requires more sample material, which explains the limited number of studies involving CBD and related molecules. Recently, Marchetti et al. [30] conducted systematic <sup>1</sup>H and <sup>13</sup>C NMR studies of non-psychoactive cannabinoids from fiber-type *Cannabis sativa* L. (hemp) extracts. They compared the obtained spectra with several recorded pure cannabinoid samples as references. The analytical potential of NMR techniques was demonstrated by presenting typical <sup>1</sup>H, <sup>13</sup>C, HSQC, and HMBC spectra of a Santhica extract. The authors demonstrated, for the first time, the competitive potential of quantitative <sup>13</sup>C NMR compared to the traditional HPLC technique for analyzing several hemp components. In 2024, Congcong Yu et al. [31] proposed a certified reference material for cannabidiol. They performed combined quantitative tests of CBD using several analytical methods: ultraviolet absorption spectroscopy (UV), infrared spectroscopy (IR), mass spectrometry (MS), nuclear magnetic resonance spectroscopy (NMR), and differential scan-

Molecules **2025**, 30, 2591 3 of 15

ning calorimetry (DSC). The reported proton and carbon chemical shifts closely matched those previously reported by Marchetti et al. [30]. Colella et al. [32] also utilized proton and carbon NMR in the metabolic analysis of natural extracts from *Cannabis sativa*. They discussed both one- and two-dimensional spectra (1D and 2D), as well as certain proton-proton coupling constants. Ohtsuki et al. [33] combined liquid-liquid-based separation techniques and NMR analysis, concluding that quantum mechanical calculations of NMR parameters play a crucial role in analyzing natural product compositions across a wide range of concentrations.

Wood et al. [34] reported the complete <sup>1</sup>H and <sup>13</sup>C NMR assignments of cannabicitran and evaluated the performance of a combination of theoretically studied geometry optimization and subsequent gauge independent atom orbital (GIAO) NMR calculations in the gas phase and chloroform approximated by polarized model of solvent (PCM). The use of the PCM model of chloroform showed no improvement. However, it is well known that the choice of functional and basis set in DFT calculations significantly affects the accuracy of predicted NMR parameters [35].

Several authors reported on detailed analysis of NMR and IR spectra, supported by theoretical calculations, of complex natural products [36–38]. Other studies [39] have investigated the impact of solvent effects on the spectroscopic properties of cannabinoid derivatives and reported that NMR chemical shifts for carbon atoms can vary by up to 7 ppm due to solvent effect. On the other hand, the changes in NMR parameters, including chemical shifts and J-couplings, can be influenced by the strength and nature of intramolecular hydrogen bonds. These interactions modify the electronic environment of nuclei, leading to variations in shielding and indirect spin-spin coupling constants, which play a key role in determining molecular conformation and stability. In the study by Denhez et al. [40], the effect of intramolecular hydrogen bonding on the conformational stability of cannabidiol derivatives was investigated using NMR, XRD, and DFT calculations. The results indicate that the conformation is influenced by the type of hydrogen bond formed, which, in turn, depends on the choice of solvent. It is important to mention that CBD has low solubility in water but is well soluble in organic solvents, such as chloroform, ethanol, and hexane. Recent research has shown that the poor solubility of CBD in water is attributed to the formation of aggregates, which further influences its physicochemical properties and bioavailability [22].

In this study, we focus on the spectroscopic properties of CBD in chloroform solution, using both IR and NMR spectroscopy to probe its conformation and the potential influence of  $OH\cdots\pi$  hydrogen bonds on its spectral parameters. By comparing experimental data with theoretical calculations, we aim to gain new insights into the conformational behavior of CBD and the role of intramolecular interactions in modulating its spectroscopic characteristics. Finally, we explored the possibility of experimental verification of the presence of the two theoretically predicted most stable CBD conformers in the gas phase and chloroform by comparing the root-mean-square (RMS) deviations between DFT-calculated chemical shifts and experimental values.

#### 2. Results and Discussion

#### 2.1. DFT Conformational Analysis

Based on our previous studies [22], it is known that the CBD molecule, in the gas phase and water, can adopt either a diequatorial (1a–1d) or diaxial (2a–2d) conformation, depending on the arrangement of substituents at the 3rd and 4th carbon atoms of the limonene ring (Figure 1). These two groups are further divided into four subgroups based on the orientation of hydroxyl groups attached to the aromatic ring of the CBD molecule. In this study, we investigate the conformational and spectroscopic properties of cannabidiol in

Molecules **2025**, 30, 2591 4 of 15

chloroform, a solvent whose dielectric constant approximates the electrostatic environment within protein interiors. Figure 2 presents the lowest-energy CBD diequatorial conformers from each subgroup, calculated using the MP2/6-311++ $G^{**}$ /B3LYP-GD3BJ/6-311++ $G^{**}$  method in chloroform, along with their corresponding energy values. The lowest-energy conformer, **1a**, is stabilized by two hydrogen bonds: one O-H··· $\pi$  and one C-H···O, formed by two hydroxyl groups (O-H(A) and O-H(B) respectively), where the first one acts as a proton donor and the second as a proton acceptor. The next conformer, **1b**, with an energy higher by only 0.48 kcal/mol, is stabilized by two O-H··· $\pi$  hydrogen bonds. In **1c** and **1d** conformers with significantly higher energy, 3.39 and 3.43 kcal/mol (see Table 1), the O-H(A) group acts as a proton acceptor, forming C(4)-H···O-H(A) hydrogen bond. This means that the energetic order of the CBD conformers is determined primarily by the O-H(A)··· $\pi$  interaction. The diaxial conformers have much higher energies, and the analysis of their conformational preferences is presented in the supplement (Figure S1, Table S3). Based on the MP2//DFT calculation results presented above, it can be assumed that CBD in chloroform exists as two diequatorial (**1a** and **1b**) conformers that are in equilibrium.

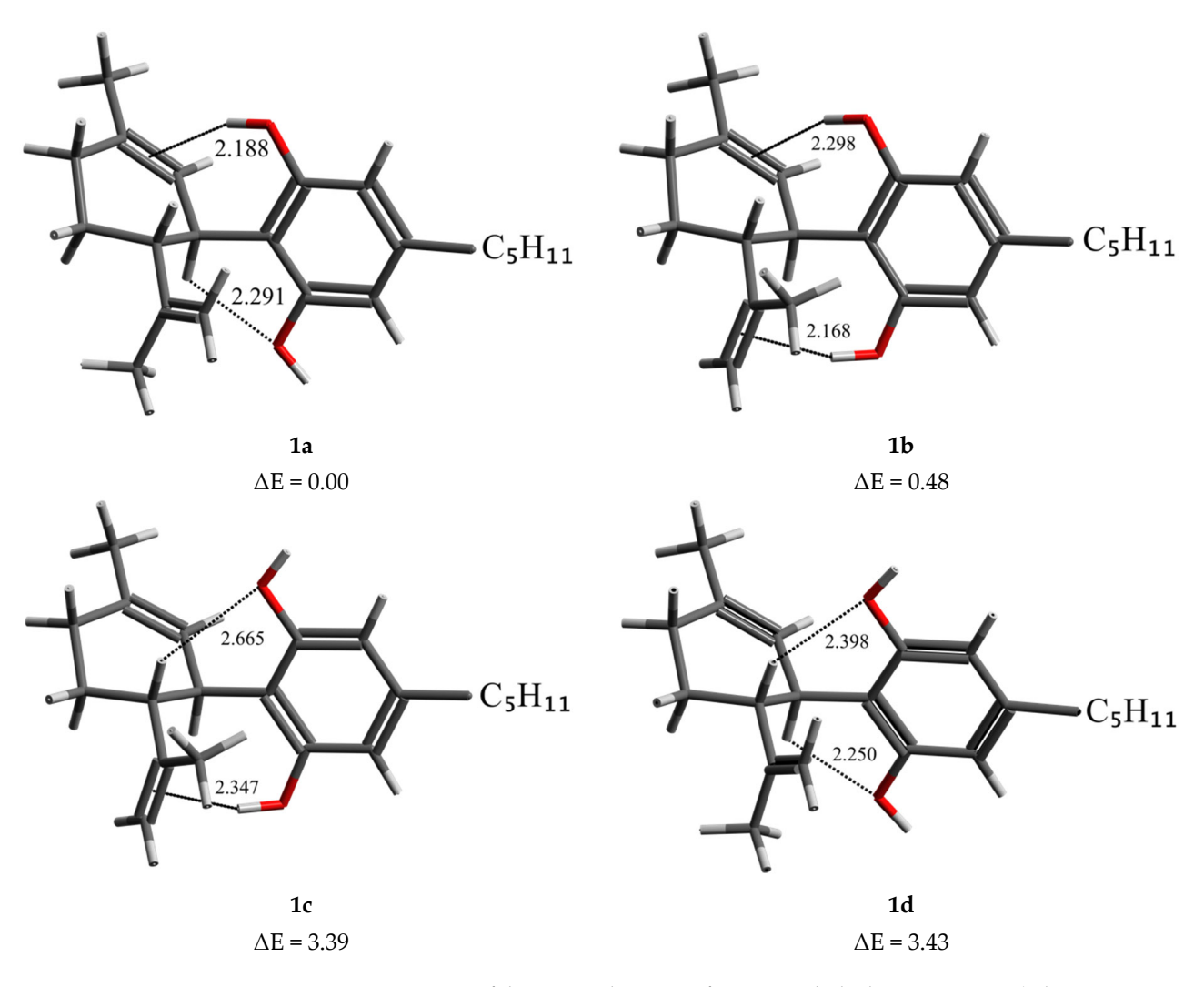


**Figure 2.** Structures of diequatorial CBD conformers with the lowest energies (relative energies  $\Delta E$  in kcal/mol) in four groups differing in OH group settings, calculated with MP2/6-311++G\*\*/B3LYP-GD3BJ/6-311++G\*\* method in chloroform. Hydrogen bonds are marked by dot lines, and the distances are given in (Å).

Molecules **2025**, 30, 2591 5 of 15

**Table 1.** The relative energies  $\Delta E$  (in kcal/mol) of the lowest diequatorial CBD conformers calculated with MP2/6-311++G\*\*/B3LYP-GD3BJ/6-311++G\*\* in gas phase and chloroform. Hydrogen bond distances are given in Å.

		Ga	s Phase	Chloroform	
Conformer	H-Bond Type	ΔΕ	Distance	ΔΕ	Distance
1a	C3-HO-H(B) O-H(A)C1=C2	0.00	2.284 2.202	0.00	2.291 2.188
1b	O-H(B)C8=C9 O-H(A)C1=C2	0.49	2.335 2.185	0.48	2.298 2.168
1c	O-H(B)C8=C9 C4-HO-H(A)	3.46	2.374 2.646	3.39	2.347 2.665
1d	C3-HO-H(B) C4-HO-H(A)	3.97	2.257 2.418	3.43	2.250 2.398

#### 2.2. FTIR Spectra

Figure 3A presents the  $v_s(O\text{-H})$  stretching region of the experimental FTIR spectra for cannabidiol (CBD) in chloroform solution. Two distinct absorption bands are observed at  $3603~\text{cm}^{-1}$  and  $3425~\text{cm}^{-1}$ . The band at  $3603~\text{cm}^{-1}$  is sharp and is attributed to the stretching vibration of the free -OH group, while the band at  $3425~\text{cm}^{-1}$  corresponds to the -OH group engaged in intramolecular hydrogen bonding. The spectra shown correspond to CBD solutions with concentrations ranging from  $2.3\times10^{-3}$  and  $9.3\times10^{-3}$  mol L<sup>-1</sup>. Notably, no shifts or changes in the shape of these bands are observed with dilution, suggesting that these bands arise from the monomeric form of CBD.

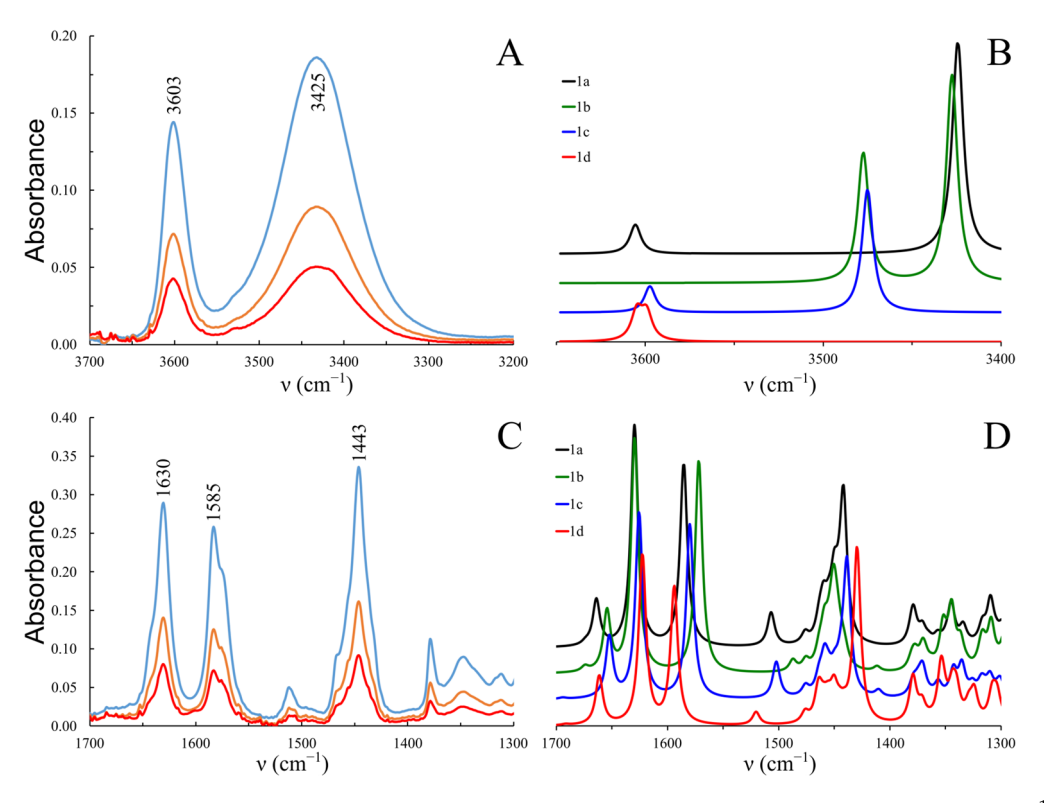


**Figure 3.** The IR spectra of CBD: (**A,B**) (the OH stretching region) and (**C,D**) (region below 1700 cm<sup>-1</sup>). (**A,C**): experimental spectra in chloroform solution, in three different concentrations ranging from  $2.3 \times 10^{-3}$  and  $9.3 \times 10^{-3}$  mol L<sup>-1</sup>; (**B,D**): spectra calculated with B3LYP-GD3BJ/6-311++G\*\* method in chloroform for the lowest diequatorial CBD conformers (**1a–1d**), scaling factors: 0.938 for OH stretching region and 0.976 for 1300–1700 cm<sup>-1</sup>.

Molecules **2025**, 30, 2591 6 of 15

Figure 3B presents the theoretically calculated vibrational spectra for the vs(O-H) stretching region of the four CBD conformers (**1a–1d**), which differ in the orientation of their -OH groups. The calculated spectrum for conformer **1a** exhibits excellent agreement with the experimental data, indicating that this conformation predominates in chloroform solution. The shift to lower frequencies observed in the stretching vibration band of the -OH(B) group, which forms a hydrogen bond with the C8=C9  $\pi$ -electrons ( $\Delta v = 130 \text{ cm}^{-1}$ ), is notably smaller than that of the -OH(A) group, which is bound to the C1=C2 double bond ( $\Delta v = 175 \text{ cm}^{-1}$ ). This difference suggests that the interaction involving the -OH(B) group is weaker than that formed by -OH(A). This observation is in agreement with the previously conducted conformational analysis of cannabidiol.

The formation of -OH··· $\pi$  hydrogen bonds also influences the position of several bands in the 1700–1300 cm<sup>-1</sup> region. Figure 3D presents this spectral range calculated for four CBD conformers. The band at 1650–1670 cm<sup>-1</sup> corresponds to the stretching vibrations of the C8=C9 bond. In conformers **1b** and **1c**, where the -OH(B)··· $\pi$  interaction is present, this band is shifted approximately 10 cm<sup>-1</sup> lower than in conformers **1a** and **1d**, which are not stabilized by this interaction. Additionally, the orientation of the -OH groups notably affects the position of the skeletal vibration bands of the aromatic ring, observed around 1630, 1585, and 1440 cm<sup>-1</sup> (Figure 3C).

#### 2.3. Experimental NMR Spectra of CBD

Intramolecular hydrogen bonds, including O-H··· $\pi$  interactions, can cause significant shifts in NMR spectra. The presence of such hydrogen bonds can lead to downfield shifts in the  $^1$ H NMR spectrum, which indirectly affects the  $^{13}$ C NMR chemical shifts due to changes in the electronic environment around the carbon atoms [41]. The size of this  $^1$ H NMR shift correlates with the strength of the hydrogen bonds.

The  $^1$ H NMR spectrum of CBD in CDCl<sub>3</sub> at 20 °C, 30 °C and 50 °C is shown in Figure 4A–C. Individual peaks are assigned according to earlier works [29,32,42,43]. It is important to notice that at 20 °C, the three peaks in the aromatic region of the spectrum are fairly broad and sharpen at 50 °C. This clearly indicates the presence of a dynamic process, probably due to the relatively fast exchange between conformers in the NMR time scale. Experimental and available literature data of  $^1$ H chemical shifts of CBD were compared with theoretically predicted values for eight conformers of CBD (four diequatorial and four diaxial; see Tables 2 and S4). Analysis of the data in Table 2 clearly shows that the chemical shift from the OH(A) group proton depends on whether this group is involved in the OH··· $\pi$  bond (6.6 ppm) or participates in the CH···O interaction (4.4 ppm). For the OH(B) group, the analogous effect is much smaller (5.8 vs. 4.5 ppm) because this group forms a weaker H-bond. A comparison of the chemical shifts of both OH groups with experimental values suggests that the OH(A) group is involved in the OH··· $\pi$  while the OH(B) group is in the C-H···O interaction.

The RMS values for theoretical proton data indicate that the smallest difference between the theoretically obtained chemical shifts and our experimental values are observed for the two lowest energy diequatorial conformers (0.37 and 0.34 for **1a** and **1b**, respectively).

This indicates that this compound prefers a structure in which the O-H (A) $\cdots\pi$  hydrogen bond occurs. For conformer **1a**, the largest differences between the experimental and the calculated chemical shift values are observed for the protons of the C(9)-H group, which may be related to the mobility of the phenyl group.

Molecules **2025**, 30, 2591 7 of 15

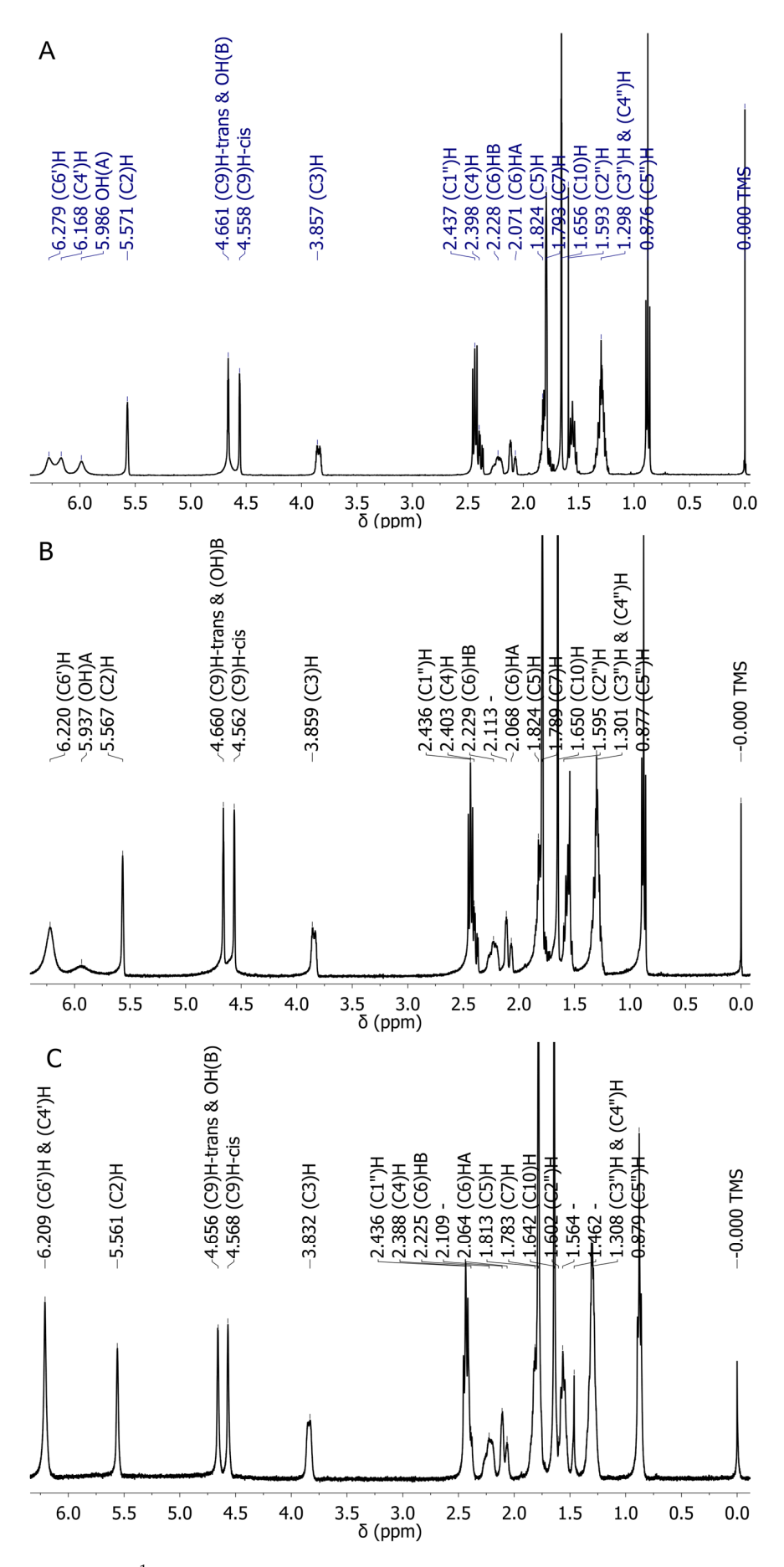


**Figure 4.** The  $^{1}$ H NMR spectrum of CBD in CDCl<sub>3</sub> at 20  $^{\circ}$ C (**A**), 30  $^{\circ}$ C (**B**) and 50  $^{\circ}$ C (**C**).

Molecules **2025**, 30, 2591 8 of 15

**Table 2.** Calculated <sup>1</sup>H chemical shifts of diequatorial CBD conformers, using B3LYP/aug-cc-pVTZ method in chloroform, compared with experiment and available literature data.

Atom	1a	1b	1c	1d	Exp. a	Lit. [42]	Lit. [29]	Lit. [43]	Lit. [32]
(OA)H	6.60	6.55	4.44	4.42	5.99	5.99	5.95	6.22	
(OB)H	4.34	5.78	5.78	4.47	4.66	5.02	4.6		
(C2)H	5.40	5.27	5.05	5.11	5.57	5.57	5.57	5.56	5.57
(C3)H	4.15	3.76	3.68	4.24	3.86	3.9	3.84	3.86	3.86
(C4)H	2.51	2.27	2.50	3.21	2.40	2.4	2.4		2.40
(C5)H	1.81	1.88	1.89	1.83	1.82	1.84	1.82		1.78-1.84
(C6)H	2.27	2.28	2.19	2.20	$H6_a = 2.07$ $H6_b = 2.23$	2.21	2.09		$H6_a = 2.05-2.09$ $H6_b = 2.22$
(C7)H	1.92	1.92	1.81	1.79	1.79	1.79	1.79		1.79
(C9)H-trans	4.10	4.78	4.73	4.04	4.66	4.64	4.67	4.66	4.64
(C9)H-cis	3.75	4.74	4.64	4.00	4.56	4.54	4.6	4.57	4.53
(C10)H	1.88	1.53	1.50	1.88	1.66	1.66	1.65		1.66
(C4')H	5.53	5.94	5.96	5.63	6.17	6.16	6.19		6.16
(C6')H	5.85	5.98	5.71	5.56	6.28	6.26	6.25		6.26
(C1")H	2.53	2.59	2.57	2.52	2.44	2.43	2.44		2.43
(C2")H	1.52	1.56	1.56	1.52	1.59	1.55	1.56		1.52-1.61
(C3")H	0.82	0.92	0.93	0.85	1.30	1.29	1.3		1.27-1.32
(C4")H	1.18	1.19	1.19	1.19	1.30	1.29	1.3		
(C5")H	0.86	0.85	0.86	0.86	0.88	0.88	0.89		0.86-0.88
RMS	0.37	0.34	0.50	0.54					

<sup>&</sup>lt;sup>a</sup> This work.

The  ${}^{13}C(-{}^{1}H)$  and  $(+{}^{1}H)$  spectra are shown in Figure 5A,B, respectively. A typical C-13 NMR spectrum is apparent from Figure 5A, and it agrees with earlier reports [29,32,42,43]. However, the proton-coupled spectrum of CBD was not reported in the literature yet (see Figure 5B). Obviously, the S/N ratio for the latter spectrum is significantly lower, and the accurate determination of several small couplings could be inaccurate. Furthermore, overlapping of some peaks enables only approximate determination of coupling constants. The enlarged aliphatic and aromatic parts of  $^{13}$ C ( $^{-1}$ H) and ( $^{+1}$ H) spectra are shown in Supplementary Materials (Figure S2). For rigid molecules, the conformation may have little effect on the <sup>13</sup>C chemical shifts. However, for flexible or cyclic molecules, conformational changes can lead to noticeable shifts in the <sup>13</sup>C NMR spectrum, and these shifts can be used to infer structural details about the molecule. For example, the chemical shift for the C1 carbon atom in the case of the OH(A)··· $\pi$  interaction is 147 ppm (Table 3, for **1a** and **1b** conformers), and in the absence of this interaction, it is approximately 136 ppm. The experimentally determined value for this atom is 143 ppm, which indicates the occurrence of the  $OH(A)\cdots\pi$  interaction in CBD conformers in chloroform. The next carbon atoms for which we observe a strong dependence on the adopted conformation are C8 and C10 atoms. For conformers with C3-H···OH(B) interactions, the chemical shifts for these atoms are 155 ppm and 20 ppm, respectively, which is very similar to the experimentally observed values. So, despite the fact that RMS values for carbon chemical shifts are relatively large (4.3 to 7.8 ppm), it is the lowest value (4.25 ppm) for the lowest energy conformer according to the DFT results. To sum up the above facts, a detailed analysis of  $^1\mathrm{H}$  and  $^{13}\mathrm{C}$  chemical shifts indicates that CBD in chloroform occurs in the form of the 1a conformer, which is stabilized by  $OH(A)\cdots\pi$  and  $C3-H\cdots OH(B)$  interactions.

#### 2.4. Indirect Spin-Spin Coupling Constants (SSCCs) of CBD Conformers

Several functionals have been shown to work well for calculating SSCC [44], but generally, the best choice depends on the specific system being studied. Therefore, for conformer 1a, we compared the coupling constants calculated using the three functionals most popular for this type of calculation: PBE0, B3LYP, and CAM-B3LYP. Proton–proton J-couplings calculated through 2–5 bonds are collected in Table 4 and compared with available literature data. Comparing the RMS values for 1a in a vacuum, it is clear that B3LYP performs the best, PBE0 is the second-best one, and CAM-B3LYP yields the worst results (Table 4). The corresponding RMS values for these functionals are 1.15, 1.27, and

Molecules **2025**, 30, 2591 9 of 15

1.3 Hz, respectively. Moreover, it was shown that the difference between the SSCC values calculated in the gas phase and those obtained using the PCM model for chloroform was small. However, the results of calculations in vacuum agree slightly better with the experimental data. Therefore, for the remaining conformers, the calculations were performed using the B3LYP functional in vacuum. Comparing the calculated coupling constants with the experimental values, it is clear that the lowest RMS value is observed for the 1a conformer, which is consistent with our hypothesis that in solution, we are dealing mainly with conformer 1a, possibly with some admixture of 1b.

**Table 3.** Calculated <sup>13</sup>C chemical shifts of diequatorial CBD conformers, with B3LYP/aug-cc-pVTZ in chloroform solvent, compared with experiment and available literature data.

Atom	1a	1b	1c	1d	Exp. a	Lit. [42]	Lit. [18]
C1	147.20	147.46	135.47	137.45	143.06	134.2	
C2	125.88	124.83	128.17	128.23	124.09	127.3	124.14
C3	41.98	50.42	51.07	41.96	37.25	37.5	37.01
C4	53.66	49.69	49.29	51.76	46.14	46.4	
C5	33.30	34.39	34.95	34.51	28.39	31.7	28.35
C6	35.92	35.86	35.56	36.05	30.64	30.7	30.36
C7	26.86	26.93	26.43	26.43	23.69	23.7	23.69
C8	155.26	168.10	169.01	158.00	149.41	150.3	
C9	109.19	106.03	103.95	107.03	110.84	110.5	110.81
C10	20.76	29.95	29.98	20.35	20.53	19.5	20.30
C1′	159.83	159.86	158.42	157.52	156.15	157.5	
C2′	112.35	114.82	116.23	114.69	113.73	115.9	
C3′	156.83	157.25	158.18	157.26	153.87	150.3	
C4'	105.13	109.98	110.25	102.81	109.76	108.3	107.92
C5′	145.31	145.84	145.15	145.03	140.09	142.7	
C6′	105.58	107.25	104.94	107.70	107.99	108.3	109.56
C1"	41.68	41.38	41.09	41.33	35.47	36.6	35.46
C2"	38.54	38.50	38.69	38.60	30.39	32.0	30.65
C3"	36.69	36.82	36.76	37.67	31.49	32.6	31.48
C4"	29.80	29.85	29.99	29.33	22.54	23.6	22.54
C5"	17.23	17.12	17.05	16.81	14.05	14.4	14.04
RMS this work	4.70	6.85	7.30	5.06		·	·

a this work.

It is known that hydrogen bond formation can influence spin–spin coupling constants by altering electronic environments, molecular conformations, and distances between nuclei, leading to variations in SSCC values. Analyzing the data collected in Table 4, it can be observed that the formation of the hydrogen bond  $OH(B)\cdots\pi$  (in 1a and 1b conformers) causes a decrease in the value of  $^2J(H9A, H9B)$  coupling constant by about 0.8 Hz. Apart from that, we did not observe any such dependencies for the long-range coupling constants. However, in the case of single-bond couplings, the situation is slightly different.

In Table 5 are gathered one-bond SSCC values for selected C-H couplings. The coupling constants are generally overestimated at the B3LYP/aug-cc-pVTZ level of theory in the gas phase, but the deviations are modest. It can be observed that the coupling constant  $^{1}$ J(CH) is larger if the C-H···O interaction occurs. A higher constant (by about 2 Hz) occurs for the C3H3 group in conformations **1a** and **1d** and for the C4H4 group in conformations **1c** and **1d**. Furthermore, the formation of an OH···· $\pi$  hydrogen bond causes an increase of the coupling constant at the methyl group substituted at the double bond by about 1 Hz. This effect is observed for  $^{1}$ J (C7H7) and  $^{1}$ J (C10H10).

Molecules **2025**, 30, 2591 10 of 15

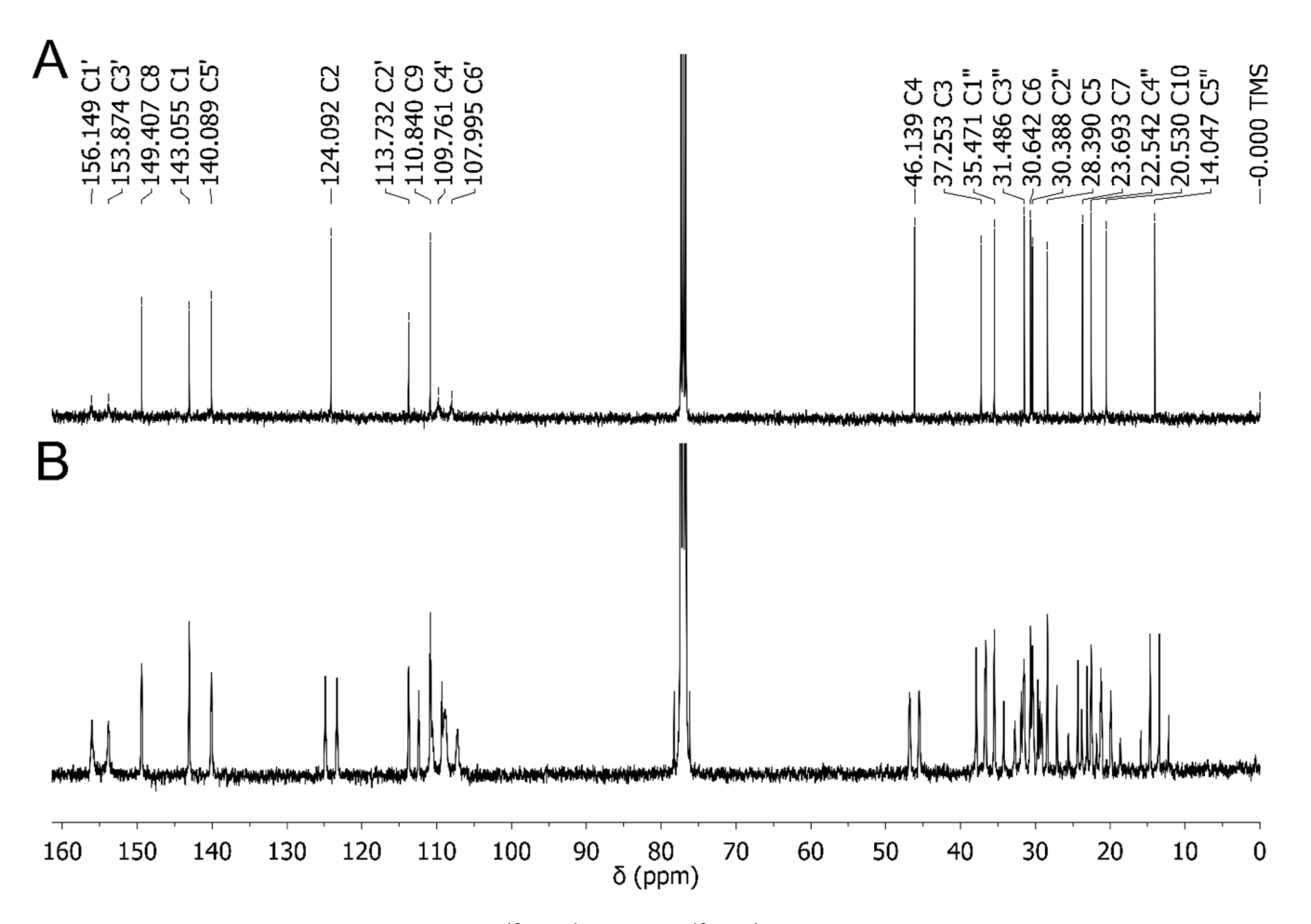


**Figure 5.** The (**A**)  $^{13}$ C ( $^{-1}$ H) and (**B**)  $^{13}$ C ( $^{+1}$ H) NMR spectra of CBD in CDCl<sub>3</sub>.

**Table 4.** Selected SSCC values for H-H couplings calculated at B3LYP, PBE0, and CAM-B3LYP/aug-cc-pVTZ level of theory in the gas phase and chloroform.

	B3L	YP	PB	E0	CAM-B3LYP		B3LYP		
	Gas	CHCl <sub>3</sub>	Gas	CHCl <sub>3</sub>	Gas		Gas		
Coupling Constants			1	a		1b	1c	1d	Lit. [33]
<sup>4</sup> J(H6′ H4′)	1.26	1.27	1.07	1.08	1.04	1.49	1.32	1.12	3.03
<sup>4</sup> J(H2 H6A)	-3.39	-3.40	-3.81	-3.82	-3.69	-3.39	-3.16	-3.20	-1.45
<sup>4</sup> J(H2 H6B)	-1.16	-1.17	-1.44	-1.44	-1.36	-1.20	-1.68	-1.63	1.35
<sup>4</sup> J(H2 H7)	-1.72	-1.12	-1.96	-1.96	-1.89	-1.73	-1.78	-1.78	-1.12
<sup>2</sup> J(H9A H9B)	3.07	3.29	0.96	1.17	2.69	2.15	2.39	3.47	2.13
<sup>3</sup> J(H3 H2)	2.92	2.88	3.28	3.23	3.31	2.84	2.58	2.62	2.85
<sup>3</sup> J(H3 H4)	10.84	10.83	10.33	10.32	11.11	10.85	10.80	11.00	10.28
<sup>5</sup> J(H3 H7)	3.27	3.24	3.32	3.30	3.43	3.22	3.12	3.22	2.49
<sup>2</sup> J(H6B H6A)	-19.20	-19.44	-19.61	-19.85	-19.58	-19.40	-18.66	-18.51	-17.75
<sup>2</sup> J(H5A H5B)	-13.45	-13.53	-14.01	-14.10	-13.61	-13.91	-13.73	-13.19	-12.88
<sup>3</sup> J(H6A H5B)	5.99	5.99	5.69	5.70	6.05	6.09	6.20	6.23	5.21
<sup>3</sup> J(H6A H5A)	12.70	12.70	11.95	11.95	12.89	12.64	12.61	12.63	11.36
<sup>3</sup> J(H6B H5B)	1.97	1.98	1.90	1.91	2.00	1.87	1.84	1.86	2.12
<sup>3</sup> J(H6B H5A)	5.66	5.65	5.34	5.32	5.76	5.64	5.85	5.92	4.94
<sup>4</sup> J(H6A H7)	-1.64	-1.62	-1.85	-1.83	-1.94	-1.65	-1.72	-1.69	-1.84
<sup>4</sup> J(H6B H7)	-0.65	-0.65	-0.83	-0.82	-0.82	-0.65	-0.76	-0.78	-1.25
RMS(H)	1.15	1.17	1.27	1.29	1.30	1.15	1.16	1.21	

Molecules **2025**, 30, 2591

**Table 5.** Selected SSCC values for CH couplings calculated at B3LYP/aug-cc-pVTZ level of theory in the gas phase.

Coupling Constants	1a	1b	1c	1d	Exp. in CDCl <sub>3</sub>
<sup>1</sup> J (C2H2)	161.42	162.54	164.14	162.48	155.14
<sup>1</sup> J (C3H3)	135.76	132.57	129.40	132.80	128.22
<sup>1</sup> J (C4H4)	133.66	133.20	135.27	136.23	127.12
<sup>1</sup> J (C5H5)	132.01	133.13	132.23	131.28	127.04
<sup>1</sup> J (C6H6)	130.02	130.18	129.39	129.24	124.75
<sup>1</sup> J (C7H7)	130.36	130.63	129.59	129.39	126.44
<sup>1</sup> J (C9H9)	162.05	161.72	161.37	161.30	154.76
<sup>1</sup> J (C10H10)	130.26	131.51	131.04	130.11	126.00
<sup>1</sup> J (C4'H4')	159.91	164.00	157.81	158.08	166.94
<sup>1</sup> J (C6'H6')	164.46	166.68	167.00	160.12	161.33
<sup>1</sup> J (C1"H1")	130.56	130.67	130.75	130.58	125.80
<sup>1</sup> J (C2"H2")	130.17	129.98	129.69	129.89	123.54
<sup>1</sup> J (C3"H3")	128.78	128.71	128.93	128.98	120.19
<sup>1</sup> J (C4"H4")	128.61	128.54	128.44	128.52	125.44
<sup>1</sup> J (C5"H5")	129.12	129.09	129.22	129.26	124.54
RMS	5.82	5.65	6.12	5.87	

## 3. Materials and Methods

#### 3.1. Experimental

FTIR spectra: The analytical grade CHCl $_3$  was dried and purified following standard methods. The IR spectra were recorded at 20 °C using a Nicolet (Madison, WI, USA) Nexus spectrometer equipped with a DTGS detector and flushed with dry nitrogen during the measurements. All spectra were recorded at 1 cm $^{-1}$  resolution and averaged using 100 scans. Solvent spectra were obtained under identical conditions and subtracted from the sample spectra. The thickness of the KBr liquid cell was 2.86 mm, and the concentration varied between  $2.3 \times 10^{-3}$  and  $9.3 \times 10^{-3}$  mol L $^{-1}$ . The spectra were analyzed with the GRAMS AI spectroscopy software suite [17]. The number and position of component bands were obtained from second derivatives and by Fourier self-deconvolution techniques as an 'initial guess'. Next, the accurate band positions were determined by a curve-fitting procedure with a mixed Gauss-Lorentz profile.

*NMR spectra:* A sample of CBD (about 5 mg in 0.6 mL CDCl<sub>3</sub>, Aldrich, Saint Louis, MO, USA) was measured with a 400 MHz ultra-shield Bruker NMR spectrometer using TMS as an internal standard. No additional sample purification was applied. For proton spectra, 16 scans were averaged at 20, 30 and 50 °C. Carbon-13 spectra decoupled from protons and coupled with protons were measured at room temperature only (needed considerably longer times of measurements).

#### 3.2. Computational Details

*Geometry optimization:* A detailed analysis of the conformational properties of cannabidiol (CBD) in the gas phase and in water was performed in our previous theoretical study [22], using the PCM/B3LYP-D3BJ/6-311++G(d,p) method. CBD conformers were categorized based on their structural differences, leading to the identification of four lowest-energy diequatorial, **1a–1d** (Figure 2) and four diaxial, **2a–2d** (Figure S1) conformers.

In this study, additional B3LYP-D3BJ/6-311++G\*\* calculations in chloroform were conducted for eight previously found CBD conformers, and their ground state structure was confirmed by the lack of imaginary frequencies. Based on the full optimization of the diaxial and diequatorial conformers, single-point calculations were performed using the B3LYP and MP2 methods, combined with the 6-311++G\*\* and aug-cc-pVTZ basis sets. All calculations were carried out using the Gaussian 16 software package [45] in both vacuum

Molecules **2025**, 30, 2591 12 of 15

and chloroform. The solvent effect of chloroform was simulated using a self-consistent reaction field (SCRF) based on the polarizable continuum model (PCM) [46].

*IR calculations*: Vibrational modes were predicted using the harmonic approximation, as implemented in Gaussian software [45], with cost-effective density functional theory (DFT) methods. However, these calculations often overestimate experimental data. To improve accuracy, empirical scaling factors have been applied to harmonic frequencies, significantly improving the agreement with observed data [47].

*NMR calculations*: For each CBD conformer, a single-point GIAO NMR calculation was performed to obtain nuclear shielding tensors using the B3LYP/aug-cc-pVTZ method in chloroform modeled by the PCM method. The raw theoretical shielding data were converted to chemical shifts using earlier predicted isotropic shieldings of reference molecules—TMS and benzene—details in Table S1 in the Supplementary Information. The <sup>1</sup>H and <sup>13</sup>C nuclear shieldings, calculated at B3LYP/aug-cc-pVTZ level of theory, are shown in Table S2.

The corresponding theoretical chemical shifts (in ppm) for atoms in the aromatic ring and double bonds were calculated as follows:

$$\delta(^{13}C(i)) = \sigma(ref) - \sigma(i) + 128.5$$

$$\delta(^{1}\text{H(i)}) = \sigma(\text{ref}) - \sigma(i) + 7.26$$

The remaining chemical shifts were referenced with respect to TMS.

The computed NMR parameters were then compared with experimental results and available literature data. Additionally, spin–spin coupling constants (SSCC), including <sup>n</sup>J(HH) and <sup>1</sup>J(CH), were modeled for the lowest-energy conformer using the B3LYP and PBE0 functionals in the gas phase and chloroform. All SSCC values were calculated with a "mixed" option of aug-cc-pVTZ basis set. Our calculated SSCC values for <sup>n</sup>J(HH) were compared with data available in the literature, whereas the theoretical SSCC values for <sup>1</sup>J(CH) were compared with values determined from our experimental NMR spectra.

## 4. Conclusions

Our investigation into the influence of weak hydrogen bonds on the conformational properties and spectral parameters of cannabidiol (CBD) has provided significant insights into its molecular behavior. The presence of the O-H··· $\pi$  intramolecular hydrogen bond has been identified as a key stabilizing factor for conformer 1a, with specific hydrogen bonding interactions, such as OH(A)··· $\pi$  and C3-H···OH(B), exerting notable effects on vibrational frequencies, chemical shifts, and coupling constants.

FTIR analysis of CBD in chloroform solution reveals distinct  $v_s(O\text{-H})$  stretching bands at 3603 cm<sup>-1</sup> and 3425 cm<sup>-1</sup>, which correspond to the free and hydrogen-bonded -OH groups, respectively. The experimental FTIR spectra are in excellent agreement with the calculated data for the CBD conformers (**1a–1d**), with conformer **1a** predominating in chloroform solution. The observed shift in the  $v_s(O\text{-H})$  band suggests a weaker hydrogen bond in the -OH(B) group compared to -OH(A), consistent with previous conformational analyses. Furthermore, the formation of -OH··· $\pi$  hydrogen bonds influences the 1700–1300 cm<sup>-1</sup> spectral region, causing shifts in the C8=C9 bond stretching vibrations and aromatic skeletal vibrations.

The proton and carbon NMR shifts, with changes of up to 2 ppm for protons and 10 ppm for carbons, highlight the impact of hydrogen bonding on the electronic environments of CBD conformers. Although the changes in coupling constants are more subtle, with variations of 1–2 Hz, they still provide evidence of the influence of these interactions on spin–spin coupling magnitudes.

Molecules **2025**, 30, 2591

Overall, our findings enhance the understanding of the structural and electronic factors that govern the behavior of CBD in solution, emphasizing the critical role of weak hydrogen bonds in determining conformational preferences and NMR spectral characteristics. This work not only advances our knowledge of cannabidiol's molecular structure but also lays the groundwork for future studies on the role of hydrogen bonding in other biomolecules and its implications for pharmacological properties.

**Supplementary Materials:** The following supporting information can be downloaded at https://www.mdpi.com/article/10.3390/molecules30122591/s1.

**Author Contributions:** Conceptualization, A.B. and M.A.B.; methodology, T.K.; software, K.R.; validation, A.B., T.K. and M.A.B.; formal analysis, A.B.; investigation, K.R.; resources, A.B.; writing—original draft preparation, A.B.; writing—review and editing, A.B.; visualization, K.R.; supervision, T.K.; project administration, A.B. All authors have read and agreed to the published version of the manuscript.

Funding: This research received no external funding.

Institutional Review Board Statement: Not applicable.

Informed Consent Statement: Not applicable.

Data Availability Statement: Data are contained within the article and Supplementary Materials.

**Acknowledgments:** Calculations have been carried out using the Wroclaw Centre for Networking and Supercomputing (https://wcss.pl).

Conflicts of Interest: The authors declare no conflict of interest.

## References

- 1. Adams, R.; Hunt, M.; Clark, J.H. Structure of Cannabidiol, a Product Isolated from the Marihuana Extract of Minnesota Wild Hemp. I. *JACS* **1940**, *62*, 196–200. [CrossRef]
- 2. Mechoulam, R.; Shvo, Y. Hashish—I: The structure of Cannabidiol. *Tetrahedron* 1963, 19, 2073–2078. [CrossRef]
- 3. Wang, X.; Zhang, H.; Liu, Y.; Xu, Y.; Yang, B.; Li, H.; Chen, L. An overview on synthetic and biological activities of cannabidiol (CBD) and its derivatives. *Bioorg. Chem.* **2023**, *140*, 106810. [CrossRef]
- 4. Burstein, S. Cannabidiol (CBD) and its analogs: A review of their effects on inflammation. *Bioorg. Med. Chem.* **2015**, 23, 1377–1385. [CrossRef]
- 5. Klein, T.W. Cannabinoid-based drugs as anti-inflammatory therapeutics. Nat. Rev. Immunol. 2005, 5, 400-411. [CrossRef]
- 6. Pisanti, S.; Malfitano, A.M.; Ciaglia, E.; Lamberti, A.; Ranieri, R.; Cuomo, G.; Abate, M.; Faggiana, G.; Proto, M.C.; Fiore, D.; et al. Cannabidiol: State of the art and new challenges for therapeutic applications. *Pharmacol. Ther.* **2017**, 175, 133–150. [CrossRef]
- 7. Atalay, S.; Jarocka-Karpowicz, I.; Skrzydlewska, E. Antioxidative and Anti-Inflammatory Properties of Cannabidiol. *Antioxidants* **2020**, *9*, 21. [CrossRef]
- 8. Boulebd, H.; Pereira, D.M.; Amine Khodja, I.; Hoa, N.T.; Mechler, A.; Vo, Q.V. Assessment of the free radical scavenging potential of cannabidiol under physiological conditions: Theoretical and experimental investigations. *J. Mol. Liq.* **2022**, 346, 118277. [CrossRef]
- 9. Borges, R.S.; Batista, J.; Viana, R.B.; Baetas, A.C.; Orestes, E.; Andrade, M.A.; Honório, K.M.; Da Silva, A.B.F. Understanding the Molecular Aspects of Tetrahydrocannabinol and Cannabidiol as Antioxidants. *Molecules* 2013, 18, 12663–12674. [CrossRef]
- 10. Thiele, E.; Marsh, E.; Mazurkiewicz-Beldzinska, M.; Halford, J.J.; Gunning, B.; Devinsky, O.; Checketts, D.; Roberts, C. Cannabidiol in patients with Lennox-Gastaut syndrome: Interim analysis of an open-label extension study. *Epilepsia* **2019**, *60*, 419–428. [CrossRef]
- 11. Hirose, S.; Tanaka, Y.; Shibata, M.; Kimura, Y.; Ishikawa, M.; Higurashi, N.; Yamamoto, T.; Ichise, E.; Chiyonobu, T.; Ishii, A. Application of induced pluripotent stem cells in epilepsy. *Mol. Cell. Neurosci.* **2020**, *108*, 103535. [CrossRef] [PubMed]
- 12. Mihailova, L.; Tchekalarova, J.; Shalabalija, D.; Geskovski, N.; Stoilkovska Gjorgievska, V.; Stefkov, G.; Krasteva, P.; Simonoska Crcarevska, M.; Glavas Dodov, M. Lipid nano-carriers loaded with *Cannabis sativa* extract for epilepsy treatment—In vitro characterization and in vivo efficacy studies. *J. Pharm. Sci.* 2022, 111, 3384–3396. [CrossRef] [PubMed]
- 13. Iseger, T.A.; Bossong, M.G. A systematic review of the antipsychotic properties of cannabidiol in humans. *Schizophr. Res.* **2015**, 162, 153–161. [CrossRef] [PubMed]

Molecules **2025**, 30, 2591 14 of 15

14. Seltzer, E.S.; Watters, A.K.; MacKenzie, D.; Granat, L.M.; Zhang, D. Cannabidiol (CBD) as a Promising Anti-Cancer Drug. *Cancers* **2020**, *12*, 3203. [CrossRef]

- 15. Li, H.; Chang, S.-L.; Chang, T.-R.; You, Y.; Wang, X.-D.; Wang, L.-W.; Yuan, X.-F.; Tan, M.-H.; Wang, P.-D.; Xu, P.-W.; et al. Inclusion complexes of cannabidiol with β-cyclodextrin and its derivative: Physicochemical properties, water solubility, and antioxidant activity. *J. Mol. Liq.* **2021**, *334*, 116070. [CrossRef]
- 16. Espel Grekopoulos, J. Construction and Validation of Quantification Methods for Determining the Cannabidiol Content in Liquid Pharma-Grade Formulations by Means of Near-Infrared Spectroscopy and Partial Least Squares Regression. *Med. Cannabis Cannabinoids* 2019, 2, 43–55. [CrossRef]
- 17. Borille, B.T.; Marcelo, M.C.A.; Ortiz, R.S.; Mariotti, K.d.C.; Ferrão, M.F.; Limberger, R.P. Near infrared spectroscopy combined with chemometrics for growth stage classification of cannabis cultivated in a greenhouse from seized seeds. *Spectrochim. Acta A* **2017**, *173*, 318–323. [CrossRef]
- 18. Tay, L.-L.; Hulse, J.; Paroli, R.M. FTIR and Raman spectroscopic characterization of cannabinoids. *Can. J. Chem.* **2022**, *100*, 751–758. [CrossRef]
- 19. Geskovski, N.; Stefkov, G.; Gigopulu, O.; Stefov, S.; Huck, C.W.; Makreski, P. Mid-infrared spectroscopy as process analytical technology tool for estimation of THC and CBD content in Cannabis flowers and extracts. *Spectrochim. Acta A* **2021**, 251, 119422. [CrossRef]
- 20. Reggio, P.H. Endocannabinoid binding to the cannabinoid receptors: What is known and what remains unknown. *Curr. Med. Chem.* **2010**, *17*, 1468–1486. [CrossRef]
- 21. El-Atawneh, S.; Goldblum, A. Candidate Therapeutics by Screening for Multitargeting Ligands: Combining the CB2 Receptor With CB1, PPARγ and 5-HT4 Receptors. *Front. Pharmacol.* **2022**, *13*, 812745. [CrossRef] [PubMed]
- 22. Buczek, A.; Rzepiela, K.; Broda, M.A.; Kupka, T.; Strodel, B.; Fatafta, H. Water modulated influence of intramolecular hydrogen-bonding on the conformational properties of Cannabidiol (CBD). *J. Mol. Liq.* **2025**, 423, 127033. [CrossRef]
- 23. Oliveira, B.G. The structures of heterocyclic complexes ruled by hydrogen bonds and halogen interactions: Interaction strength and IR modes. *Spectrochim. Acta A* **2014**, 124, 208–215. [CrossRef]
- 24. Buczek, A.; Wałęsa, R.; Broda, M.A. β-turn tendency in N-methylated peptides with dehydrophenylalanine residue: DFT study. *Biopolymers* **2012**, *97*, 518–528. [CrossRef]
- 25. Broda, M.A.; SiodŁak, D.; Rzeszotarska, B. Conformational investigation of α,β-dehydropeptides. XV: N-acetyl-α,β-dehydroamino acid N 'N '-dimethylamides: Conformational properties from infrared and theoretical studies. *J. Pept. Sci.* **2005**, *11*, 546–555. [CrossRef]
- 26. Mayr, T.; Grassl, T.; Korber, N.; Christoffel, V.; Bodensteiner, M. Cannabidiol revisited. IUCrData 2017, 2, x170276. [CrossRef]
- 27. Jaremko, Ł.; Jaremko, M.; Buczek, A.; Broda, M.A.; Kupka, T.; Jackowski, K. 1H and 13C shielding measurements in comparison with DFT calculations performed for two 2-(acetyloamino)-N,N-dimethyl-3-phenylacrylamide isomers. *Chem. Phys. Lett.* **2015**, 627, 1–6. [CrossRef]
- 28. Joshi, B.D.; Srivastava, A.; Honorato, S.B.; Tandon, P.; Pessoa, O.D.L.; Fechine, P.B.A.; Ayala, A.P. Study of molecular structure, vibrational, electronic and NMR spectra of oncocalyxone A using DFT and quantum chemical calculations. *Spectrochim. Acta A* **2013**, *113*, 367–377. [CrossRef]
- 29. Barthlott, I.; Scharinger, A.; Golombek, P.; Kuballa, T.; Lachenmeier, D.W. A Quantitative (1)H NMR Method for Screening Cannabinoids in CBD Oils. *Toxics* **2021**, *9*, 136. [CrossRef]
- 30. Marchetti, L.; Brighenti, V.; Rossi, M.C.; Sperlea, J.; Pellati, F.; Bertelli, D. Use of (13)C-qNMR Spectroscopy for the Analysis of Non-Psychoactive Cannabinoids in Fibre-Type Cannabis sativa L. (Hemp). Molecules 2019, 24, 1138. [CrossRef]
- 31. Yu, C.; Long, R.; Cao, F.; Zhao, X.; Lan, T.; Xu, D. Development of Pure Certified Reference Material of Cannabidiol. *Molecules* **2024**, 29, 921. [CrossRef] [PubMed]
- 32. Colella, M.F.; Salvino, R.A.; Gaglianò, M.; Litrenta, F.; Oliviero Rossi, C.; Le Pera, A.; De Luca, G. NMR Spectroscopy Applied to the Metabolic Analysis of Natural Extracts of *Cannabis sativa*. *Molecules* **2022**, 27, 3509. [CrossRef] [PubMed]
- 33. Ohtsuki, T.; Friesen, J.B.; Chen, S.N.; McAlpine, J.B.; Pauli, G.F. Selective Preparation and High Dynamic-Range Analysis of Cannabinoids in "CBD Oil" and Other *Cannabis sativa* Preparations. J. Nat. Prod. 2022, 85, 634–646. [CrossRef]
- 34. Wood, J.S.; Gordon, W.H.; Morgan, J.B.; Williamson, R.T. Calculated and Experimental 1 H and 13 C NMR Assignments for Cannabicitran. *Magn. Reson. Chem.* **2021**, *60*, 196–202. [CrossRef]
- 35. Tasdemir, H.U. Effects of intramolecular hydrogen bonding on nuclear magnetic resonance, electron paramagnetic resonance and molecular docking studies: Mexiletine molecule. *J. Mol. Model.* **2024**, *30*, 41. [CrossRef]
- Mololina, A.A.; Sobornova, V.V.; Belov, K.V.; Krestyaninov, M.A.; Khodov, I.A. Role of non-covalent interactions in the conformational stability of bicalutamide in different solvent environments: Insights from quantum-chemical calculations and NMR spectroscopy. J. Mol. Liq. 2025, 423, 126921. [CrossRef]
- 37. Tolstoy, P.M.; Tupikina, E.Y. IR and NMR Spectral Diagnostics of Hydrogen Bond Energy and Geometry. In *Spectroscopy and Computation of Hydrogen-Bonded Systems*; Wiley-VCH: Weinheim Germany, 2023; pp. 345–407. [CrossRef]

Molecules **2025**, 30, 2591 15 of 15

38. Oparin, R.D.; Kiselev, M.G. A near-infrared spectroscopic study of the conformational equilibria of lidocaine molecules in a highly concentrated lidocaine solution in supercritical CO<sub>2</sub>. *J. Mol. Liq.* **2024**, 396, 123916. [CrossRef]

- 39. Prado, R.C.; Filho, V.S.; Portes, S.A.; Colherinhas, G.; Oliveira, L.B.A. Solvent effects on the spectroscopic properties of cannabinoids derivatives: A theoretical study using PCM. *Int. J. Quantum Chem.* **2024**, 124, e27417. [CrossRef]
- 40. Denhez, C.; Lameiras, P.; Berber, H. Intramolecular OH/π versus C–H/O H-Bond-Dependent Conformational Control about Aryl–C(sp3) Bonds in Cannabidiol Derivatives. *Org. Lett.* **2019**, *21*, 6855–6859. [CrossRef]
- 41. Abraham, R.J.; Mobli, M. An NMR, IR and theoretical investigation of 1H Chemical Shifts and hydrogen bonding in phenols. *Magn. Reson. Chem.* **2007**, *45*, 865–877. [CrossRef]
- 42. Choi, Y.H.; Hazekamp, A.; Peltenburg-Looman, A.M.; Frédérich, M.; Erkelens, C.; Lefeber, A.W.; Verpoorte, R. NMR assignments of the major cannabinoids and cannabiflavonoids isolated from flowers of *Cannabis sativa*. *Phytochem. Anal.* **2004**, *15*, 345–354. [CrossRef] [PubMed]
- 43. Siciliano, C.; Bartella, L.; Mazzotti, F.; Aiello, D.; Napoli, A.; De Luca, P.; Temperini, A. 1H NMR quantification of cannabidiol (CBD) in industrial products derived from *Cannabis sativa* L. (hemp) seeds. *IOP Conf. Ser. Mater. Sci. Eng.* **2019**, 572, 012010. [CrossRef]
- 44. Kupka, T.; Makieieva, N.; Jewgiński, M.; Witek, M.; Blicharska, B.; Rahmonov, O.; Doležal, K.; Pospíšil, T. Caffeine—Legal Natural Stimulant with Open Research Perspective: Spectroscopic and Theoretical Characterization. *Molecules* **2024**, 29, 4382. [CrossRef] [PubMed]
- 45. Frisch, M.J.; Trucks, G.W.; Schlegel, H.B.; Scuseria, G.E.; Robb, M.A.; Cheeseman, J.R.; Scalmani, G.; Barone, V.; Petersson, G.A.; Nakatsuji, H.; et al. *Gaussian 16, C 0.1*; Gaussian, Inc.: Wallingford, CT, USA, 2019.
- 46. Tomasi, J.; Mennucci, B.; Cammi, R. Quantum Mechanical Continuum Solvation Models. *Chem. Rev.* **2005**, *105*, 2999–3094. [CrossRef]
- 47. Scott, A.P.; Radom, L. Harmonic vibrational frequencies: An evaluation of Hartree-Fock, Møller-Plesset, quadratic configuration interaction, density functional theory, and semiempirical scale factors. *J. Phys. Chem.* **1996**, *100*, 16502–16513. [CrossRef]

**Disclaimer/Publisher's Note:** The statements, opinions and data contained in all publications are solely those of the individual author(s) and contributor(s) and not of MDPI and/or the editor(s). MDPI and/or the editor(s) disclaim responsibility for any injury to people or property resulting from any ideas, methods, instructions or products referred to in the content.

## **Supplementary Material**

for

# Impact of O-H $\cdots\pi$ hydrogen bond on IR and NMR parameters of cannabidiol (CBD): theoretical and experimental study

Aneta Buczek\*, Kacper Rzepiela, Małgorzata A. Broda, Teobald Kupka

Faculty of Chemistry and Pharmacy, University of Opole, 48, Oleska Street, 45-052 Opole, Poland

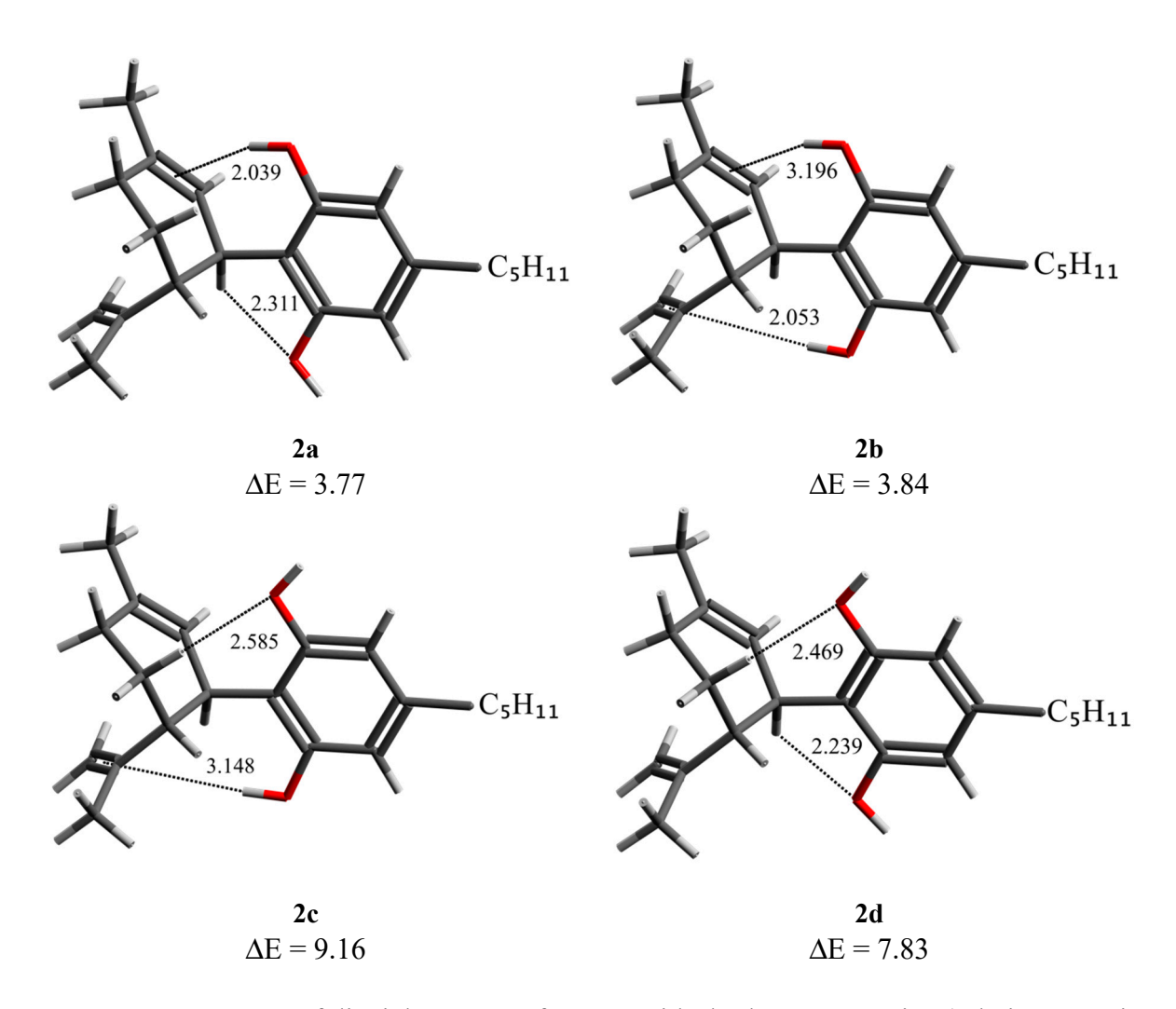


**Figure S1.** Structures of diaxial CBD conformers with the lowest energies (relative energies  $\Delta E$  in kcal/mol, the relative energy was calculated in comparison to the lowest energy of CBD with diequatorial conformation) in four groups differing in OH group settings, calculated with MP2/6-311++G(d,p)//B3LYP-GD3BJ/6-311++G(d,p) method in chloroform. Hydrogen bonds are marked by dot lines and the distances are given in (Å).

**Table S1.** <sup>1</sup>H and <sup>13</sup>C nuclear shieldings of TMS and benzene as reference molecules calculated at B3LYP/aug-cc-pVTZ level of theory.

Atom	Gas	CHCl <sub>3</sub>								
TMS										
C	184.127	184.512								
H	31.671	31.665								
Benzene										
C	49.546	49.326								
Н	24.017	23.907								

**Table S2.** <sup>1</sup>H and <sup>13</sup>C nuclear shieldings for diequatorial (**1a - 1d**) and diaxial (**2a - 2d**) CBD conformers, calculated at B3LYP/aug-cc-pVTZ level of theory in gas phase.

ers, carculate	u at D31	_ I F/aug	3-сс-р v	IZ level of theory in gas phase			phase.	
Atom	1a	1b	1c	1d	2a	2b	2c	2d
(OA)H	27.89	26.36	26.10	27.78	27.74	27.26	26.80	27.64
(OB)H	25.40	25.62	27.80	27.77	23.73	24.18	27.95	27.87
(C2)H	25.65	25.78	26.04	25.99	25.39	25.43	25.78	25.81
(C3)H	27.53	27.97	29.46	27.43	27.58	28.25	28.36	27.54
(C4)H	29.13	29.38	28.06	28.56	29.47	29.42	29.53	29.55
(C5)H	29.87	29.81	29.80	29.87	29.83	29.78	29.77	29.72
(C6)H	29.45	29.44	29.52	29.50	29.64	29.66	29.65	29.75
(C7)H	29.78	29.78	29.88	29.89	29.81	29.77	29.88	29.90
(C9)H-trans	26.99	26.40	26.41	27.09	26.54	26.41	26.43	26.52
(C9)H-cis	27.31	26.40	26.49	27.14	26.69	26.65	26.54	26.55
(C10)H	29.81	30.17	30.18	29.79	29.80	29.76	29.77	29.84
(C4')H	25.23	25.13	25.11	25.71	25.63	25.14	25.08	25.55
(C6')H	25.74	25.14	25.60	25.66	25.26	25.27	25.72	25.72
(C1")H	29.18	29.11	29.13	29.19	29.30	29.09	29.28	29.19
(C2")H	30.16	30.13	30.15	30.18	30.25	30.00	30.24	30.14
(C3")H	30.82	30.73	30.70	30.80	30.34	30.67	30.34	30.69
(C4")H	30.50	30.49	30.49	30.50	30.34	30.28	30.34	30.47
(C5")H	30.81	30.82	30.80	30.80	30.67	30.79	30.66	30.78
C1	33.00	33.25	43.69	42.60	32.81	30.51	40.51	40.40
C2	50.07	50.75	49.06	49.70	51.31	54.28	52.55	52.18
С3	142.51	133.84	132.98	142.10	140.09	138.78	138.41	141.40
C4	131.21	135.03	135.17	132.47	131.57	131.64	131.45	131.00
C5	151.11	150.01	149.40	150.22	158.57	158.80	157.61	158.21
С6	148.36	148.45	148.83	149.15	154.56	153.70	154.91	153.35
C7	157.44	157.45	157.83	157.56	157.44	157.69	156.84	157.01
C8	24.71	10.82	9.80	21.02	22.74	23.15	21.56	22.52
С9	67.37	72.23	73.71	69.83	71.04	70.18	70.37	72.02
C10	163.68	154.44	154.35	163.95	158.96	158.83	158.53	157.62
C1'	21.40	20.49	20.00	18.92	16.13	17.37	20.94	20.00

C2'	66.24	64.52	62.17	61.98	65.76	68.87	64.99	60.54
С3'	17.60	18.17	18.87	20.54	21.10	21.24	18.67	19.17
C4'	71.31	70.29	66.92	72.31	75.73	70.95	71.27	74.83
C5'	33.21	32.54	33.60	34.26	31.22	32.63	31.21	33.96
C6'	73.50	67.31	74.28	73.94	69.49	70.47	74.12	70.00
C1"	142.44	142.78	143.09	142.78	140.15	146.73	140.33	142.69
C2"	145.82	145.82	145.49	145.70	141.11	147.65	141.15	145.46
C3"	147.72	147.46	147.65	147.76	144.18	151.29	143.96	147.87
C4"	154.52	154.41	154.22	154.43	154.11	157.91	154.23	154.27
C5"	167.05	167.14	167.26	167.06	167.03	167.18	167.23	167.31

**Table S3.** The relative energies  $\Delta E$  (in kcal/mol) of the lowest diaxial CBD conformer calculated with MP2/6-311++G(d,p)//B3LYP-GD3BJ/6-311++G(d,p) in gas phase and

chloroform. Hydrogen bonds distances are given in Å.

	ΔE			Distance		
Conformer	Gas phase CHCl <sub>3</sub>		H-bond type	gas phase	CHCl <sub>3</sub>	
2a	3.99	3.77	C3-H···O-H(B)	2.301	2.311	
			O-H(A)···C1=C2	2.050	2.039	
2b	3.87	3.84	O-H(B)···C8=C9	3.183	3.196	
			O-H(A)···C1=C2	2.073	2.053	
20	0.02	9.16	O-H(B)··· C8=C9	3.137	3.148	
2c	9.03	9.10	C4-H···O-H(A)	2.593	2.585	
2d	8.34	7,83	С3-Н···О-Н(В)	2.239	2.239	
			C4-H···O-H(A)	2.459	2.469	

**Table S4.** Calculated <sup>1</sup>H chemical shifts of diaxial CBD conformers, with B3LYP/aug-cc-pVTZ in gas phase, compared with experiment and available literature data.

p v 12 m gas phase, compared with experiment and available merature data.									
Atom	2a	2b	2c	2d	Exp. this work	Lit.1	Lit.2	Lit.3	Lit.4
(OA)H	7.94	7.50	3.72	3.80	5.99	5.99	5.95	6.22	
(OB)H	3.93	4.41	4.87	4.03	4.66	5.02	4.6		
(C2)H	5.78	5.75	5.40	5.36	5.57	5.57	5.57	5.56	5.57
(C3)H	4.09	3.42	3.31	4.13	3.86	3.9	3.84	3.86	3.86
(C4)H	2.20	2.25	2.14	2.12	2.40	2.4	2.4		2.40
(C5)H	1.84	1.89	1.90	1.95	1.82	1.84	1.82		1.78–1.84
(C6)H	2.03	2.01	2.02	1.92	$H6_a = 2.07,$ $H6_b = 2.23$	2.21	2.09		H6a = 2.05-2.09, H6b = 2.22
(C7)H	1.86	1.90	1.79	1.77	1.79	1.79	1.79		1.79
(C9)H- trans	4.64	4.77	4.75	4.65	4.66	4.64	4.67	4.66	4.64
(C9)H-cis	4.49	4.52	4.63	4.63	4.56	4.54	4.6	4.57	4.53
(C10)H	1.87	1.91	1.90	1.83	1.66	1.66	1.65		1.66
(C4')H	5.54	6.04	6.09	5.63	6.17	6.16	6.19		6.16
(C6')H	5.92	5.90	5.46	5.46	6.28	6.26	6.25		6.26
(C1")H	2.38	2.58	2.39	2.48	2.44	2.43	2.44		2.43
(C2")H	1.42	1.67	1.43	1.53	1.59	1.55	1.56		1.52–1.61
(C3")H	1.33	1.00	1.33	0.98	1.30	1.29	1.3		1.27–1.32
(C4")H	1.33	1.40	1.33	1.20	1.30	1.29	1.3		
(C5")H	1.01	0.88	1.01	0.89	0.88	0.88	0.89		0.86-0.88
RMS exp. this work	0.53	0.41	0.60	0.60					

**Table S5.** Calculated <sup>13</sup>C chemical shifts of diaxial CBD conformers, with B3LYP/aug-cc-pVTZ in vacuum, compared with experiment and available literature data.

vacuum, compared with experiment and available merature data.								
Atom	2b	<b>2</b> b	2c	2d	Exp. this work	Lit.1	Lit.2	
C1	145.24	147.54	137.53	137.65	143.06	134.2		
C2	126.74	123.77	125.50	125.86	124.09	127.3	124.14	
С3	44.04	45.35	45.72	42.73	37.25	37.5	37.01	
C4	52.56	52.48	52.68	53.13	46.14	46.4		
C5	25.56	25.33	26.52	25.92	28.39	31.7	28.35	
C6	29.57	30.43	29.22	30.77	30.64	30.7	30.36	
C7	26.69	26.44	27.29	27.12	23.69	23.7	23.69	
C8	155.31	154.90	156.48	155.53	149.41	150.3		
С9	107.01	107.87	107.68	106.02	110.84	110.5	110.81	
C10	25.17	25.29	25.60	26.50	20.53	19.5	20.30	
C1'	161.92	160.68	157.11	158.05	156.15	157.5		
C2'	112.29	109.18	113.05	117.51	113.73	115.9		
C3'	156.95	156.81	159.37	158.88	153.87	150.3		
C4'	102.32	107.09	106.77	103.22	109.76	108.3	107.92	
C5'	146.83	145.41	146.84	144.08	140.09	142.7		
C6'	108.56	107.57	103.93	108.05	107.99	108.3	109.56	
C1"	43.97	37.40	43.80	41.44	35.47	36.6	35.46	
C2"	43.02	36.48	42.98	38.67	30.39	32.0	30.65	
C3"	39.95	32.84	40.17	36.26	31.49	32.6	31.48	
C4"	30.02	26.22	29.90	29.86	22.54	23.6	22.54	
C5"	17.10	16.94	16.89	16.82	14.05	14.4	14.04	
RMS this work	5.73	4.10	5.80	4.90				

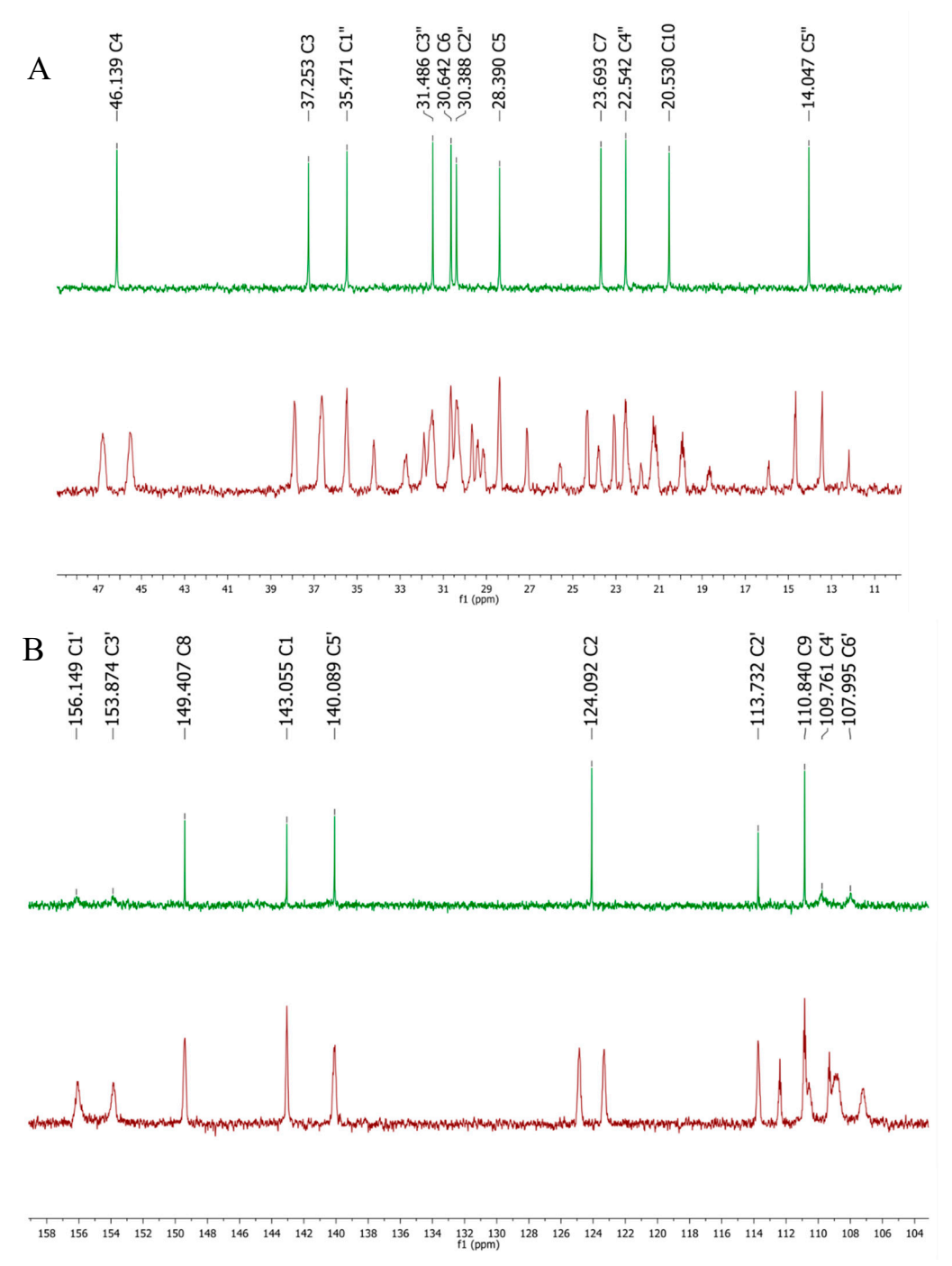


**Figure S2.** The enlarged aliphatic (A) and aromatic (B) fragments of <sup>13</sup>C (-<sup>1</sup>H) (green) and (+<sup>1</sup>H) (red) NMR spectrum of CBD in CDCl<sub>3</sub>.

# 10.5 P5: Water modulated influence of intramolecular hydrogen-bonding on the conformational properties of Cannabidiol (CBD)



## Journal of Molecular Liquids

Volume 423, 1 April 2025, 127033



# Water modulated influence of intramolecular hydrogen-bonding on the conformational properties of Cannabidiol (CBD)

 $\frac{\text{Aneta Buczek} \, ^{\text{a}} \overset{\triangle}{\sim} \, \boxtimes}{\text{Strodel}} , \\ \frac{\text{Kacper Rzepiela} \, ^{\text{a}} \, \text{b}}{\text{Strodel}} , \\ \frac{\text{b} \, ^{\text{c}}}{\text{Strodel}} , \\ \frac{\text{c} \, ^{\text{c}}}{\text{Strodel}$ 

https://doi.org/10.1016/j.molliq.2025.127033 7

Get rights and content ↗

## Highlights

- DFT calculations show CBD's stable conformation involves diequatorial substitution.
- The energy of <u>CBD</u> <u>conformers</u> depends on the orientation of both OH groups.
- $OH{\cdots}\pi$  <u>hydrogen bonding</u> stabilizes CBD's preferred structure.
- MD simulations reveal that single <u>CBD</u> molecule retain their conformation in water.
- <u>CBD</u> molecules in water tend to form clusters.

### **Abstract**

Cannabidiol (CBD), a non-psychoactive phytocannabinoid from *Cannabis sativa*, has gained significant attention due to its diverse therapeutic properties, including anti-inflammatory, antioxidant, and anxiolytic effects. However, its clinical application is hindered by poor water solubility, which limits its bioavailability. The aim of this study is to deepen our understanding of the conformational properties of <u>CBD</u>, and investigate how these properties affect its solubility. Using Density Functional Theory (DFT) calculations, we analyzed the axial and equatorial positions of substituents on the limonene ring and the arrangement of both hydroxyl groups. Our findings indicate that the most stable conformation of <u>CBD</u> involves diequatorial substitution on the limonene ring, stabilized by specific  $-OH\cdots\pi$  hydrogen bonding interactions. All-atom Molecular Dynamics (MD) simulations in an aqueous environment revealed that while single <u>CBD</u> molecules maintain their conformation, multiple CBD molecules tend to cluster. These insights provide a comprehensive understanding of the molecular interactions that underlies CBD's low aqueous solubility and suggests potential strategies for enhancing its bioavailability, which could optimize its therapeutic potential.

## 11. Co-author statements

Mgr inż. Kacper Rzepiela

September 29, 2025

Faculty of Chemistry and Pharmacy,

University of Opole,

ul. Oleska 48, 45-052 Opole, Poland

Statement:

I state that in the articles:

P1. Aneta Buczek\*, Kacper Rzepiela, Teobald Kupka, Małgorzata A. Broda and Tapas Kar\*,

Uracil-water interaction revisited - in search of single H-bonded secondary minima,

Physical Chemistry Chemical Physics, 2024,26, 5169-5182. DOI: https://doi.org/10.1039/D3CP04057G

P2. Kacper Rzepiela, Aneta Buczek, Teobald Kupka, Tapas Kar and Małgorzata A. Broda\*, Modelowanie właściwości wiązań wodorowych na przykładzie kompleksów układ amidowy-woda. (MODELING THE PROPERTIES OF HYDROGEN BONDS. AN EXAMPLE OF AMIDE-WATER COMPLEX) Wiadomości Chemiczne 2023, 77 (7-8), 629-645, DOI: <a href="https://doi.org/10.53584/wiadchem.2023.07.1">https://doi.org/10.53584/wiadchem.2023.07.1</a>

P3. Kacper Rzepiela, Jakub Kaminský\*, Aneta Buczek, Małgorzata A. Broda and Teobald Kupka\*, Electron Correlation or Basis Set Quality: How to Obtain Converged and Accurate NMR Shieldings for the Third-Row Elements?, Molecules, 2022, 27(23), 8230. DOI: <a href="https://doi.org/10.3390/molecules27238230">https://doi.org/10.3390/molecules27238230</a>

P4. Aneta Buczek, Kacper Rzepiela, Teobald Kupka, Małgorzata A. Impact of OH····  $\pi$  Hydrogen Bond on IR and NMR Parameters of Cannabidiol: Theoretical and Experimental Study. Molecules 2025, 30 (12), 2591, DOI: <a href="https://10.3390/molecules30122591">https://10.3390/molecules30122591</a>

P5. Aneta Buczek\*, Kacper Rzepiela, Małgorzata A. Broda, Teobald Kupka, Birgit Strodel, Hebah Fatafta\*, Water modulated influence of intramolecular hydrogen-bonding on the conformational properties of Cannabidiol (CBD), Journal of Molecular Liquids 423 (2025) 127033 DOI: <a href="https://doi.org/10.1016/j.molliq.2025.127033">https://doi.org/10.1016/j.molliq.2025.127033</a>

My contribution included: reviewing the literature, co-developing the research hypothesis, conducting calculations, the analysis of results, preparation of FTIR and NMR samples, editing of the manuscripts, and visualization of figures.

co-author signature

Keyer Repuls

Faculty of Chemistry and Pharmacy,

University of Opole,

ul. Oleska 48, 45-052 Opole, Poland

Statement:

I state that in the articles:

P1. Aneta Buczek\*, Kacper Rzepiela, Teobald Kupka, Małgorzata A. Broda and Tapas Kar\*,

Uracil-water interaction revisited – in search of single H-bonded secondary minima,

Physical Chemistry Chemical Physics, 2024,26, 5169-5182. DOI: https://doi.org/10.1039/D3CP04057G

- P2. Kacper Rzepiela, Aneta Buczek, Teobald Kupka, Tapas Kar and Małgorzata A. Broda\*, Modelowanie właściwości wiązań wodorowych na przykładzie kompleksów układ amidowy-woda. (MODELING THE PROPERTIES OF HYDROGEN BONDS. AN EXAMPLE OF AMIDE-WATER COMPLEX) Wiadomości Chemiczne 2023, 77 (7-8), 629-645, DOI: <a href="https://doi.org/10.53584/wiadchem.2023.07.1">https://doi.org/10.53584/wiadchem.2023.07.1</a>
- P3. Kacper Rzepiela, Jakub Kaminský\*, Aneta Buczek, Małgorzata A. Broda and Teobald Kupka\*, Electron Correlation or Basis Set Quality: How to Obtain Converged and Accurate NMR Shieldings for the Third-Row Elements?, Molecules, 2022, 27(23), 8230. DOI: <a href="https://doi.org/10.3390/molecules27238230">https://doi.org/10.3390/molecules27238230</a>
- P4. Aneta Buczek, Kacper Rzepiela, Teobald Kupka, Małgorzata A. Impact of OH····  $\pi$  Hydrogen Bond on IR and NMR Parameters of Cannabidiol: Theoretical and Experimental Study. Molecules 2025, 30 (12), 2591, DOI: https://10.3390/molecules30122591
- P5. Aneta Buczek\*, Kacper Rzepiela, Małgorzata A. Broda, Teobald Kupka, Birgit Strodel, Hebah Fatafta\*, Water modulated influence of intramolecular hydrogen-bonding on the conformational properties of Cannabidiol (CBD), Journal of Molecular Liquids 423 (2025) 127033 DOI: <a href="https://doi.org/10.1016/j.molliq.2025.127033">https://doi.org/10.1016/j.molliq.2025.127033</a>

My contribution was writing – review & editing, conceptualization, methodology, project administration, formal analysis and supervision.

co-author signature

Faculty of Chemistry and Pharmacy,

University of Opole,

ul. Oleska 48, 45-052 Opole, Poland

Statement:

I state that in the articles:

P1. Aneta Buczek\*, Kacper Rzepiela, Teobald Kupka, Małgorzata A. Broda and Tapas Kar\*,

Uracil-water interaction revisited – in search of single H-bonded secondary minima,

Physical Chemistry Chemical Physics, 2024,26, 5169-5182. DOI: https://doi.org/10.1039/D3CP04057G

- P2. Kacper Rzepiela, Aneta Buczek, Teobald Kupka, Tapas Kar and Małgorzata A. Broda\*, Modelowanie właściwości wiązań wodorowych na przykładzie kompleksów układ amidowy-woda. (MODELING THE PROPERTIES OF HYDROGEN BONDS. AN EXAMPLE OF AMIDE-WATER COMPLEX) Wiadomości Chemiczne 2023, 77 (7-8), 629-645, DOI: <a href="https://doi.org/10.53584/wiadchem.2023.07.1">https://doi.org/10.53584/wiadchem.2023.07.1</a>
- P3. Kacper Rzepiela, Jakub Kaminský\*, Aneta Buczek, Małgorzata A. Broda and Teobald Kupka\*, Electron Correlation or Basis Set Quality: How to Obtain Converged and Accurate NMR Shieldings for the Third-Row Elements?, Molecules, 2022, 27(23), 8230. DOI: <a href="https://doi.org/10.3390/molecules27238230">https://doi.org/10.3390/molecules27238230</a>
- P4. Aneta Buczek, Kacper Rzepiela, Teobald Kupka, Małgorzata A. Impact of OH····  $\pi$  Hydrogen Bond on IR and NMR Parameters of Cannabidiol: Theoretical and Experimental Study. Molecules 2025, 30 (12), 2591, DOI: <a href="https://10.3390/molecules30122591">https://10.3390/molecules30122591</a>
- P5. Aneta Buczek\*, Kacper Rzepiela, Małgorzata A. Broda, Teobald Kupka, Birgit Strodel, Hebah Fatafta\*, Water modulated influence of intramolecular hydrogen-bonding on the conformational properties of Cannabidiol (CBD), Journal of Molecular Liquids 423 (2025) 127033 DOI: <a href="https://doi.org/10.1016/j.molliq.2025.127033">https://doi.org/10.1016/j.molliq.2025.127033</a>

My contribution was writing – review & editing, conceptualization, methodology, project administration, formal analysis and supervision.

co-author signature

Aneta Bussel

Faculty of Chemistry and Pharmacy,

University of Opole,

ul. Oleska 48, 45-052 Opole, Poland

Statement:

I state that in the articles:

P1. Aneta Buczek\*, Kacper Rzepiela, Teobald Kupka, Małgorzata A. Broda and Tapas Kar\*,

Uracil-water interaction revisited – in search of single H-bonded secondary minima,

Physical Chemistry Chemical Physics, 2024,26, 5169-5182. DOI: https://doi.org/10.1039/D3CP04057G

- P2. Kacper Rzepiela, Aneta Buczek, Teobald Kupka, Tapas Kar and Małgorzata A. Broda\*, Modelowanie właściwości wiązań wodorowych na przykładzie kompleksów układ amidowy-woda. (MODELING THE PROPERTIES OF HYDROGEN BONDS. AN EXAMPLE OF AMIDE-WATER COMPLEX) Wiadomości Chemiczne 2023, 77 (7-8), 629-645, DOI: <a href="https://doi.org/10.53584/wiadchem.2023.07.1">https://doi.org/10.53584/wiadchem.2023.07.1</a>
- P3. Kacper Rzepiela, Jakub Kaminský\*, Aneta Buczek, Małgorzata A. Broda and Teobald Kupka\*, Electron Correlation or Basis Set Quality: How to Obtain Converged and Accurate NMR Shieldings for the Third-Row Elements?, Molecules, 2022, 27(23), 8230. DOI: <a href="https://doi.org/10.3390/molecules27238230">https://doi.org/10.3390/molecules27238230</a>
- P4. Aneta Buczek, Kacper Rzepiela, Teobald Kupka, Małgorzata A. Impact of OH····  $\pi$  Hydrogen Bond on IR and NMR Parameters of Cannabidiol: Theoretical and Experimental Study. Molecules 2025, 30 (12), 2591, DOI: <a href="https://10.3390/molecules30122591">https://10.3390/molecules30122591</a>
- P5. Aneta Buczek\*, Kacper Rzepiela, Małgorzata A. Broda, Teobald Kupka, Birgit Strodel, Hebah Fatafta\*, Water modulated influence of intramolecular hydrogen-bonding on the conformational properties of Cannabidiol (CBD), Journal of Molecular Liquids 423 (2025) 127033 DOI: <a href="https://doi.org/10.1016/j.molliq.2025.127033">https://doi.org/10.1016/j.molliq.2025.127033</a>

My contribution was writing – review & editing, conceptualization, methodology, project administration, formal analysis and supervision.

co-author signature

M. Smola

September 29, 2025

(Professor)

Institute of Biological Information Processing: Structural Biochemistry (IBI-7),

Forschungszentrum Jülich, Building 5.8v, Room 3024,

52425 Jülich, Germany

Statement

I state that in the article:

P5. Aneta Buczek\*, Kacper Rzepiela, Małgorzata A. Broda, Teobald Kupka, Birgit Strodel, Hebah Fatafta\*

Water modulated influence of intramolecular hydrogen-bonding on the conformational properties of Cannabidiol (CBD), Journal of Molecular Liquids 423 (2025) 127033

DOI: https://doi.org/10.1016/j.molliq.2025.127033

my contribution was writing – review & editing, Supervision, Resources and Conceptualization.

co-author signature

int too be

Dr. Hebah Fatafta 27, 2025 September

\_\_\_\_

Department of Engineering and Communication,

Bonn-Rhein-Sieg University of Applied Sciences,

Grantham-Allee 20 53757 Sankt Augustin, Germany

Statement

I state that in the article:

P5. Aneta Buczek\*, Kacper Rzepiela, Małgorzata A. Broda, Teobald Kupka, Birgit Strodel, Hebah Fatafta\*

Water modulated influence of intramolecular hydrogen-bonding on the conformational properties of Cannabidiol (CBD), Journal of Molecular Liquids 423 (2025) 127033

DOI: https://doi.org/10.1016/j.molliq.2025.127033

My contribution was Writing – review & editing, Writing. – original draft, Validation, Supervision, Methodology and Conceptualization.

Hiba Fatafta

co-author signature

Dr. Jakub Kaminský

September 26, 2025

(Senior Researcher)

Institute of Organic Chemistry and Biochemistry,

Czech Academy of Sciences,

Flemingovo nám. 2, 166 10 Prague, Czech Republic

Statement

I state that in the article:

P3. Kacper Rzepiela, Jakub Kaminský\*, Aneta Buczek, Małgorzata A. Broda and Teobald Kupka\*

Electron Correlation or Basis Set Quality: How to Obtain Converged and Accurate NMR Shieldings for the Third-Row Elements?, Molecules, 2022, 27(23), 8230.

DOI: https://doi.org/10.3390/molecules27238230

My contribution was calculating zero-point vibrational corrections with the S4 program, and in general: investigation, supervision, methodology, and writing—review and editing

co-author signature

Kamis \